INSIGHTS INTO RETINAL HEALTH AND DISEASE FROM HUMAN STEM CELL BASED SYSTEMS

by
Alyssa Kallman

A dissertation submitted to Johns Hopkins University in conformity with the requirements for the degree of Doctor of Philosophy

Baltimore, Maryland

August 2020

Abstract

Retinal health and function is dependent on the function of various cell types, and genetic insult or injury to these cells can result in vision loss. The inherited retinal degenerations constitute a heterogeneous group of orphan diseases, with multiple causative genes and highly varied disease phenotypes. Many of the genes involved in photoreceptor degeneration are also involved in development, and understanding both of these facets of photoreceptor health is critical to understanding disease. While photoreceptor death is a leading cause of vision loss, other cell types are also affected in retinal disease. Retinal ganglion cells are also commonly affected in retinal diseases such as glaucoma and optic neuritis, and their axons are myelinated by oligodendrocytes. Because of the importance of myelin, oligodendrocyte health is an additional important aspect of retinal health and vision. Multiple sclerosis, a demyelinating disorder, often presents as optic neuritis, a condition marked by retinal ganglion cell demyelination. As such, a better understanding of oligodendrocyte development and myelination is important for identifying remyelination therapeutic targets. In this study, we utilized stem cell based systems combined with single-cell transcriptomics to better understand development of photoreceptors and oligodendrocytes, as well as photoreceptor degeneration. We utilized retinal organoids differentiated from a patient-derived stem cell line harboring a homozygous mutation in *NRL*, a transcription factor required for rod development and whose loss leads to Enhanced S Cone Syndrome. These organoids lacked rods and had a higher proportion of *OPN1SW+* photoreceptors, with the *OPN1SW+* cells being separable into two distinct populations. Additionally, we identified MEF2C as a candidate regulator of cone development. We also utilized retinal organoids to develop models of Leber Congenital Amaurosis due to loss of either CRB1 or RPGRIP1. We identified distinct histological pathologies in these models and convergence upon DDIT3 induction as a shared

degenerative pathway, thus making endoplasmic reticulum stress an attractive therapeutic target. Finally, we characterized oligodendrocyte precursor cell development into either oligodendrocytes or astrocytes and identified heterogeneity within the precursor population, as well as transcription factors and microRNAs that could be important in directing formation of oligodendrocytes or astrocytes.

Thesis Readers

Don Zack, M.D., Ph.D

Ophthalmology, JHUSOM

David Valle, M.D

Genetic Medicine, JHUSOM

Preface

A huge thanks to everyone in the Zack lab and our collaborators for making this work possible. Especially Don, Cindy, and Xitiz for their continued mentorship and support over the years. I would also like to thank our collaborators in the labs of David Gamm, Jiang Qian, and Jeff Wang for their indispensable contributions to this work.

Table of Contents

List of Abbreviations

ALC	Astrocyte lineage cell
CNS	Central nervous system
ER	Endoplasmic reticulum
ESCS	Enhanced S Cone Syndrome
GO	Gene ontology
hESC	Human embryonic stem cell
hPSC	Human pluripotent stem cell
ICC	Immunocytochemistry
IHC	Immunohistochemistry
iPSC	Induced pluripotent stem cell
KO	Knockout
LCA	Leber Congenital Amaurosis
MS	Multiple Sclerosis
OL	Oligodendrocyte
OLLC	Oligodendrocyte lineage cell
ONL	Outer nuclear layer
OPC	Oligodendrocyte precursor cell
scRNAseq	Single cell RNA sequencing
TF	Transcription factor
t-SNE	T-distributed stochastic neighbor embedding
UMAP	Uniform manifold approximation and projection
UMI	Unique molecular identifier
WT	Wild type

List of Tables

List of Figures

Chapter 2 Figures

Chapter 2 Supplementary Figures

Chapter 1: Introduction

The neural retina is critical for visual function, with light detection first occurring in photoreceptors followed by signal transduction via the optic nerve to the brain (1, 2). This process and overall retinal health depends on proper function and coordinated activity of the many cell types of the retina, including photoreceptors, bipolar cells, amacrine cells, horizontal cells, retinal ganglion cells, muller glia, and retinal pigmented epithelium (3). Retinal health and vision are susceptible to a multitude of genetic and environmental insults, and retinal disease can present with both Mendelian and non-Mendelian inheritance patterns (4). There is vast heterogeneity in the causes of retinal degenerations in the cells affected, role of environmental factors, phenotypic presentation and severity, genes mutated, and the specific mutant alleles. This heterogeneity complicates treatment of retinal diseases, as many individuals globally are affected, but they vary significantly in the cause of their retinal dysfunction. To understand retinal disease, it is critical to also understand retinal development. Development and degeneration are closely linked, with many genes important for development involved in retinal degeneration (5-8).

I sought to better understand both of these facets of retinal health through analysis of human models of both development and degeneration. Many different retinal pathologies have been described, with Enhanced S Cone Syndrome (ESCS) representing a sort of developmental defect and Leber Congenital Amaurosis (LCA) representing the most severe form of photoreceptor degeneration (9-12). ESCS is inherited in an autosomal recessive manner and patients usually lack the transcription factor NR2E3, or occasionally NRL, the transcription factor upstream of NR2E3 (11-13). The combined functions of NRL and NR2E3 are critical for rod photoreceptor development, and loss of either leads to development of an apparent cone-dominant

retina. Patients with ESCS manifest with enhanced blue cone function and an absence of rod function, as well as some degree of retinal degeneration (11, 12). As ESCS presents more of a developmental aberration than a degeneration, this disease provides an attractive model to study cone development and the results of loss of a critical developmental transcription factor. While mouse models of Nrl loss have been studied extensively, the work here represents the first molecular investigation of NRL loss using a human model (14-18). Additionally, previous studies had analyzed population transcriptomics in describing Nrl null photoreceptors, while this study presents in depth single-cell transcriptomic characterization which enabled discovery of subpopulations of NRL null photoreceptors.

On the other end of the disease spectrum is LCA, a severe photoreceptor degeneration in which patients are either born blind or suffer significant vision loss within the first year of life (9, 10). There are over 20 genes known to cause LCA, which can present with either autosomal recessive or autosomal dominant inheritance patterns (9). In addition to the genetic heterogeneity of LCA, there is also heterogeneity in the affected cell type, with mutations affecting either photoreceptors or retinal pigmented epithelium function. Dysfunction of either of these cell types can lead to photoreceptor cell death. Additionally, LCA can vary in whether rod or cone photoreceptors are more severely affected (9, 10). Many mouse models of LCA have been described, and recently there have been efforts to characterize human models of LCA, specifically LCA caused by mutation of CEP290 and AIPL1 (19-26). While there have been advances in LCA treatment, specifically the success of RPE65 gene therapy, the inherited retinal degenerations remain largely untreatable (27). In this work, I sought to characterize CRB1 and RPGRIP1 knockout LCA disease models and identify possible degenerative pathways targetable for treatment strategies. Better understanding of both

developmental and degenerative diseases can provide critical insights into photoreceptor health and possibly identify targets for therapeutic intervention.

While photoreceptor degeneration is a major cause of vision loss, it is also important to better understand the other cell populations important for retinal health. Specifically, retinal ganglion cells, whose axons form the neuronal component of the optic nerve and ultimately transmit visual signals to the brain, are also frequently affected in retinal disease (28, 29). In addition to cell stress within the retinal ganglion cells themselves, demyelination can also promote cell death and visual impairment (30). Myelination insulates the axons of neurons and aids in nerve conduction, with oligodendrocytes myelinating cells of the central nervous system, including retinal ganglion cells (31). Loss of myelin in the central nervous system occurs in Multiple Sclerosis, and a subset of patients experience optic neuritis in which retinal ganglion cell demyelination occurs (32). As such, a better understanding of oligodendrocyte development may provide insights into myelination and possible treatment avenues. Many recent studies have isolated and characterized both human and murine oligodendrocytes, while this study describes the development of stem cell derived oligodendrocyte precursor cells (OPCs) and characterizes their possible cell fates (33-35). By understanding how oligodendrocytes develop and begin expressing myelin, it may be possible to promote myelination in diseased tissue. Myelination and its relationship to retinal ganglion cell health is an additional aspect of retinal health and disease that warrants further investigation.

Rapidly evolving molecular biology and genetics tools such as stem cell differentiation strategies and single cell RNA sequencing (scRNAseq) have enabled important advances in disease research. While mouse models have provided many insights into development and disease, stem cell differentiation allows for studying these processes in a human system. Stem cell derived retinal organoids have become an

important human model to characterize retinal development and disease (22, 23, 36-51). Retinal organoids develop all major cell types of the retina and closely mimic *in vivo* retinal architecture, with an organized outer nuclear layer (ONL) of photoreceptors capable of responding to light stimuli (51). Many recent studies have used retinal organoids to describe both retinal development and disease, providing important complementary insights to mouse models. In addition to 3D organoid models, 2D culture systems can provide important insights into how a specific cell population develops. Stem cell derived OPCs are an attractive model for studying oligodendrocyte development and myelination, as OPCs are not abundant *in vivo* and there are distinct differences in murine vs human OPCs development (52, 53). While murine OPCs are fated to form oligodendrocytes, human OPCs are not restricted to solely oligodendrocyte fates, thus human models can provide important insights not possible in mouse models (52, 53). In addition to stem cell strategies, scRNAseq has become an invaluable tool to investigate retinal biology. Recent studies have utilized scRNAseq to characterize retinal development in murine retinas, human retinal organoids, primate retinas, and human fetal and adult retinas (37, 44, 46, 50, 54-60). The combinatorial use of stem cell differentiation strategies and scRNAseq provides a model to investigate human development and disease at high resolution and identify critical transcriptomic alterations in a population-specific manner, thus providing an attractive system for retinal disease research.

In this study, scRNAseq and stem cell differentiation strategies were used to investigate three critical aspects of retinal health. First, I analyzed the transcriptomic alterations resulting from loss of NRL in patient derived retinal organoids to characterize photoreceptor development in ESCS. In the absence of NRL, rods development does not occur, and instead the retinal organoids have a higher abundance of S opsin+ photoreceptors. However, these photoreceptors fall into two discrete populations, one

population more representative of typical S cones and the other being rod-cone intermediates, or "cods." The cod population exhibited high S opsin expression, but lack of substantial rod or cone gene expression profiles and a great degree of differential gene expression when compared to both rods and cones. In addition to the cod population, we identified MEF2C as a candidate regulator of cone development or maturation due to its RNA and protein expression pattern. Second, I generated stem cell lines harboring CRB1 or RPGRIP1 null alleles to model a time course of LCA in retinal organoids with the goal of identifying common degenerative pathways that could be therapeutically targeted. Both models exhibited distinct histological aberrations, the RPGRIP1 KO photoreceptors incapable of outer segment disc morphogenesis and CRB1 KO mature rhodopsin expressing rods mislocalized within the RCVRN+ ONL. Despite exhibiting different histological changes, both KO's induced DDIT3 and the endoplasmic reticulum (ER) stress pathway. While the onset and duration of ER stress varied across the two KO's, possibly resulting from the different temporal expression patterns of CRB1 and RPGRIP1, this represented a common degenerative pathway that may provide targets for therapeutic intervention for LCA and other photoreceptor degenerations involving ER stress. Finally, we characterized development of stem cell derived OPCs into either astrocytes and oligodendrocytes. By analyzing the developmental trajectory reconstructed from 3 time points, we identified possible transcription factors and microRNAs important for regulating this cell fate decision. This study also verified that, unlike the mouse, human OPCs have the potential to form either astrocytes or oligodendrocytes and this branch in cell fate can be recapitulated *in vitro*. Collectively, this work has created a more detailed picture of human retinal health and disease, taking into account both development and degeneration across various models.

Chapter 2: Photoreceptor development in a human model of NRL loss

Investigating cone photoreceptor development using patient-derived NRL null retinal organoids

This work has been published and is reprinted here with permission from Communications Biology.

Kallman, A., Capowski, E.E., Wang, J., Kaushik, A.M, Jansen, A.D, Edwards, K.L, Chen, L., Berlinicke, C.A, Phillips, M.J., Pierce, E.A, Qian, J., Wang, T-H., Gamm, D.M, Zack, D.J. Investigating cone photoreceptor development using patient-derived NRL null retinal organoids. Commun Biol 3, 82 (2020). https://doi.org/10.1038/s42003-020-0808-5

Abstract

Photoreceptor loss is a leading cause of blindness, but mechanisms underlying photoreceptor degeneration are not well understood. Treatment strategies would benefit from improved understanding of gene-expression patterns directing photoreceptor development, as many genes are implicated in both development and degeneration. Neural retina leucine zipper (NRL) is critical for rod photoreceptor genesis and degeneration, with *NRL* mutations known to cause enhanced S-cone syndrome and retinitis pigmentosa. While murine Nrl loss has been characterized, studies of human NRL can identify important insights for human retinal development and disease. We utilized iPSC organoid models of retinal development to molecularly define developmental alterations in a human model of NRL loss. Consistent with the function of NRL in rod fate specification, human retinal organoids lacking NRL develop S-opsin dominant photoreceptor populations. We report generation of two distinct S-opsin

expressing populations in NRL null retinal organoids and identify *MEF2C* as a candidate regulator of cone development.

Introduction

Normal visual function requires light detection by photoreceptors followed by signal transduction through the neural retina to the brain. Mammalian retinas contain rod and cone photoreceptors, with rods responsible for dim-light and peripheral vision and cones for color, high acuity, and central vision. Rods and cones arise from a common precursor, and photoreceptor cell fate is dictated by key transcription factors (61). Neural retina leucine zipper (NRL) is required for rod development, and it activates Nuclear Receptor Subfamily 2 Group E Member 3 (NR2E3), which suppresses expression of cone-specific genes, promoting the rod developmental program (13). Previous murine studies have shown that Nrl loss leads to development of cone dominant retinas; specifically, an increase in S-cones (17).

Like the murine phenotype, loss of NRL in humans can cause enhanced S-cone syndrome, a rare retinal disease characterized by supranormal blue cone function due to an increased proportion of S-cones and night blindness due to the absence of rods (11, 12). However, the range of clinical phenotypes caused by *NRL* mutations is broad, with dominant missense mutations leading to a clinical picture more akin to retinitis pigmentosa (11, 12, 62). Similarly, enhanced S-cone syndrome can result from mutations in genes other than *NRL*, usually *NR2E3*. Using an induced pluripotent stem cell (iPSC) line derived from a patient carrying a homozygous *NRL* mutation, we sought to characterize the developmental and molecular effects of NRL loss in human stem cell-derived retinal organoids. Retinal organoids, which closely mirror *in vivo* retinal development, provide a human model for studying retinal development and degeneration (36, 40, 42, 45, 49, 51, 63-70). Organoids closely mimic retinal structure and apical-

basal polarity, with an outer layer of photoreceptors capable of ribbon synapse formation and inner layers of retinal ganglion, amacrine, horizontal, and bipolar cells.

In addition to histological characterization of human retinal organoids, transcriptomics, particularly at the single-cell level, can identify and characterize distinct cell populations. Dropseq, a single-cell RNA sequencing (scRNAseq) method utilizing microfluidics and barcoded beads to capture the transcriptomes of single cells, has proven powerful for characterizing mouse retinas and identifying subtypes of mouse bipolar cells (57, 59). More recently, scRNAseq studies with developing and adult retinal tissue have offered insight into *in vivo* human retinal cell populations (55, 56, 60). While previous studies have utilized scRNAseq to identify cell types of developing retinal organoids, they have not discerned distinct photoreceptor sub-populations (37, 44, 46). Additionally, while transcriptomics have been used to characterize Nrl loss in murine photoreceptors, these analyses were not performed at a single-cell level, thus limiting the potential to identify and characterize sub-populations (16, 71, 72).

Here, we present histological and single-cell transcriptomic characterization of human iPSC-derived retinal organoids with and without functional NRL (73). We show that retinal organoids lacking NRL develop S-opsin+ dominant photoreceptor populations. In contrast to previous studies, we provide evidence that, in the absence of NRL, two distinct populations of S-opsin expressing photoreceptors emerge; one population more representative of typical cones, and the other of rod/cone intermediates. Finally, our analyses identified a putative novel regulator of cone photoreceptor development. This study further defines photoreceptor subpopulations in a human model of NRL loss and provides a platform for characterizing aberrant photoreceptor development.

Methods

Generation of iPSC lines:

Tissue samples were obtained with written informed consent in adherence with the Declaration of Helsinki and with approval from institutional review boards at the University of Wisconsin-Madison and Massachusetts Eye and Ear Infirmary. The patient received clinical ophthalmic care from Dr. Eric Pierce in the ophthalmology clinic at the Children's Hospital of Philadelphia. The patient was recruited by Dr. Pierce to participate in research on the genetics of inherited retinal diseases. Participation involved consenting to collection of both blood and tissue samples. Informed consent was obtained from all donors of cells and tissues. A fibroblast biopsy from patient OGI-019-047 was reprogrammed via Sendai virus delivery of *OCT3/4, KLF4, SOX2* and *cMYC* by the Waisman Center iPSC core (University of Wisconsin-Madison) (73). The patient mutation (*NRL* c.233dup(C),p.(L75Pfs19X)) was confirmed in iPSCs and organoids by PCR amplifying a 770 nt genomic region surrounding the duplication with F-5'-TCCCTGCTCCTGGTTC-3' and R-5'-CACCATCCCTCTGGCTTTCC-3' followed by Sanger sequencing (University of Wisconsin Biotech Center, Madison, WI) with the F primer. Karyotype analysis was performed on iPSCs by WiCell (Madison, WI).

Cell lines and retinal differentiation:

Three independent clones were used for all experiments and compared to three WT lines: WA09 (WiCell), 1013 and 1581 (36). All plasticware and reagents unless otherwise stated, were from ThermoFisher. All hPSCs were maintained on Matrigel in either mTeSR1 (WiCell) or StemFlex and passaged with either Versene or ReLeSR (STEMCELL Technologies). Retinal differentiation has been described (36). Briefly, embryoid bodies (EB) were lifted with either 2 mg/ml dispase or ReLeSR and weaned

into Neural Induction Media (NIM: DMEM:F12 1:1, 1% N2 supplement, 1x MEM nonessential amino acids (MEM NEAA), 1x GlutaMAX and 2 mg/ml heparin (Sigma)) over the course of 4 days. On day 6 (d6), 1.5 nM BMP4 (R&D Systems) was added to fresh NIM and on d7, EBs were plated on Matrigel at a density of 200 EBs per well of a 6-well plate. Half the media was replaced with fresh NIM on d9, d12 and d15 to gradually dilute the BMP4 and on d16, the media was changed to Retinal Differentiation Media (RDM: DMEM:F12 3:1, 2% B27 supplement, MEM NEAA, 1X antibiotic, anti-mycotic and 1x GlutaMAX). On d25-30, optic vesicle-like structures were manually dissected and maintained as free floating organoids in poly HEMA (Sigma)-coated flasks with twice weekly feeding of 3D-RDM (RDM + 5% FBS (WiCell), 100 uM taurine (Sigma) and 1:1000 chemically defined lipid supplement) to which 1 uM all-trans retinoic acid (Sigma) was added until d100. Live cultures were imaged on a Nikon Ts2-FL equipped with a DS-fi3 camera or on a Nikon Ts100 equipped with a qImaging CE CCD camera.

Immunocytochemistry and transmission electron microscopy:

Human prenatal eyes were obtained from the Laboratory of Developmental Biology (University of Washington-Seattle). Tissue collection methods adhered to Institutional Review Board requirements, NIH guidelines and the Helsinki declaration. Organoids were fixed in 4% paraformaldehyde at room temperature for 40 min, cryopreserved in 15% sucrose followed by equilibration in 30% sucrose, and sectioned on a cryostat. Slides were blocked for 1 hr at RT in 10% normal donkey serum, 5% BSA, 1% fish gelatin and 0.5% Triton then incubated overnight at 4°C with primary antibodies diluted in block. Supplementary Table 2 lists primary antibodies, dilutions and sources. Slides were incubated with species-specific fluorophore-conjugated secondary antibodies diluted 1:500 in block, for 30 minutes in the dark at RT (Alexa Fluor 488, AF546 and AF647). For co-visualization of ML and S opsin, the rabbit α-ML opsin

antibody (Millipore) was directly conjugated to AF555 using the Apex Alexa Fluor 555 labeling kit (ThermoFisher) according to manufacturer's instructions, mixed with unlabeled rabbit α-S opsin (Millipore) and detected with an anti-rabbit AF488 secondary. Sections were imaged on a Nikon A1R-HD laser scanning confocal microscope. Cone and rod counts were performed on at least 6 random images from at least 3 different organoids from each of the 3 WT lines and each of the 3 L75Pfs clones using Nikon Elements D annotations and measurements module. *P*-values were calculated with an unpaired two-tailed Student's *t*-test (Mann-Whitney test) using Graph-Pad Prism 6.

Organoids were fixed for TEM in 3% glutaraldehyde and 1% paraformaldehyde in 0.08M sodium cacodylate buffer (all from Electron Microscopy Sciences) overnight with gentle rocking at 4°C, washed with 0.1M cacodylate buffer and post-fixed in 1% Osmium Tetroxide for 2 hrs at RT. The organoids were dehydrated in a graded ethanol series, further dehydrated in propylene oxide and embedded in Epon epoxy resin. Ultra-thin sections were cut with a Leica EM UC6 Ultramicrotome and collected on pioloform-coated 1 hole slot grids (Ted Pella, Inc.). Sections were contrasted with Reynolds lead citrate and 8% uranyl acetate in 50% EtOH and imaged on a Philips CM120 electron microscope equipped with an AMT BioSprint side-mounted digital camera and AMT Capture Engine software.

RT-qPCR:

Stage 2/3 organoids from two differentiations each from three WT and 3 L75Pfs clones were collected at d160 (when PRs were starting to mature) and RNA was extracted using the RNAeasy mini spin kit (Qiagen) according to manufacturer's instructions, including the optional DNAse step. 1 ug of RNA was reverse transcribed using the iScript cDNA synthesis kit (BioRad), diluted 1:10 and qPCR was performed

with SSO Advanced Sybr Green Master mix (BioRad) on a StepOne Plus qPCR machine (ABI). A list of primers can be found in Supplementary Table 3. ΔC(q)s were calculated from the geometric mean of two housekeeping genes and variability for all six lines was visualized by subtracting the ΔC(q) for each differentiation from the avg ΔC(q) for all six WT samples. $2^{-\Delta\Delta C(q)}$ were plotted and *P*-values were calculated using an unpaired two-tailed Student's *t*-test (Mann-Whitney test) using Graph-Pad Prism 6.

Lentiviral rescue:

Full length human NRL coding sequence was PCR-amplified from human adult neuroretina cDNA using F-5'-ATGGCCCTGCCCCCCAGC-3' and R-5'-TCAGAGGAAGAGGTGGGAGGGGTC-3' with a BamHI site added 5' and a SalI site added 3' to facilitate cloning into the pSIN-WP-mpgk lentiviral shuttle vector (74). Lentivirus was produced via transfection of HEK293T cells, concentrated 40-fold by ultracentrifugation and titered on hiPSCs to calculate a working titer (75). D90, early stage 2 organoids were infected every 3 days 3 times with effective titer to give >70% infection of iPSCs, by adding virus to the media. Control pgkGFP virus infection was monitored by live fluorescence. Organoids were maintained in culture for 100 days to allow sufficient time for RHO expression, whereupon they were fixed and processed for ICC as described above. The pgkNRL infection was repeated 4 times- once with each clone except for clone 7 which was infected twice.

Single cell dissociation and sample preparation:

At d100, cell lines used were 1013 and 1581 for WT and L75Pfs clones 9 and 11. D170 organoids were 1013 for WT and clones 7 and 9 for L75Pfs. Organoids were dissociated to single cells with papain (Worthington) to 1 mg/ml and 5 uL DNase (Roche) per mL, using 200 uL papain mix per organoid. After 1-2 hours when organoids

appeared fully dissociated the reaction was quenched with media containing 10% FBS (Gibco). Single cells were resuspended in HBSS (Gibco) and 0.1 mg/mL BSA at 120,000 cells per mL. Single cell capture was performed using a home-made Dropseq setup according to the published Dropseq protocol (57)[21]. Cells were combined in oil (Biorad) and barcoded beads (Chemgenes) in ~1 nL droplets. Droplets were broken using 6x SSC and perfluorooctanol (Sigma) to collect beads. Reverse transcription was performed using Maxima reverse transcriptase (Thermo Fisher Scientific) and cDNA was amplified using Kapa (Roche). cDNA was quantified using a Bioanalyzer DNA High Sensitivity Chip (Agilent). cDNA was fragmented and libraries were created using the Nextera XT library prep kit (Illumina). Libraries with quantified by Qubit dsDNA HS (Thermo Fisher Scientific) and sequenced via Illumina HiSeq 2500.

Bioinformatics:

Fastq files were processed according to the published Dropseq analysis pipeline and aligned to GRCh38 to extract expression matrices. Canonical component analysis, t-distributed stochastic neighbor embedding, and clustering was performed using the Seurat R package (version 2) (76). To remove low quality cells, cells with less than 200 genes or greater than 20% (d170) or 15% (d100) mitochondrial RNA content were filtered out. Genes expressed in a minimum of 2 cells were included for downstream analysis. The union of the top 2000 highly variable genes of WT and L75Pfs were used for canonical component analysis and 20 (d170) and 17 (d100) canonical components and were used to align subspaces and cluster cells. Cell populations were identified using previously published marker genes (Supplementary Table 1) and differential gene expression analysis was performed within each cluster to identify genes that varied by genotype. Differential expression analysis within each population between WT and L75Pfs cells was performed using a Wilcoxon rank sum test. Bonferroni corrected p-

values were calculated using the number of genes expressed at each time point (23645 for d100 and 25622 for d170). Cell populations at each age were compared to published fetal retinal cell populations and adult peripheral versus foveal populations (55, 60). For each population, the average expression of each gene expressed in both datasets was input for correlation analysis. Spearman correlation tests were performed for each cell population against its corresponding fetal and adult populations. Photoreceptor clusters of d100 and d170 were subsetted out for analysis using the Monocle R package (version 2) (77). A semi-supervised differential gene expression test was used on WT cells to identify genes that varied by age and cell type (NR2E3=rod, ARR3=cone, neither=undifferentiated photoreceptor). The top 780 non ribosomal or mitochondrial genes were used for ordering and trajectory reconstruction for both the WT trajectory and combined trajectory. Differential gene expression analysis was performed on the node in the WT trajectory to identify genes with rod/cone branch dependent expression. Similar analyses were performed on published adult photoreceptors (60). Peripheral and foveal photoreceptors combined, and rod/cone designations were retained for the analysis. A differential gene expression test was performed to identify genes differentially expressed across cell types, and genes with q values < 0.00001 (602 genes) were used for trajectory reconstruction. Additional differential gene expression tests were performed on subsets of the merged trajectory to characterize L75Pfs photoreceptors compared to WT rods and cones. All differential gene expression analysis in Monocle was performed using a likelihood ratio test on the 14,657 genes expressed in a minimum of 10 cells and a Bonferroni corrected p-value. To analyze possible regulation by MEF2C, human retinal ATAC-seq data was queried for genes with MEF2C binding sites (78). The resulting gene list (475 genes with MEF2C binding sites) was compared against genes expressed in at least 10 cells of the photoreceptor dataset (14,657 genes) and against genes differentially expressed (791 genes) between the WT

cones and L75Pfs rod-like cells. The percentage of expressed genes and differentially expressed genes with MEF2C binding sites were compared against the expected percentages using a two-tailed Student's T test. To estimate expected frequency in expressed genes, 14,657 genes were randomly chosen from all 28,040 human genes and the number of genes with MEF2C binding sites was determined and this process was repeated for 1000 iterations. This process was repeated for differentially expressed genes, randomly choosing 791 genes of the 14,657 expressed genes to determine the expected frequency of differentially expressed genes with MEF2C binding sites.

Results

Differentiation of patient and control retinal organoids

Fibroblasts from a patient with a homozygous null mutation, a frame shift and premature stop (c.223dupC, p.L75Pfs*19) in the *NRL* gene, were reprogrammed to hiPSCs (73). Three independent, karyotypically normal L75Pfs clones (Supplementary Fig. 1) were compared with WA09 and two wildtype (WT) hiPSC lines (1013 and 1581) (36). All lines were indistinguishable in their ability to make stage 1 organoids, characterized by a phase bright, neuroepithelial appearance and the presence of ganglion cells and proliferative retinal progenitor cells (Supplementary Fig. 2) (36). CRX+/RCVN+ photoreceptor precursor production was comparable between early stage 2 WT and L75Pfs organoids, when photoreceptor subtype specification begins (Fig. 1; compare Fig. 1B, 1C, merge in 1E to 1G, 1L, 1Q, 1H, 1M, 1R, merges in 1J, 1O and 1T) (36). However, NRL+ rod photoreceptors were never detected in L75Pfs organoids (compare Fig. 1D to 1I, 1N and 1S). As photoreceptors matured and formed outer segments (the "hair-like" surface projections in Figure 2C and 2I), L75Pfs organoids showed a striking S-opsin dominant photoreceptor phenotype (Fig. 2) (36). Unlike WT organoids, which possess a single layer of ML-opsin+ cones and rare S-opsin+ cones

along the outermost aspect of the outer nuclear layer (ONL) (Fig. 2A), L75Pfs organoids contained S-opsin expressing cells throughout the ONL and in greater abundance than ML-opsin expressing cells (Fig. 2B; also compare Fig. 2E, 2G to Fig. 2K, 2M). Quantification of ARR3+ cones and NR2E3+ rods as a percent of total nuclei in the ONL (Fig. 2D-H and J-N) revealed a dramatic reduction in rods and an increase in cones in the L75Pfs ONL (Fig. 2O). Interestingly, while WT organoids had rare ARR3-/NR2E3- nuclei in the ONL, ~20% of the L75Pfs ONL nuclei expressed neither marker. Since ARR3 is normally expressed >60 days after cone progenitors are detected, these ARR3-/NR2E3- cells may represent rod progenitor-derived cells that either have not committed to a cone fate or do not yet express ARR3. We quantified the ML- or S-opsin expressing cells as a fraction of the total ARR3+ cells and detected a 38-fold shift in the ML:S-opsin cone ratio, from 19:1 in WT to 1:2 in L75Pfs organoids (Fig. 2P). Additional analyses of rod and cone gene expression by RT-qPCR revealed that rod developmental genes were downregulated in L75Pfs organoids relative to WT organoids, while S-opsin expression was significantly increased in the L75Pfs organoids (Fig. 2Q, $p<0.005$, Mann-Whitney test). Thus, in L75Pfs human retinal organoids, rods appeared shifted toward an S-cone fate, consistent with the *Nrl-/-* mouse phenotype (15, 17). Finally, we examined the inner nuclear layer (INL) of L75Pfs organoids and found it indistinguishable from WT organoids (Supplementary Fig. 3A-N), including comparable production of PKCα+ rod bipolar cells (consistent with the *Nrl-/-* mouse phenotype) (79). However, in contrast to the *Nrl-/-* mouse, L75Pfs organoids displayed an intact outer limiting membrane (OLM) with no increase in rosette formation compared to WT organoids (Supplementary Fig. 3O-Y) (17, 80).

Reintroduction of WT NRL restores rod formation

To confirm that the observed L75Pfs phenotypes were indeed due to lack of NRL, we introduced functional *NRL* to determine whether NRL expression could rescue the phenotype. We ectopically expressed WT *NRL* in d90 L75Pfs retinal organoids using a lentivirus expression cassette. Of note, d90 corresponds to the onset of NRL protein detection in WT organoids (36). After 100 additional days in culture, organoids transduced with virus containing either a control *GFP* expression cassette (without *NRL*) or a WT *NRL* expression cassette were examined by immunocytochemistry for NRL, rhodopsin (RHO), and S-opsin expression. Figure 3A-D shows co-expression of GFP in ARR3+ cones of control cassette-treated L75Pfs NRL organoids, which remained NRL-/RHO- and expressed S-opsin throughout the ONL (Fig. 3E-L), similar to untreated L75Pfs organoids. In contrast, WT *NRL* expression cassette-treated organoids showed NRL protein in patches of nuclei within the ONL (Fig. 3M-X). Furthermore, all cells with restored NRL expression did not express S-opsin (Fig. 3M-T). Additionally, rare RHO+ cells (Fig. 3Q and 3W), which were never observed in untreated or pgkGFP-transduced (Fig 3I-L) L75Pfs organoids, were observed and were uniformly negative for S-opsin (Fig. 3T) and ARR3 (Fig. 3X). Of note, the localization of RHO to outer segments in some lenti-pgkNRL transduced cells (Fig. 3W) is reminiscent of RHO immunostaining in WT organoids (Supplementary Figure 4A-D). Thus, restoring NRL protein expression to L75Pfs photoreceptor precursor cells restricted S-opsin expression and could promote, although at low efficiency, RHO expression.

scRNAseq to identify and analyze organoid cell types

After establishing that the observed L75Pfs phenotype was due to NRL loss, we sought to identify and transcriptomically analyze the cell populations in WT and L75Pfs retinal organoids. We performed scRNAseq via the Dropseq platform on WT and L75Pfs organoids differentiated to early (100-103 days) or late (170 days) stage 2 (36,

57). At the earlier time, 4 WT and 4 L75Pfs organoids yielded transcriptional profiles of 5,294 and 4,787 cells, respectively. Cells were clustered by t-distributed stochastic neighbor embedding (tSNE) using the Seurat R package (76). The even distribution of cells classified either by number of genes expressed or number of unique molecular identifiers (UMIs) throughout the clusters confirmed that these factors were not driving clustering (Supplementary Fig. 5). Rather, based on known marker genes (Supplementary Table 1, Supplementary Fig. 6), the clusters represent stereotypical retinal populations present in both WT and L75Pfs organoids (Fig. 4A). Both rod and cone photoreceptors were present, with almost all *NR2E3* expressing cells being WT (Fig. 4B). Spearman correlations were performed between WT cells of each population and published fetal and adult retinal scRNAseq datasets (Supplementary Fig. 7-8) (55, 60). This analysis revealed d100 organoids yielded amacrine, horizontal, and retinal ganglion cells more similar to fetal retinal populations. Rods most closely resembled adult peripheral rods, while cones and Müller glia more closely resembled adult foveal cells. Differential gene expression tests were performed between WT and L75Pfs cells of each cluster, and genes with significantly different expression and an average natural log fold change greater than 0.5 (~1.6 fold) are summarized in Supplementary Data 1. Of genes enriched in L75Pfs cells of the rod cluster, the presence of the cone transducin, *GNGT2,* indicates that this population is acquiring a cone-like profile.

At d170, 3 WT and 6 L75Pfs organoids yielded 8,920 and 15,447 single cell transcriptomes, respectively. Cell populations identified by marker gene expression (Supplementary Table 1) showed that mature retinal cells were captured, including bipolar cells and opsin-expressing photoreceptors (Fig. 4C, Supplementary Fig. 9). Loss of retinal ganglion cells was also observed. Possible explanations for retinal ganglion cell loss include microfluidic bias favoring other cell types or death of retinal ganglion cells due to the lack of vasculature in retinal organoids. Notably, age-dependent retinal

ganglion cell loss has been reported in retinal organoids (36). Again, Spearman correlations were performed between WT cells of each population and published fetal and adult retinal scRNAseq datasets (Supplementary Fig. 10-11) (55, 60). Like d100, organoids at d170 yielded amacrine and horizontal cells more similar to fetal cells. Rods and bipolar cells more closely resembled adult peripheral cells, and, similarly to d100, cones and Müller glia were more highly correlated with adult foveal cells. Two cone opsin-expressing populations were identified, one that expressed both ML-opsin and S-opsin and the other consisting of cells that primarily express S-opsin. Due to the identity of the M- and L-opsin 3' UTRs that were captured via our analysis, we could not distinguish between M- and L-opsin transcripts. Interestingly, 1.5% of WT cone opsin-expressing cells co-expressed both ML- and S-opsin (Fig. 4D). The number of UMIs and genes expressed by these cells suggests they are not doublets (Fig. 4E).

We performed differential gene expression analysis on these 3 cone opsin-expressing populations (ML-, ML/S-, or S- expressing) to identify novel markers of developing cone subtypes. As expected, there were only minimal differences in gene expression between the cone populations. We identified *MYL4* as a possible ML-cone marker and *CCDC136* and *DCT* as possible S-cone markers (Fig. 4F). *CCDC136* is preferentially expressed in mouse S- and S/M-cones and recently has been shown to be enriched in primate S-cones (58, 81). Interestingly, Peng et al. identified *MYH4*, the heavy chain complement to MYL4, as a transcript distinguishing ML-cones from S-cones (58). *NUP93, SLC12A6, PDRG1,* and *TRAPP2CL* were significantly enriched in the ML/S-cone population compared to the ML or S- expressing cell populations. Further studies are necessary to determine if this ML/S-co-expressing cone population exists *in vivo*.

To determine altered transcriptional profiles at d170, within each cell population we identified differentially expressed genes with an average natural log fold change

greater than 0.5 (~1.6-fold) between WT and L75Pfs cells (Supplementary Data 2). Within the rod cluster, WT cells had significantly higher expression of many rod-specific genes including *GNAT1, ROM1, SAMD7, NR2E3, CNGB1, GNB1,* and *PDE6G,* while cone-specific phosphodiesterase, *PDE6H* (Fig. 4G), was enriched in L75Pfs cells, suggesting a more cone-like character of these cells. Despite loss of NRL protein, the *NRL* transcript is still detectable in L75Pfs cells, possibly due to the presence of transcripts that have yet to be removed by nonsense mediated decay. Of differentially expressed genes in the S-opsin expressing population (Fig. 4H), L75Pfs S-opsin expressing photoreceptors were enriched for *OPN1SW* and *GNGT1*, a rod-enriched transducin (Fig. 4G). Despite enrichment of *MYL4* in WT compared to L75Pfs S-cones, this gene exhibited substantially higher expression in ML-cones compared to S-cones, supporting its designation as enriched in ML-cones (Fig. 4F). To identify whether NRL loss alters the distribution of photoreceptor subtypes, we compared expression of *OPN1SW, OPN1MW,* and *NR2E3* within each cell population of d170 WT and L75Pfs organoids, as well as total expression of these genes across both genotypes (Fig. 4I). *OPN1SW* was detected in more cells and more clusters in L75Pfs organoids compared to WT, while *OPN1MW* was primarily detected in only the cone cluster of both the WT and L75Pfs organoids. Since NRL activates *NR2E3* transcription, L75Pfs organoids had (as expected) lower expression of *NR2E3* and fewer *NR2E3* expressing cells compared to WT. Quantification of *OPN1SW, OPN1MW,* and *NR2E3* expression levels and percentage of expressing cells in d170 organoids can be found in Table 1. Although WT and L75Pfs organoids had significantly different relative numbers of cells expressing *OPN1SW* vs *OPN1MW,* on an individual cell basis the *OPN1SW* and *OPN1MW* expressing cells expressed comparable levels of *OPN1SW* and *OPN1MW*. However, for *NR2E3,* both the percentage of expressing cells and the expression level within individual expressing cells was significantly lower in L75Pfs cells. Taken together, this

data suggests that NRL loss has a profound effect on rod development, shifting them towards an S-cone identity.

Trajectory reconstruction of WT photoreceptor development

After identifying retinal populations, we used the 5,144 WT photoreceptors identified from both time points to create a pseudotemporal trajectory of WT photoreceptor development (77). While the population contained contaminating bipolar cell precursors (44/5,144 cells with *VSX1* or *VSX2* expression), this small population is unlikely to impact trajectory construction (we could have removed these cells, but felt that selectively removing small subpopulations of cells was more likely to produce an artifact than leaving them in). To determine the gene set for ordering the trajectory, we performed a semi-supervised differential gene expression test for genes varying by age and assigned cell type within the WT photoreceptor dataset. After removing mitochondrial and ribosomal genes, the top 780 genes by p-value were used for ordering (Supplementary Data 3). Importantly, neither *VSX1* nor *VSX2* were present in this list, verifying that the contaminating bipolar cells did not affect the trajectory reconstruction. The resulting WT trajectory had one node separating rod and cone photoreceptors, with *OPN1SW* or *OPN1MW* expressing cells in state 2 and *NR2E3/SAG* expressing cells in state 3 (Fig. 5A-D). 590 genes were significantly differentially expressed at this node and the top 100 non-ribosomal genes were used to create a heatmap of genes enriched along the rod versus cone branches (Supplementary Data 4, Fig. 5E). While many of these genes are known as rod- or cone-specific, we identified some novel cone- or rod-enriched genes. In addition to *MPP4* and *CC2D2A*, genes already shown to be enriched in human fetal cones, we identified *GNAI3, CA2, MAP4, MYL4, MCF2, KIF2A,* and *KIF21A* as cone-enriched, and *PTPRZ1, CABP5, IRX6, B2M,* and *PRUNE2* as rod-enriched (Supplementary Fig. 12) (50). We checked published adult human scRNAseq

data and confirmed significant enrichment of *MAP4, MYL4, MCF2,* and *KIF2A* in cones, and *CABP5* and *IRX6* in rods ($p<0.05$, one-sided T-test) (60). We performed similar trajectory analyses using adult photoreceptor data to compare the organoid trajectory to *in vivo* photoreceptors (Supplementary Fig. 13) (60). The resulting trajectory separated rods and cones, and the top 100 non-ribosomal differentially expressed genes between the state 1 rods and state 4 cones were used to create a heatmap for comparison to organoid development. 30 genes were differentially expressed in both datasets, with all but *MALAT1, TMSB10,* and *EEF1A1* exhibiting the same enrichment pattern. The expression patterns of known markers confirm that our trajectory accurately recapitulates photoreceptor development and validate its utility for analysis of perturbations occurring in NRL null photoreceptors.

Reconstruction of the combined WT and L75Pfs trajectory

After creating a WT trajectory that accurately represented photoreceptor development, we applied the same parameters to create a trajectory of 13,317 combined WT and L75Pfs photoreceptors to elucidate the shift in development resulting from the absence of NRL (Fig. 6A-D). Again, there were few contaminating bipolar cell precursors (254/13,317 cells with *VSX1* or *VSX2* expression) that likely did not affect trajectory reconstruction. The combined trajectory indicated 9 cell states, compared to 3 states of the WT-only trajectory. We sought to characterize these states by their gene expression and gene ontology (GO). After the start of pseudotime with state 1, the first node separated two populations of immature photoreceptors. To characterize the photoreceptors in state 9, we input genes enriched in this state to a GO tool (82). The enriched GO terms included various cell differentiation and cell stress processes (Supplementary Fig. 14). The remaining portions of the trajectory included developing photoreceptors (states 2, 3, and 4), and 4 branches corresponding to 2 rod and 2 cone

cell fates. States 2, 3, and 4 were defined as developing photoreceptors due to expression of *CRX, OTX2,* and *RCVRN* and absence of WT cells with substantial rod or cone gene expression patterns (Supplementary Fig. 15B-D). These states have some cells expressing *NRL* or *ARR3*, but the low numbers and level of expression, compared to the more clearly-defined rod and cone populations of states 5, 6, 7, and 8, suggests they are developing photoreceptors (Fig. 6E). Expression of *NR2E3* and *SAG* in WT cells identified states 7 and 8 as rod/rod-like cell fates and *OPN1MW* expression defined states 5 and 6 as cone fates. To differentiate between cone states 5 and 6, we utilized GO analysis on gene sets enriched in each fate (Supplementary Fig. 15E). State 5 cones were enriched for GO terms relating to electron transport chain and guanylate cyclase activity, whereas state 6 cones had enrichment for retinal development and photoreceptor differentiation terms, suggesting that state 6 cones may be less mature than the more metabolically active cones of state 5. Despite apparent differences in maturity and metabolism, cells in these states were combined into a single cone population for downstream analyses due to confidence in their identity as cone photoreceptors. We performed similar analyses on states 7 and 8 to distinguish between the two rod/rod-like populations (Supplementary Fig. 15F). While both populations were enriched for terms related to photoreceptor activity, state 8 cells appear to have stronger rod profiles due to enrichment in rhodopsin signaling terms. As with the cone states, cells of these two rod states were combined into one rod population for downstream analysis. This analysis identified the L75Pfs photoreceptor populations and their WT counterparts, thus allowing for further comparison of mature L75Pfs photoreceptor populations to WT rods and cones.

Characterization of L75Pfs S-opsin expressing cells

Because previous murine studies described Nrl-/- photoreceptors as possible "cods", we sought to determine if this would hold for human NRL null photoreceptors[3]. To better characterize the L75Pfs photoreceptors, we determined genes differentially expressed compared to WT cells in each photoreceptor subset. Comparison of genes enriched in either WT or L75Pfs cone states (combined states 5 and 6) revealed 184 genes, few of which were rod- or cone-specific genes (Supplementary Data 5). Importantly, nearly all cone-specific genes showed no significant differential expression between WT and L75Pfs cones (Fig. 6F). Exceptions included *ARR3, GRK7,* and *OPN1SW*, which were more highly expressed in L75Pfs cells, and *PDE6H*, which showed slight enrichment in WT cells. Lower *OPN1SW* expression in WT cones was expected as ML-cones are the dominant cone subtype in WT organoids (Fig. 2P). The low number of differentially expressed genes and comparable expression levels of most cone genes between WT and L75Pfs cones suggests that this population of L75Pfs cones is essentially normal.

To characterize L75Pfs photoreceptors in the rod/rod-like branches (states 7 and 8), we compared them to both WT rods and WT cones by performing differential gene expression analysis according to the schematic in Fig. 7A (L75Pfs rod-like red cells vs WT rod purple cells; L75Pfs rod-like red cells vs WT cone blue cells). L75Pfs photoreceptors of the rod-like states had high *OPN1SW* expression, while also exhibiting WT rod levels of *OPN1MW* expression and WT cone levels of *NR2E3/SAG* expression (Fig. 7B). In comparing L75Pfs and WT rods/rod-like cells, 397 genes were differentially expressed (Supplementary Data 6), with L75Pfs photoreceptors expressing significantly lower levels of the rod-specific genes *CNGB1, GNAT1, GNB1, GNGT1, NR2E3, NRL, PDE6G, ROM1,* and *SAG* than their WT counterparts (Fig. 7C). The expression levels of these rod genes in L75Pfs rod-like cells were comparable to their expression levels in WT cones (Supplementary Fig. 16A). The low expression of these genes compared to

WT rods is likely due to the loss of NRL. In comparing L75Pfs rod-like cells to WT cones, 791 genes were differentially expressed, including many cone-specific genes (Supplementary Data 7). Compared to WT cones, L75Pfs rod-like cells had significantly lower expression of *ARR3, CNGB3, GNAT2, GNB3, GNGT2, GUCA1C, PDE6C,* and *PDE6H* (Fig. 7D). Except for *ARR3* and *PDE6H*, all of these genes were expressed at comparable levels in L75Pfs rod-like cells and WT rods (Supplementary Fig. 16B). Interestingly, L75Pfs rod-like cells also had significantly higher expression of *GNGT1*, a rod transducin also associated with foveal cones (58). The high *OPN1SW* expression, rod levels of expression of cone genes, cone levels of expression of rod genes, and degree of differential gene expression compared to WT rods and cones suggests that L75Pfs rod-like cells are human analogs of "cods".

MEF2C as a candidate regulator of cone cell fate

Because the cod expression pattern is not completely consistent with either rods or cones, the presence of this population suggests that NRL is not the only transcription factor directing rod versus cone photoreceptor fate specification. We postulated that other transcription factor(s) with higher expression in cones than L75Pfs cods could play a previously unappreciated role in regulating cone development. We identified 75 transcription factors of the 791 genes differentially expressed between WT cones and L75Pfs cods, with *MEF2C* as a potential candidate due to its higher expression level in both WT and L75Pfs cones compared to L75Pfs cods and WT rods (Fig. 7E). Interestingly, MEF2C has been shown to act downstream of *Nrl* in mice; however, in our dataset *MEF2C* showed significant enrichment in cone photoreceptors, suggesting a potential difference between human and murine photoreceptor fate determination (83). To determine if *MEF2C* could be involved in human photoreceptor gene regulation, we queried human retinal ATAC-seq data for regions of open chromatin with MEF2C

binding sites (78). After identifying 475 genes with MEF2C binding sites, we tested for enrichment of MEF2C-regulated genes in our dataset. 375 genes (80%) were expressed in at least 10 cells in this photoreceptor dataset, a significant enrichment compared to the expected 50% for random genes (Fig. 7F). Furthermore, 34 genes (7.2%) were differentially expressed between L75Pfs cods and WT cone cells, a significant enrichment compared to 4.2% expected for random genes (Fig. 7G). This enrichment in expressed genes and differentially expressed genes suggests a possible role for MEF2C in photoreceptor development, and specifically rod versus cone cell fate specification. Consistent with our transcriptome data, MEF2C protein was detected exclusively in ARR3+ photoreceptors in both WT and L75Pfs retinal organoids at d160 (Fig. 7H, Supplementary Fig. 17A-J). MEF2C expression was also detected in d122 human fetal retina within a single cell layer adjacent to NR2E3+ developing rod nuclei, consistent with cone localization (Supplementary Fig. 17K-N). Strong MEF2C expression was also detected in peripheral adult monkey retina in infrequent cells next to NR2E3+ rod nuclei, also corresponding to cones (Supplementary Fig. 17O-R), and within a line of INL nuclei likely corresponding to Müller glia. Additionally, faint expression was detectable in rod nuclei (Supplementary Fig. 17Q). Furthermore, analysis of published adult human scRNAseq data confirmed enrichment of *MEF2C* expression in cones relative to rods ($p=0.04489$, one-sided T-test) (60). This protein localization profile, adult human photoreceptor expression analysis, and enrichment both in expressed genes and differentially expressed genes in our dataset suggests a possible role for *MEF2C* in human cone photoreceptor development or maturation.

Discussion

We have used an *in vitro* human stem cell-based system to investigate photoreceptor development in *NRL* null human retinal organoids. L75Pfs has been

identified as a null allele, and L75Pfs-derived retinal organoids have a phenotype similar to the phenotype of the *Nrl* null mouse (12, 15, 17). Rods were not detected by immunocytochemistry (Fig. 1 and 2) and the portion of the ONL typically populated by rods in WT organoids instead contained S-opsin+ photoreceptors. This perturbation of photoreceptor cell fate determination was accompanied by a dramatic shift in the ratio of S- to ML-opsin+ photoreceptors (Fig. 2). Additionally, we confirmed that this phenotype was due to lack of NRL by reintroducing functional *NRL* and demonstrating restriction of S-opsin expression and promotion of RHO expression in mutant photoreceptors (Fig. 3).

To better understand the identity of the photoreceptor populations that develop in the absence of NRL, we performed scRNAseq to characterize the cell populations of WT organoids compared to L75Pfs organoids. Previous studies have analyzed retinal organoid development using scRNAseq; however, the findings were limited by an inability to resolve cell clusters, the loss of INL cell populations, or incomplete characterization of photoreceptor populations (37, 44, 46). Using transcriptomics, our analyses verified that retinal organoids generate all major neuronal cell types present in *in vivo* retina (Fig. 4). Our findings also enabled comparison of the timeline of retinal organoid and *in vivo* fetal retinal development. Previous fetal retinal bulk RNAseq analysis characterized three "epochs" of retinal development, with photoreceptor development occurring during the third epoch (84). In comparing the timeline of retinal organoid development to that of the fetal retina, the organoids used in this study corresponded to this final epoch. Similar to *in vivo* retinal development, retinal organoids exhibit an early emergence of horizontal and amacrine cells, expression of cone-opsin prior to rhodopsin, and the later development of bipolar cells. Through our analyses we have generated a more comprehensive picture of the transcriptome of retinal organoids and provided a platform to further "stage" *in vitro* retinal organoid development compared to that of *in vivo* fetal retinas (36).

In addition to characterizing retinal organoid development in a WT system, we also provided a comprehensive picture of human photoreceptor development in the absence of NRL. Similar to a recent study characterizing cone photoreceptor development in human retinal organoids in the absence of the transcription factor THRB, we determined how loss of the rod transcription factor, NRL, affects rod and cone photoreceptor genesis (40). While Nrl loss has been studied extensively in mice, to our knowledge this work represents the first transcriptomic characterization of human NRL null photoreceptors, and demonstrates similarities and differences between murine and human retinal development (14-18). In both humans and mice, loss of NRL leads to development of an S-opsin+ photoreceptor dominant retina at the expense of rods. Murine Nrl null photoreceptors exhibited absent or decreased expression of *Rho, Gnat1, Nr2e3, Rom1, Rcvrn, Gnb1,* and *Cnga1*, consistent with our observations of decreased expression of these genes in human retinal organoids (17, 18). While *Sag* is expressed in murine Nrl null photoreceptors, albeit at lower levels, we detected no *SAG* expression in human NRL null photoreceptors (Fig. 6E). Human NRL null photoreceptors also exhibited substantial expression of the rod transducin *GNGT1,* which is not expressed in Nrl null mice. Consistent with upregulation of cone-specific genes in murine Nrl null photoreceptors, we also detected higher expression of *OPN1SW, GNAT2, GNGT2,* and *GNB3* in NRL null photoreceptors compared to WT. However, studies of Nrl null mice utilized population transcriptomics and thus only characterized the expression pattern of the average Nrl null photoreceptor (16). Through single cell analysis, we identified two distinct populations of NRL null photoreceptors, with one population bioinformatically indistinguishable from WT cones and the other representing a cod population with high *OPN1SW* expression but significantly lower expression of other rod- or cone- specific genes. This finding differs from previous studies that characterized Nrl null photoreceptors as “normal” S-cones (17, 18). Our model of two distinct *OPN1SW*

expressing populations is compatible with the phenotype of enhanced S-cone syndrome due to the preservation of cone function in concert with retinal degeneration (12). It is possible that preservation of S-cone function stems from the "normal" NRL null S-cone population, whereas the cod population may explain the degenerative phenotype. Of note, patients with enhanced S-cone syndrome lack normal retinal architecture, a phenotype not recapitulated in NRL null retinal organoids, and this disorganization may contribute to the degeneration observed *in vivo* (12).

In addition to characterizing photoreceptor populations, the availability of NRL null retinal organoids provided a platform for novel transcription factor discovery. Kim et al. (2016) combined transcriptomics and epigenetics in the context of Nrl null mice to identify candidate regulators of photoreceptor cell fate (16). We utilized a similar methodology to identify *MEF2C* as a candidate regulator of cone cell fate specification due to its higher expression in cones and enrichment of differentially expressed genes with MEF2C binding sites. Interestingly, *MEF2C* had been identified through analyses of Nrl null mice, but as a transcription factor involved in conferring rod identity (83). These opposing roles may be due to differences in human and murine retinal development, the existence of MEF2C splice variants, or the temporal expression pattern of *MEF2C* during retinogenesis, as Hao et al. (2011) detected *MEF2C* exclusively in mature murine retinas and not during development (83). In both developing organoids and fetal human retina, MEF2C was primarily detected in cones and remained cone-enriched in adult primate retina (Fig. 7H, Supplementary Fig. 17). While our immunocytochemical evidence of MEF2C enrichment in developing cones supports a possible role for MEF2C in cone development, further studies, such as cell type-specific gain- and loss-of function experiments, will be necessary to determine experimentally the possible role of *MEF2C* in cone cell fate specification and/or maturation.

Table 1: Percent of d170 cells expressing select rod and cone markers and level of expression[1] of these markers showing altered expression of *NR2E3* and *OPN1SW* in L75Pfs organoids.

Table 1

[1]Statistically significant differences are highlighted in yellow.

	% Cells expressing		Average (normalized) expression level within expression group		Average (normalized) total expression level	
	WT	L75Pfs	WT	L75Pfs	WT	L75Pfs
OPN1SW	0.796	8.021	3.648	3.793	0.029	0.304
OPN1MW	3.711	2.278	2.612	2.654	0.097	0.060
NR2E3	7.735	0.667	3.084	2.657	0.239	0.018

Figure 1: Photoreceptors from L75Pfs retinal organoids lack NRL protein expression. A-T) Confocal images of d100 (stage 2) organoids from a WT line **(A-E)** or 3 individual clonal lines of the L75Pfs mutant **(F-T)** showing photoreceptors immunostained for RCVN **(B, G, L, Q)**, CRX **(C, H, M, R)**, or NRL **(D, I, N, S). (A, F, K, and P:** nuclei (blue); **E, J, O** merge in **T).** Scale bars = 50 microns.

Figure 1

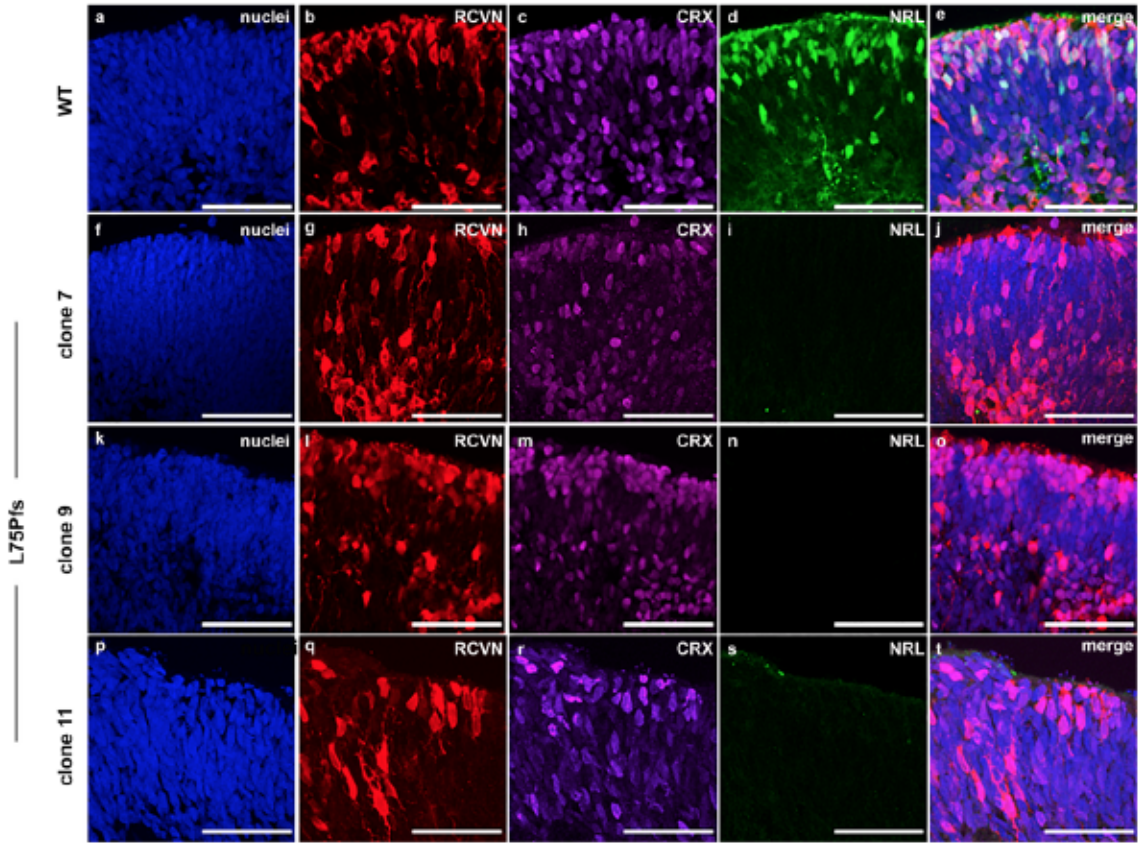

Figure 2: L75Pfs retinal organoids display an overabundance of S-opsin expressing cells at the expense of rods compared to WT organoids. **A-B)** Confocal images from stage 3 organoids (i.e., presence of photoreceptor outer segments) showing a single layer of cones with few S-cones (green) in WT organoids (**A**) versus an abundance of S-cones (green) distributed throughout the ONL in L75Pfs organoids (**B**). ML-cones are shown in orange. Scale bars = 25 microns. **C-N)** Photoreceptor characterization of WT and L75Pfs retinal organoids. Bright field (**C**, **I**) and confocal (**D-H** and **J-N**) images showing S-opsin+/ARR3+ cones (**K**, **L**) distributed throughout the ONL of L75P(fs) organoids that do not express the rod marker NR2E3 (**M**) (a transcription factor whose expression is controlled by NRL). This finding is in contrast to WT organoids that display ordered expression of cones (**E**, **F**) along the outermost ONL with a multicellular layer of NR2E3+ rod nuclei (**G**) internal to the cone layer, as well as an overall low number of S-opsin+ (**E**) cones. Scale bars: **C**, **I** = 250 microns; **D-H** and **J-N** = 25 microns. **O-P)** Quantification of photoreceptors in confocal images of stage 3 organoids from 3 WT lines and 3 L75Pfs clones. **O-P)** Quantification of photoreceptors in confocal images of stage 3 organoids from 3 WT lines and 3 L75Pfs clones. **O)** NR2E3+ rod and ARR3+ cone abundance as a percentage of total nuclei in the ONL: 15 images from 5 organoids per line or clone were counted. **P)** ML- and S-cone abundance as a percentage of total ARR3+ cones in the ONL: 11 WT images from 4 organoids per line and 15 L75Pfs images from 5 organoids per clone were counted. **Q)** RT-qPCR from stage 2-3 organoids showing a reduction in rod transcripts and an increase in S-opsin transcripts in L75Pfs organoids relative to WT organoids. $p < 0.005$, Mann-Whitney test.

Figure 2

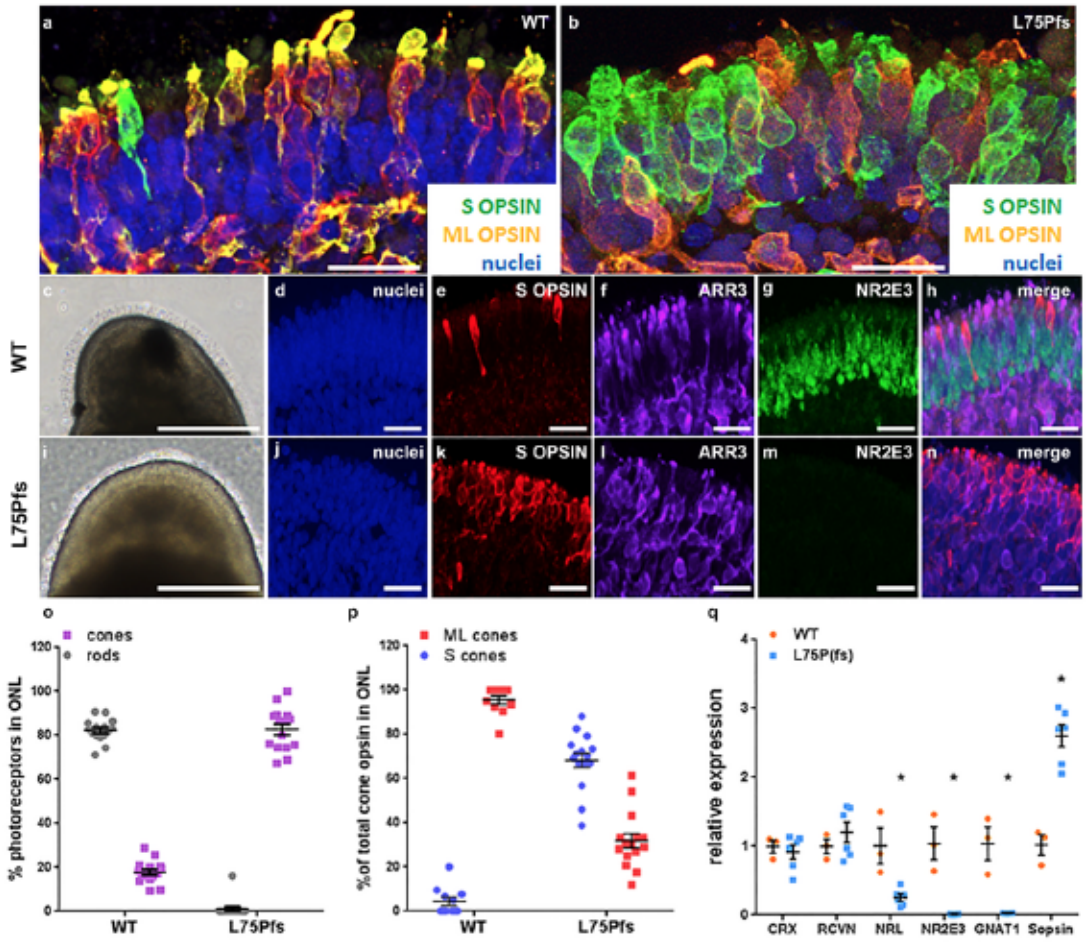
a
WT
b
L75Pfs
S OPSIN
ML OPSIN
nuclei
S OPSIN
ML OPSIN
nuclei
WT
L75Pfs
c
d
nuclei
e
S OPSIN
f
ARR3
g
NR2E3
h
merge
i
j
nuclei
k
S OPSIN
l
ARR3
m
NR2E3
n
merge
o
% photoreceptors in ONL
cones
rods
WT
L75Pfs
p
%of total cone opsin in ONL
ML cones
S cones
WT
L75Pfs
q
relative expression
WT
L75P(fs)
CRX
RCVN
NRL
NR2E3
GNAT1
Sopsin

Figure 3: RHO expression is found in L75Pfs organoids following viral transduction with an *NRL*-expression cassette. A-H) Confocal images from L75Pfs organoids transduced with a control lentivirus carrying a pgkGFP expression cassette. GFP (**C**) was found in ARR3+ (**B**) cones; NRL (**G**) was not detected, and S-opsin+ cones (**F**) were localized throughout the ONL and no RHO (**K**) expression was detected, as expected in the absence of ectopic WT NRL expression. **M-X)** Confocal images from L75Pfs organoids transduced with lentivirus carrying a pgkNRL expression cassette reveal patches of NRL expression within the ONL (**O** and **S**) and no NRL co-expression with S-opsin (**N** and **R;** merges in **P** and **T**). However, ectopically expressed NRL does co-express with RHO (**Q;** merge in **T**), a rod marker that was never present in control transduced L75Pfs organoids. In pgkNRL-transduced organoids, RHO (**W**) did not co-localize with the cone marker ARR3 (**V**; merge in **X**). Scale bars = 25 microns.

Figure 3

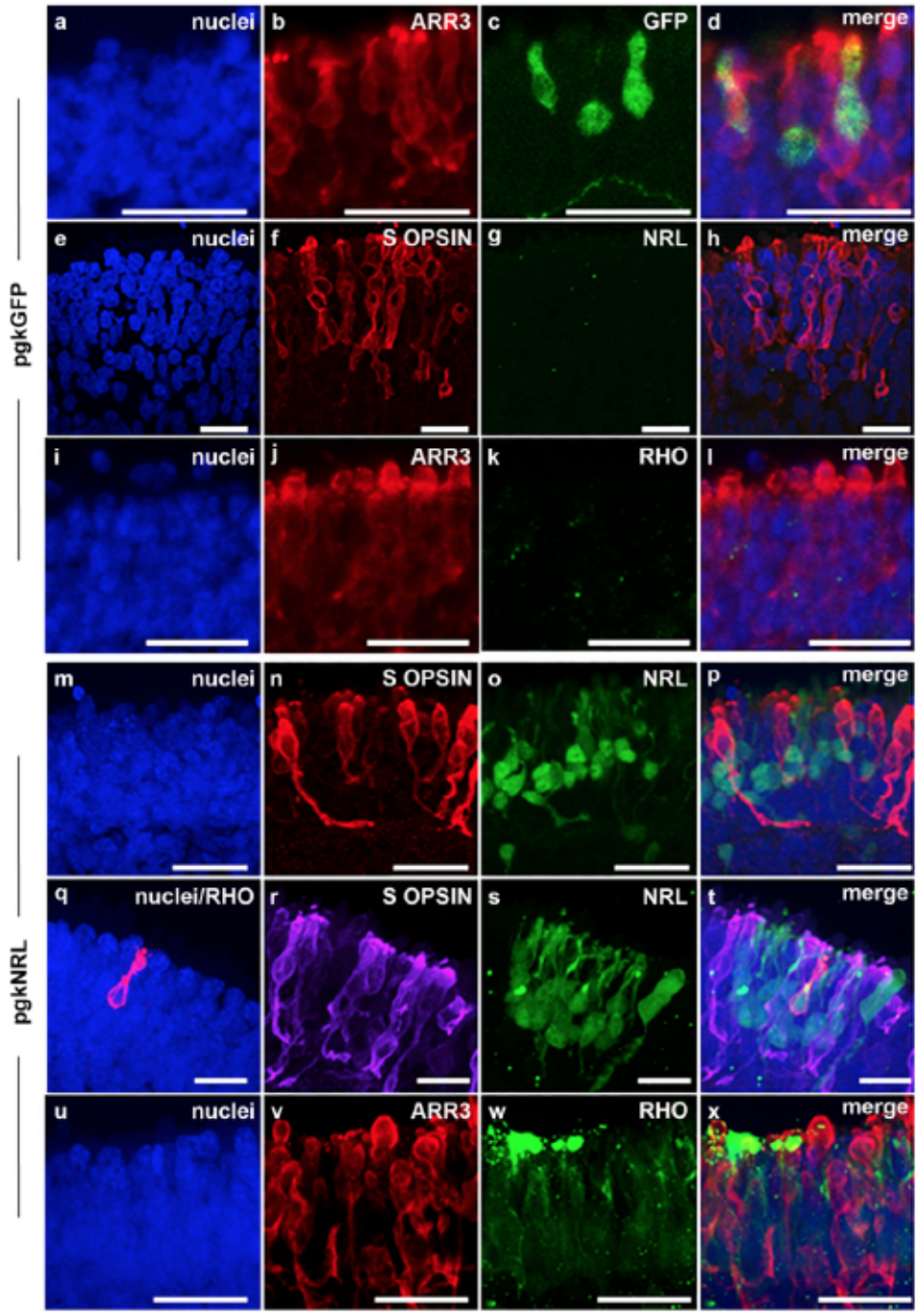
pgkGFP
pgkNRL
a nuclei
b ARR3
c GFP
d merge
e nuclei
f S OPSIN
g NRL
h merge
i nuclei
j ARR3
k RHO
l merge
m nuclei
n S OPSIN
o NRL
p merge
q nuclei/RHO
r S OPSIN
s NRL
t merge
u nuclei
v ARR3
w RHO
x merge

Figure 4: Identification and characterization of cell populations present in WT and L75Pfs retinal organoids by scRNAseq. A) tSNE plot showing cell populations present in all d100 organoids. **B)** Expression of *NR2E3* in WT (top) compared to L75Pfs (bottom) cells, showing that nearly all expression is in WT cells. **C)** tSNE plot showing cell populations present in all d170 organoids. **D)** Scatter plot of *OPN1SW* and *OPN1MW* expression at d170 indicating 6 co-expressing cells. **E)** Scatter plot showing the number of UMIs and genes expressed by the 6 co-expressing cells from D. **F)** Violin plots showing specific enrichment of novel cone marker genes across WT ML-cones, ML/S-cones, and S-cones. **G and H)** Heatmap of genes differentially expressed in d170 rod (**G**) and S-cone (**H**) clusters between WT and L75Pfs cells. **I)** Comparison of expression of *OPN1SW, OPN1MW,* and *NR2E3* by cell population of WT and L75Pfs organoids, and total expression of *OPN1SW, OPN1MW,* and *NR2E3* within all WT and L75Pfs cells.

Figure 4

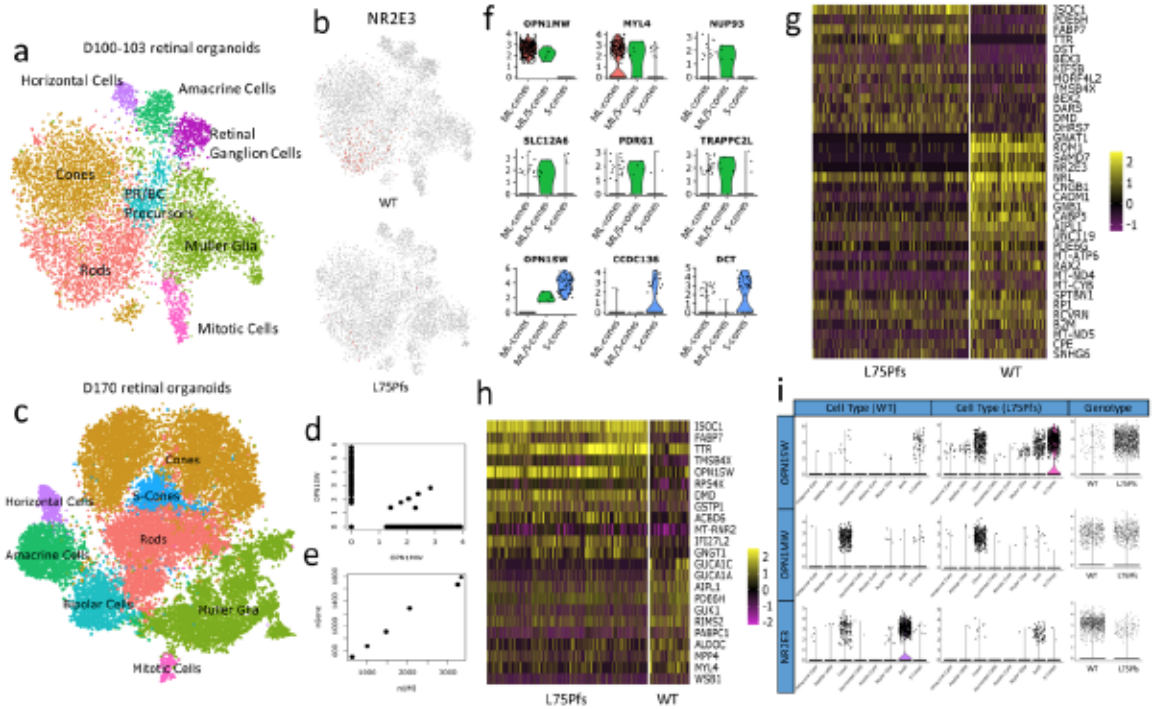

Figure 5: Reconstruction of a WT photoreceptor developmental trajectory. A-C) Trajectory of 5144 WT photoreceptors colored by state (**A**), pseudotime (**B**), and age (**C**). **D)** Expression of photoreceptor markers used to distinguish the identity of each branch of the trajectory. **E)** Heatmap of the top 100 non-ribosomal differentially expressed genes at the node separating rods and cones. Genes are hierarchically clustered into 4 clusters based on expression pattern. The center of the heatmap is the beginning of pseudotime, with cell maturity moving horizontally to the left (cones) and right (rods).

Figure 5

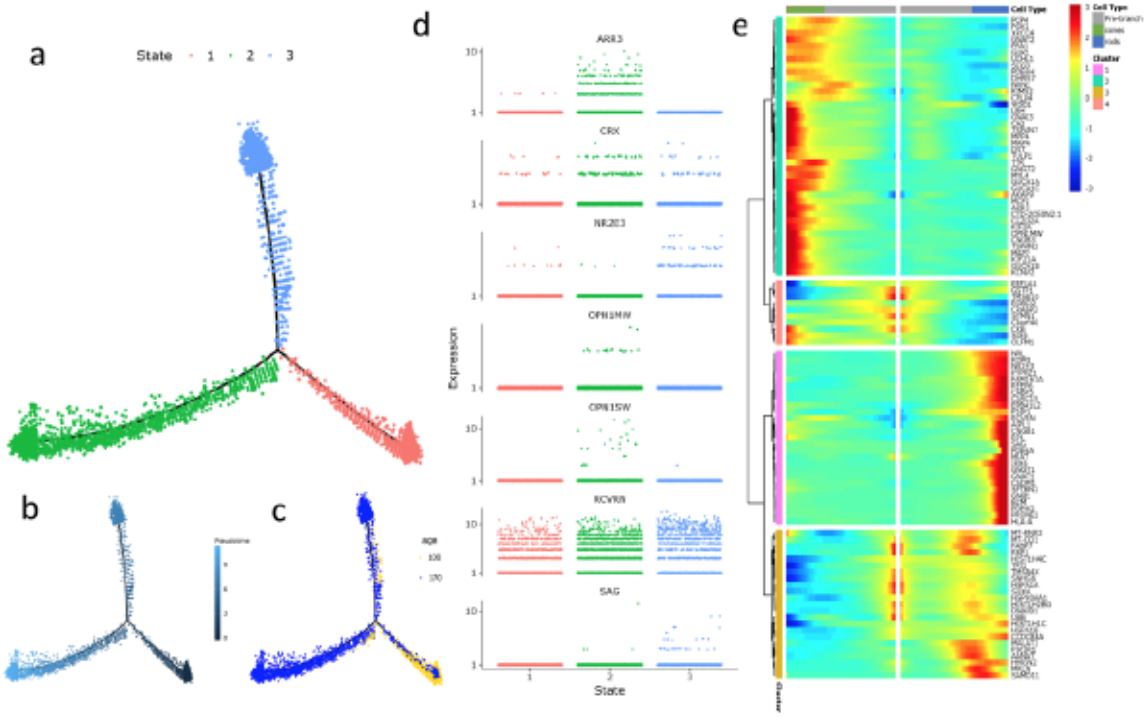

Figure 6: Combined analysis of WT and L75Pfs photoreceptor populations. A-D) Trajectory of combined WT and L75Pfs photoreceptors colored by state (**A**), genotype (**B**), pseudotime (**C**), or age (**D**). **E)** Expression of rod and cone marker genes by state, with L75Pfs cell populations on the left and WT cell populations on the right. WT expression of *NR2E3* and *SAG* was used to assign states 7 and 8 as rods, and expression of *OPN1MW* to assign states 5 and 6 as cones. **F)** Expression levels of cone markers in states 5 and 6 by genotype, with the position of the largest dot indicating the average level for each marker. All genes are expressed at comparable levels except *ARR3, GRK7, OPN1SW,* and *PDE6H.*

Figure 6

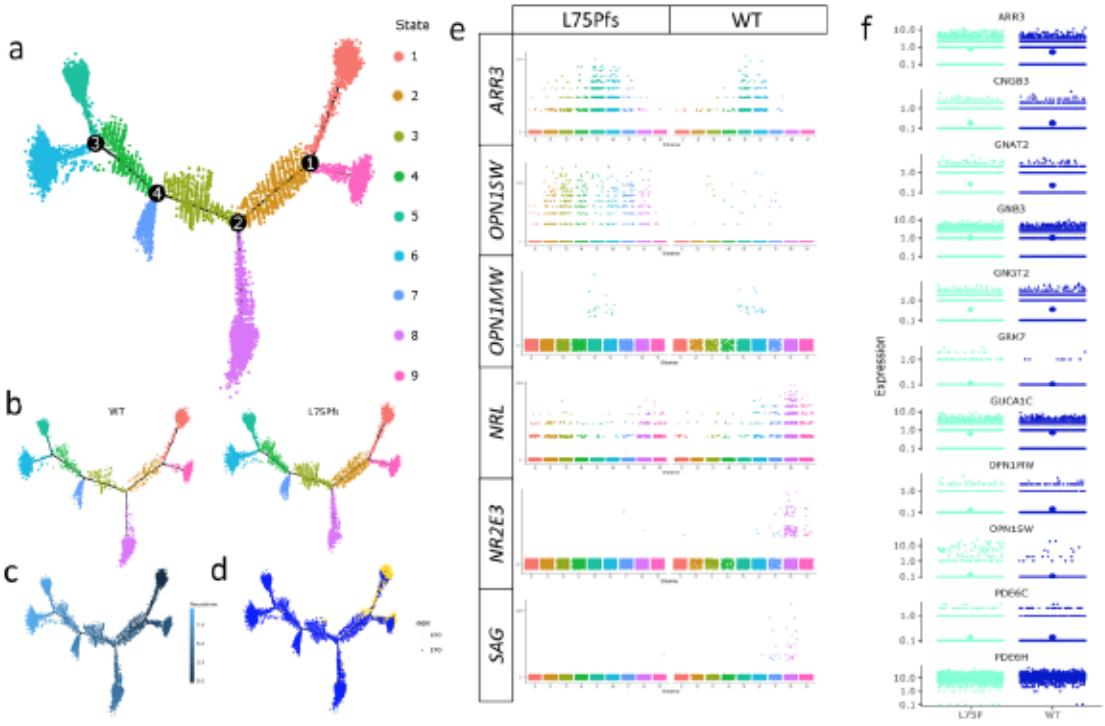

Figure 7: Comparative analysis of L75Pfs photoreceptors identifies 2 populations of S-opsin expressing photoreceptors, with one population having gene expression inconsistent with WT S-cones, and identification of MEF2C as a candidate regulator of cone cell fate specification. A) Plot depicting the differential expression analysis. Gene expression in the cells highlighted in red (L75Pfs rod-like cells) was separately compared to expression in the cells highlighted in blue (WT cones) and the cells highlighted in purple (WT rods). **B)** Expression levels of *NR2E3, OPN1MW, OPN1SW,* and *SAG* across the 3 cell groups (red, blue, and purple) used for differential analysis. **C-D)** Expression levels of rod- and cone-specific genes differentially expressed between L75Pfs rod-like cells and WT rods (**C**), or WT cones (**D**). The position of the largest dots indicate average gene expression levels for **B-D**. **E)** Expression level of *MEF2C* in cells in the cone states (5 and 6) on the left versus the rod states (7 and 8) on the right, with cells colored by genotype (black = L75Pfs, teal = WT). **F-G)** Percentage of *MEF2C* regulated genes expressed in a minimum of 10 cells (**F**) and differentially expressed between the red (L75Pfs rod-like cells) and blue (WT cones) groups (**G**) versus random genes. **H)** Confocal images demonstrating MEF2C (green) co-expression with ARR3 (purple) in cone photoreceptors of WT (left) and L75Pfs (right) organoids at d160. NR2E3+ nuclei (red) are present in WT but not in L75Pfs organoids. Scale bar = 10 microns.

Figure 7

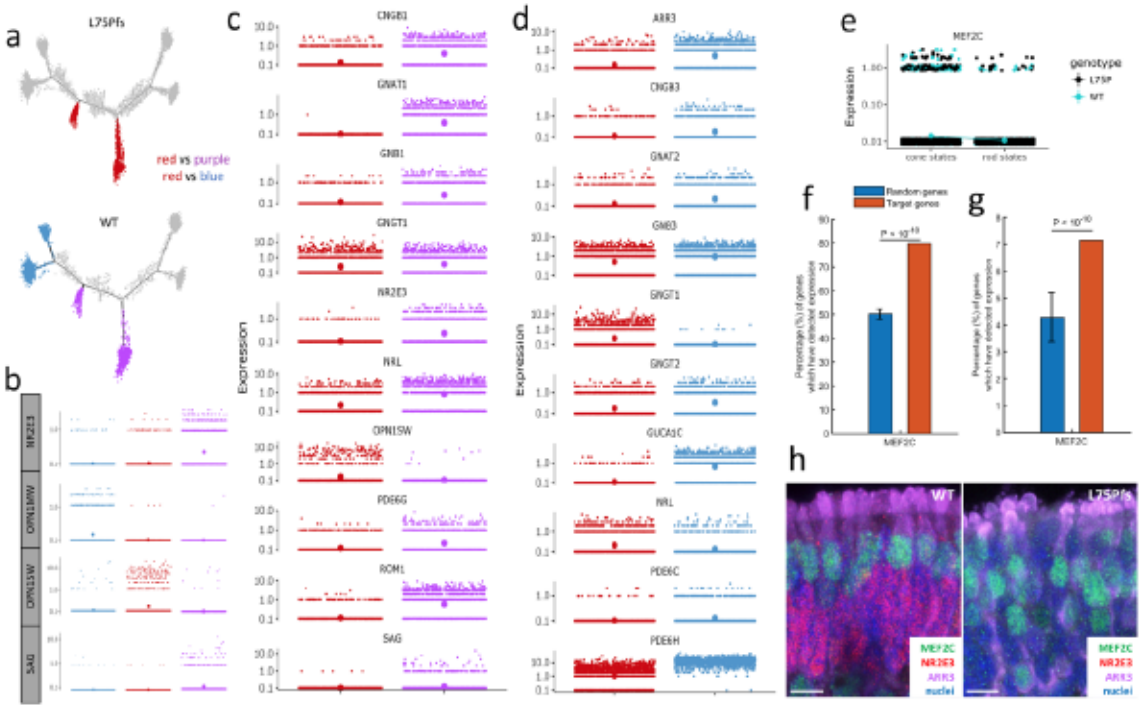
a
L75Pfs
red vs purple
red vs blue
WT
b
NR2E3
OPN1MW
OPN1SW
SAG
c
CNGB1
GNAT1
GNB1
GNGT1
NR2E3
NRL
OPN1SW
PDE6G
ROM1
SAG
Expression
d
ARR3
CNGB3
GNAT2
GNB3
GNGT1
GNGT2
GUCA1C
NRL
PDE6C
PDE6H
Expression
e
MEF2C
Expression
genotype
L75P
WT
cone states
rod states
f
Random genes
Target genes
MEF2C
g
MEF2C
h
WT
L75Pfs
MEF2C
NR2E3
ARR3
nuclei

Supplementary Materials

Supplementary Figure 1: Confirmation of normal karyotypes and the presence or absence of *NRL* mutations in the L75Pfs or WT iPSC lines, respectively. A-D) Normal karyotypes were confirmed for hPSCs from WT and 3 independent L75Pfs clones. **E-H)** Sequence of PCR amplicon surrounding *NRL* c.223 from WT iPSCs (**E**) and three L75Pfs clones (**F-H**) (c.233dupC outlined by dotted pink box). **I-W**) Bright field (**I, N, S**) and confocal (**J-M, O-R, T-W**) images of the three L75Pfs iPSC clones confirming the morphology and presence of pluripotency markers. Scale bars = 50 microns.

Figure 8

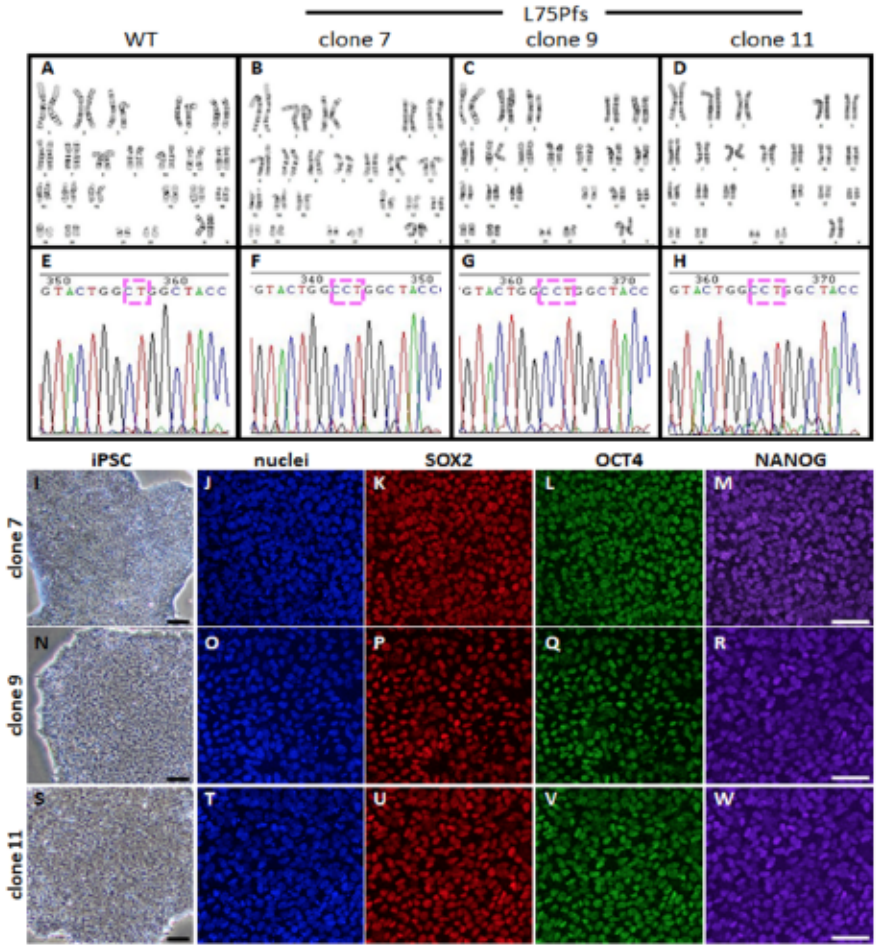

Supplementary Figure 2: All three L75Pfs hiPSC clones display normal early (stage 1) retinal organoid differentiation. Bright field and confocal images of stage 1 retinal organoids demonstrating normal bright field morphology (**A**, **G**, **M**, **S**), as well as the expected presence of proliferative Ki67+/VSX2+ (**C, D**, **I, J**, **O, P**, **U, V**) retinal progenitor cells, and SNCG+ (**E**, **K**, **Q**, **W**) retinal ganglion cells from WT (**A-F**) and L75Pfs organoids from 3 independent lines (**G-X**). Scale bars = 250 microns.

Figure 9

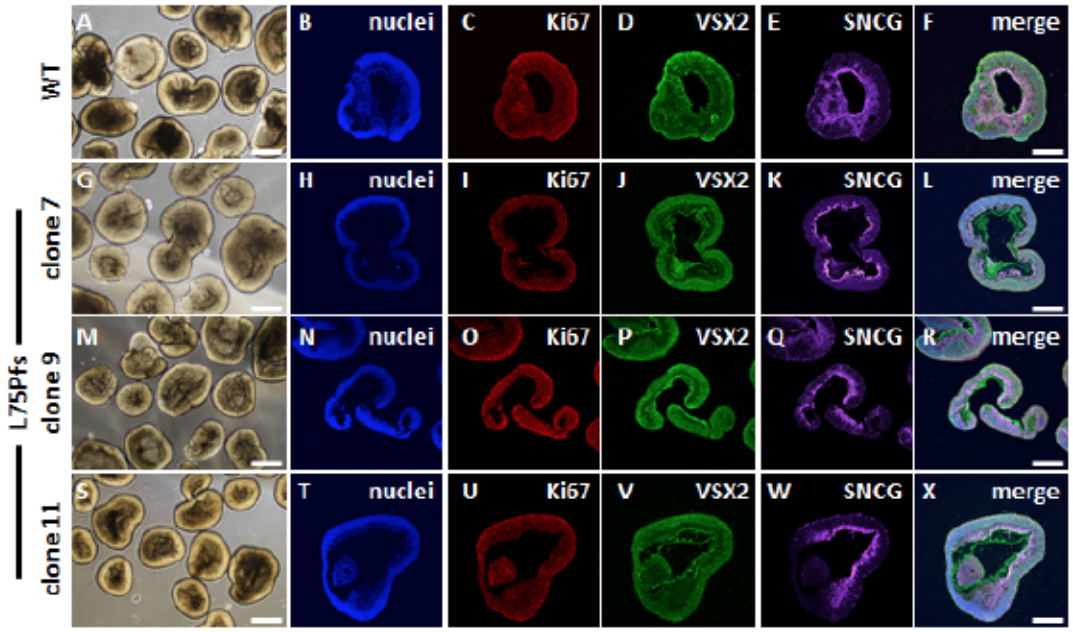

Supplementary Figure 3: The inner nuclear layer (INL), rod ON bipolar cells, and the outer limiting membrane (OLM) develop normally in L75Pfs retinal organoids. **A-J)** G0α ON bipolar cells (**B, G**) and the presynaptic marker VGLUT (**C, H**) are detected in the INL and outer plexiform-like region (respectively) of WT (**A-E**) and L75Pfs (**F-J**) retinal organoids. **K-N)** G0α+/PKCα+ rod ON bipolar cells (**G**, **H;** merge in **I**) differentiate along with G0α+/PKCα- cone ON bipolar cells in L75Pfs organoids despite the absence of NRL+ rods. **O-X)** F-actin (**Q, V**) and CRALBP+ Müller glia (**P, U**) form an intact OLM in WT (**O-S**) and L75Pfs (**T-X**) retinal organoids (also visualized in L75Pfs by TEM in panel **Y**). Scale bars **A-N** = 25 microns; **Y** = 2 microns

Figure 10

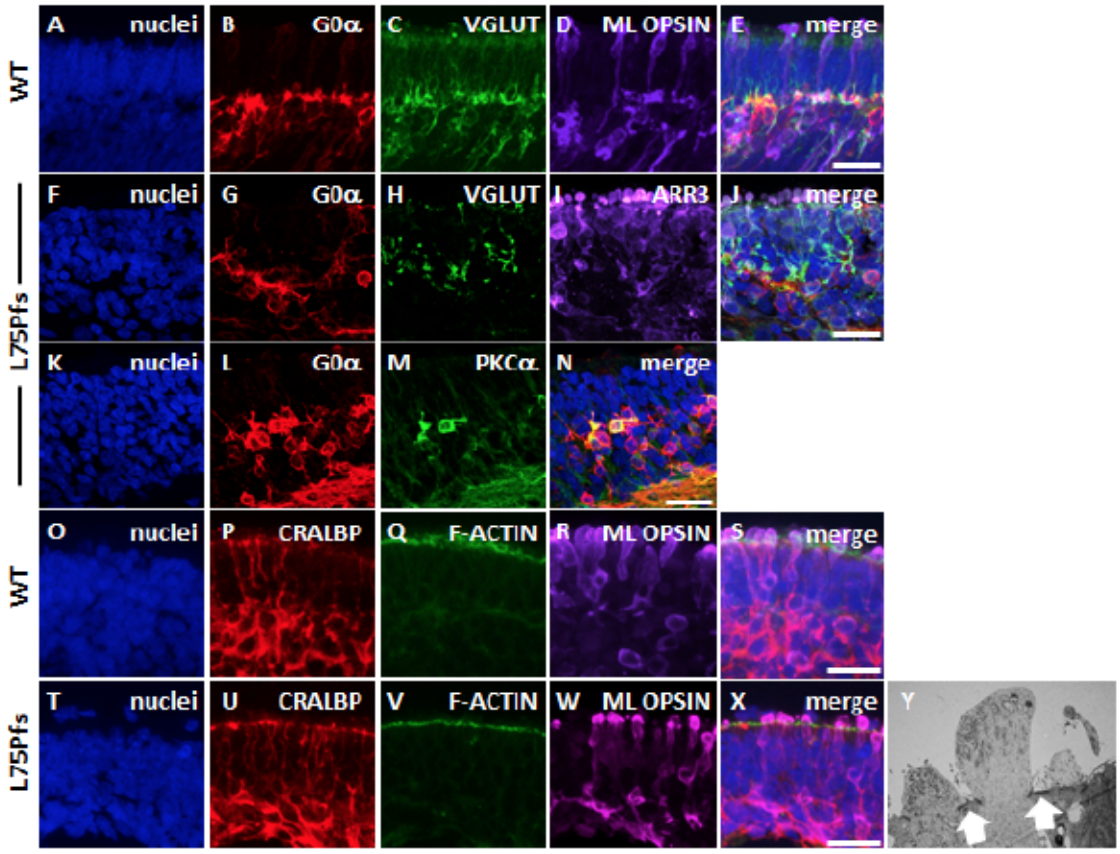

Supplementary Figure 4: Rods and cones in WT organoids at d240. Confocal images of ARR3 positive cones (**B**) and RHO positive rods (**C**, merge in **D**; DAPI-stained nuclei are shown in **A**) in a WT d240 stage 3 organoid for comparison to RHO protein expression seen in L75Pfs photoreceptors transduced with lenti-pgkNRL in Figure 3U-X. Scale bar = 25 microns.

Figure 11

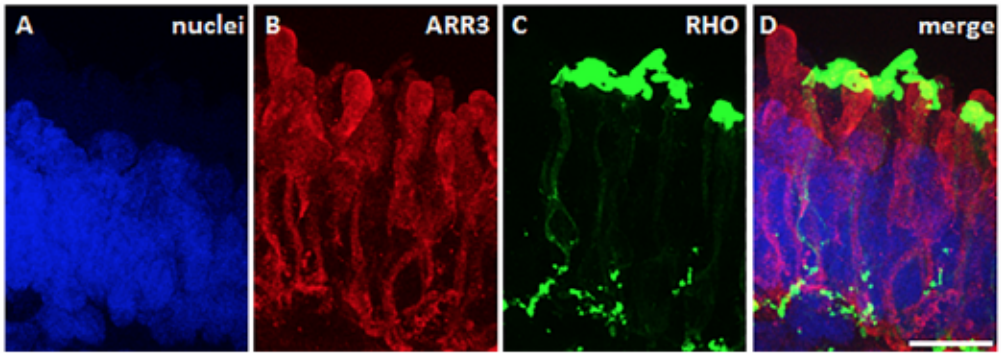

Supplementary Figure 5: UMIs and transcript number per cells mapped onto tSNE plots and pseudotime trajectories.

Figure 12

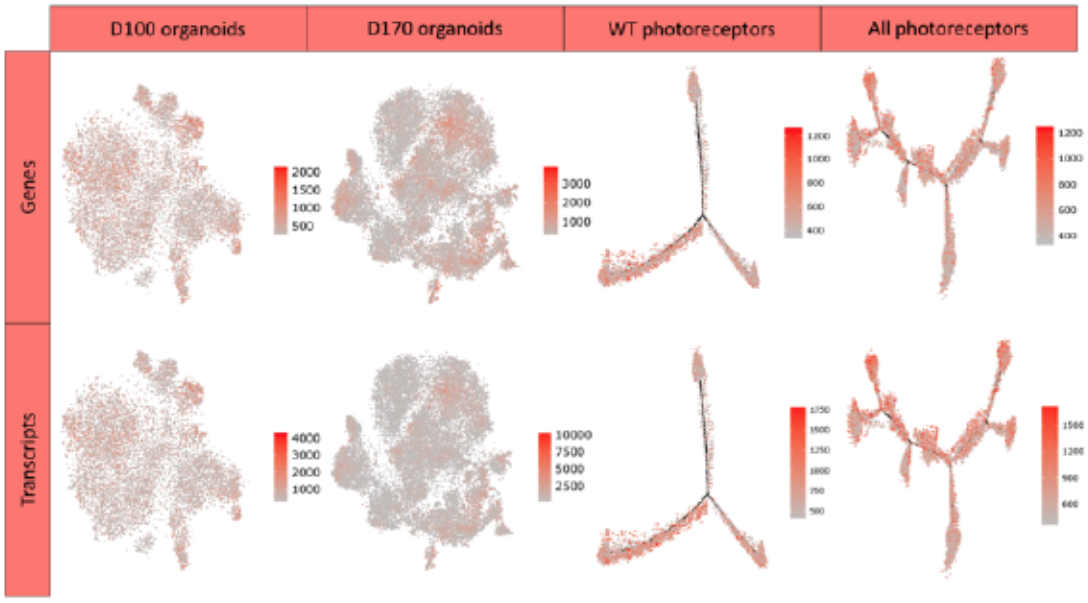

Supplementary Figure 6: Identification of d100 organoid cell populations by marker gene expression. A) tSNE plot showing cell populations present in all d100 organoids. **B)** tSNE plot from panel A showing only WT cells (left) or L75Pfs cells (right). **C-M)** Expression pattern of marker genes used to assign cluster identity

Figure 13

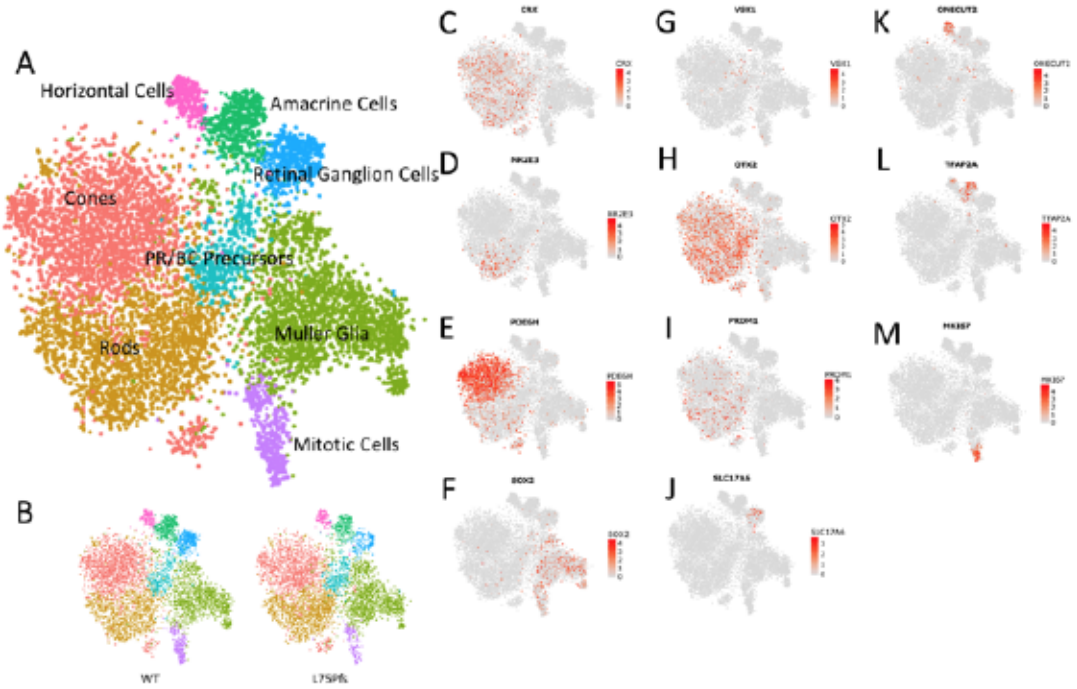

Supplementary Figure 7: Correlation of d100 retinal cell populations with fetal retina scRNAseq data. **A-F)** Scatter plots and spearman correlations of amacrine cells **(A)**, horizontal cells **(B)**, rods **(C)**, cones **(D)**, retinal ganglion cells **(E)**, and Müller glia **(F)**.

Figure 14

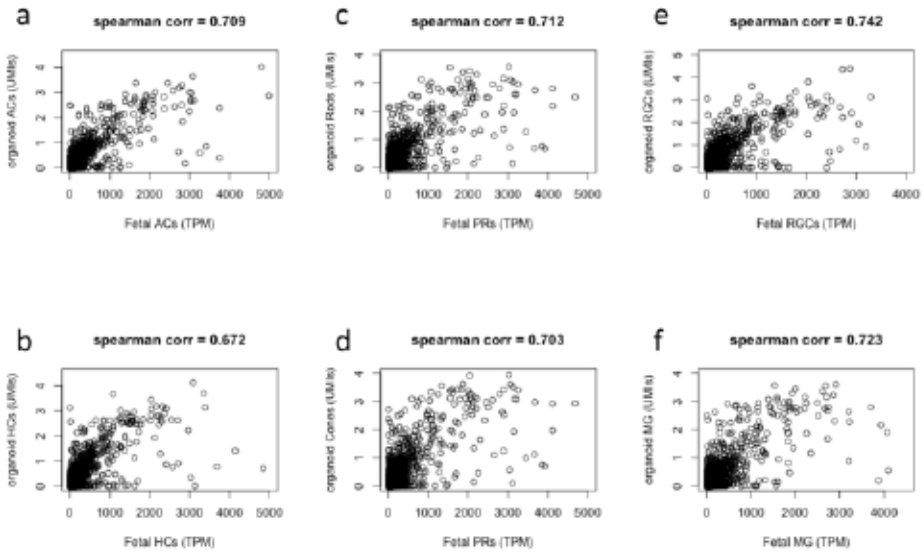

Supplementary Figure 8: Correlation of d100 retinal cell populations with adult peripheral and foveal retina scRNAseq data. **A-L)** Scatter plots and spearman correlations with peripheral **(A)** and foveal **(B)** amacrine cells, peripheral **(C)** and foveal **(D)** horizontal cells, peripheral **(E)** and foveal **(F)** rods, peripheral **(G)** and foveal **(H)** cones, peripheral **(I)** and foveal **(J)** retinal ganglion cells, and peripheral **(K)** and foveal Müller glia **(L)**.

Figure 15

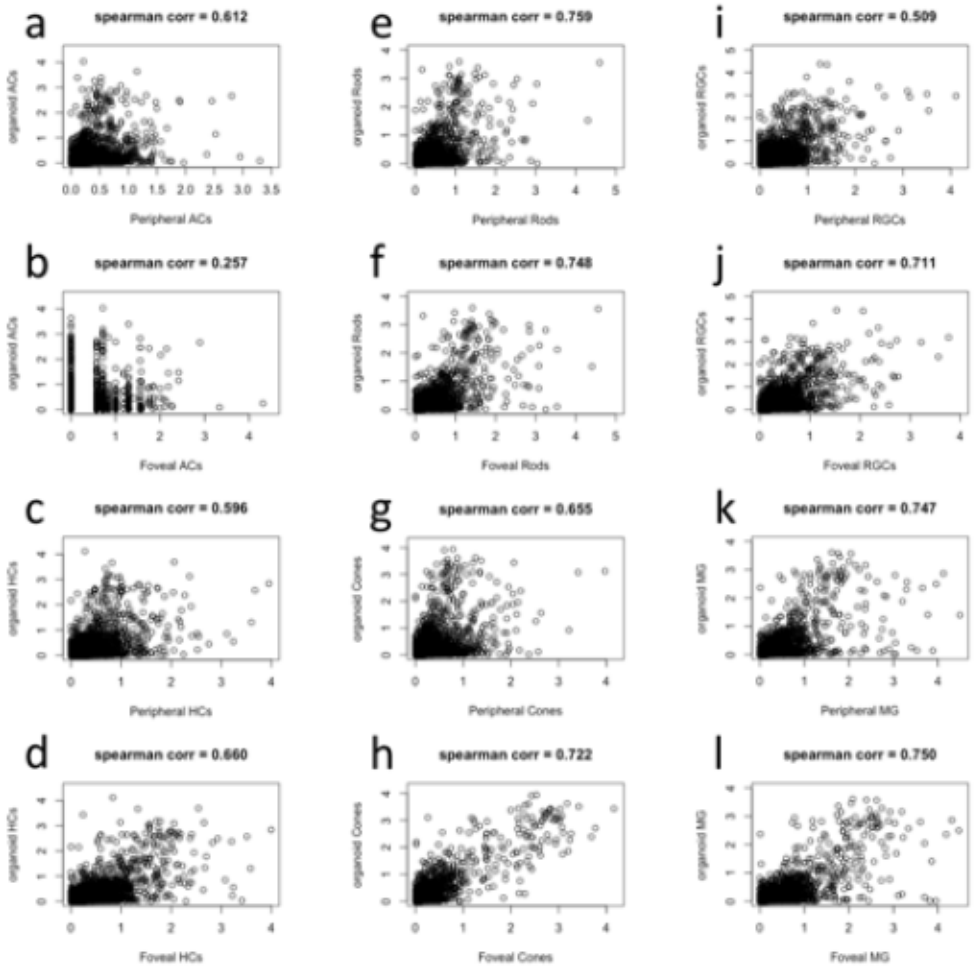

Supplementary Figure 9: Identification of d170 organoid cell populations by marker gene expression. A) tSNE plot showing cell populations present in all day 170 organoids. **B)** tSNE plot from panel A showing only WT cells (left) or L75Pfs cells (right). **C-K)** Expression patterns of marker genes used to assign cluster identity. For *NRL* expression **(F)**, only WT cells are shown.

Figure 16

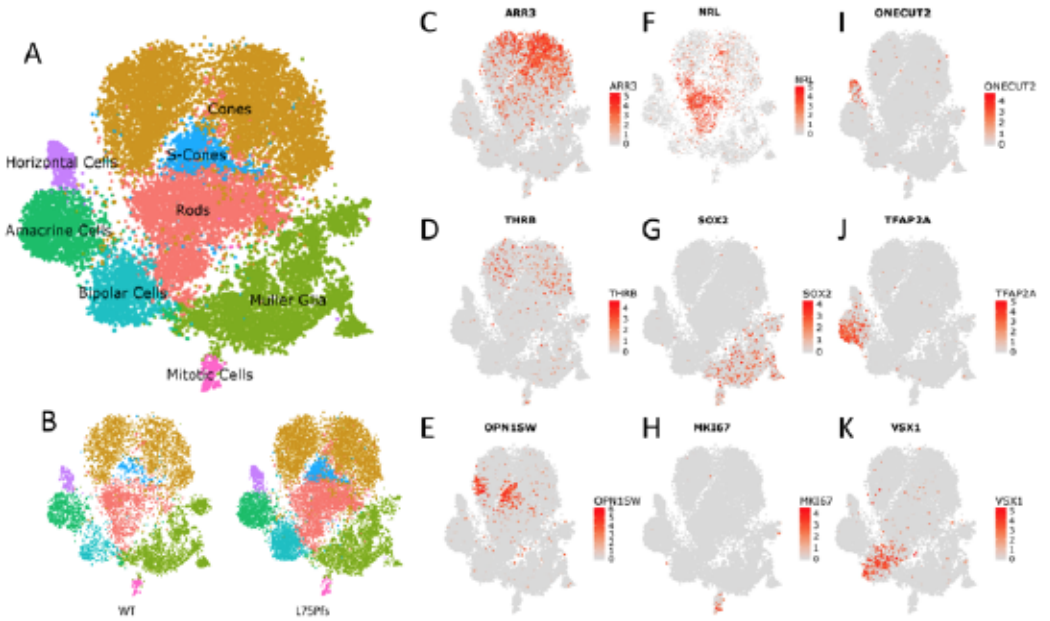

Supplementary Figure 10: Correlation of d170 retinal cell populations with fetal retina scRNAseq data. **A-G)** Scatter plots and Spearman correlations of amacrine cells **(A)**, horizontal cells **(B)**, bipolar cells **(C)**, rods **(D)**, cones **(E)**, S cones **(F)**, and Müller glia **(G)**.

Figure 17

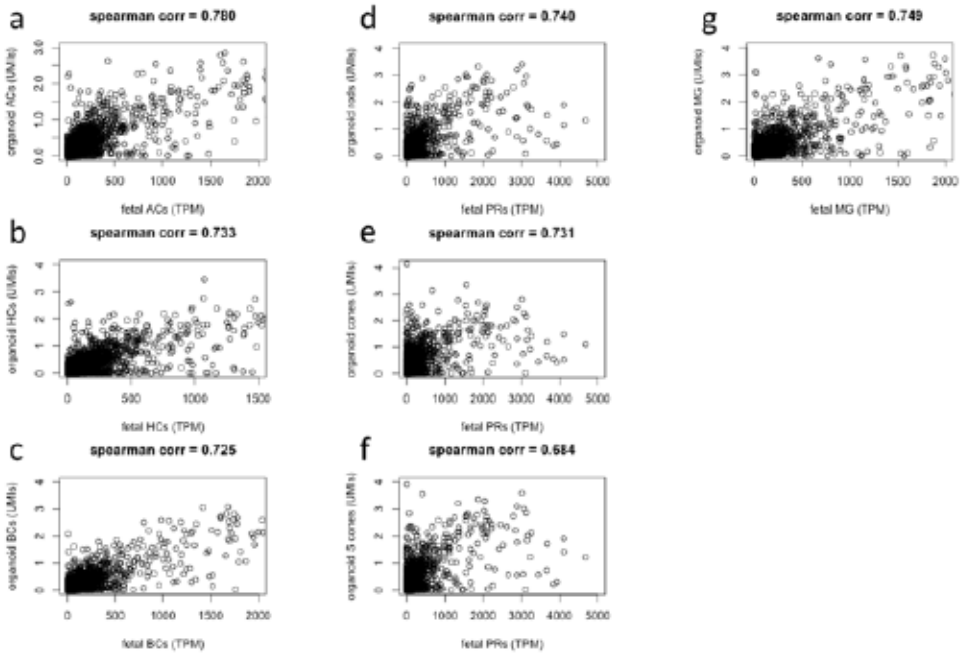

Supplementary Figure 11: Correlation of d170 retinal cell populations with adult peripheral and foveal retina scRNAseq data. **A-N)** Scatter plots and Spearman correlations with peripheral **(A)** and foveal **(B)** amacrine cells, peripheral **(C)** and foveal **(D)** horizontal cells, peripheral **(E)** and foveal **(F)** bipolar cells, peripheral **(G)** and foveal **(H)** rods, peripheral **(I)** and foveal **(J)** cones, S-cones with peripheral **(K)** and foveal **(L)** cones, and peripheral **(M)** and foveal Müller glia **(N)**.

Figure 18

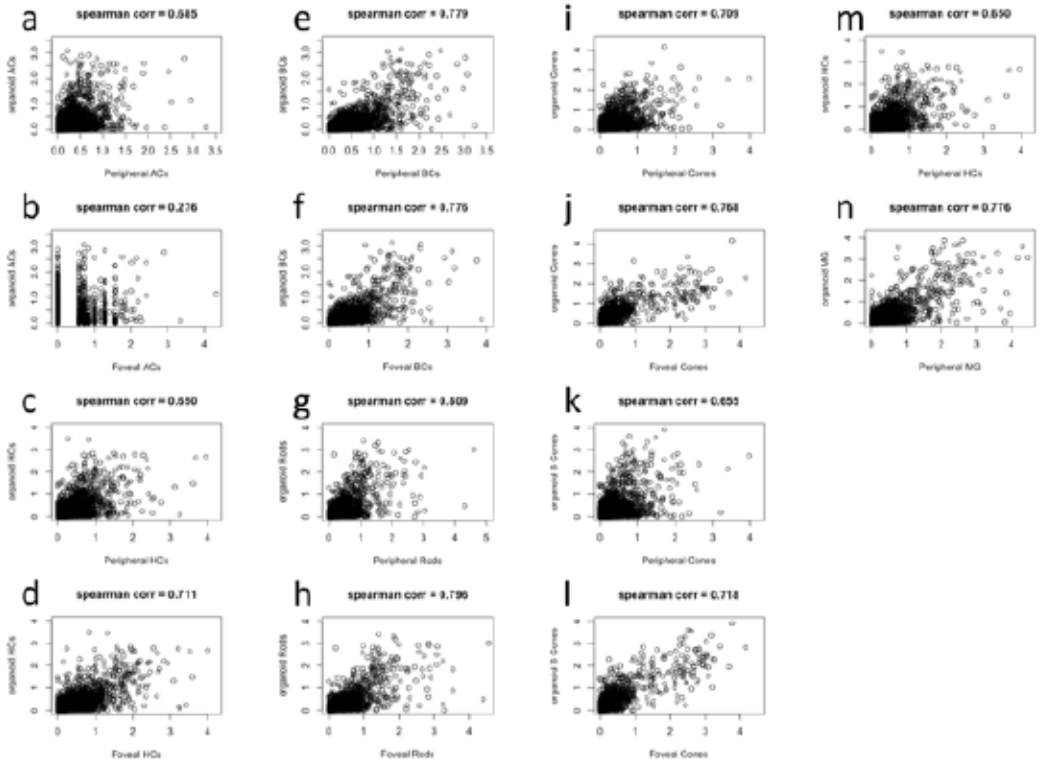

Supplementary Figure 12: Identification of novel rod- and cone-enriched genes from differential gene expression analysis at the node separating rods and cones. **A)** Trajectory of 5144 WT photoreceptors colored by state (state 2 = cones, state 3 = rods). **B-C)** Expression pattern of novel rod-enriched (**B**) and cone-enriched (**C**) genes, with the largest dot indicating average level of expression of each gene of interest.

Figure 19

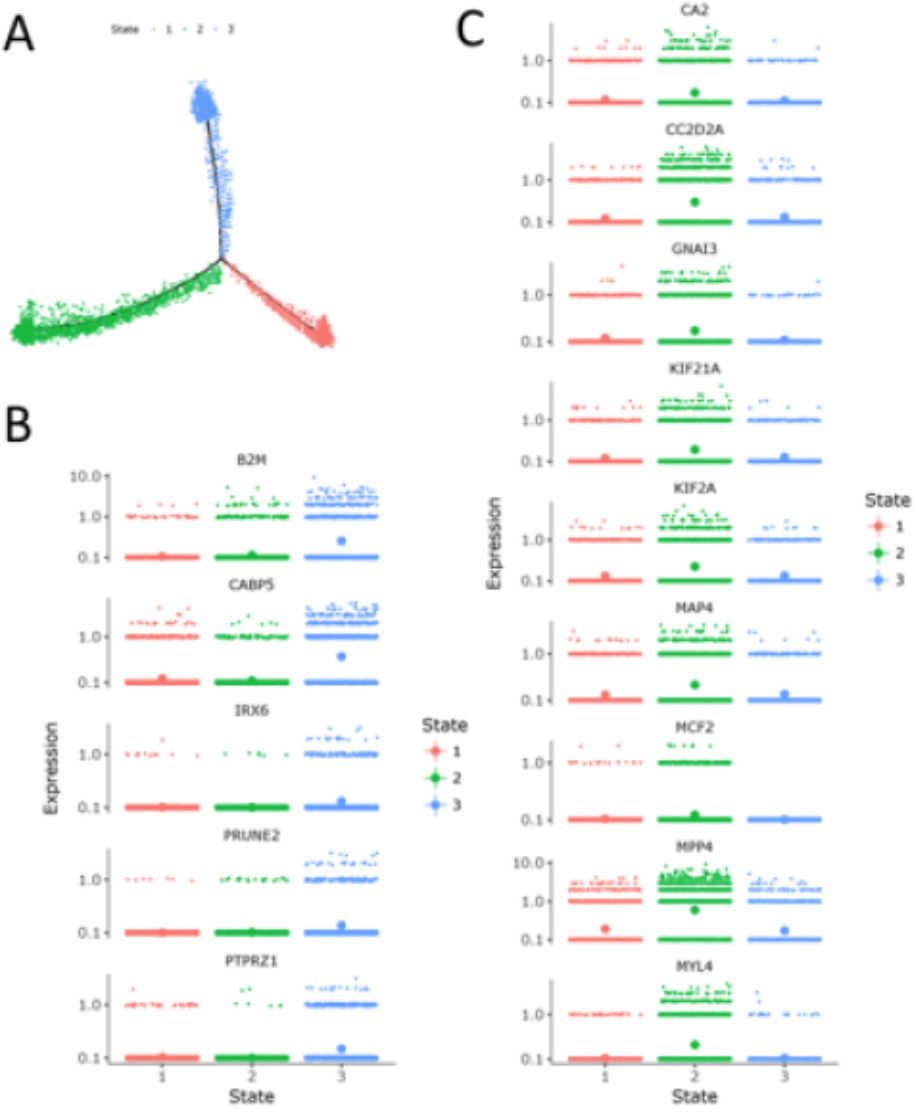

Supplementary Figure 13: Developmental trajectory of adult *in vivo* photoreceptors. A-C) Trajectory colored by state **(A)**, pseudotime **(B)**, and cell type **(C)**. **D-E)** Expression patterns of RHO **(D)** and ARR3 **(E)** along the trajectory. **F)** Heatmap of the top 100 non-ribosomal differentially expressed genes between states 1 (rods) and 4 (cones).

Figure 20

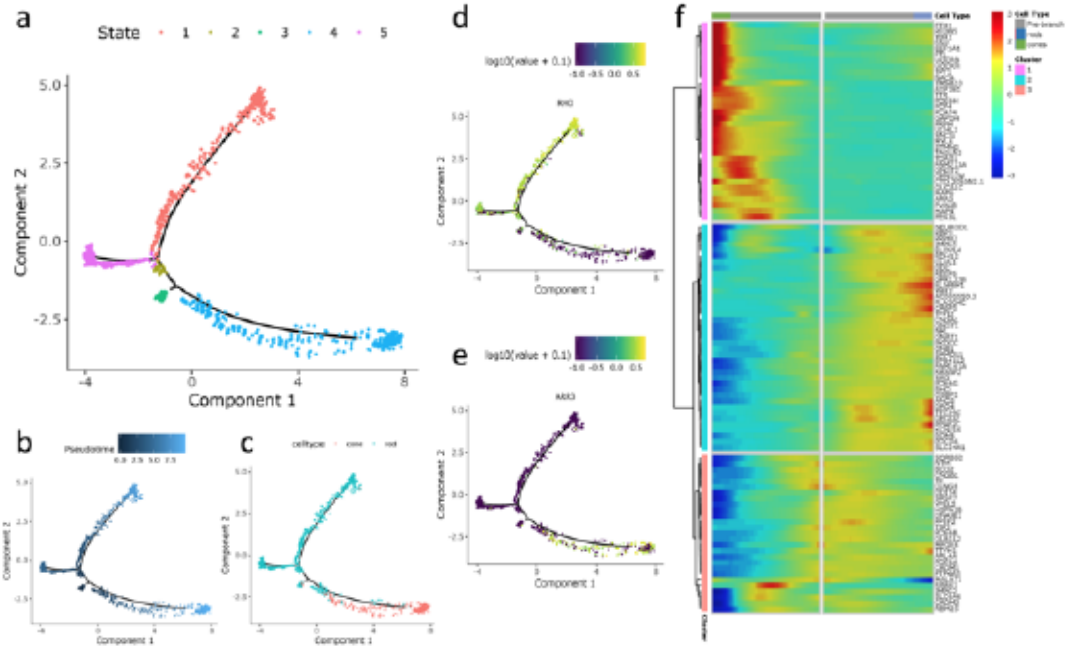

Supplementary Figure 14: Gene ontology enrichment analysis used to characterize the photoreceptors of state 9. A) Trajectory of combined WT and L75Pfs cells highlighting state 9 in pink. **B)** Heatmap of all genes differentially expressed at node 1, with genes hierarchically clustered. Clusters 3, 4, and 6 are highly enriched in state 9. **C)** GO term enrichment for genes in clusters 3, 4, and 6 (p values are Bonferroni corrected).

Figure 21

A

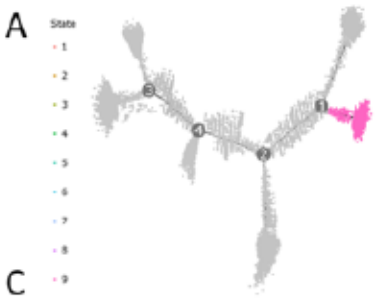

B

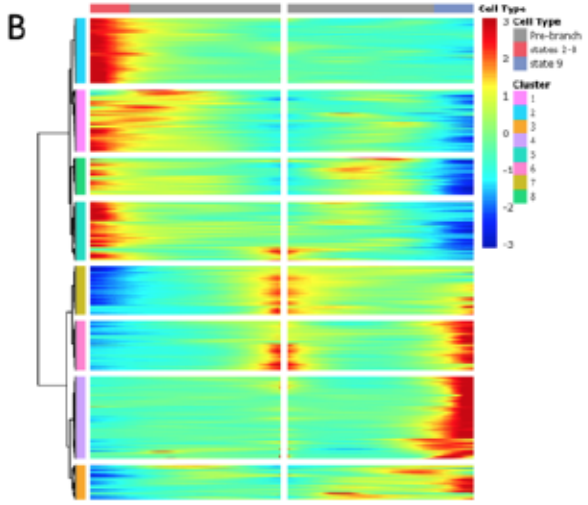

C

GO term	Fold change	p value
regulation of timing of cell differentiation	32.25	1.42E-02
protein refolding	22.57	8.06E-04
regulation of cellular response to heat	13.19	6.28E-04
oligodendrocyte differentiation	11.47	8.52E-03
cellular response to heat	10.12	1.97E-02
regulation of neural precursor proliferation	9.38	3.27E-02
endocrine system development	9.21	3.69E-02
cellular response to toxic substance	8.38	1.37E-02
response to reactive oxygen species	8.12	1.74E-02
response to unfolded protein	6.08	3.49E-03
mRNA splicing, via spliceosome	5.15	3.34E-02
epithelial cell differentiation	4.35	2.42E-03
gland development	4.28	1.35E-02
brain development	3.56	6.75E-05
sensory organ development	3.48	4.94E-02
generation of neurons	3.39	5.52E-03
negative regulation of cell differentiation	3.21	4.68E-02
negative regulation of transcription, DNA templated	2.6	3.93E-03
positive regulation of developmental process	2.53	1.52E-02
negative regulation of cell communication	2.44	2.77E-02

Supplementary Figure 15: Gene expression and GO enrichment analyses used to identify developing photoreceptors and to characterize differences between the 2 cone states and the 2 rod states. **A)** Trajectory of combined WT and L75Pfs photoreceptors colored by state. **B-D)** Expression pattern of *OTX2* (**B**), *CRX* (**C**), and *RCVRN* (**D**) along the trajectory. **E)** Heatmap of genes differentially expressed between cone states 5 and 6 and their corresponding gene ontology enrichment based on gene clusters (gene cluster 1 is enriched in state 6; gene clusters 2 and 3 are enriched in state 5). **F)** Heatmap of genes differentially expressed between rod states 7 and 8 and their corresponding gene ontology enrichment based on gene clusters (gene clusters 1, 3, and 6 are enriched in state 7; gene clusters 2, 4, and 5 are enriched in state 8).

Figure 22

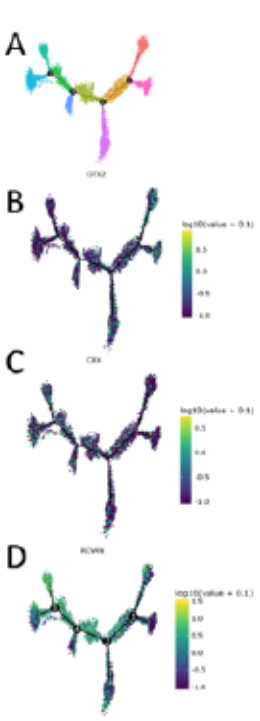

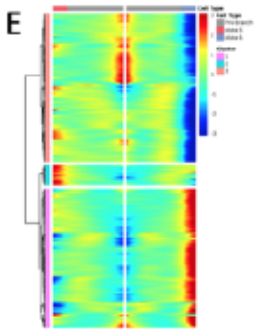

GO terms – State 5 enriched	fold enrichment	p value
Positive regulation of guanylate cyclase activity	>100	3.96E-03
mitochondrial coupled ATP synthesis coupled proton transport	38.4	2.25E-09
cristae formation	23.74	1.56E-08
mitochondrial electron transport, NADH to ubiquinone	23.46	3.82E-13
proteasomal ubiquitin independent protein catabolic process	21.86	1.06E-03
mitochondrial respiratory chain complex I assembly	17.08	6.94E-13
ATP hydrolysis coupled cation transmembrane transport	13.89	1.55E-05
aerobic respiration	9.32	5.91E-04
translation	3.54	3.65E-03
symbiont process	2.88	2.15E-02

GO terms – State 6 enriched	fold enrichment	p value
neural retina development	11.64	1.11E-02
photoreceptor cell differentiation	10.15	1.94E-02
brain development	3	1.61E-02
regulation of multicellular organismal process	1.92	2.10E-02

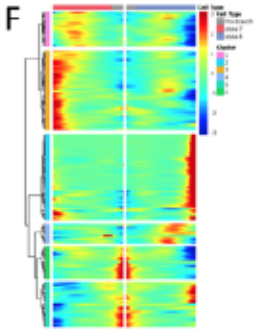

GO terms – State 7 enriched	fold enrichment	p value
positive regulation of guanylate cyclase activity	>100	4.31E-02
phototransduction	27.94	1.11E-02
neural retina development	26.24	1.31E-03
visual perception	7.88	6.15E-03

GO terms – State 8 enriched	fold enrichment	p value
rhodopsin mediated signaling pathway	>100	8.21E-07
negative regulation of inclusion body assembly	>100	3.14E-02
protein refolding	69.81	3.66E-03
platelet aggregation	66.49	4.69E-03
regulation of rhodopsin mediated signaling pathway	55.61	2.40E-05
chaperone cofactor dependent protein refolding	51.71	1.13E-02
eye photoreceptor cell development	37.89	2.83E-03
regulation of tumor necrosis factor mediated signaling pathway	35.8	4.31E-02
visual perception	20.74	6.90E-12
response to unfolded protein	15.18	1.96E-02
regulation of myeloid cell differentiation	15.18	1.96E-02
anatomical structure homeostasis	12.58	1.38E-03
leukocyte activation	6.61	4.07E-02
cellular response to organic substance	4.59	1.18E-04

Supplementary Figure 16: Comparison of rod and cone genes in L75Pfs rod-like cells reveals low expression levels of rod or cone genes. A) Expression levels of rod genes in L75Pfs rod-like cells is comparable to WT cone expression levels of rod genes. **B)** Expression levels of most cone genes in L75Pfs rod-like cells is comparable to WT rod expression levels of cone genes. Exceptions include *ARR3* and *PDE6H.*

Figure 23

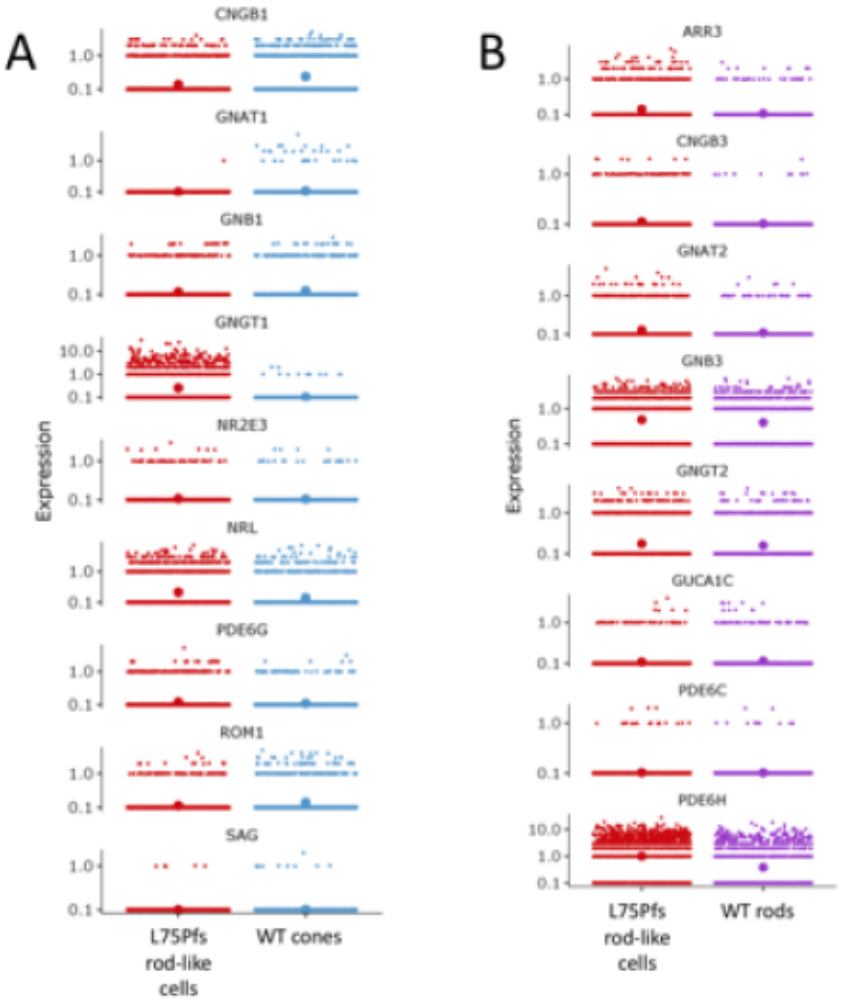

Supplementary Figure 17: Co-expression of MEF2C with ARR3, but not NR2E3, in hPSC-derived retinal organoids and human fetal retina supports a role for MEF2C in cone development. A-J) Confocal images of WT (**A-E**) or L75Pfs (**F-J**) d160 stage 3 (i.e., photoreceptor outer segment-containing) retinal organoids showing MEF2C (**C, H**) co-localization with ARR3 (**D, I**, merge in **E** and **J**), but not with NR2E3 in WT (**B**). **K-N)** Day 122 human fetal retina demonstrating localization of MEF2C (**M**) to the single layer of cone nuclei external to NR2E3+ developing rods (**L**, merge in **N**). **O-R)** Section from an adult monkey peripheral retina showing MEF2C (**Q**) localizing to two NR2E3-negative (**P**) nuclei in the ONL and a row of possibly Müller glia nuclei in the ONL (**Q**). Nuclei (blue) are shown in **A**, **F** and **K**. Scale bars: **A-E** and **F-J** = 10 microns. **K-N** and **O-R** = 50 microns.

Figure 24

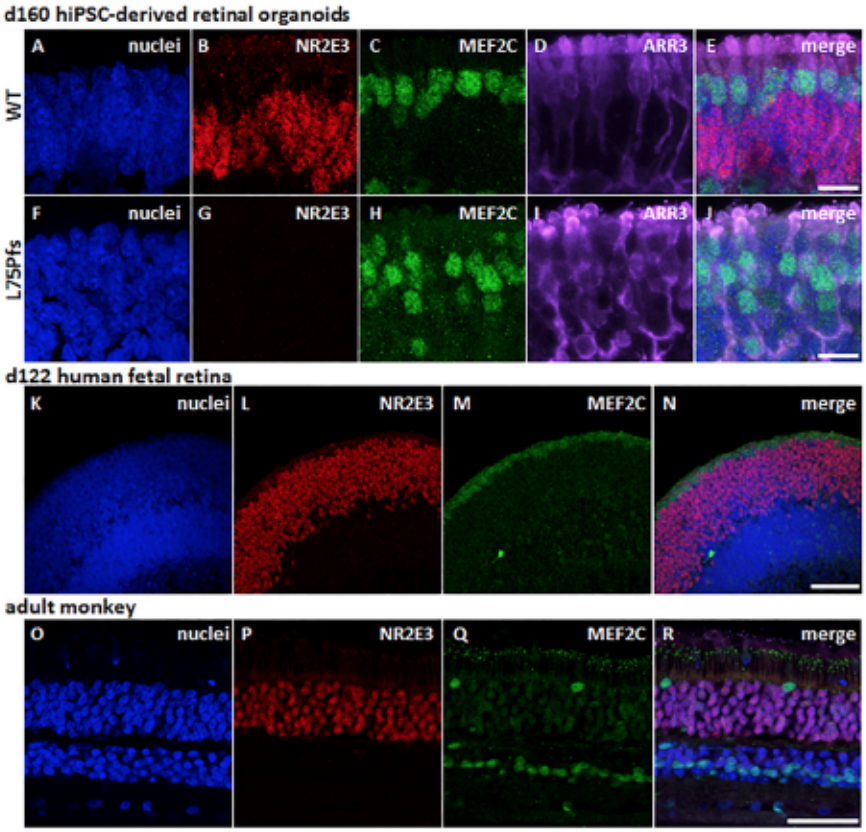

Supplementary Table 1: Marker genes used to call cluster identity

Table 2

Cell type	Gene(s)
Rod photoreceptors	*NR2E3, NRL* (wild type cells only), *GNGT1, SAG*
Cone photoreceptors	*PDE6H, ARR3, OPN1MW, OPN1SW, GUCA1C , GNAT2*
Bipolar cells	*VSX1, VSX2, TMEM215, ISL1*
Photoreceptor/Bipolar precursors	*CRX, OTX2, PRDM1, VSX1*
Amacrine cells	*TFAP2A, GAD1, GAD2, CALB2*
Horizontal cells	*ONECUT1, ONECUT2, TFAP2B, PROX1*
Retinal ganglion cells	*SLC17A6, GAP43, NEFL, NEFM*
Muller glia	*SOX2, SOX9, VIM, CLU, DKK3*
Mitotic cells	*MKI67, TOP2A, NUSAP1, CENPF*

Supplementary Table 2: primary antibodies

Table 3

ARR3	rabbit	LS Bio	1:100
ARR3	goat	Novus	1:100
CRALBP	mouse	Abcam	1:250
CRX	mouse	Abnova	1:100 0
Ki67	rabbit	Abcam	1:100
G0 ✔	mouse	Millipore	1:500
ML OPSIN	rabbit	Millipore	1:500
MEF2C	rabbit	Abnova	1:100
hNANOG	rabbit	Stemgent	1:100
NRL	goat	R&D Systems	1:300
NR2E3	mouse	Abcam	1:300
OCT3/4	mouse	Santa Cruz	1:100
PHALLOIDIN (f-actin)		Invitrogen	1:300
PKC ✔	rabbit	Sigma	1:50
RECOVERIN	rabbit	Millipore	1:200 0
RHO (4D2 clone)	mouse	Millipore	1:100
SNCG	mouse	Abnova	1:500
S OPSIN	rabbit	Millipore	1:500
SOX2	goat	R&D Systems	1:500
VGLUT	guinea	Millipore	1:200

	pig		0
VSX2	sheep	Exalpha	1:200

Supplementary Table 3: qPCR primers

Table 4

actin	GCGAGAAGATGACCCAGATC CCAGTGGTACGGCCAGAGG
CRX	TTTGCCAAGACCCAGTACCCAGA TGCATTTAGCCCTCCGGTTCTTGA
GNAT1	ACGGGTACTCGCTGGAAGA TCTCCGTACTGGATGTTGAGTG
NRL	CACGGTTCTCTGCATCGTTA AAATTCGGGCATGACTTGAG
NR2E3	CCAGTCCCAAGTGATGCTGAG GCGTTCCGCAGTGATAAACC
OPN1SW	TACGGCTTGTCACCATTCCT GGATTCATCTGTCATGGCCT
RCVN	CTCCTTCCAGACGATGAAAACA GCCAGTGTCCCCTCAATGAA
YWHAZ	ACTTTTGGTACATTGTGGCTTCAA CCGCCAGGACAAACCAGTAT

Supplementary Table 4: Genes differentially expressed between WT and L75Pfs cells at d100. Differential expression analysis was performed within each cluster and only genes with a statistically significant Bonferroni corrected p value and average natural log fold change > 0.5 were included. The "genotype" column indicates in which genotype each gene is enriched.

Table 5

	rods		
gene	p_val	avg_logFC	genotype
FABP7	1.01E-120	0.995792946	L75P
TMSB4X	3.52E-75	0.738379346	L75P
RPS4X	2.54E-55	0.518785789	L75P
HSPB1	1.17E-44	1.054698665	L75P
MORF4L2	1.14E-38	0.917795418	L75P
PRDX1	1.44E-31	0.550007809	L75P
JUN	1.10E-29	0.518981986	L75P

HIST1H2AC	1.24E-27	0.742851409	L75P
DCT	5.14E-24	0.519263633	L75P
TUBB4B	1.02E-23	0.588024008	L75P
GNGT2	1.05E-18	0.541317235	L75P
ENAH	3.33E-17	0.606954284	L75P
MRLN	9.39E-17	0.51051175	L75P
RPS29	4.94E-31	0.509582459	WT
RCVRN	9.53E-19	0.633849629	WT
RPS26	8.72E-15	0.703015996	WT
SOX4	2.34E-13	0.520008073	WT
HIST1H4C	4.15E-10	0.518819473	WT
SNHG5	7.82E-08	0.507361582	WT

cones

gene	p_val	avg_logFC	genotype
FABP7	1.00E-48	1.545604327	L75P
JUN	2.37E-39	0.930841165	L75P
MORF4L2	1.17E-29	0.708205314	L75P
DNAJB1	1.57E-18	0.507938903	L75P
HIST1H2AC	2.27E-17	0.555392651	L75P
RPS4Y1	1.42E-98	1.938586877	WT
RPS29	2.73E-56	0.555415921	WT
RPS26	2.37E-52	1.151773035	WT

precursors

gene	p_val	avg_logFC	genotype
HSPB1	5.17E-12	1.372489499	L75P
HIST1H2BG	1.36E-07	0.821379059	L75P
HSPE1	1.67E-07	0.853934927	L75P
HIST1H1C	2.24E-07	1.009205073	L75P
RPS29	2.76E-07	0.504701745	WT
UQCRB	1.01E-06	0.563615499	WT

amacrine cells

gene	p_val	avg_logFC	genotype
MT-RNR2	6.65E-17	0.624859657	L75P
RPS4X	3.46E-12	0.595809545	L75P
BEX3	3.22E-09	0.573927191	L75P
TMSB4X	5.79E-09	0.590928868	L75P
DCX	5.24E-07	0.696150823	L75P
RPS29	2.21E-08	0.515712121	WT
RPS26	9.14E-07	0.820239857	WT

horizontal cells

gene	p_val	avg_logFC	genotype
TMSB4X	2.37E-10	0.922944897	L75P
RPS29	9.64E-10	0.761781003	WT

RGCs

gene	p_val	avg_logFC	genotype
RPS4X	3.87E-20	0.699783958	L75P
TMSB4X	8.14E-08	0.53411685	L75P
PAK3	1.93E-06	0.721365865	L75P
ELAVL4	2.42E-08	1.032914048	WT

muller glia

gene	p_val	avg_logFC	genotype
RPS4X	2.65E-67	0.613527588	L75P
HSPB1	2.06E-39	1.085397705	L75P
DNAJB1	2.99E-38	0.852191406	L75P
HSPA1A	4.61E-31	0.685157368	L75P
H3F3B	6.94E-31	0.512879932	L75P
GPM6B	4.78E-30	0.638019347	L75P
UBB	1.03E-28	0.566669059	L75P
HIST1H2BG	6.54E-22	0.660879498	L75P
HSPE1	1.27E-17	0.66252755	L75P
JUN	1.00E-16	0.610637589	L75P
MORF4L2	1.80E-16	0.594465074	L75P
RPS26	9.59E-37	0.948610013	WT
SNHG5	2.32E-15	0.502226316	WT
MARCKSL1	4.64E-13	0.553916441	WT

mitotic cells

gene	p_val	avg_logFC	genotype
RPS4X	1.37E-23	0.84960342	L75P
HSPB1	1.19E-21	1.626375337	L75P
DNAJB1	2.79E-14	1.034338953	L75P
CRABP1	2.78E-13	0.619383315	L75P
HSPA1A	3.70E-13	0.79534223	L75P
RPL29	2.16E-08	0.646389483	L75P
HSP90AB1	7.67E-08	0.531263919	L75P
HSPA1B	1.06E-07	0.592300677	L75P
GPM6B	1.83E-07	0.561379599	L75P
TSC22D1	4.30E-07	0.789525386	L75P
HSPE1	5.59E-07	0.639963456	L75P
SAT1	6.94E-07	0.679520174	L75P
MORF4L2	1.47E-06	0.521626731	L75P

HMGB1	5.18E-10	0.628014473	WT

Supplementary Table 2: Genes differentially expressed between WT and L75Pfs cells at d170. Differential expression analysis was performed within each cluster and only genes with a statistically significant Bonferroni corrected p value and average natural log fold change > 0.5 were included. The "genotype" column indicates in which genotype each gene is enriched.

Table 6

	rods		
gene	p_val	avg_logFC	genotype
ISOC1	6.75E-134	1.420203442	L75P
PDE6H	5.30E-119	1.047735534	L75P
FABP7	5.06E-114	1.118235809	L75P
TTR	5.66E-111	2.597353629	L75P
DST	2.30E-68	0.815270436	L75P
BEX3	1.97E-50	0.737834434	L75P
KIF5B	4.04E-50	0.691487476	L75P
MORF4L2	1.73E-47	0.787215074	L75P
TMSB4X	9.67E-43	0.60829967	L75P
BEX2	2.18E-34	0.607093783	L75P
DARS	7.61E-30	0.624042159	L75P
DMD	8.20E-30	0.582155106	L75P
DHRS7	7.19E-27	0.512947955	L75P
GNAT1	0	2.733077526	WT
ROM1	0	2.35218798	WT
SAMD7	2.09E-215	2.004164253	WT
NR2E3	2.31E-194	1.866285046	WT
NRL	6.87E-177	1.154957632	WT
CNGB1	3.06E-173	1.634450354	WT
CADM1	4.11E-171	1.43880041	WT
GNB1	1.33E-126	1.53340333	WT

CABP5	4.69E-113	1.246339374	WT
AIPL1	5.58E-110	0.900281898	WT
UNC119	9.49E-83	0.727873735	WT
PDE6G	1.67E-71	1.184937722	WT
MT-ATP6	8.76E-69	0.863775243	WT
RAX2	1.41E-61	0.978619335	WT
MT-ND4	4.41E-61	0.78160685	WT
MT-CYB	6.45E-54	0.73073916	WT
SPTBN1	3.78E-53	0.95180123	WT
RP1	1.88E-46	0.678355449	WT
RCVRN	3.32E-44	0.63155199	WT
B2M	1.54E-41	0.833760907	WT
MT-ND5	5.70E-32	0.621477734	WT
CPE	6.59E-21	0.54691214	WT
SNHG6	1.26E-16	0.514533058	WT

s-cones

gene	p_val	avg_logFC	genotype
ISOC1	1.31E-28	1.04562069	L75P
FABP7	6.03E-26	1.673303622	L75P
TTR	2.12E-25	1.460829661	L75P
TMSB4X	7.59E-24	0.916453538	L75P
OPN1SW	2.18E-22	1.003985625	L75P
RPS4X	4.70E-19	0.554637307	L75P
DMD	1.11E-13	0.757071046	L75P
GSTP1	1.17E-12	0.662777357	L75P
ACBD6	2.36E-10	0.941707364	L75P
MT-RNR2	9.04E-10	0.512769937	L75P
IFI27L2	2.41E-08	0.742860975	L75P
GNGT1	1.86E-07	0.805969101	L75P
GUCA1C	1.41E-19	1.221055427	WT
GUCA1A	6.26E-16	1.044351104	WT
AIPL1	4.11E-15	0.651782898	WT
PDE6H	1.22E-12	0.563568523	WT
GUK1	4.26E-12	0.724160081	WT
RIMS2	1.48E-09	0.610574651	WT
PABPC1	2.19E-09	0.569746701	WT
ALDOC	1.08E-08	0.687527699	WT
MPP4	1.56E-07	0.659382448	WT
MYL4	4.30E-07	0.595757039	WT
WSB1	1.06E-06	0.648389602	WT

cones

gene	p_val	avg_logFC	genotype
RPS4X	3.36E-69	0.548124222	L75P
DMD	2.86E-63	0.765920576	L75P
TMSB4X	6.29E-42	0.635381977	L75P
CNGB1	6.24E-31	0.500668904	WT

amacrine cells

gene	p_val	avg_logFC	genotype
MORF4L2	2.27E-17	0.572881136	L75P
BEX2	5.51E-17	0.593265019	L75P
NAP1L3	4.41E-14	0.613732647	L75P
MEG3	3.91E-122	2.316728077	WT
RPS2	4.87E-29	0.672867603	WT
RBP1	4.04E-13	0.677167175	WT

bipolar cells

gene	p_val	avg_logFC	genotype
CADPS	4.91E-14	0.891476451	L75P
RPS2	1.47E-17	0.635965313	WT
RBP1	1.34E-10	0.631031801	WT

horizontal cells

gene	p_val	avg_logFC	genotype
BEX3	8.70E-12	0.582649378	L75P
RPS4X	2.01E-10	0.515039488	L75P
TMSB4X	7.61E-08	0.644309947	L75P
RPL34	5.69E-07	0.511195932	L75P

muller glia

gene	p_val	avg_logFC	genotype
CRYM	1.48E-113	1.364777743	L75P
RPS4X	7.47E-109	0.521077363	L75P
RPL34	6.69E-73	0.509805998	L75P
BEX3	2.96E-62	0.511569624	L75P
GPM6B	3.23E-56	0.578177728	L75P
CP	2.55E-46	0.783598839	L75P
SFRP2	3.07E-37	0.5163643	L75P
MORF4L2	2.03E-34	0.588025759	L75P
LGALS3	4.61E-27	0.70323864	L75P
DAPL1	1.11E-25	0.502402476	L75P
CRYAB	1.43E-06	0.566652901	L75P
RPS4Y1	0	1.973974043	WT
RPS2	2.46E-143	0.634459379	WT
CCND1	3.12E-42	0.914379747	WT

IGFBP5	3.00E-39	0.711245142	WT
HILPDA	1.34E-38	0.864366509	WT
AKAP12	5.68E-38	0.912076661	WT
	mitotic cells		
gene	p_val	avg_logFC	genotype
RPL34	8.75E-11	0.840320655	L75P
RPS4X	7.76E-08	0.526520658	L75P
RPS4Y1	7.23E-18	1.748814912	WT
RBP1	3.23E-07	0.802800764	WT
TUBA1A	1.05E-06	0.534320228	WT

Supplementary Table 3: Ordering genes used for trajectory reconstruction.

Table 7

	gene
1	ARR3
2	CRABP2
3	GUCA1A
4	GUCA1B
5	GUCA1C
6	MAP1B
7	NR2E3
8	PDE6H
9	TMSB4X
10	GNAT1
11	GNGT1
12	NRL
13	ROM1
14	TMSB10
15	SAMD7
16	PCP4
17	UNC119
18	CNGB1
19	RP1
20	GSTP1
21	PTMA
22	AKAP9
23	B2M
24	MYL4
25	RCVRN

26	CADM1
27	FABP7
28	RIMS2
29	PDC
30	HSPA1A
31	CC2D2A
32	MPP4
33	MALAT1
34	AIPL1
35	KCNV2
36	PDE6G
37	ARL6IP5
38	CABP5
39	COX7C
40	CFL1
41	GUK1
42	HIST1H4C
43	GNB1
44	SPTBN1
45	PRCD
46	SNHG6
47	CTD-2050N2.1
48	CRABP1
49	HIST1H2BG
50	CNGB3
51	DNAJB1
52	MYL6
53	CKB
54	ITM2C
55	ATP5E
56	SOX4
57	DST
58	MAP2
59	ELOVL4
60	TUBB
61	HSP90AB1
62	XRCC4
63	HSP90AA1
64	LMO4

65	CPE
66	STMN1
67	PTPN13
68	RS1
69	PPDPF
70	CPLX4
71	HNRNPA1
72	ENO2
73	STMN2
74	IMPG1
75	OPN1MW
76	GNGT2
77	TPI1
78	TUBB2B
79	TTR
80	TSPAN7
81	EPB41L2
82	GNAT2
83	PTMS
84	PPA1
85	PKIB
86	NDUFA13
87	NDUFB11
88	RAX2
89	SLC25A6
90	AHI1
91	EEF1A1
92	PRPH2
93	SAG
94	SYNE2
95	RGS9
96	ASPH
97	KIF21A
98	EEF2
99	ACTB
100	ZFAS1
101	ROMO1
102	PRUNE2
103	GNB3
104	ALDOA

105 PIK3R1
106 KIF2A
107 SERF2
108 LAPTM4B
109 HSPB1
110 SNRPE
111 PDE6A
112 MIR7-3HG
113 GNAI3
114 ITM2B
115 PRDX2
116 UQCR11
117 TAPT1
118 STX3
119 CA2
120 MAP4
121 CREG1
122 FSTL5
123 LBH
124 BICD1
125 MTND1P23
126 GPR160
127 DMD
128 ELOB
129 ISOC1
130 ATP5J2
131 RABL3
132 C4orf48
133 HMGA1
134 SLC38A5
135 RBP1
136 TUBA1A
137 OTX2
138 HLA-B
139 ALDOC
140 GOLGA4
141 YWHAE
142 TULP1
143 LRRC39
144 RXRG

145 OPN1SW
146 PALMD
147 HLTF
148 NAP1L1
149 FAM161A
150 SNHG5
151 HSPE1
152 PSIP1
153 IRX6
154 SEPT4
155 USMG5
156 PROM1
157 HSPA1B
158 TMEM14B
159 ATP5I
160 HSPA6
161 DZIP3
162 DCT
163 POLR2L
164 TOMM7
165 GNG5
166 RHOBTB1
167 FTH1
168 BTG1
169 NDUFA3
170 SNAP25
171 CORO7
172 UBB
173 COTL1
174 HLA-A
175 COX8A
176 MAK
177 NEUROD4
178 PTPRZ1
179 DDIT3
180 REEP6
181 UBA52
182 RTN4
183 CHN2
184 CADM3

185 SNRPF
186 TAGLN3
187 CMSS1
188 ANKRD33
189 ATP5L
190 UCHL1
191 PDE6C
192 UBL5
193 HMGN2
194 FAU
195 RBP3
196 CAMK1D
197 HMGB1
198 PPP2R2B
199 MATN2
200 HOOK1
201 ACTG1
202 GRINA
203 PRMT1
204 DCAF1
205 OST4
206 ALDH2
207 C8orf46
208 NDUFS5
209 HIST1H2AC
210 MRLN
211 GPX4
212 NFKBIZ
213 EEF1B2
214 NDUFA11
215 CD24
216 RBP4
217 TECR
218 EID1
219 DDX17
220 SRRM3
221 EIF3E
222 PLEKHB1
223 SAMD11
224 CLUL1

225 HMGN1
226 MARCKSL1
227 APLP2
228 NOS1AP
229 HINT1
230 TMA7
231 GNAS
232 C16orf74
233 AC090602.2
234 LIMA1
235 SRSF3
236 COX6C
237 PLA2G5
238 COPS9
239 ZNF428
240 DCBLD2
241 RPGR
242 UQCRQ
243 BEX3
244 ZNF326
245 LINC02115
246 CRX
247 DTNBP1
248 MCF2
249 HSPD1
250 MAP1LC3B
251 NME1
252 CANX
253 NRN1
254 DPYSL3
255 BMP7
256 PGRMC1
257 LGI4
258 CFAP36
259 HDAC2
260 GPR155
261 RD3
262 UGCG
263 RPGRIP1
264 TPD52

265	PDZPH1P
266	C14orf2
267	BHLHE41
268	BLOC1S2
269	NPM1
270	ANP32E
271	TSPAN3
272	QPRT
273	MOAP1
274	MINOS1
275	APEX1
276	PCBP4
277	MIF
278	SPON2
279	COMMD6
280	TPM1
281	MLXIP
282	SNRPG
283	WI2-1896O14.1
284	LRRIQ1
285	YBX1
286	HNRNPDL
287	MEGF9
288	SCG3
289	TMSB15A
290	LUC7L3
291	KCNQ1OT1
292	FKBP3
293	CCDC88A
294	LGALSL
295	TMF1
296	HIST1H1C
297	TMEM14A
298	NDUFC2
299	MAP1LC3A
300	COX6A1
301	CCDC82
302	TAF7
303	HN1

304 SLC38A1
305 RASSF2
306 EGR1
307 NDUFB1
308 PGK1
309 ABCA5
310 HMGN5
311 MIAT
312 IMPG2
313 DHRS7
314 HRASLS
315 RAD17
316 CHCHD10
317 PPM1N
318 CALCOCO2
319 CADM2
320 BAZ2B
321 TRAC
322 SCAMP1
323 BTF3
324 ARHGAP10
325 LMOD1
326 ROBO2
327 PRDX1
328 RAB3IP
329 TMEM176B
330 ECHDC2
331 HEG1
332 EMB
333 C9orf16
334 SIX6
335 HLA-C
336 NEDD4L
337 ANK3
338 SLC24A2
339 HPRT1
340 GSG1
341 GAPDH
342 FAM162A
343 PCSK1N

344 TMEM258
345 ARMC9
346 RNF170
347 SYK
348 SUCO
349 ARHGAP42
350 SRPRA
351 C6orf62
352 CPLX2
353 COX7A2
354 ISL2
355 ETF1P2
356 TROVE2
357 PLCD4
358 HSPH1
359 PARP1
360 CLTB
361 MXRA5
362 AANAT
363 GABRG2
364 CHCHD5
365 SLC6A6
366 YBX3
367 FOS
368 PPFIA2
369 LIMCH1
370 GOLGB1
371 CABP4
372 AC007349.7
373 NCL
374 ACTN1
375 SHISA5
376 CASC15
377 MAP3K7CL
378 COBLL1
379 PDE6D
380 SLC2A11
381 DLL3
382 KIF5C
383 PNISR

384	ANKRD33B
385	RSPH1
386	MYLK
387	FZD3
388	VOPP1
389	MROH8
390	SMARCB1
391	SARAF
392	EFR3A
393	SMC3
394	KCNB1
395	SNRPD2
396	NXNL2
397	OLFM1
398	DOCK8
399	ITGA6
400	SPECC1
401	RICTOR
402	WASF3
403	PSMA7
404	NAPB
405	SLC12A2
406	EGFLAM
407	FAM84B
408	BLOC1S1
409	COBL
410	WAPL
411	FAM57B
412	POU2AF1
413	IGFBP7
414	C4orf3
415	LYPLA1
416	CD46
417	MEF2C
418	FAM213A
419	CTD-2524L6.3
420	BNIP3
421	ATP2B1
422	POLR2I

423	SNRPN
424	PDCD4
425	CD63
426	MFSD11
427	KCNB2
428	TMEM244
429	TMEM50B
430	EPS8
431	PRELID2
432	GNB5
433	DNAJA1
434	ATF4
435	FAM19A4
436	PKM
437	PDE6B
438	BEX1
439	RAB41
440	NIPAL1
441	UFL1
442	C7orf33
443	CTD-2287O16.1
444	ORMDL1
445	ATP1A3
446	CACYBP
447	GNB2
448	SERINC1
449	SPEF2
450	SEZ6L2
451	COL4A3
452	SLC25A4
453	MED18
454	ASB13
455	COX7B
456	PPP4R4
457	COX6B1
458	ST5
459	RGS20
460	LINC00888
461	PRDX5

462	OSBPL1A
463	MBNL1
464	ABCA1
465	SPTSSA
466	TAX1BP1
467	SLC1A2
468	SLC24A4
469	ADD1
470	STC1
471	NEBL
472	MTDH
473	TMEM256
474	GAS5
475	SAMD15
476	PSAP
477	CGNL1
478	TBCA
479	SYTL4
480	NDUFA1
481	SCAMP5
482	FMC1
483	CTC-487M23.6
484	ATP5G2
485	GREM2
486	SLC39A5
487	SELENOF
488	AC002075.4
489	RP1L1
490	COPE
491	DYNLL1
492	LARP6
493	CSRP2
494	WSB1
495	CEP290
496	DICER1-AS1
497	FSCN1
498	MAP9
499	LAMTOR4
500	LINC02154

501	PTH2
502	KTN1
503	DEFB119
504	NDUFA4
505	BCO2
506	OTX2-AS1
507	TERF2IP
508	NPPC
509	GOLGA1
510	VPS36
511	HIST1H2BD
512	H1F0
513	YPEL5
514	SLIRP
515	AC007246.3
516	CCKBR
517	NEDD8
518	H3F3A
519	TUBA1B
520	CTC-209L16.1
521	DPP4
522	SSB
523	METTL9
524	BASP1
525	RDH12
526	PPFIBP1
527	EIF1
528	SEC62
529	SMC5
530	ACSL3
531	PPIA
532	EPRS
533	CCDC186
534	TACC1
535	CRHBP
536	DMBX1
537	WBP11
538	RAI14
539	CHRNA3

540	SCAF11
541	FUS
542	TNRC6B
543	TP53I11
544	TMEM107
545	PCOLCE2
546	GRSF1
547	ZBTB38
548	TRAM1
549	EPHX2
550	SPG20
551	CLCN4
552	CLCN3
553	PPM1J
554	ZDHHC2
555	TPT1
556	MTATP6P1
557	LIPG
558	ESD
559	RAX
560	B3GAT2
561	EPB41L3
562	AP000997.1
563	PRKD3
564	RNPC3
565	PLP1
566	ATP5G3
567	TYW5
568	BRWD1
569	ZNF540
570	RTN3
571	RIC3
572	CYB5D2
573	NNAT
574	CTR9
575	AC004453.8
576	CNNM4
577	ANK2
578	PLOD2
579	TRAK1

580	RRAD
581	ERGIC3
582	MACF1
583	MPDZ
584	PPP1R9A
585	MCUR1
586	VTN
587	IGSF9
588	PRDM1
589	RUFY3
590	C20orf194
591	KIAA1841
592	ANXA4
593	BARD1
594	DNAJC3
595	WWC2
596	AC007969.5
597	KIF1B
598	OSBPL8
599	PPP3CC
600	UNC80
601	PARP6
602	POC5
603	TRIM37
604	BBS7
605	SLC25A37
606	CDHR1
607	MAP6
608	C1orf226
609	IFT88
610	CLK4
611	FAIM
612	XIAP
613	SEC11A
614	LLNLR-245B6.1
615	SSX2IP
616	LRIT3
617	ADD3
618	CEP70

619	CTA-228A9.4
620	NOL4
621	CEP95
622	C8orf59
623	HK2
624	IQGAP2
625	PARD6B
626	TMED9
627	CTD-2034I21.1
628	WDR83OS
629	SMARCE1
630	IL6ST
631	SVOP
632	ADCY1
633	SEMA3C
634	SCAPER
635	RNF157
636	KLHL18
637	HILPDA
638	DNAJC25
639	PFN1
640	SLC44A1
641	CBX1
642	NOP10
643	F10-AS1
644	SHPRH
645	FMN2
646	SYT1
647	VSTM2A
648	AGPAT3
649	ATP1B2
650	CD47
651	GABARAPL2
652	SH3BGRL
653	CEP112
654	CDK13
655	TUBB2A
656	CEP126
657	JAKMIP2

658	CASQ1
659	GCC2
660	TMEM243
661	CCDC14
662	CCSER1
663	EBLN3P
664	GPBP1
665	NDUFA7
666	DAPL1
667	NDUFB2
668	PSMA2
669	FMN1
670	GLYATL1
671	C6orf48
672	GDI1
673	UBE2I
674	AC012146.7
675	GPX1
676	CHD9
677	ACSL6
678	CTC-425K20.1
679	RIDA
680	PAFAH1B3
681	NIPAL3
682	NFE2L2
683	ACBD5
684	SRSF5
685	TMEM97
686	FXYD7
687	TTC3
688	PERP
689	ITSN1
690	FXYD6
691	ZNF83
692	BANF1
693	BCL2L1
694	JAK1
695	ABCA4
696	ADIPOR1

697 SHTN1
698 ABCA7
699 MAGEH1
700 FHOD3
701 MAGED2
702 DRAP1
703 RAB3A
704 ST3GAL5
705 HIST1H2AE
706 CFDP1
707 SPINK4
708 MREG
709 DNAJC15
710 NCKAP5
711 PPIG
712 TMEM230
713 DAXX
714 SPOP
715 CNTN2
716 ARHGAP12
717 TLX2
718 NDNF
719 IFI27
720 HSPA8
721 ANKRD26
722 CAMK2N1
723 FAM171B
724 CHGB
725 INHBB
726 INTU
727 ROGDI
728 NT5DC1
729 SON
730 MBD3L2
731 DEK
732 SNX29
733 EPAS1
734 IQSEC1
735 NEUROD1
736 RTBDN

737 CNGA1
738 LEMD1
739 FAM174A
740 CROT
741 WRB
742 MDK
743 PDCD5
744 DGKE
745 PCNA
746 COPB1
747 TIMM13
748 FSD1L
749 FAM13A
750 ATCAY
751 FAM210A
752 HTRA1
753 TCF25
754 CEP120
755 SELENOH
756 LBHD1
757 LYST
758 AC003075.4
759 PHB2
760 RPAIN
761 BNIP3L
762 OSTF1
763 SORL1
764 OCIAD2
765 POLB
766 ARHGAP5
767 SNRPB
768 FRMPD2
769 HES6
770 EMC1
771 DDRGK1
772 PTMAP5
773 EZH2
774 POLR2E
775 NACA
776 RGS2

777	MINDY2
778	LDLRAD4
779	PFKP
780	SEC61G

Supplementary Table 4: Genes differentially expressed at the node separating WT rods and cones.

Table 8

gene	pval
GNGT1	0
GUCA1A	0
NRL	0
PDE6H	0
TMSB4X	0
ROM1	8.47E-272
GNAT1	3.10E-264
GUCA1B	5.47E-230
MT-RNR2	1.85E-228
CABP5	8.53E-227
GUCA1C	6.55E-215
ARR3	1.17E-206
PCP4	5.15E-194
MALAT1	1.45E-181
NR2E3	2.29E-144
GUK1	1.96E-130
DST	1.01E-125
B2M	4.33E-125
MPP4	7.30E-124
PDE6G	2.78E-113
CADM1	8.98E-110
GNB1	7.85E-96
MYL4	1.16E-94
FABP7	1.30E-84
RPS6	1.34E-82
RPLP1	9.00E-82
GSTP1	1.85E-81
CC2D2A	3.93E-77
CNGB1	1.60E-69
PIK3R1	2.11E-69
GNAT2	1.99E-65

PPA1	5.91E-64
RCVRN	4.98E-62
PTPRZ1	1.58E-61
MRLN	2.17E-59
AIPL1	9.42E-58
HIST1H2BG	1.00E-55
LBH	1.45E-55
CNGB3	2.12E-54
DNAJB1	3.98E-54
SCG3	3.04E-52
RIMS2	2.05E-51
HSP90AA1	3.97E-51
SPTBN1	3.75E-50
SAG	1.41E-49
CPLX4	3.29E-49
CTD-2050N2.1	4.48E-49
GNAI3	3.43E-48
RPL13	6.56E-48
HMGN2	3.83E-47
RPLP0	6.08E-47
XRCC4	6.10E-47
REEP6	2.44E-45
SAMD11	6.52E-45
FAM161A	7.70E-45
PRUNE2	1.25E-44
TPI1	1.34E-44
HIST1H4C	1.80E-43
PDE6A	5.02E-43
RP1	1.96E-42
MAP2	2.93E-42
KCNV2	2.38E-41
IRX6	3.81E-41
CA2	5.18E-40
SNHG6	6.73E-40
NRN1	1.21E-38
STMN1	2.55E-38
TMSB10	2.56E-38
RPL32	4.81E-38
MT-CO1	6.79E-38
HSPA1B	1.22E-37
RPL19	6.86E-37
EEF1A1	8.72E-37

KIF2A	2.14E-36
RPS14	3.92E-36
WSB1	4.70E-36
RPS13	7.76E-36
HSPA1A	2.66E-35
HLA-A	3.08E-35
RPS11	1.50E-34
RPL13A	1.72E-34
UCHL1	3.32E-34
MIAT	6.27E-34
TSPAN7	7.08E-34
SIX6	1.22E-33
RPS4X	2.53E-33
RPS27	1.49E-32
RPL23	2.42E-32
CRABP2	6.84E-32
ROBO2	9.31E-32
EPB41L2	2.44E-31
RPL3	1.45E-30
GNGT2	2.25E-30
OLFM1	2.38E-30
CKB	3.25E-30
AANAT	4.65E-30
DHRS7	1.16E-29
UBB	4.67E-29
RBP1	9.34E-29
PGK1	1.00E-28
CCDC88A	8.43E-28
KIF21A	1.28E-27
CASC15	1.32E-27
PSIP1	1.66E-27
TTR	1.68E-27
HIST1H1C	2.57E-27
MCF2	2.72E-27
OPN1MW	3.50E-27
RPS18	5.57E-27
SOX4	6.94E-27
TSPAN3	1.00E-26
RPL37A	2.05E-26
C8orf46	2.18E-26
TULP1	9.41E-26
MAP4	2.59E-25
AKAP9	3.76E-25

CLUL1	4.60E-25
RPLP2	4.79E-25
BICD1	5.19E-25
RPL6	5.29E-25
RPL8	1.26E-24
RPL10A	1.65E-24
RPS16	1.67E-24
OTX2	2.12E-24
RPL30	2.78E-24
FAM162A	6.14E-24
HMGN5	1.06E-23
B3GAT2	1.12E-23
GNB3	2.01E-23
OPN1SW	3.66E-23
RPS27A	4.37E-23
RPS3A	4.50E-23
BLOC1S2	5.18E-23
CFAP36	5.22E-23
ARL6IP5	6.17E-23
ENO2	7.83E-23
RS1	1.66E-22
STC1	1.77E-22
LINC02115	2.37E-22
RACK1	2.64E-22
RPS9	3.12E-22
RHOBTB1	3.37E-22
CHCHD10	6.12E-22
ITSN1	7.64E-22
RPL27A	7.70E-22
WI2-1896O14.1	8.35E-22
PDE6B	1.12E-21
EZH2	1.20E-21
RPL21	1.24E-21
TAPT1	1.27E-21
PDE6C	1.28E-21
MAP1B	1.42E-21
SAMD7	1.57E-21
GPR160	1.82E-21
ITM2B	1.92E-21
CCDC82	2.24E-21
PKIB	2.28E-21
NIPAL1	5.14E-21

TUBA1B	5.66E-21
FAU	1.09E-20
RPL7	1.11E-20
TPT1	1.27E-20
RPL34	2.85E-20
RPS15A	3.93E-20
RPS19	4.96E-20
CREG1	5.86E-20
UBA52	7.26E-20
RPL10	7.34E-20
RRAD	8.17E-20
NDUFA4	9.81E-20
GNAS	1.39E-19
RP11-240M16.1	2.60E-19
NFKBIZ	3.43E-19
RPS2	7.58E-19
PDZPH1P	8.60E-19
CGNL1	8.78E-19
PGRMC1	9.01E-19
DCT	9.57E-19
RPL24	1.00E-18
CTD-2524L6.3	1.09E-18
RPL5	2.11E-18
SPECC1	2.65E-18
HLA-B	2.89E-18
RPL27	3.33E-18
RPS24	3.58E-18
RPS23	3.81E-18
YBX1	4.38E-18
ATP2B1	6.36E-18
H3F3B	7.68E-18
RPL11	8.98E-18
RPS25	1.16E-17
ANXA4	1.33E-17
RPS5	1.41E-17
ELOVL4	2.02E-17
RPS3	2.20E-17
BAZ2B	2.28E-17
PTMA	3.60E-17
SPINK4	3.70E-17
CAMK1D	4.36E-17

HIST1H1E	4.88E-17
RPS8	5.18E-17
RPS15	5.77E-17
SYTL4	8.74E-17
LIMA1	1.16E-16
PTPN13	1.19E-16
FAM213A	1.39E-16
WWC1	1.43E-16
IGF2BP3	1.45E-16
ACTG1	1.58E-16
COTL1	2.02E-16
RPS7	2.04E-16
FTL	2.05E-16
HSPA6	2.08E-16
MT-ND5	2.35E-16
PABPC1	2.40E-16
FAM57B	2.86E-16
RPL31	4.19E-16
BNIP3	4.61E-16
COL4A3	4.66E-16
LRRC4C	4.78E-16
RPL35A	5.98E-16
MATN2	6.41E-16
GPR155	6.66E-16
NACA	7.35E-16
GNG5	9.02E-16
RPL12	1.43E-15
MEGF9	1.63E-15
LMO4	1.96E-15
KCNB2	1.98E-15
PDC	2.63E-15
RPL41	2.77E-15
HRASLS	3.41E-15
MT-CO2	3.58E-15
TACC1	6.92E-15
PEX5L	6.99E-15
LGALSL	7.45E-15
NXNL2	9.02E-15
HES6	1.04E-14
MAP6	1.09E-14
FAM155A	1.24E-14
MXRA5	2.37E-14
RBP4	2.37E-14

IMPG1	2.95E-14
RPL38	3.07E-14
PPP4R4	3.32E-14
PBX1	5.04E-14
ATP1B1	5.34E-14
RPL7A	7.41E-14
ATF4	7.86E-14
PRCD	8.27E-14
EMC1	8.52E-14
TOX	9.18E-14
RPL4	1.20E-13
RPS12	1.34E-13
ITM2C	1.36E-13
MT-CYB	1.69E-13
RPL35	1.94E-13
LUZP2	2.70E-13
APP	3.39E-13
MT-CO3	3.96E-13
ALDH2	4.84E-13
DEFB119	5.66E-13
RP11-96L14.7	5.84E-13
RGS2	5.96E-13
DAXX	7.33E-13
GABRG2	7.37E-13
SLC44A1	1.20E-12
ACTB	1.30E-12
TMEM14B	1.37E-12
MIR7-3HG	1.85E-12
PROM1	2.35E-12
HIST1H2AC	2.65E-12
MOAP1	2.69E-12
GPM6A	2.84E-12
DYNLL1	3.18E-12
SCAMP1	3.40E-12
RPL18A	3.56E-12
SLC24A4	4.98E-12
UGCG	5.85E-12
SON	5.91E-12
OCIAD2	6.95E-12
UQCRB	8.24E-12
RP11-395G23.3	8.99E-12

LMOD1	1.01E-11
GABRR3	1.07E-11
PRELID2	1.09E-11
SLC24A2	1.22E-11
KLHL18	1.27E-11
TSPAN13	1.51E-11
SMC3	1.71E-11
PFDN5	1.71E-11
RPS29	1.71E-11
MBNL1	1.76E-11
SEMA3C	2.04E-11
ISOC1	2.25E-11
RPL15	2.25E-11
SEC61G	2.64E-11
MLLT11	2.71E-11
TUBB4B	2.82E-11
C4orf3	3.08E-11
RPGRIP1	3.27E-11
MAPT	3.55E-11
HEG1	3.82E-11
WAPL	4.02E-11
RP11-169K17.3	4.67E-11
RPL26	5.37E-11
KLF6	6.10E-11
EDIL3	6.20E-11
ANKRD33	7.52E-11
ZBTB20	8.09E-11
LYRM1	8.62E-11
HIST1H2BD	9.10E-11
ELOB	9.94E-11
OTX2-AS1	1.07E-10
GAPDH	1.16E-10
FGF12	1.27E-10
ARMC9	1.33E-10
RPL23A	1.34E-10
CADPS	1.36E-10
PLEKHB1	1.40E-10
HNRNPA2B1	1.51E-10
ASPH	1.62E-10
NDUFB4	1.88E-10
FNBP1L	2.04E-10
DPYSL5	2.34E-10

RP11-87G24.2	2.37E-10
ABCA1	2.37E-10
GNG4	2.61E-10
TUBA4A	2.62E-10
CORO7	2.62E-10
TTC3	2.88E-10
RPL18	2.96E-10
TMEM176B	3.07E-10
SSX2IP	3.09E-10
EMB	3.12E-10
RPS20	3.18E-10
RP11-1069G10.1	3.30E-10
VAV3	3.35E-10
CCKBR	3.43E-10
DUSP1	4.23E-10
RPL36	4.24E-10
HSPB1	4.92E-10
HSPH1	4.93E-10
ISL2	5.10E-10
ABCA5	5.81E-10
FAIM	6.88E-10
DPYSL3	7.05E-10
MLXIP	7.49E-10
BTF3	8.63E-10
ABCA7	1.05E-09
SEMA6D	1.09E-09
GATM-AS1	1.09E-09
HIST1H2AE	1.09E-09
RPS21	1.13E-09
CHGA	1.38E-09
RSPH1	1.41E-09
NEGR1	1.42E-09
THSD7A	1.44E-09
DTNBP1	1.48E-09
DDIT3	1.49E-09
BTG1	1.58E-09
RPS17	1.58E-09
NEUROD1	1.62E-09
MAP1LC3B	1.78E-09
TENM2	1.86E-09
UBL5	1.89E-09

PCOLCE2	1.92E-09
MGST3	2.32E-09
LRRC57	2.36E-09
RP11-5O24.1	2.48E-09
RPL14	2.56E-09
RP11-531A24.3	2.70E-09
ATP1B2	2.83E-09
CROCC	2.86E-09
RASSF2	3.29E-09
LRRC39	3.69E-09
MAGEH1	3.91E-09
APMAP	4.22E-09
SND1	4.35E-09
CHN2	4.65E-09
CD27-AS1	4.91E-09
UQCRH	5.17E-09
FAM84B	5.49E-09
SLC29A4	5.51E-09
ALDOC	5.54E-09
MGLL	5.65E-09
DDRGK1	6.00E-09
NRG1	6.02E-09
CEP112	6.20E-09
RBP7	6.36E-09
OSBPL8	6.76E-09
RABL3	6.96E-09
MT-ND4	7.10E-09
RAB41	7.23E-09
TIMELESS	7.70E-09
RTN4	7.81E-09
PGRMC2	7.87E-09
DDX5	8.00E-09
HNRNPDL	8.26E-09
RNF8	8.37E-09
RAB3B	8.50E-09
SYCE1L	8.88E-09
SNCA	8.93E-09
AKAP7	9.01E-09
ARRDC3	9.80E-09
DMD	9.86E-09
SRSF3	9.90E-09

EEF1B2	1.10E-08
PKP2	1.14E-08
DYNC1I2	1.27E-08
HLTF	1.49E-08
IFI27L2	1.53E-08
RAX	1.62E-08
SH3GL2	1.65E-08
SLC6A17	1.83E-08
RPL39	1.91E-08
PRDX5	1.92E-08
KIF19	1.93E-08
TP53INP2	1.94E-08
PKM	2.18E-08
WDR54	2.23E-08
AMER2	2.24E-08
TXNDC12	2.30E-08
ZFHX4	2.33E-08
BARD1	2.40E-08
PCSK1N	2.43E-08
VOPP1	2.53E-08
NEDD4L	2.67E-08
TXNIP	2.75E-08
IFI16	3.05E-08
ARHGAP42	3.08E-08
SYNE2	3.20E-08
TPBG	3.40E-08
NREP	3.43E-08
CYCS	3.44E-08
PPM1J	3.47E-08
ARHGAP10	3.94E-08
NME1	3.98E-08
DAP	4.04E-08
SLC6A6	4.21E-08
FEZ2	4.22E-08
MYL6	4.30E-08
SPTSSA	4.35E-08
ACLY	5.23E-08
PRDX1	6.01E-08
HIST2H2BE	6.02E-08
UBXN4	6.23E-08
SPAG16	6.33E-08
ZFAS1	6.52E-08
RXRG	6.82E-08

NFE2L2	6.93E-08
SRRM4	7.20E-08
AMOTL2	7.58E-08
EEF2	7.61E-08
UNC13C	7.64E-08
CNGA1	7.78E-08
ITGA6	7.86E-08
KIAA1217	8.12E-08
PARP9	8.64E-08
ALDOA	1.01E-07
OPTN	1.06E-07
VDAC1	1.07E-07
TAGLN2	1.08E-07
OSBP2	1.09E-07
RAX2	1.12E-07
ATP5E	1.13E-07
CNTNAP2	1.23E-07
NPPC	1.23E-07
MT-ATP6	1.24E-07
SELENOM	1.27E-07
DCAF1	1.36E-07
THRB	1.42E-07
YBX3	1.43E-07
TDRG1	1.50E-07
SNRPD2	1.55E-07
NFASC	1.68E-07
ECHDC2	1.81E-07
CD63	1.92E-07
SLC38A1	1.94E-07
UBC	1.95E-07
FAM19A4	2.04E-07
LEMD1	2.08E-07
NEIL2	2.10E-07
GLYATL1	2.13E-07
INTS13	2.34E-07
CDK5R1	2.45E-07
CTC-304I17.6	2.46E-07
SCD5	2.49E-07
GRSF1	2.64E-07
OGFOD1	2.75E-07
DPP4	2.93E-07
IGSF9	3.14E-07

CCDC144CP	3.36E-07
RPL9	3.48E-07
DPCD	3.53E-07
EIF3H	3.75E-07
BCL2L11	3.97E-07
SEC62	4.05E-07
ATP5G2	4.09E-07
RTN3	4.22E-07
CABP2	4.31E-07
ANK2	4.44E-07
POLR2L	4.60E-07
TIA1	4.65E-07
NOS1AP	4.70E-07
HOOK1	4.72E-07
TMEM14A	4.76E-07
NKD1	4.79E-07
STAT4	4.83E-07
TLE1	4.99E-07
RBP3	5.05E-07
XKR4	5.10E-07
NEUROG1	5.43E-07
GADD45A	5.43E-07
PPFIBP1	5.69E-07
GSTA4	5.80E-07
RAI14	5.90E-07
SYT13	5.98E-07
PPP1R21	6.27E-07
PPP2R2B	6.39E-07
NUCB2	6.55E-07
RP11-490M8.1	6.66E-07
CRYBG3	6.77E-07
NBEA	6.79E-07
EID1	7.02E-07
EIF1	7.08E-07
H2AFV	8.17E-07
METTL16	8.24E-07
KIF5C	8.27E-07
PNPLA3	8.77E-07
TMA7	9.11E-07
OGFRL1	9.13E-07
MED18	1.03E-06
ORAI2	1.04E-06

RP4-604A21.1	1.05E-06
SEMA3A	1.05E-06
TMEM237	1.05E-06
RP11-25K19.1	1.07E-06
MRPL17	1.07E-06
FMN2	1.11E-06
ARHGEF4	1.14E-06
CANX	1.21E-06
STIP1	1.31E-06
DGKD	1.31E-06
BBX	1.32E-06
ERN1	1.34E-06
MRPS25	1.35E-06
C8orf34	1.36E-06
SNTB2	1.36E-06
CACYBP	1.37E-06
GRB2	1.38E-06
SCRN1	1.38E-06
TFPI2	1.49E-06
AHI1	1.59E-06
ACIN1	1.60E-06
HSPD1	1.74E-06
AKAP13	1.77E-06
RP11-434D9.1	1.82E-06
MAOA	1.85E-06
CCT7	1.86E-06
IDH1	1.95E-06
COX7C	1.98E-06
FUS	2.10E-06
SAT2	2.12E-06
CLSTN1	2.14E-06
SULF1	2.17E-06
FAM171B	2.19E-06
SUCO	2.21E-06
NEBL	2.21E-06
RPL28	2.31E-06
FMN1	2.33E-06
MTUS1	2.39E-06
AC003075.4	2.44E-06
WEE1	2.50E-06
ANKRD6	2.58E-06

RPS4Y1	2.62E-06
ANXA5	2.68E-06
BHLHE41	2.71E-06
H3F3A	2.72E-06
RICTOR	2.86E-06
LIN7A	2.88E-06
CHRNA3	2.90E-06
FAM135B	2.92E-06
LRIT3	2.96E-06
FAM19A3	3.06E-06
EWSR1	3.07E-06
ANK1	3.08E-06
ANK3	3.12E-06
NR3C1	3.14E-06
RTBDN	3.22E-06

Supplementary Table 5: Genes differentially expressed between WT and L75Pfs cones.

Table 9

gene	pval
RPS4X	1.80E-159
RPS4Y1	1.49E-146
OPN1SW	1.79E-62
RPL34	2.35E-57
TTR	2.05E-52
TMSB4X	1.49E-47
MALAT1	3.04E-47
DDX3Y	2.71E-46
MT-ND4	2.68E-44
MAP1B	2.08E-43
GSTP1	1.80E-42
MT-CYB	1.35E-39
TXLNGY	2.04E-37
GNGT1	5.78E-37
DMD	5.39E-36
MT-ND5	4.40E-32
CABP5	4.16E-27
TTTY15	3.84E-25
USP9Y	9.45E-24

MT-ATP6	1.74E-23
COX6C	3.26E-23
HRASLS	8.32E-23
NDUFA4	3.06E-22
CKB	6.64E-21
ARR3	1.29E-20
RS1	1.27E-19
FTH1	1.78E-18
NRL	3.07E-18
YBX1	5.24E-18
PDE6H	1.53E-17
AIPL1	2.28E-17
RPL35A	2.97E-17
NREP	3.09E-17
BEX3	4.44E-17
NDUFS5	4.63E-17
RSPH1	5.75E-17
RP5-958B11.2	7.41E-16
CRABP2	9.35E-16
MORF4L2	1.04E-15
COX7A2	1.14E-15
GNAT1	2.76E-15
RPS2	5.40E-15
TYW3	5.55E-15
RP5-958B11.1	1.10E-14
EIF1AY	1.67E-14
PCP4	2.94E-14
RPL27	2.98E-14
GAPDH	3.96E-14
SMS	4.87E-14
ANK2	5.43E-14
JPX	6.54E-14
CCDC141	6.81E-14
TTN	8.50E-14
RPL13P12	8.99E-14
RPL24	1.00E-13
RPL21	2.38E-13
RPL41	3.11E-13
ACSL4	6.11E-13

RP11-155D18.13	6.90E-13
ITM2C	7.89E-13
PSMD5-AS1	2.08E-12
UQCRQ	2.09E-12
BLOC1S2	2.27E-12
SMARCA1	3.42E-12
RAD17	3.75E-12
MATN2	7.25E-12
CPE	7.55E-12
GYG2P1	8.32E-12
UBB	8.62E-12
BEX2	1.29E-11
DCT	2.11E-11
COX7B	2.72E-11
ROM1	2.91E-11
CCDC173	3.67E-11
ENO2	5.03E-11
PSMD10	6.45E-11
RPS15	6.45E-11
UTY	1.82E-10
ISOC1	2.11E-10
RCVRN	2.47E-10
PCBP4	2.54E-10
RPL37A	2.76E-10
NME1	3.47E-10
PABPC1	4.26E-10
SLC39A5	5.74E-10
UQCRB	5.96E-10
ZNF880	8.51E-10
GRK7	9.42E-10
HPRT1	1.05E-09
CHCHD2	1.10E-09
PGK1	1.14E-09
FSIP2	1.73E-09
NDUFB4	1.78E-09
RPL38	2.27E-09
HIST1H4C	2.58E-09
PRDX4	2.76E-09
CNGB1	3.01E-09

NR2E3	3.25E-09
GABRG2	3.87E-09
NDUFB11	4.13E-09
COX7C	4.14E-09
TERF2IP	5.07E-09
TAPT1	5.16E-09
ELOB	5.21E-09
RPL35	6.90E-09
RPLP2	7.70E-09
ATP5G3	8.12E-09
ETF1P2	8.38E-09
SCG3	1.23E-08
CRYZ	1.87E-08
HSP90AA1	2.06E-08
HLA-V	2.14E-08
RBP3	2.19E-08
C1D	2.21E-08
TCEAL3	2.34E-08
CCDC136	2.44E-08
RP4-604A21.1	2.70E-08
WSB1	2.73E-08
GPM6B	2.93E-08
WDR66	2.99E-08
UBA52	3.00E-08
PARK7	3.28E-08
RPS7	4.03E-08
MOAP1	5.83E-08
PTMA	6.61E-08
COX6B1	6.78E-08
RPS19	7.42E-08
LAPTM4B	7.98E-08
RPL23	9.14E-08
AF127577.8	9.93E-08
RPS27A	1.08E-07
TTC3	1.38E-07
GJC1	1.41E-07
AHI1	1.48E-07
POMP	1.48E-07
RPL36	1.58E-07

IFI27	1.64E-07
COPS9	1.66E-07
RRAD	1.79E-07
HINT1	1.82E-07
RPS8	1.92E-07
RPL10A	2.14E-07
USP11	2.23E-07
RPLP0	2.45E-07
DCBLD2	2.65E-07
GABPB1-AS1	2.66E-07
RP11-87G24.2	2.78E-07
C8orf46	3.18E-07
EIF2S3	3.53E-07
TMA7	3.67E-07
NDUFB2	4.02E-07
BAZ2B	4.76E-07
ATP5H	4.82E-07
RPS24	5.25E-07
UQCR10	5.43E-07
UBL5	6.94E-07
SAMD7	7.29E-07
HIST1H1C	8.51E-07
AGGF1	8.85E-07
JHDM1D-AS1	9.44E-07
SLC40A1	1.14E-06
RPL7	1.28E-06
RPL31	1.36E-06
ZCWPW2	1.36E-06
MRPS18C	1.40E-06
RPL8	1.40E-06
ITM2B	1.47E-06
STAG2	1.50E-06
TTC3P1	1.53E-06
AP1S2	1.60E-06
GNB1	1.67E-06
AC004556.1	1.67E-06
UNC119	2.16E-06
SEC11C	2.18E-06

FRG1HP	2.25E-06
TCEAL9	2.28E-06
LHX3	2.36E-06
LINC02208	2.70E-06
DYNLL1	2.75E-06
C14orf2	3.03E-06
PRDX5	3.18E-06
EFCAB1	3.23E-06
ZNF37A	3.30E-06
BEX4	3.36E-06

Supplementary Table 6: Genes differentially expressed between WT rods and L75Pfs rod-like cells.

Table 10

gene	pval
ROM1	0
TTR	0
GNAT1	0
FABP7	2.90E-307
NRL	1.35E-229
SAMD7	1.33E-210
ISOC1	3.04E-174
CADM1	2.28E-168
AIPL1	5.42E-168
CNGB1	2.93E-166
RCVRN	5.09E-164
OPN1SW	6.47E-154
NR2E3	1.45E-136
GNB1	1.55E-126
RPS4Y1	5.83E-114
CABP5	5.27E-106
UNC119	1.81E-93
PDE6H	2.58E-90
DST	1.06E-84
PDE6G	1.76E-80
MT-ATP6	1.32E-69
EEF1A1	3.16E-69
SAG	2.51E-63

RAX2	3.25E-63
KIF5B	7.53E-58
RPLP1	9.90E-58
DMD	1.60E-55
RPS6	2.87E-50
TMSB4X	3.05E-50
GPR160	3.98E-47
CKB	6.25E-46
PCP4	3.21E-45
RPL13A	6.97E-45
B2M	6.57E-44
MT-ND4	7.77E-44
PTPRZ1	2.26E-43
SPTBN1	2.88E-42
MT-CYB	8.68E-41
REEP6	2.10E-40
RP1	1.49E-35
DDX3Y	6.00E-35
WI2-1896O14.1	3.27E-34
ARR3	1.42E-33
PDE6A	1.53E-32
ROBO2	1.55E-32
SLC29A4	4.13E-32
NCKAP5	1.75E-31
MORF4L2	2.19E-30
SNHG6	9.11E-30
CADPS	2.95E-29
RPS4X	4.52E-28
PRDX1	5.17E-28
DCT	2.37E-26
ALDOC	2.96E-26
PRUNE2	3.67E-26
CCDC136	2.19E-25
ACBD6	2.89E-25
RPS2	1.23E-24
ZNF326	2.37E-24
CTD-2524L6.3	3.15E-24
HLTF	3.46E-24
PRNP	3.65E-24

DARS	7.68E-24
CASC15	1.35E-23
HMGN2	9.52E-23
BEX3	1.09E-22
SPTSSA	3.04E-22
RPS16	3.13E-22
PDC	3.88E-22
MTATP6P1	2.09E-21
TXLNGY	2.67E-21
MT-RNR1	4.22E-21
RPL13	7.80E-21
TTN	1.14E-20
CLUL1	1.26E-20
STC1	1.50E-20
LHX4	2.44E-20
FTH1	3.25E-20
ATP1B1	3.61E-20
RPL10	1.19E-19
JPX	1.24E-19
PEX5L	1.80E-19
ALDH2	2.65E-19
VSX1	6.43E-19
RPS11	6.48E-19
C8orf46	6.89E-19
CPE	7.92E-19
MAP2	8.95E-19
MIAT	1.08E-18
NIPAL1	4.20E-18
MAPT	7.55E-18
DDIT3	9.08E-18
SAMD11	1.02E-17
SHTN1	1.69E-17
ARHGAP10	1.69E-17
BEX2	2.26E-17
PDE6B	2.52E-17
DHRS7	2.71E-17
MXRA5	3.97E-17
RPL27A	5.63E-17
CADM3	8.84E-17
MT-ND5	9.33E-17

PLEKHA5	9.79E-17
TTTY15	9.81E-17
ITGA6	1.23E-16
PALMD	1.28E-16
RPL6	1.38E-16
RPL19	1.45E-16
MT-CO1	2.10E-16
RPS14	2.29E-16
EIF1AY	2.58E-16
RBP1	3.08E-16
SERPINF1	3.14E-16
ZDHHC22	4.35E-16
C6orf48	5.29E-16
NAP1L3	7.38E-16
NEIL2	2.18E-15
PRDM1	4.58E-15
ARL4D	5.02E-15
RPL3	6.94E-15
RPS5	8.56E-15
PIK3R1	9.19E-15
RPS13	1.28E-14
RPLP0	1.29E-14
RPS7	1.47E-14
RPS23	1.58E-14
FAM161A	1.84E-14
H2AFZ	2.89E-14
RORB	2.98E-14
EMC1	6.61E-14
USP9Y	7.58E-14
ITM2C	8.45E-14
RPL4	1.15E-13
MAP1LC3B	1.76E-13
RASSF2	1.84E-13
MAP3K7CL	2.01E-13
RPS27	2.09E-13
AANAT	2.49E-13
PRKG2	3.10E-13
EIF1	3.26E-13
HIST1H2BG	3.31E-13
TCEAL9	4.80E-13

NEUROD1	5.82E-13
PLP1	6.01E-13
CHN2	6.55E-13
RPL7A	7.83E-13
PSMD5-AS1	7.87E-13
PSMD10	8.12E-13
FOS	8.38E-13
MBNL1	9.50E-13
LNPK	1.83E-12
SPAG16	3.53E-12
TDRD9	3.63E-12
RPS3	3.92E-12
GNAT2	4.69E-12
RP11-6E9.5	4.83E-12
RPS3A	6.47E-12
PPP2R2B	7.66E-12
GSTP1	1.08E-11
SEC14L2	1.11E-11
TMX4	1.38E-11
FRMD4A	1.43E-11
TPM1	1.61E-11
PSIP1	1.78E-11
SMARCA1	1.89E-11
GABRR3	2.86E-11
TPI1	2.88E-11
HSP90AB1	3.24E-11
BICD1	3.45E-11
RPS9	3.62E-11
CCKBR	3.93E-11
NDNF	4.30E-11
RUFY3	6.67E-11
WASF3	6.71E-11
CLCN3	7.81E-11
HPRT1	8.58E-11
NREP	8.75E-11
RPS12	8.96E-11
KCNH6	1.08E-10
CC2D2A	1.34E-10
CRABP2	1.39E-10

PHF6	1.49E-10
SPECC1	1.69E-10
GREM2	1.87E-10
TAGLN2	1.90E-10
FSIP2	2.26E-10
KCNAB1	2.36E-10
UTY	2.38E-10
RPS18	2.60E-10
RPL23	3.35E-10
FTX	3.52E-10
ABCA5	4.27E-10
RPS15A	4.37E-10
CNGB3	4.74E-10
SLITRK6	5.00E-10
KIF5C	5.69E-10
OSBPL8	5.78E-10
STMN4	6.05E-10
SMS	6.11E-10
ELFN1	6.23E-10
WAPL	6.95E-10
USP11	7.38E-10
COPZ1	1.03E-09
MT-RNR2	1.05E-09
CADM3-AS1	1.11E-09
MYL6	1.27E-09
MSX1	1.29E-09
MEG3	1.29E-09
EPB41L2	1.36E-09
UGCG	1.40E-09
ENAH	1.67E-09
CYCS	1.79E-09
GABPB1-AS1	2.30E-09
GNB5	2.85E-09
SLC27A6	3.02E-09
KLK10	3.09E-09
METTL16	3.23E-09
GNGT1	3.48E-09
PRDX4	4.14E-09
MAPRE2	4.28E-09

CNGA1	4.87E-09
SEC62	5.05E-09
GSTM3	5.41E-09
CLCN4	5.45E-09
DAXX	5.64E-09
FHOD3	5.64E-09
NDUFAB1	5.90E-09
TTC3P1	6.03E-09
GADD45A	6.29E-09
PCSK5	7.82E-09
HSPA1A	7.82E-09
RP5-958B11.1	7.90E-09
GPR180	8.43E-09
TXLNG	8.55E-09
GNAI3	8.62E-09
CANX	9.91E-09
PPA1	1.01E-08
STAG2	1.06E-08
FAR2P1	1.10E-08
4-Sep	1.16E-08
EFR3A	1.17E-08
EIF2S3	1.18E-08
FZD10-AS1	1.25E-08
RIDA	1.25E-08
NEUROG1	1.28E-08
RGS2	1.44E-08
NEBL	1.50E-08
TCEAL8	1.56E-08
FAM107A	1.60E-08
MT-ND1	1.63E-08
RBBP7	1.65E-08
EFHC1	1.69E-08
PTPRE	1.73E-08
MCC	1.75E-08
KIF19	1.98E-08
EZH2	2.05E-08
FAM19A4	2.39E-08
TMEM138	2.55E-08
IGSF9	2.61E-08

EIF5	2.87E-08
SARS	3.04E-08
TCEAL1	3.12E-08
TXNIP	3.31E-08
ESAM	3.36E-08
GNAO1	3.50E-08
TRAK2	3.84E-08
SIX6	3.96E-08
SYAP1	4.44E-08
CLTB	4.50E-08
DAP3	4.53E-08
DDHD2	4.65E-08
ABCA1	4.70E-08
H3F3B	4.85E-08
CCDC141	5.03E-08
TUBB4B	5.32E-08
ATF4	5.56E-08
KCNG4	5.70E-08
SLC38A1	5.78E-08
PAFAH1B1	5.85E-08
YBX1	6.41E-08
PHACTR2	6.45E-08
UNC13C	6.48E-08
TYW3	6.88E-08
UPP1	7.15E-08
GUK1	7.32E-08
RHOBTB3	7.83E-08
SLC6A17	7.91E-08
KCNIP4	8.32E-08
COL16A1	8.43E-08
PLA2G12A	8.57E-08
KIF21A	9.34E-08
TACC1	9.35E-08
FABP12	9.48E-08
RIMS2	9.61E-08
PPEF2	9.71E-08
LBH	1.11E-07
TRAM1	1.23E-07
OCIAD2	1.29E-07
RPL37A	1.52E-07

ATP5C1	1.58E-07
MAP6	1.77E-07
NCAPG	1.87E-07
CPLX2	1.94E-07
UBE2E3	1.97E-07
ACSL4	2.07E-07
HMGN5	2.07E-07
CROCC	2.16E-07
RACK1	2.45E-07
DDRGK1	2.47E-07
TDRD7	2.62E-07
HOOK1	2.67E-07
STMN1	2.84E-07
KLHL18	2.87E-07
RPL30	2.89E-07
SUPT16H	2.92E-07
HSPH1	3.10E-07
CUL1	3.10E-07
UBE2E2	3.11E-07
TMEM108	3.26E-07
NPTX1	3.35E-07
RP11-395G23.3	3.65E-07
RPS20	3.97E-07
RPS25	4.00E-07
CNTNAP2	4.11E-07
MRPS6	4.21E-07
OPTN	4.50E-07
YPEL2	4.61E-07
COX14	4.69E-07
RAB9B	4.82E-07
CHRM3	4.83E-07
SYCE1L	4.91E-07
TLK1	5.12E-07
OGFRL1	5.22E-07
LEMD1	5.35E-07
PLEKHB1	5.41E-07
DUSP1	5.63E-07
MEGF10	5.79E-07
AKAP9	5.94E-07

MT-ND2	6.19E-07
SMC3	6.20E-07
PLCD3	6.24E-07
NPPB	6.31E-07
SPG20	6.57E-07
SLC3A2	6.67E-07
ANK2	6.76E-07
ATP5A1	6.95E-07
R3HCC1	7.03E-07
ACLY	7.23E-07
TMEM38B	7.57E-07
RP11-490M8.1	7.99E-07
HMGN1	8.43E-07
GRIK1	8.48E-07
NAA25	8.97E-07
MDM2	9.16E-07
CREG1	9.41E-07
JUNB	9.67E-07
TMCC1	9.95E-07
ADGRL3	1.01E-06
ARL5C	1.03E-06
BTG1	1.06E-06
RGS9	1.13E-06
RXRG	1.14E-06
SNTB2	1.17E-06
SH2D4A	1.20E-06
ANKRD33B	1.20E-06
VAV3	1.21E-06
LUZP2	1.22E-06
ATCAY	1.26E-06
ETNK2	1.28E-06
CEBPG	1.37E-06
WWC1	1.44E-06
COX6C	1.53E-06
DGKD	1.56E-06
ZFAS1	1.58E-06
RRAGD	1.58E-06
ABCA7	1.60E-06
ITSN1	1.61E-06

MARK3	1.80E-06
ZSCAN30	1.84E-06
GYG1	1.88E-06
WDR44	1.89E-06
SCAMP1	2.03E-06
TYW5	2.05E-06
ZFYVE16	2.09E-06
RP11-379K17.4	2.15E-06
CNGA3	2.15E-06
HSPA9	2.26E-06
PRCD	2.32E-06
CDKN1C	2.61E-06
CCS	2.64E-06
LCORL	2.68E-06
MRLN	2.75E-06
STRIP2	2.81E-06
PDLIM3	2.91E-06
RPLP2	3.14E-06
HLA-A	3.31E-06
CPEB1	3.41E-06

Supplementary Table 7: Genes differentially expressed between WT cones and L75Pfs rod-like cells.

Table 11

gene	pval
CKB	0
FABP7	0
GUCA1A	0
GUCA1B	0
GUCA1C	0
GUK1	0
ISOC1	0
MALAT1	0
PDE6H	0
TMSB4X	0
GNGT1	2.70E-303
UNC119	1.08E-245

TTR	1.17E-230
MPP4	5.11E-221
ARR3	7.25E-210
MT-CYB	4.40E-188
SAMD7	4.01E-187
MT-ND4	7.72E-171
MYL4	5.89E-168
OPN1SW	1.48E-154
KCNV2	6.37E-143
MT-ND5	2.05E-131
RPS4Y1	2.99E-117
DMD	3.24E-101
MT-ATP6	1.05E-98
ITM2C	5.12E-96
MT-RNR2	1.14E-92
RCVRN	1.80E-83
MRLN	1.63E-81
AIPL1	2.74E-80
PDC	1.95E-79
KIF5B	1.66E-74
CA2	9.09E-74
IRX6	2.87E-73
TUBA1B	1.27E-72
ATP1B1	2.40E-72
PRCD	4.19E-72
OPN1MW	1.32E-71
CPE	1.87E-71
RPS4X	5.26E-71
MAP1B	1.73E-70
HSP90AA1	2.67E-69
NREP	4.07E-66
SOX4	2.97E-65
MYL6	1.27E-62
EIF1	1.81E-60
SEPT4	3.80E-60
CC2D2A	9.89E-60
CTD-2050N2.1	2.35E-59
CNGB3	1.04E-56
PLEKHB1	1.17E-55

RAX2	2.66E-55
H3F3B	1.63E-52
TMSB10	1.76E-52
XRCC4	1.21E-51
PPA1	1.06E-50
MOAP1	1.43E-50
WSB1	1.26E-49
LBH	1.31E-49
DNAJB1	7.96E-47
GNGT2	1.38E-46
RP11-240M16.1	1.61E-44
GNAT2	3.75E-43
CNGB1	7.21E-43
RIMS2	8.35E-43
ARL6IP5	1.25E-42
OTX2	9.88E-42
PCP4	1.31E-41
COTL1	1.43E-41
PRDX1	4.46E-41
RPL34	1.09E-40
ENO2	2.26E-40
DDX3Y	1.12E-39
LMOD1	6.66E-39
RBP3	2.27E-37
ITSN1	4.64E-37
MCF2	7.35E-37
CCDC136	5.50E-36
DTNBP1	6.19E-36
PDE6C	1.92E-35
UCHL1	2.19E-35
GNB3	2.76E-35
CPLX4	8.99E-35
FTH1	1.29E-34
PLA2G5	2.85E-34
B2M	7.44E-34
DCT	1.68E-33
TSPAN7	6.19E-33
TULP1	9.28E-33
CABP5	1.88E-32

PIK3R1	3.76E-32
SCG3	3.93E-32
KIF2A	9.45E-32
TXLNGY	1.71E-31
ITM2B	1.86E-31
STMN1	3.65E-31
TMEM14B	4.76E-31
MORF4L2	1.22E-30
CADM3	1.24E-30
PKIB	1.79E-30
OLFM1	1.80E-30
RABL3	2.06E-30
DPYSL3	2.38E-30
MT-CO2	3.83E-30
GADD45A	5.20E-30
NEUROD4	6.19E-30
RSPH1	2.01E-29
CFAP36	7.11E-29
PROM1	1.04E-28
TPM1	1.13E-28
GAPDH	1.21E-28
EEF1A1	1.48E-28
HSPH1	5.34E-28
HIST1H4C	7.72E-28
SMS	1.13E-27
VOPP1	3.29E-27
FAM57B	4.33E-27
TSPAN3	6.40E-27
NXNL2	7.49E-27
CHRNA3	1.25E-26
NRL	1.45E-26
PPP4R4	1.67E-26
HRASLS	2.39E-26
PGRMC1	2.42E-26
CCDC82	3.29E-26
FAM155A	3.64E-26
RRAD	7.39E-26
GNAI3	9.25E-26
RHOBTB1	2.49E-25
RP11-	2.76E-25

1069G10.1	
GABRG2	3.88E-25
BLOC1S2	4.66E-25
RP11-356I2.4	5.47E-25
ACBD6	6.19E-25
MTATP6P1	6.90E-25
FAM107A	9.01E-25
TMEM14A	1.28E-24
HES6	1.54E-24
ALDOC	1.56E-24
MT-RNR1	4.98E-24
TENM2	5.83E-24
MRPS6	6.25E-24
GPR155	1.03E-23
GSTP1	1.19E-23
MEGF9	2.07E-23
NDUFA4	4.31E-23
RPLP0	5.73E-23
BMP7	6.22E-23
LIMA1	9.60E-23
ZDHHC22	1.01E-22
SLC39A5	1.25E-22
MAP2	1.30E-22
CRYBG3	1.82E-22
C6orf48	2.16E-22
DARS	3.64E-22
RS1	4.64E-22
PPP2R2B	6.21E-22
ROM1	1.10E-21
CREG1	1.57E-21
ANXA4	5.34E-21
GREM2	1.12E-20
TTTY15	1.21E-20
MATN2	1.64E-20
PLP1	2.54E-20
MAP4	2.72E-20
SLC24A2	4.13E-20
SIX6	5.42E-20
AKAP9	6.68E-20
RPL41	1.08E-19

COL4A3	1.40E-19
LHX4	1.45E-19
GNAT1	1.90E-19
USP9Y	2.14E-19
AHI1	2.21E-19
ANKRD33	2.90E-19
PABPC1	3.45E-19
MT-CO1	3.48E-19
MEF2C	5.03E-19
NCKAP5	8.52E-19
ACTB	1.22E-18
VSX1	1.44E-18
NME1	1.62E-18
LINC02115	1.69E-18
KCNB2	1.81E-18
BAZ2B	2.71E-18
GNAS	2.75E-18
EZR	2.94E-18
BEX3	4.26E-18
EMB	4.26E-18
HLA-B	4.34E-18
TUBA4A	4.99E-18
FOS	5.57E-18
SLC3A2	6.30E-18
RTBDN	6.33E-18
PALMD	8.30E-18
H2AFZ	9.01E-18
TMX4	9.18E-18
PDE6D	9.65E-18
DZIP3	1.08E-17
PRDM1	1.09E-17
HSPA1B	1.26E-17
NFKBIZ	1.29E-17
PTPN13	1.45E-17
SELENOW	1.45E-17
KIF21A	1.49E-17
RNF8	1.81E-17
RPGRIP1	2.29E-17
RGS9	2.39E-17
ELOVL4	2.55E-17

HIST3H2A	2.83E-17
MLXIP	3.75E-17
MT-CO3	3.96E-17
FHOD3	4.39E-17
CADM3-AS1	4.87E-17
HLA-A	5.10E-17
JPX	5.72E-17
ZFHX4	1.25E-16
EGR1	1.61E-16
PARP1	2.33E-16
HSPE1	2.60E-16
BAIAP2L1	2.67E-16
TUBA1A	2.98E-16
AC007349.7	3.54E-16
HSPA6	3.72E-16
TAPT1	3.87E-16
IGFBP7	4.52E-16
GSG1	4.99E-16
LRRC4C	5.23E-16
EIF5	5.31E-16
RP11-531A24.3	5.96E-16
HIST1H1C	7.12E-16
LAPTM4B	8.36E-16
PKM	9.36E-16
NRN1	1.07E-15
THRB	1.12E-15
NPPC	1.17E-15
ASPH	1.35E-15
NOS1AP	1.47E-15
PPM1J	1.83E-15
CCDC88A	2.00E-15
TTN	2.14E-15
B3GAT2	2.56E-15
ZNF326	3.58E-15
PHYHIPL	4.75E-15
ARMC9	6.17E-15
SON	6.36E-15
IMPG1	6.75E-15
TDRG1	7.57E-15

CGNL1	1.01E-14
IFI16	1.09E-14
HPRT1	1.10E-14
RPL27	1.35E-14
DYNLL1	1.40E-14
STAG2	1.49E-14
CHCHD10	1.50E-14
MT-ND4L	1.68E-14
TPI1	1.89E-14
TDRD9	1.96E-14
PGK1	1.99E-14
HEG1	2.30E-14
FGF12	2.48E-14
PHACTR2	2.79E-14
MT-ND1	3.47E-14
WBP11	3.54E-14
HIST1H2BG	3.71E-14
RGS20	5.27E-14
KCNG4	6.27E-14
CPLX2	6.53E-14
SLC27A6	6.63E-14
CHGA	6.94E-14
CAPS2	7.77E-14
PSMD10	8.05E-14
PTMA	8.19E-14
RPL38	8.23E-14
RICTOR	9.19E-14
WEE1	9.31E-14
RPS15	1.11E-13
HSPD1	1.40E-13
CACYBP	1.66E-13
DEFB119	1.68E-13
PBX1	1.70E-13
HSP90AB1	1.73E-13
RDH12	1.78E-13
RPLP2	1.80E-13
MFSD11	2.41E-13
MIR7-3HG	2.42E-13
TMEM35A	2.54E-13
RPL13P12	2.74E-13

RPS2	2.79E-13
LCORL	2.90E-13
NCAPG	3.70E-13
GYG2P1	4.00E-13
TMEM176B	6.24E-13
HNRNPH1	6.38E-13
SEMA6D	7.12E-13
ATF3	7.24E-13
MAP3K7CL	7.47E-13
CAMK1D	7.60E-13
MTHFD2	8.46E-13
TMEM108	8.67E-13
RP11-442N1.1	8.95E-13
SAMD15	1.04E-12
NUCKS1	1.08E-12
RP5-958B11.2	1.17E-12
C4orf3	1.49E-12
CDKN1A	1.67E-12
CTD-2034I21.1	1.74E-12
BEX2	1.95E-12
ZNF292	1.99E-12
TYW3	2.24E-12
EIF2S3	2.53E-12
SESN2	2.58E-12
ZNF83	2.86E-12
CADPS	2.89E-12
TERF2IP	3.02E-12
FAM162A	3.72E-12
PRELID2	3.81E-12
FAIM	3.88E-12
NEAT1	4.77E-12
TXLNG	4.97E-12
STMN4	5.03E-12
PHPT1	5.20E-12
RP11-155D18.13	5.52E-12
PRL	5.66E-12
RP5-958B11.1	6.02E-12

RPL10A	6.64E-12
SRSF3	6.77E-12
HERPUD1	6.80E-12
DYNC1LI2	6.86E-12
NCL	7.70E-12
MMD	7.72E-12
SARS	8.05E-12
TMEM47	8.69E-12
PCSK5	8.76E-12
HIST1H1D	9.80E-12
PGRMC2	1.03E-11
CCS	1.06E-11
GLYATL1	1.07E-11
FSIP2	1.28E-11
SPINK4	1.34E-11
BZW2	1.38E-11
PBX3	1.43E-11
PLCD4	1.55E-11
GPM6A	1.95E-11
RAD17	1.99E-11
RP11-314C16.1	2.00E-11
RBP7	2.28E-11
SNAP25	2.39E-11
CHRM3	2.45E-11
MGST3	2.73E-11
RP1L1	2.82E-11
ADD1	2.99E-11
RD3	3.00E-11
IARS	3.18E-11
EIF1AY	3.19E-11
NCAM1	3.25E-11
TLK1	3.52E-11
NKTR	3.53E-11
PDZPH1P	3.58E-11
TCEAL9	4.50E-11
RBBP7	4.89E-11
NOP10	4.90E-11
CMSS1	5.38E-11
SCD5	5.64E-11

ASB13	6.07E-11
JHDM1D-AS1	6.31E-11
SRRM3	6.58E-11
CCNI	6.59E-11
UTP14A	7.41E-11
HSPB1	7.41E-11
SYAP1	7.57E-11
NFIB	7.61E-11
PDE1C	9.05E-11
BBX	9.32E-11
MEGF10	9.42E-11
PKP2	1.04E-10
SOX11	1.14E-10
DCAF1	1.17E-10
FTL	1.22E-10
GPBP1	1.24E-10
SLC29A4	1.26E-10
FZD10-AS1	1.27E-10
LMCD1	1.36E-10
GNG5	1.46E-10
MAP6	1.49E-10
NRXN1	1.56E-10
CEBPG	1.71E-10
LNPK	1.71E-10
GPR160	1.75E-10
FNBP1L	1.87E-10
DCBLD2	1.89E-10
MT-ND2	1.89E-10
PSMD5-AS1	2.18E-10
RAB41	2.18E-10
USP11	2.36E-10
SEC14L5	2.52E-10
ASNS	2.54E-10
CAMK2N1	2.70E-10
CCDC141	2.76E-10
UBXN4	2.92E-10
NELL2	3.03E-10
ATP5G2	3.33E-10
RP11-96L14.7	3.41E-10

PCOLCE2	3.62E-10
POMP	3.83E-10
SLC25A3	3.91E-10
ATP2B1-AS1	3.99E-10
PLEKHA5	3.99E-10
LIN7A	4.05E-10
RPL35	4.11E-10
APP	4.24E-10
CADM1	4.24E-10
NAP1L3	4.28E-10
EGFLAM	4.36E-10
VDAC1	4.68E-10
TBC1D23	4.73E-10
RPL37	4.82E-10
BCLAF1	4.87E-10
SCAMP1	4.96E-10
FABP12	5.17E-10
LINC00575	5.54E-10
AF131216.5	5.70E-10
BARD1	5.72E-10
U2SURP	6.34E-10
HNRNPDL	6.98E-10
GOLGA1	7.41E-10
RPL24	7.80E-10
STIP1	7.84E-10
FAR2P1	8.13E-10
PHGDH	8.13E-10
LMO4	8.14E-10
HIST1H1E	8.16E-10
DDAH2	8.86E-10
PCMTD1	9.04E-10
REV3L	1.04E-09
GNB2	1.12E-09
FAM161A	1.14E-09
LPCAT1	1.17E-09
UBB	1.19E-09
RPL13A	1.22E-09
LIPG	1.23E-09
MLLT11	1.24E-09
JAM3	1.34E-09

H2AFY2	1.40E-09
NDFIP1	1.40E-09
DPF3	1.49E-09
RASA2	1.57E-09
TOX	1.57E-09
AGAP1	1.60E-09
FARP1	1.61E-09
PDLIM3	1.64E-09
RPL35A	1.77E-09
LHX3	1.88E-09
XIAP	2.12E-09
ZADH2	2.37E-09
PAPOLA	2.67E-09
ELSPBP1	2.71E-09
GTF2I	2.78E-09
CBX3	2.80E-09
PCBP4	2.93E-09
ATP5A1	2.97E-09
HIST1H2BD	3.09E-09
DCLK2	3.22E-09
FRMPD2	3.51E-09
GRIK1	3.51E-09
FMN1	3.57E-09
WDR54	3.57E-09
8-Mar	3.73E-09
RPL36	3.74E-09
VPS26A	3.80E-09
CLSTN1	3.87E-09
FAM135B	4.14E-09
TRMT44	4.19E-09
HNRNPA3	4.24E-09
RNF170	4.55E-09
C10orf76	4.73E-09
ERN1	4.73E-09
MCC	4.74E-09
CTNNA1	4.85E-09
CCT4	4.91E-09
RCN1	5.90E-09
ISL2	6.03E-09
ATP5G1	6.17E-09

UBC	6.20E-09
TRIM37	6.24E-09
PBRM1	6.31E-09
PRDX3	6.38E-09
GABPB1-AS1	6.83E-09
TSPAN13	7.07E-09
FAM19A3	7.11E-09
XPC	7.18E-09
TCEAL8	7.72E-09
WASF3	7.78E-09
PPM1N	7.81E-09
GOLGA4	7.97E-09
EPB41L1	8.47E-09
IDH1	8.68E-09
CCDC39	9.24E-09
QPRT	9.65E-09
SNX29	9.74E-09
PAQR9-AS1	9.90E-09
GOLIM4	1.01E-08
ECHDC2	1.03E-08
ATP2C1	1.05E-08
CEBPD	1.05E-08
WDR47	1.06E-08
NUDC	1.10E-08
UBE2Q2	1.16E-08
C1orf226	1.17E-08
FAM84B	1.19E-08
PHF6	1.21E-08
NRIP1	1.25E-08
GOLGB1	1.25E-08
DPYSL5	1.26E-08
NSUN6	1.27E-08
WDR1	1.30E-08
FTX	1.32E-08
HEBP2	1.32E-08
SLC2A11	1.39E-08
CD55	1.43E-08
ST13	1.51E-08
RCAN3	1.60E-08
RTN4	1.60E-08

CRYZ	1.62E-08
SHTN1	1.74E-08
CLSTN2	1.74E-08
TRIM36	1.82E-08
EPB41L3	1.84E-08
PKN2	1.84E-08
CACNA2D4	1.86E-08
R3HCC1	1.87E-08
ENOX2	1.92E-08
KIAA0408	1.94E-08
RPL26	1.97E-08
H2AFX	2.01E-08
TLN2	2.09E-08
AHSA1	2.19E-08
ORAI2	2.25E-08
TEX2	2.29E-08
AANAT	2.32E-08
TMEM98	2.43E-08
TTC3P1	2.52E-08
CTC-304I17.5	2.63E-08
KDM5B	2.70E-08
BHLHE41	2.78E-08
CTC-304I17.6	2.80E-08
RAB3B	2.81E-08
SCAMP5	2.96E-08
IDS	3.06E-08
EIF4EBP1	3.19E-08
DDX46	3.34E-08
RLF	3.38E-08
C1QTNF4	3.66E-08
PLA2G4C	3.67E-08
TFPI2	4.02E-08
SDC2	4.08E-08
MAGED2	4.13E-08
ARHGAP10	4.22E-08
RAB6B	4.33E-08
YTHDC1	4.47E-08
SMC4	4.48E-08
NISCH	4.55E-08

BAG3	4.55E-08
ARL4D	4.56E-08
DPCD	4.65E-08
HSPA4	4.78E-08
ANK1	4.88E-08
PIGF	4.95E-08
ZFHX3	5.04E-08
EML4	5.12E-08
SCAMP1-AS1	5.14E-08
MT-ND6	5.20E-08
TRAK2	5.21E-08
TCEAL3	5.40E-08
RP11-169K17.3	6.11E-08
LGALSL	6.13E-08
DLL1	6.28E-08
UTY	6.47E-08
TLX2	6.59E-08
REST	6.72E-08
MRPL58	7.09E-08
LINC00599	7.37E-08
LGMN	7.48E-08
KIF9	7.56E-08
SNCA	7.71E-08
RPS18	7.74E-08
RAB2A	7.77E-08
CALCOCO2	8.02E-08
BRINP1	8.51E-08
AMER2	8.63E-08
FAM218A	8.92E-08
NPPB	8.95E-08
DDIT3	9.18E-08
TBX2	9.25E-08
ROBO2	9.27E-08
NANOS1	9.47E-08
CABP4	9.69E-08
MARK3	1.03E-07
SLC6A6	1.15E-07
ZCCHC7	1.26E-07
HNRNPM	1.27E-07

GRSF1	1.28E-07
RUFY2	1.29E-07
PTPN11	1.33E-07
ELFN1	1.33E-07
F5	1.36E-07
ELOB	1.37E-07
RPL3	1.41E-07
RIMS1	1.43E-07
FYN	1.49E-07
KCNAB1	1.54E-07
MAK	1.55E-07
ARID4B	1.55E-07
KCNH6	1.62E-07
MAP1LC3B	1.73E-07
C1GALT1	1.73E-07
TAF1B	1.83E-07
HMGN1	1.86E-07
INTS13	1.89E-07
TUBB4B	1.97E-07
GJD2	2.06E-07
MYO16	2.10E-07
KCTD20	2.12E-07
SLC8A1	2.22E-07
MTFR1	2.23E-07
ZEB2	2.35E-07
ST3GAL5	2.36E-07
MRFAP1	2.40E-07
RBP4	2.41E-07
SAT2	2.49E-07
NXNL1	2.51E-07
RPS16	2.58E-07
CWC15	2.60E-07
DAB1	2.66E-07
RPS27	2.75E-07
TCF7L2	2.80E-07
NPC2	2.81E-07
EXOSC8	2.86E-07
PGP	2.87E-07
PRDX5	2.94E-07
ALDOA	2.98E-07

PRSS23	3.02E-07
YWHAE	3.23E-07
SELENOF	3.32E-07
AHSA2	3.33E-07
DNPH1	3.39E-07
RPL37A	3.43E-07
MYLK	3.59E-07
QTRT2	3.67E-07
PLD4	3.68E-07
OTX2-AS1	3.82E-07
RHEB	3.88E-07
RPS17	3.91E-07
MCUR1	3.99E-07
HNRNPH3	4.01E-07
TBX2-AS1	4.04E-07
RPL23	4.10E-07
ZFAND5	4.10E-07
NUP62	4.12E-07
C7orf73	4.15E-07
CASK	4.40E-07
MPST	4.43E-07
BCL2L13	4.65E-07
PLA2G4C-AS1	4.74E-07
PAK3	4.76E-07
AMN1	4.84E-07
NEURL1	4.87E-07
BEND5	4.90E-07
TXNDC12	4.94E-07
LHFP	4.98E-07
NME5	5.00E-07
GAS7	5.17E-07
GARS	5.32E-07
HLA-DPB2	5.36E-07
RP11-384P7.7	5.39E-07
KLF6	5.40E-07
SYTL4	5.59E-07
KMT2A	5.63E-07
NUDT15	5.67E-07
GABARAPL2	5.78E-07

RAB9A	5.79E-07
EAPP	5.85E-07
PRPF6	5.88E-07
RPL36AL	6.60E-07
SQSTM1	6.70E-07
PRKG2	6.77E-07
PTPRR	6.98E-07
HNRNPA2B1	6.99E-07
PTPRE	7.15E-07
TCEAL4	7.36E-07
MEIS2	7.36E-07
SLC44A1	7.94E-07
RIOX2	8.42E-07
IFT22	8.60E-07
NRXN3	8.76E-07
H1F0	8.80E-07
CTD-2521M24.11	8.85E-07
NRSN1	8.89E-07
ANAPC16	9.04E-07
PUM2	9.06E-07
HSPA9	9.11E-07
PAX6	9.37E-07
PTPRZ1	9.38E-07
SPEN	9.47E-07
VANGL1	9.53E-07
RB1CC1	9.54E-07
THOC1	9.74E-07
FIGN	1.00E-06
ACTG1	1.01E-06
ANKMY2	1.02E-06
ATP6V0E2	1.05E-06
GPM6B	1.05E-06
ADGRL3	1.08E-06
MOSPD1	1.09E-06
SLC1A7	1.11E-06
PPP1R21	1.11E-06
ZFX	1.12E-06
EPHX2	1.13E-06
RPS3	1.13E-06

RP11-352M15.2	1.14E-06
ISCU	1.16E-06
S100A6	1.18E-06
CFAP97	1.22E-06
SLC6A15	1.22E-06
WFDC1	1.22E-06
MDM2	1.23E-06
AEN	1.28E-06
TMEM251	1.29E-06
SULT1A1	1.29E-06
PRKAA2	1.31E-06
SMARCE1	1.37E-06
IGF2BP3	1.37E-06
VPS36	1.38E-06
LINC00632	1.42E-06
OLAH	1.45E-06
RPL30	1.46E-06
TLE1	1.48E-06
CDR1-AS	1.48E-06
C16orf74	1.52E-06
ABHD14A	1.55E-06
CCDC77	1.55E-06
HSP90B1	1.60E-06
CREBRF	1.62E-06
SNRPE	1.62E-06
FAM138D	1.62E-06
RAB9B	1.66E-06
TBL1XR1	1.66E-06
AIFM1	1.68E-06
CNRIP1	1.72E-06
EZH2	1.78E-06
SLC2A1	1.86E-06
GPLD1	1.91E-06
FRMD4A	1.92E-06
PSAT1	1.97E-06
TTLL7	2.13E-06
UQCRH	2.13E-06
PRPH2	2.15E-06
NPM1	2.22E-06

SLK	2.27E-06
BEX4	2.36E-06
TRIM14	2.37E-06
MYO10	2.39E-06
CEP95	2.41E-06
TOP1	2.43E-06
RTF1	2.44E-06
RHOC	2.48E-06
C11orf58	2.61E-06
VAPA	2.64E-06
GON7	2.65E-06
FAM213A	2.68E-06
BTF3	2.69E-06
HNRNPU	2.71E-06
RBPJ	2.79E-06
CADM2	2.83E-06
SCARB2	2.90E-06
BCO2	2.90E-06
FRG1HP	2.91E-06
TCF25	2.97E-06
ANKRD33B	2.98E-06
MAP7D1	3.02E-06
UQCR10	3.06E-06
PRDX6	3.12E-06
CD200	3.13E-06
NELFCD	3.19E-06
CFAP221	3.20E-06
TRAK1	3.21E-06
MIAT	3.21E-06
FXR1	3.24E-06
AP1AR	3.30E-06
TBL1X	3.38E-06
TRMT112	3.39E-06

Chapter 3: Modeling LCA in human stem cell derived retinal organoids

Characterization of CRB1 and RPGRIP1 KO human retinal organoid models of LCA and identification of ER stress as a common degenerative pathway

Abstract

Photoreceptor loss is a largely untreatable cause of blindness, and LCA is the most severe form of retinal degeneration, with patients being severely visually impaired within the first year of life. There are over 20 known causative genes, and identification of degenerative pathways shared across different genetic models could provide targets for therapeutic development. To address this need, we generated retinal organoid models of LCA due to CRB1 or RPGRIP1 loss and characterized these models histologically and transcriptomically over a time course of development. Mutant organoids exhibited different histological aberrations, with CRB1 KO organoids developing a thickened ONL and aberrant rhodopsin expression pattern, while RPGRIP1 KO organoids suffered ONL thinning and an absence of outer segment discs. Despite histological differences, we report convergence upon DDIT3 induction and ER stress as a common degenerative pathway across these genetically different LCA models, and this pathway may provide therapeutic targets for retinal degeneration treatment.

Introduction

Normal visual perception begins with a series of signal transduction events in the neural retina, with photoreceptors detecting photons of lights and ultimately transmitting this signal to the brain (1, 2). Vision can be impaired by various genetic and environmental insults, and disorders of the retina typically result from degeneration of retinal ganglion cells, retinal pigmented epithelium, and photoreceptors. Inherited retinal

degeneration is an important cause of irreversible vision loss, with over 200 genes known to cause this heterogeneous set of disorders (RetNet). Photoreceptor cell death can result from a variety of diseases, including Macular Degeneration, Retinitis Pigmentosa, and Leber Congenital Amaurosis (LCA) (85). While great advances in gene therapy have recently been made for the treatment of LCA due to RPE65 mutation, the other forms of inherited retinal degeneration remain largely untreatable (27). Better understanding of the complex gene expression patterns directing photoreceptor degeneration could elucidate the mechanisms of photoreceptor death and identify potential therapeutic targets.

LCA is the most severe form of inherited retinal degeneration, with patients exhibiting blindness or severe visual impairment within the first year of life (9, 10). There are over 20 genes known to cause LCA, and they manifest as a variety of inheritance patterns and phenotypes (9). LCA can exhibit autosomal dominant or recessive inheritance patterns, affect either photoreceptor or retinal pigmented epithelium function, and photoreceptor death can occur as either rod-cone or cone-rod dystrophies (9, 10). Mouse models have been useful to study the degenerative phenotype of different forms of LCA, including LCA due to mutation of Aipl1, Crb1, Gucy2e, Nmnat1, Rpe65, Lrat, and Rpgrip1 (19-21, 24-26). While murine studies have provided important insights into the pathology of LCA, human models of LCA could facilitate identification of new therapeutic targets. Importantly, due to the heterogeneity of LCA and other inherited retinal degenerations, mutation and gene independent treatment options could be effective across many subsets of patients.

Recently, stem cell-derived retinal organoid culture has become a well-established system for modeling retinal development and disease in a human system (22, 23, 36-51, 86). Retinal organoids have been shown to provide valuable insights into both development and degeneration, including models of retinal disease due to

mutations in NRL, CEP290, RPGR, CRB1, and AIPL1 (22, 23, 38, 47, 86). In addition to advances in tissue culture systems in studying retinal disease, single cell RNA sequencing (scRNAseq) has proven powerful across many retinal development and degeneration models (37, 44, 46, 50, 54-60). scRNAseq has enabled elucidation of the critical gene expression alterations occurring in both murine and human retinal development, as well as disease. We have previously shown the utility of combining scRNAseq and retinal organoids to gain insights into another form of inherited retinal degeneration, Enhanced S Cone Syndrome (86).

In this study, we utilized a similar methodology to characterize photoreceptor degeneration in two human models of LCA. We used CRISPR/Cas9 genome engineering to generate human induced pluripotent stem cell (iPSC) lines lacking either functional CRB1 or RPGRIP1, genes known to harbor null alleles causing autosomal recessive forms of LCA, and differentiated these cells into retinal organoids to model a time course of LCA (87, 88). Over 6 time points from days 70 to days 225, we have performed immunohistochemistry (IHC) and scRNAseq to identify both transcriptional and histological alterations occurring over disease progression. We have identified distinct histological aberrations in both knockouts (KO's), as well as induction of DNA Damage Inducible Transcript 3 (DDIT3) and endoplasmic reticulum stress as a common degenerative pathway. Our identification of a shared photoreceptor cell stress pathway may provide targets for therapeutic intervention in the treatment of LCA and possibly other diseases of photoreceptor degeneration.

Methods

Cell and retinal organoid culture

EP1 stem cells were grown in mTeSR1 (Stem cell tech 05850) on matrigel (BD Biosciences 354230) coated plates and maintained by passaging with accutase (Sigma

A6964-100ml). After passaging cells were plated in mTesr with blebbistatin (Sigma B0560-1mg). Organoids were differentiated according to Wahlin et al 2017. Stem cells were dissociated to single cells then plated at 3000 cells per well in 96 well U-bottom plates in mTesr with 5 uM blebbistatin. On day 1 organoids were fed BE6.2 media (10 mL E6 stock [100 mL water, 97 mg insulin (Roche 11376497001), 53.5 mg holo-transferrin (Sigma T0665-500MG), 320 mg L-ascorbic acid (Sigma A8960-5G), 5 uL of 14 mg/mL sodium selenite (Sigma S5261-10G)], 5 mL B27 without vitamin A (Gibco 12587010), 2.5 mL Glutamax (Gibco 16140071), 2.5 mL MEM NEAA (Gibco 11140-050), 2.5 mL sodium pyruvate (Gibco 11360-070), 1 mL 219 g/L NaCl, DMEM (Gibco to 250 mL) plus 2% v/v matrigel and 3 uM Wnt inhibitor (EMD Millipore 681669). On days 2-3 organoids were fed with BE6.2 plus 1% v/v matrigel and 3uM Wnt inhibitor, then 50% media exchange with BE6.2 plus 1% v/v and 3 uM Wnt inhibitor on days 4-7. 50% exchange was continued on days 8-9 with only BE6.2. On day 10 organoids were transferred to 10 cm dishes and fed with BE6.2 plus 100 nM SAG (EMD Millipore 364590-63-6) until day 12. Optic vesicles were manually excised from organoids using tungsten needles from days 10-14. Organoids were fed with LTR medium (125 mL F12 (Gibco 11765), 50 mL FBS (Gibco 16140071), 10 mL B27 (Gibco 17504044), 5 ml Glutamax, 5 mL MEM NEAA, 5 ml sodium pyruvate, 500 uL 1M taurine (Sigma T-8691), and DMEM up to 500 mL) plus 100 nM SAG until day 18. Organoids were fed with only LTR medium on days 18-19. From days 20-27, organoids were fed with LTR plus 500 nM retinoic acid (Sigma R2625-50mg), and days 28-42 with LTR plus 500 nM retinoic acid and 10 uM DAPT (Calbiochem 565770). Organoids were fed with LTR plus 500 nM retinoic acid until day 120, then fed with only LTR.

CRISPR gene editing

EP1 stem cells were dissociated and plated in at ~50,000 cells per well in a 24 well plate with mTeSR plus blebbistatin. The following day, transfection was performed by applying a mixture of 50 uL OptiMEM (Thermofisher 31985062), 2 uL Lipofectamine Stem (Thermofisher STEM00015), and 350-500 ng plasmid containing the gRNA, Cas9 gene, and puromycin resistance cassette. Cells were treated with 0.9 ug/uL puromycin (Sigma P8833) ~40 hours after transfection to select for cells that had taken up the guide plasmid. Cells were then passaged, plated as single cells, and colonies were screened for loss of the wild type allele using HpyAV (NEB R0621S) for RPGRIP1 and Taq$^{\alpha}$1 (NEB R0149S) or MseI (NEB R0525S) for CRB1. Clones containing mutations were sanger sequenced to determine the mutated sequence. Genomic integrity after gene editing was confirmed by karyotyping (KaryoStat, Thermofisher).

Fixation and immunohistochemistry

Organoids were fixed on ice in 4% PFA (Electron Microscopy Sciences 15710) in 0.1 M PB-5% sucrose for 25 minutes then immersed in 6.75% sucrose-PBS for 1 hour, 12.5% sucrose-PBS for 1 hour, 25% sucrose-PBS overnight, and 2:1 25% sucrose-PBS/OCT (Tissue-Tek 4583) for one hour. Frozen 10 um sections were mounted on Superfrost plus slides (Thermofisher) and stored at -80. Sections were blocked in PBS with 0.5% Triton X-100 (Sigma 10789704001) and 10% normal donkey serum (Sigma D9663). Primary antibodies were incubated overnight at 4 degrees in PBS with 2% normal donkey serum and 0.15% Triton X-100. The list of primary antibodies can be found in Supplementary Table 8. Secondary antibodies (Invitrogen, 1:1000) were incubated for 1.5-2 hours at room temperature in PBS with 2% normal donkey serum. Antibody conjugations to distinguish between primary antibodies of the same species were performed using APEX Antibody Labeling Kits (Invitrogen).

Imaging and quantification

Images were taken using either an EVOS microscope or Zeiss LSM 510 confocal. Expression of DDIT3 and RCVRN in confocal images were quantified by total pixel intensity and pixel area of the maximum intensity Z projection. Nested ANOVAs were performed using sections (4-6 per organoid) nested within biological replicates (3 per genotype).

Electron microscopy

Organoids were fixed in cold 2.5% glutaraldehyde/2% PFA in 0.1N cacodylate buffer (pH 7.3), post fixed in cold 1% osmium tetroxide, dehydrated using a graded series of EtOH and embedded in LX112 resin (Ladd Research Industries, Williston, VT). Ultra-thin sections (68nm) were cut on a Leica UC7 ultramicrotome and stained with uranyl acetate and lead citrate and imaged using transmission electron microscopy (Hitachi H7600).

Single cell dissociation and capture

Organoids were individually dissociated to single cells for up to 2 hours with 200 uL of papain solution containing 700 uL water, 100 uL cysteine (6 mg/mL, Sigma W326305), 100 uL EDTA (10mM, Corning 46-034-CI), 10 uL BME (60 mM, Sigma M6250), papain to 1 mg/mL (Worthington LS003126), and 5 uL DNAse (Roche 04716728001). Dissociations were quenched with media containing 10% FBS plus 5 uL DNAse. Dissociated cells were applied to a cell strainer, washed with HBSS, and resuspended at 120,000 cells per mL in HBSS plus 1% BSA (10 mg/mL). Single cells were captured with dropseq beads via a home made Dropseq platform and beads were processed according to the published Dropseq protocol (Macosko et al 2015). Multiplexed libraries were sequenced on the Illumina NovaSeq.

Bioinformatics

Fastq files were processed according to the Dropseq cookbook to extract digital expression matrices (57). Expression matrices were read into R and analyzed using the Seurat v3 R package (89). Cells with greater than 5000 UMIs, less than 200 genes, or greater than 15% mitochondrial content were excluded from the analysis. The WT dataset was merged with either the RPGRIP1 KO dataset or the CRB1 KO dataset by identifying integration anchors with which to integrate the datasets. Differential gene expression within each identified cell population was performed using the fit models function in the Monocle3 R package to identify genes differentially expressed based on genotype (90). For non-photoreceptor populations, a less stringent threshold of 3 cells expressing each gene tested was used for differential gene expression. Photoreceptor populations were extracted from WT, RPGRIP1 KO, and CRB1 KO datasets and read into the Monocle3 R package and analyzed separately as all rods and all cones. Differential gene expression was performed using the fit models function to identify genes expressed in at least 10 cells that were differentially expressed based on genotype and age. These genes were then organized into modules of covarying genes to track how expression of each module varied across time in each genotype.

Results

Generation and histological characterization of LCA organoids

CRISPR/Cas9 was used to perform gene editing via non-homologous end joining on a previously characterized iPSC line, EP1 (49). Compound heterozygotes were generated for both CRB1 and RPGRIP1 and karyotypes were confirmed to be normal by karyostat (Supplementary Fig. 1A-D). CRB1 KO was confirmed by IHC, with only WT organoids exhibiting CRB1 expression along the outer limiting membrane

(Supplementary Fig. 1E). We then sought to characterize possible alterations to the outer nuclear layer (ONL) over a time course of development in WT and KO organoids. Organoids were stained for nuclei and CRX expression at days 90, 120, 150, 190, and 225 and the width of the CRX+ ONL was measured relative to the nuclei dense, organized retinal region of the organoid (Fig. 1A-O). In comparing CRB1 KO (Fig. 1A-E) to WT (Fig. 1F-J) organoids, the ONL thickness was comparable across most time points. However, at day 225, CRB1 organoids exhibited ONL thickening relative to WT, similar to that observed in CRB1 KO LCA patients (Fig. 1E and J) (91). Unlike most retinal degenerations where the ONL thins over time, patients with LCA due to CRB1 loss demonstrate thick, disorganized retinas (91). This thickening at day 225 *in vitro* was statistically significant, with quantification of CRB1 KO versus WT ONL thickness shown in Figure 1P (Wilcoxon Rank Sum Test, p=0.05). In comparing RPGRIP1 KO (Fig. 1K-O) to WT (Fig. 1F-J) organoids, the ONL thickness was comparable at the early time points, but showed ONL thinning at later time points. Quantification showed significant ONL thinning at day 150, and increased thinning at days 190 and 225. At day 225, the ONL comprised ~45% of the optic vesicle thickness in the WT organoids, compared to ~30% for RPGRIP1 KO (Wilcoxon Rank Sum Test, p=0.05) (Fig. 1Q). Of note, the difference at day 150 was predominantly driven by one RPGRIP1 KO replicate, while all replicates at days 190 and 225 had consistently thinner ONL's compared to WT. This dramatic loss of ONL thickness over time indicated that RPGRIP1 KO photoreceptors were dying as the organoids matured.

After characterizing gross ONL dynamics over time, we performed histological characterization in mature, opsin-expressing rods and cones via IHC staining for RCVRN, RHO, and ML-opsin in day 225 sections. While overall organization of RPGRIP1 KO opsin-expressing photoreceptors appeared comparable to WT (Supplementary Fig. 2A-H), CRB1 KO organoids exhibited a striking RHO+ rod

phenotype (Fig. 1, WT in R-U, CRB1 KO in V-Y). In all three CRB1 KO d225 organoids imaged, RHO expressing rods were not present adjacent to ML-opsin+ cones, rather disorganized patches of RHO expression were detectable in the most interior part of the ONL. Additionally, these RHO+ rods lacked apparent outer segment-like projections. Because of the role of CRB1 in maintaining adherens junctions, it is possible that mature photoreceptors lose their ability to maintain cell-cell adhesion, causing their abnormal localization within the ONL (91, 92). This localization could prevent proper interactions with bipolar cells to transmit signals or improperly localize opsins and thus prevent photon detection, either of which could contribute to visual loss for LCA patients. While organization of RPGRIP1 KO organoids appeared comparable to WT, photoreceptor morphology did not appear normal (Supplementary Fig. 2A-H). Opsin staining localized primarily to cell bodies and little staining was observed in outer segments. We sought to characterize possible defects in RPGRIP1 KO photoreceptor morphology, as RPGRIP1 is thought to interact with RPGR to support outer segments (93). Additionally, a similar study of RPGR KO organoids identified various morphological aberrations in outer segment morphology. Because of the close interactions between RPGR and RPGRIP1, as well as the opsin staining in day 225 photoreceptor cell bodies, we postulated that the RPGRIP1 KO organoids may also produce abnormal outer segments (38). We performed electron microscopy on WT and RPGRIP1 KO organoids at day 245. All 3 WT organoids imaged had evidence of discs in the outer segments, while 0/3 RPGRIP1 organoids had produced discs (Fig. 1Z). While discs were absent in RPGRIP1 KO photoreceptors, gross outer segment morphology appeared comparable to WT. This data provides evidence that disc morphogenesis does not occur in the absence of RPGRIP1 *in vitro,* which may contribute to vision loss suffered by LCA patients lacking RPGRIP1. Lack of disc morphogenesis may prevent proper localization of opsins and

other critical phototransduction proteins in the outer segments, thus severely limiting ability to detect and respond to light.

scRNAseq characterization of LCA organoids

To gain further insights into the molecular aberrations occurring in the absence of CRB1 or RPGRIP1, we performed scRNAseq via Dropseq over days 70, 90, 120, 150, 190, and 225 (57). Across all 6 time points 20,849 cells were captured from WT organoids, 31,138 from CRB1 KO, and 36,067 from RPGRIP1 KO. Each KO dataset was integrated with WT and cells were clustered using UMAP in Seurat (89). All stereotypical cell populations were present in each genotype, including neural progenitor cells, retinal progenitor cells, retinal ganglion cells, horizontal cells, amacrine cells, bipolar cells, retinal pigmented epithelium, muller glia, rods, and cones (Fig. 2A-B, Supplementary Fig. 3 and 4). We also identified an unknown cluster expressing some ciliary margin genes (Supplementary Fig. 5A-B). The distribution of mitochondrial gene content, number of genes captured, and number of transcripts captured confirmed that these features were not driving clustering (Supplementary Fig. 6A-F). For each cell population, we performed differential gene expression tests using Monocle3 to identify genes differentially expressed between each KO and WT (90). As expected, most cell types had very few genes differentially expressed between WT and KO. In comparing CRB1 KO and RPGRIP1 KO to WT, amacrine cells, horizontal cells, bipolar cells, retinal pigmented epithelium, and the unknown cluster all had less than 35 genes differentially expressed (Supplementary Tables 1 and 2). The lack of many differentially expressed genes in these non-photoreceptor cell types serves as an important internal control for batch effects. While retinal ganglion cells, retinal progenitor cells, and neural progenitor cells had >70 genes differentially expressed between KO and WT, gene ontology analysis did not reveal any clear biologically significant pathways from the differentially

expressed gene sets (Supplementary Tables 3 and 4). Of non-photoreceptor populations, muller glia were the most different in WT versus KO organoids, with 879 genes and 788 genes differentially expressed between CRB1 KO and RPGRIP1 KO muller glia compared to WT, respectively. This degree of differential gene expression was unsurprising considering the role of muller glia in retinal degeneration and photoreceptor cell death (94). We performed gene ontology analysis on gene sets enriched in KO muller glia compared to WT (82). Interestingly, both RPGRIP1 KO and CRB1 KO muller glia were highly enriched for terms related to chaperone mediated autophagy (CMA) (Table 1). CMA has been shown to be an important pathway in both photoreceptors and retinal pigmented epithelium during retinal degeneration, as dysregulation of protein and organelle homeostasis contributes to cell stress (95-97). To our knowledge, there have been no reports of CMA dysregulation in muller glia of degenerating retinas. While reactive gliosis of muller glia is known to contribute to retinal degeneration, further investigation into the role of muller glia CMA could provide additional insights into the extent of muller glia involvement in degenerative phenotypes (94).

We then sought to identify and characterize transcriptomic alterations in photoreceptor populations over the time course of differentiation. Photoreceptors of all 3 genotypes were subsetted and reclustered in Monocle3 (Fig. 2C, Supplementary Fig. 7) (90). We then performed differential gene expression tests based on age and genotype separately for rods and cones. 534 and 789 genes were differentially expressed in the rod and cone populations, respectively (Supplementary Table 5). Of note, the number of genes differentially expressed for the photoreceptor populations is lower than that of the muller glia as more stringent thresholds were set for photoreceptors to limit the effect of possible uninteresting sources of variation and batch effects (minimum 10 cells expressed for photoreceptor genes compared to 3 for non-photoreceptors). These

genes were then clustered into modules of differentially expressed genes to create a heatmap of expression level of each module in each group of cells, with cell groups designated with the genotype and time point. For differentially expressed genes in cones, modules 1, 4, 8, 9, 12, 13, 15, and 16 were enriched at the earlier time points, whereas modules 2, 3, 5, 6, 7, 10, 11, 14, and 17 were enriched at the later time points (Fig. 2D). As expected, the modules expressed highly at the later time points were enriched for GO terms related to more mature photoreceptor characteristics such as guanylate cyclase activity and cone development, while the modules enriched in the less mature cells corresponded to GO terms not specific to photoreceptor function (Supplementary Table 6). For rods, modules 2, 3, 4, 6, 8, 9, and 10 were enriched at earlier time points, while modules 1, 5, 7, and 13 were enriched at later time points (Fig. 2E). Modules 11 and 12 did not seem to exhibit a clear pattern over age. GO analysis for rods revealed similar results to cones, with modules expressed in mature rods highly enriched for GO terms related to rhodopsin signaling and guanylate cyclase activity. These time point-dependent modules confirmed expected transitions towards photoreceptor-specific functions as organoid photoreceptors matured.

We then sought to identify modules that were enriched based on genotype using a minimum expression difference of 0.5 between WT and KO photoreceptors. For cones, modules 12 and 13 were enriched in WT and depleted in both KO's (Fig. 3A). The genes in these modules were enriched for the mitochondrial ATP synthesis coupled electron transport GO term (p value = 3.93e-7, fold enrichment = 16.16), indicating that the WT cones may be more metabolically active, whereas the KO cones seem to be downregulating energy production. Modules 9 and 14 were enriched in both CRB1 KO and RPGRIP1 KO cones compared to WT, which corresponded to GO terms related to the unfolded protein response, cell stress, and aggrephagy (Supplementary Table 7). Modules 9 and 14 included many heat shock genes, and interestingly the endoplasmic

reticulum (ER) stress induced pro-apoptotic gene DDIT3 (98). The enrichment of these genes in both KO's compared to WT cones indicated that ER stress may be involved in photoreceptor degeneration. Additionally, the most highly enriched GO term related to NOD2 signaling, a pathway that has been shown to mediate ER stress (99). Taken together, these results suggest that ER stress may be an important degenerative pathway in KO cones. In rods, modules 2, 8, 9, and 12 were enriched in WT compared to KO photoreceptors (Fig. 3B). These genes corresponded primarily to GO terms related to translational and ribosomal processes (Supplementary Table 7). Modules 1, 3, 5, 7, 11, and 13 were enriched in KO rods. While these modules also included many heat shock genes and DDIT3, the enriched GO terms were predominantly related to rhodopsin signaling and photoreceptor development (Supplementary Table 7), possibly due to lower capture of WT rods at later time points. The similarity between GO terms corresponding to WT rod enriched modules and early age dependent modules provides additional support for the effect of maturity distributions on genotype dependent modules in rods.

To determine if DDIT3 and other cell death-related genes were enriched in KO photoreceptors regardless of age distributions, we next regressed out the effect of age prior to differential gene expression analysis. Using a list of cell death related genes obtained from Qiagen, we performed differential gene tests between KO and WT rods and cones (Table 2). DDIT3 was significantly enriched in RPGRIP1 KO rods, CRB1 KO rods, and CRB1 KO cones, with average expression level and percent of cells expressing DDIT3 shown in Figure 3C-D. Many genes enriched in WT compared to KO were protective against stress and cell death, including BAG1, DAD1, GSTP1, PRDX5. Interestingly, GSTP1, the only gene consistently downregulated compared to WT across all photoreceptor groups, has been shown to be protective against neurotoxic conditions (100). Altogether, the single cell transcriptomics and differential gene expression

analysis suggest that induction of DDIT3 and ER stress may serve as a common pathway underlying the photoreceptor degeneration seen with RPGRIP1 and CRB1 associated LCA.

ER stress in LCA organoids

Next we sought to validate DDIT3 enrichment at the protein level by performing IHC for DDIT3 and RCVRN and comparing both the relative area and intensity of DDIT3 signal to RCVRN over all time points. At day 150, the area and intensity of DDIT3 expression were significantly enriched in CRB1 KO organoids, but not RPGRIP1 KO organoids, relative to WT (Fig. 4A-K) (Nested ANOVA, $p<0.05$). Of note, RPGRIP1 KO replicate 1 was excluded from the area analysis due to significant inter-replicate variation. Interestingly, this outlier organoid was also the main driver of significant ONL thinning relative to WT at day 150. At day 190, both KO's exhibited significant enrichment of both area and intensity of DDIT3 expression relative to WT (Fig. 4L-V) (Nested ANOVA, $p<0.05$). While both KO's appear to be converging on a shared ER stress response and induction of DDIT3, the duration and onset differs between KO's. CRB1 KO organoids appear to activate DDIT3 earlier and maintain ER stress over a longer time range, whereas RPGRIP1 KO organoids exhibited a rapid spike in DDIT3 expression and ER stress at day 190. It is possible that these differences in onset and duration are due to the specific roles and temporal expression patterns of CRB1 and RPGRIP1 in photoreceptor development and maturation. Despite these differences, the convergence upon ER stress provides a possible degenerative pathway to target for therapeutic intervention. Examination of other LCA models for evidence of ER stress could provide further support for this pathway as a therapeutic target.

Discussion

In this study, we have characterized the histological and transcriptomic changes occurring over development in two genetically distinct retinal organoid models of LCA, and identified DDIT3 induction and ER stress as a common degenerative pathway across both models. In the case of the CRB1 KO organoids, we report thickening of the ONL and aberrant ONL organization at day 225, with RHO expression occurring in patches in the most internal region of the ONL. These findings partially recapitulate the Crb1 KO mouse model, *rd8*, in which mice exhibit retinal disorganization (92). Homozygous *rd8* mice suffer structural alterations due to the loss of adherens junctions, and this loss could also explain both the abnormal localization of RHO+ rods within the ONL and patchy expression of RHO+ within the photoreceptors (92). Similarly, a second Crb1 KO mouse model also recapitulates the phenotype of photoreceptor displacement due to the loss of adhesion between photoreceptors in the ONL (92). The presence of this phenotype in both murine models of Crb1 loss and our retinal organoid model supports the role of CRB1 in maintaining organization of the ONL in both mice and humans. While organization is disrupted in both murine and human models, *rd8* mice also suffer rosette formation and thinning of the ONL, findings not recapitulated in the CRB1 KO organoids described here (92, 101). Despite the absence of these phenotypes in CRB1 KO organoids, these observations were reported for aging mice whose time course of degeneration was likely beyond the window of organoid development in this study. It is possible that organoids at a later time point more consistent with aged mice could recapitulate these phenotypes *in vitro*. Additionally, both murine and other human organoid models of retinitis pigmentosa due to CRB1 mutation report loss of outer limiting membrane integrity (47, 92, 101). The CRB1 KO organoids described here differ from previously described retinal organoids differentiated from patient iPSC lines with CRB1 mutations in that we did not observe disruptions to

outer limiting membrane integrity (47). However, previous organoid models of CRB1 mutation produced a variant protein, as opposed to total loss of CRB1 protein in the organoids described here, which could explain the differences in phenotype (47). While the CRB1 KO organoids displayed some differences to other *in vitro* human models and *in vivo* mouse models, the retinal thickening and abnormal organization are consistent with observations of LCA patients with CRB1 loss (91, 92).

In the case of the RPGRIP1 KO organoids, we report dramatic thinning of the ONL over time, opsin expression incorrectly localizing primarily to photoreceptor cell bodies, and absence of outer segment discs. ONL thinning due to photoreceptor loss and abnormal pattern of opsin staining are both phenotypes also present in two mouse models of RPGRIP1 loss (102, 103). In both the Rpgrip1^{tm1Tili} and Rpgrip1^{nmf247} mouse models, opsins are mislocalized to cell bodies rather than photoreceptor outer segments (102, 103). This is consistent with the RPGRIP1 KO organoid phenotype, and improper localization of opsins in both murine and human models supports the proposed role of RPGRIP1 in trafficking proteins to the outer segments. While ONL thinning and mislocalization of opsins are phenotypes consistent with mouse models of Rpgrip1 loss, the outer segment phenotype is different from the murine phenotypes. This may be due to the different cellular localization of RPGRIP1 in humans and mice, with human RPGRIP1 localizing to outer segments and murine Rpgrip1 localizing to the connecting cilium (102-104). In the Rpgrip1^{tm1Tili} mouse, disc morphogenesis does occur, however discs appear swollen with a larger than normal diameter (103). This is in contrast to the Rpgrip1^{nmf247} mouse, which exhibits a more severe phenotype in which photoreceptors rarely develop outer segments (102). The RPGRIP1 KO organoids described here differ from both of these murine phenotypes, with an intermediate severity of outer segment formation but absence of discs. Because genetic background affects the outer segment phenotype in Rpgrip1 KO mice, it is possible that other human models of RPGRIP1 loss

may also exhibit a range of severity with regard to outer segments and disc morphogenesis. Because RPGRIP1 is thought to interact with RPGR to facilitate ciliary transport in photoreceptors, the phenotypes associated with RPGRIP1 loss could be expected to overlap with RPGR phenotypes (104). A previous study of retinal organoids with RPGR loss reported abnormal photoreceptor morphology, as well as a decrease in photoreceptor cell number relative to control organoids (38). These findings are consistent with the RPGRIP1 KO organoid phenotypes reported here. While both RPGR and RPGRIP1 KO organoids exhibit photoreceptor loss and abnormal morphology, the morphological changes differ. RPGR KO organoids exhibited RHO staining in outer segments, but abnormal outer segment morphology, whereas RPGRIP1 KO organoids had primarily RHO expression in the cell body portion of the photoreceptor (38). These differences in opsin localization may be attributed to the different severities of disease due to RPGR or RPGRIP1 loss and the degree of impact on ciliary transport. Because LCA is more severe than retinitis pigmentosa caused by RPGR loss, ciliary transport may be more affected leading to a more severe trafficking defect and the opsin expression pattern seen in RPGRIP1 KO organoids.

While CRB1 and RPGRIP1 KO organoids represent different genetic causes of LCA and exhibit different histological pathologies, both models converge on ER stress as a common degenerative pathway. At the later time points, both KO's exhibited induction of DDIT3, a key event in ER stress mediated cell death (98). Our results are consistent with previous reports that ER stress has been shown to be an important cause of cell death in various forms of neurodegeneration, including retinal degeneration, possibly due to the sensitivity of neurons to cell stress (105). In retinal degeneration, ER stress is a common mechanism of cell death due to misfolding and accumulation of mutant rhodopsin (106-108). While protein misfolding is a frequent cause of ER stress, photoreceptors have also been shown to induce DDIT3 and ER stress mediated in cell in

environmental models of excess light exposure (108, 109). The CRB1 and RPGRIP1 KO organoids described here differ from these causes of ER stress in that there is an absence of a critical protein, as opposed to accumulation of misfolding proteins or environmental stressors. Rather, based on the histological findings in these KO's, it is likely that ER stress resulted from improper protein trafficking to outer segments. In the case of CRB1 KO organoids, we have shown that RHO does not localize to outer segments, and is rather expressed in patches in the internal most part of the ONL. This finding and the role of CRB1 in establishing photoreceptor polarity suggest that opsins are not properly trafficked to the outer segments. Similarly, RPGRIP1 KO organoids also likely exhibit a protein trafficking defect. The complete absence of outer segment discs and predominantly cell body staining of opsins is also suggestive of a defect in trafficking of opsins and other phototransduction proteins. Improper protein trafficking has also been previously identified as a cause of ER stress and photoreceptor cell death in models of achromatopsia and LCA due to loss of Lrat (110-113). Specifically, cone opsin mistrafficking leads to ER stress and cell death in Lrat KO LCA mice and achromatopsia mouse models of Cnga3 or Cngb3 loss (111-113). These findings support opsin mistrafficking in CRB1 KO and RPGRIP1 KO organoids as a potential cause of ER stress and cell death. Because both LCA models described here induced DDIT3 expression and ER stress, targeting this pathway may decrease the degree of photoreceptor cell death and lessen the severity of visual impairment for patients. Inhibition of ER stress has been shown to promote photoreceptor survival in P23H rats, making this an attractive target for therapeutic intervention (114). However, because the P23H mutations leads to an accumulation of mutant rhodopsin, further studies are required to determine if inhibition of ER stress can attenuate photoreceptor degeneration resulting from protein mistrafficking, as well as the utility of targeting this pathway in retinal degeneration treatment.

DATA AVAILABILITY

All fastq files and expression matrices can be found on GEO accession GSE152212.

Table 1: GO enrichment analysis of genes differentially expressed between WT and KO muller glia.

Table 12

CRB1 KO muller glia

GO biological process (parent)	fold enrichment	raw P value	FDR
chaperone-mediated protein transport involved in chaperone mediate autophagy	93.08	6.65E-04	3.88 E-02
positive regulation of intrinsic apoptotic signaling pathway by p53 class mediator	55.85	6.38E-05	5.55 E-03
positive regulation of tau-protein kinase activity	53.19	3.87E-06	4.46 E-04
SRP-dependent cotranslational protein targeting to membrane	43.63	1.01E-54	1.62 E-50
viral transcription	36.42	7.28E-52	2.32 E-48
mammalian oogenesis stage	34.91	1.84E-04	1.39 E-02
nuclear-transcribed mRNA catabolic process, nonsense-mediated decay	34.91	3.51E-51	9.32 E-48
retinoic acid biosynthetic process	31.03	2.43E-04	1.76 E-02
translational initiation	29.29	2.50E-48	4.42 E-45
negative regulation of ubiquitin protein ligase activity	27.93	3.13E-04	2.10 E-02

WT muller glia (compared to CRB1 KO)

GO biological process (parent)	fold enrichment	raw P value	FDR
receptor-mediated virion attachment to host cell	21.06	1.07E-03	3.79 E-02
positive regulation of axon extension involved in axon guidance	20.06	1.65E-04	9.47 E-03
SREBP signaling pathway	15.6	3.41E-04	1.66 E-02
commissural neuron axon guidance	11.7	8.13E-04	3.12 E-02

epithelial cell maturation	10.97	2.26E-04	1.20E-02
apical protein localization	10.8	1.04E-03	3.72E-02
cellular response to low-density lipoprotein particle stimulus	9.75	3.57E-04	1.71E-02
mRNA splice site selection	9.06	9.53E-06	1.07E-03
regulation of cholestrol biosynthetic process	8.98	2.18E-07	5.11E-05
positive regulation of transcription from RNA polymerase II promoter involved in cellular response to chemical stimulus	8.78	1.48E-04	8.72E-03

RPGRIP1 KO muller glia

GO biological process complete (parent)	fold enrichment	raw P value	FDR
chaperone-mediated protein transport involved in chaperone-mediated autophagy	99.77	5.80E-04	3.31E-02
negative regulation of polynucleotide adenylyltransferase activity	99.77	5.80E-03	3.30E-02
positive regulation of nucleotide-binding oligomerization domain containing 2 signaling pathway	66.51	9.61E-04	4.78E-02
protein targeting to lysosome involved in chaperone-mediated autophagy	66.51	9.61E-04	4.76E-02
positive regulation of tau-protein kinase activity	57.01	2.95E-06	3.52E-04
SRP-dependent cotranslational protein targeting to membrane	32.22	1.30E-34	2.07E-30
chaperone cofactor dependent protein refolding	28.06	2.09E-10	3.96E-08
viral transcription	27.76	5.73E-34	1.82E-30
chaperone-mediated protein complex assembly	27.71	2.67E-06	3.24E-04
negative regulation of inclusion body assembly	27.21	3.23E-04	2.05E-02

WT muller glia (compared to RPGRIP1 KO)

GO biological process complete (parent)	fold enrichment	raw P value	FDR
metanephric nephron tubule formation	29.84	4.76E-04	2.52E-02
positive regulation of axon extension involved in axon guidance	22.74	1.03E-04	7.50E-03
transmembrane receptor protein tyrosine phosphatase signaling pathway	19.9	1.10E-03	4.94E-02
SREBP signaling pathway	17.69	2.14E-04	1.36E-02

commissural neuron axon guidance	13.26	5.14E-04	2.66E-02
otic vesicle development	10.61	1.03E-03	4.66E-02
cellular response to sterol	9.47	3.73E-04	2.11E-02
neuron projection regeneration	9.28	2.78E-05	2.80E-03
regulation of cholestrol biosynthetic process	8.33	4.30E-06	6.64E-04
cholestron biosynthetic process	7.76	2.30E-05	2.40E-03

Table 2: Differential gene expression of cell death related genes between WT and KO photoreceptors. Positive estimate indicates WT enrichment.

Table 13

	RKO cones			RKO rods	
gene	estimate	q value	gene	estimate	q value
BAG1	0.505	2.86E-06	DDIT3	-0.411	8.08E-04
DAD1	0.277	2.14E-04	GPX1	0.461	3.93E-03
GSTP1	0.33	1.40E-21	GSTP1	0.21	4.26E-04
GADD45G	0.464	8.62E-06	HSPA5	-0.524	1.85E-08
PRDX5	0.247	7.72E-06	PTPN13	-0.254	8.93E-05
			YWHAE	-0.278	3.67E-04

	C13 cones			C13 rods	
gene	estimate	q value	gene	estimate	q value
APP	0.346	4.35E-03	BNIP3	0.395	1.71E-07
BAG1	0.35	8.16E-03	DAD1	0.394	1.49E-02
CLU	-0.563	9.27E-03	DDIT3	-0.421	1.22E-04
DAD1	0.463	2.60E-13	GSTP1	0.159	2.10E-02
DDIT3	-0.297	1.20E-04	HSPA5	-0.449	1.76E-06
GSTP1	0.349	4.96E-25	JUN	0.251	3.83E-03
JUN	-0.252	2.17E-04	JUNB	-0.798	2.80E-02
NPM1	0.131	1.74E-02	PTPN13	-0.324	2.60E-10
YWHAE	-0.195	8.24E-04	TNFAIP3	-1.21	1.39E-04
GADD45G	0.569	9.17E-09	YWHAE	-0.388	3.73E-11
MTCH1	0.414	4.52E-05	GADD45G	0.629	6.26E-09
PRDX5	0.291	1.61E-08	MTCH1	0.486	1.78E-02
NLRP2	0.739	3.81E-02			

Figure 1: Histological characterization of LCA organoids. A-O) Staining for nuclei (blue) and CRX (red) over days 90 **(A, F, L)**, 120 **(B, G, L)**, 150 **(C, H, M)**, 190 **(D, I, N)** and 225 **(E, J, O)** in CRB1 KO **(A-E)**, WT **(F-J)**, and RPGRIP1 KO **(K-O)** organoids showing increase in ONL thickness in CRB1 KO organoids and ONL thinning in RPGRIP1 KO organoids. **P-Q)** Quantification of ONL thickness in CRB1 KO **(P)** and RPGRIP1 KO **(Q)** organoids relative to WT. Red asterisk denotes statistically significant differences. **R-Y)** Staining for ML opsin **(R, V)**, RHO **(S,W)**, and RCVRN **(T,X)** and merge **(U,Y)** in WT **(R-U)** and CRB1 KO **(V-Y)** organoids at day 225 showing aberrant RHO+ expression in CRB1 KO organoids. **Z)** Electron microscopy images of day 245 WT (upper) and RPGRIP1 KO (lower) organoids showing outer segment discs present in WT and absent from RPGRIP1 KO photoreceptor outer segments.

Figure 25

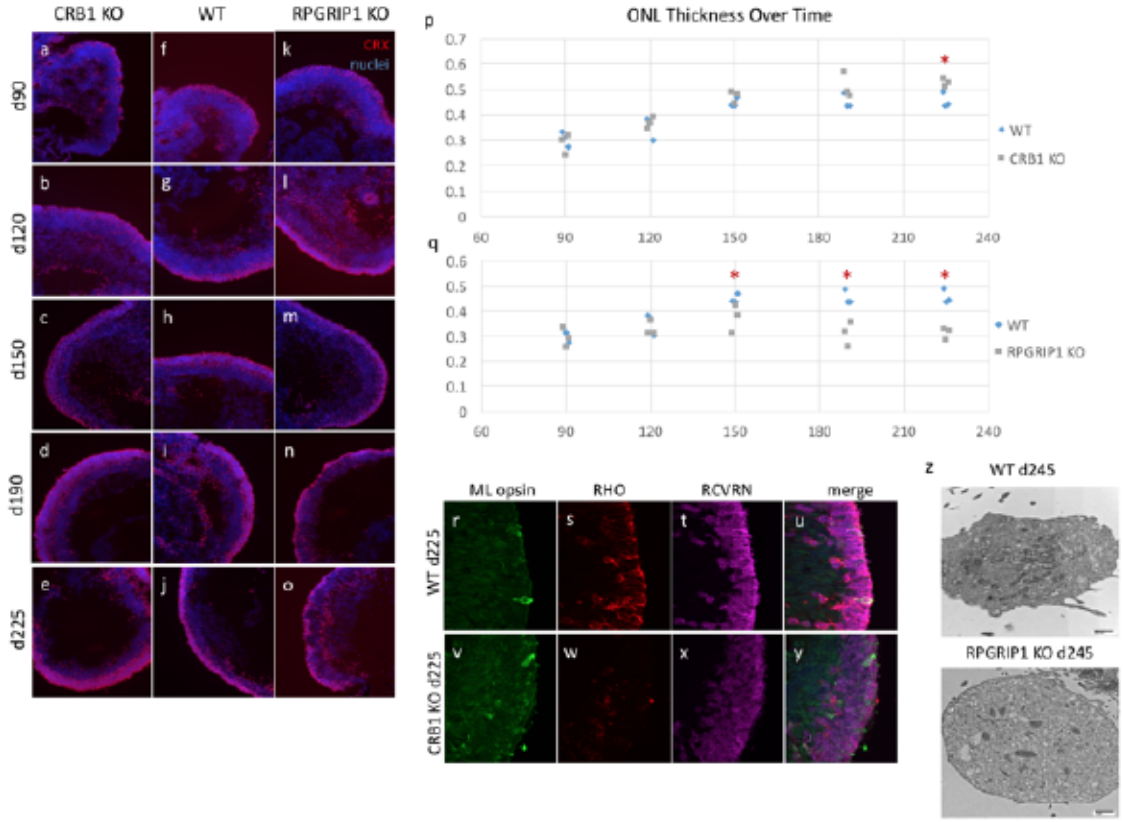

Figure 2: Single cell clustering of organoids over all time points and identification of modules of co-regulated genes in cones and rods. A-B) UMAP clustering of WT cells merged with CRB1 KO **(A)** and RPGRIP1 KO **(B)** cells showing presence of all stereotypical retinal cell populations. **C)** Subsetted and reclustered photoreceptors from all 3 genotypes. **D-E)** Modules of covarying differentially expressed genes across age and genotype in cones **(D)** and rods **(E)**.

Figure 26

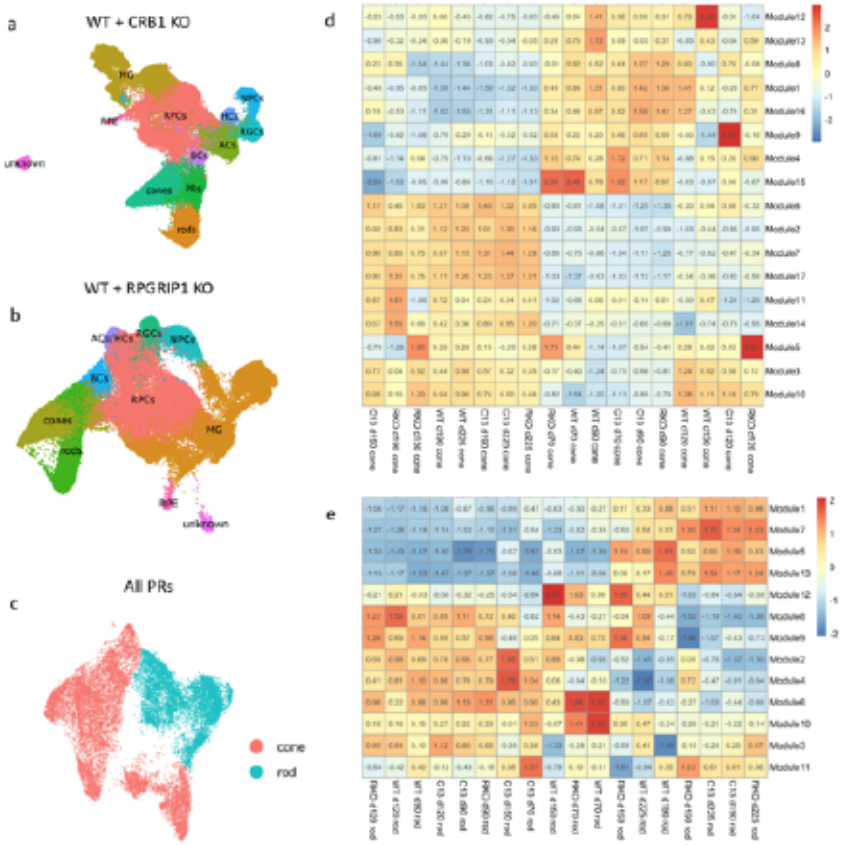

Figure 3: Gene modules varying by genotype and identification of KO enrichment of DDIT3. A-B) Expression of modules of covarying differentially expressed genes by genotype in cones **(A)** and rods **(B)**. **C-D)** Average expression level and percent of cells expressing DDIT3 by genotype in cones **(C)** and rods **(D)** showing enrichment of DDIT3 in RPGRIP1 KO rods and CRB1 KO rods and cones.

Figure 27

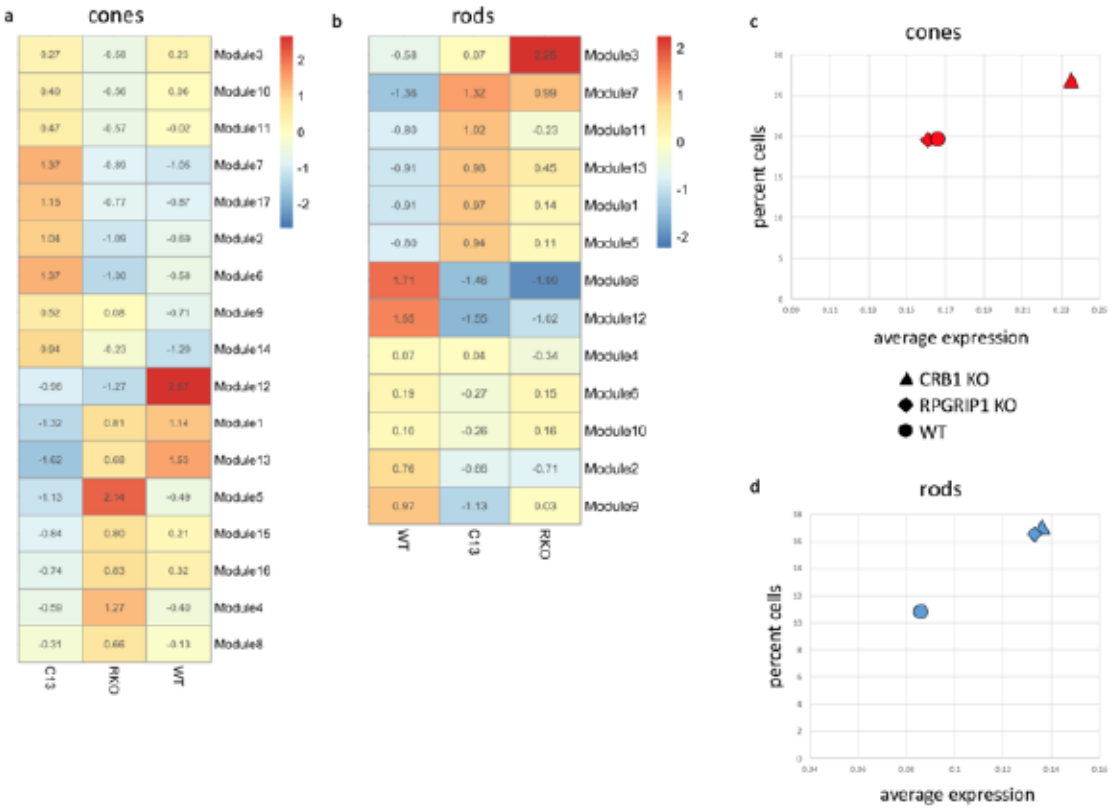

Figure 4: DDIT3 protein is enriched in KO organoids relative to WT at days 150 and 190. A-I) Expression of RCVRN **(A, D, G)** and DDIT3 **(B, E, H)**, merge in **C, F, I,** in CRB1 KO **(A-C)**, WT **(D-F)**, and RPGRIP1 KO **(G-I)** organoids at day 150. **J-K)** Quantification of DDIT3 expression relative to RCVRN in terms of pixel intensity **(J)** and pixel area **(K)** shows significant enrichment of DDIT3 in CRB1 KO organoids. RPGRIP1 KO replicate 1 was removed from the analysis due to significant inter-organoid variability. **L-T)** Expression of RCVRN **(L, O, R)** and DDIT3 **(M, P, S)**, merge in **N, Q, T**, in CRB1 KO **(L-N)**, WT **(O-Q)**, and RPGRIP1 KO **(R-T)** organoids at day 190. **U-V)** Quantification of DDIT3 expression relative to RCVRN in terms of pixel intensity **(U)** and pixel area **(V)** shows significant enrichment of DDIT3 in CRB1 KO and RPGRIP1 KO organoids. Error bars represent standard deviation of sections.

Figure 28

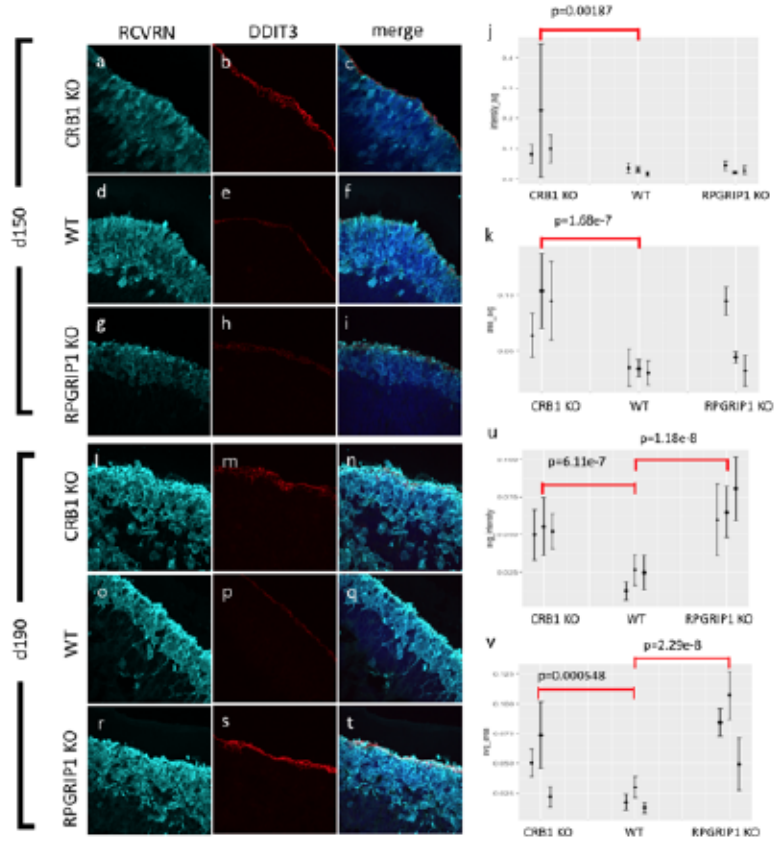

Supplementary Materials

Supplementary Figure 1: Generation and validation of LCA KO's. A-B) CRISPR generated mutations in CRB1 **(A)** and RPGRIP1 KO **(B)** cell lines. **C-D)** Genomic integrity of CRB1 KO (**C**) and RPGRIP1 KO **(D)** cell lines by karyostat. **E)** Validation of CRB1 KO by IHC for nuclei (blue) and CRB1 (green) in WT (left) and CRB1 KO (right) organoids at day 225 showing no CRB1 protein in CRB1 KO organoids.

Figure 29

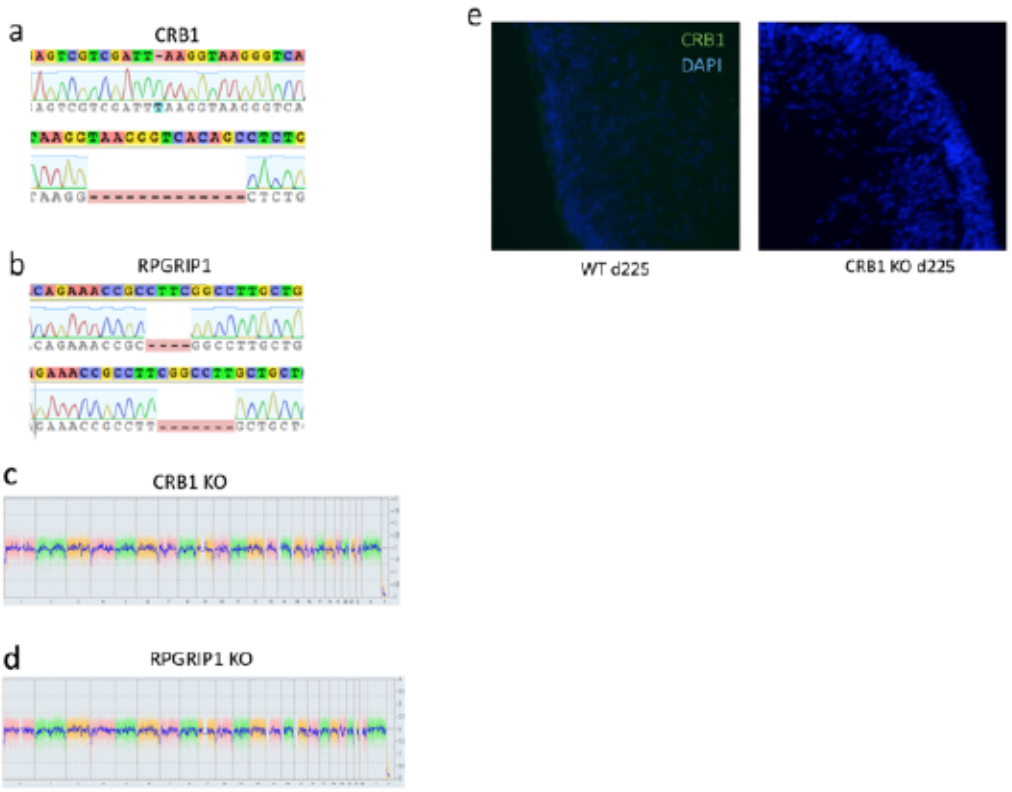

Supplementary Figure 2:

RPGRIP1 KO organoids have normal retinal organization but abnormal photoreceptor morphology. A-H) Staining for ML opsin **(A, E)**, RHO **(B, F)**, RCVRN **(C, G)**, and merge **(D, H)**, in WT **(A-D)** and RPGRIP1 KO **(E-H)** organoids at day 225.

Figure 30

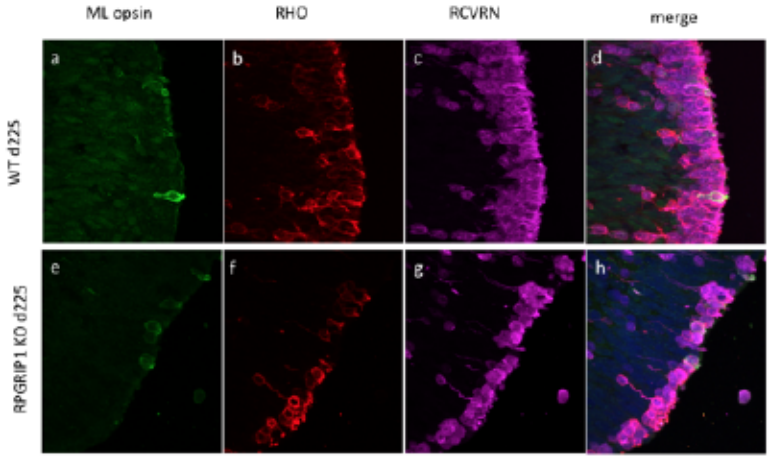

Supplementary Figure 3: Cell populations of merged WT and CRB1 KO organoids. **A-B)** UMAP showing only WT **(A)** and CRB1 KO **(B)** cells. **C)** Cells colored by age of organoid. **D)** Marker gene expression used to call population identity.

Figure 31

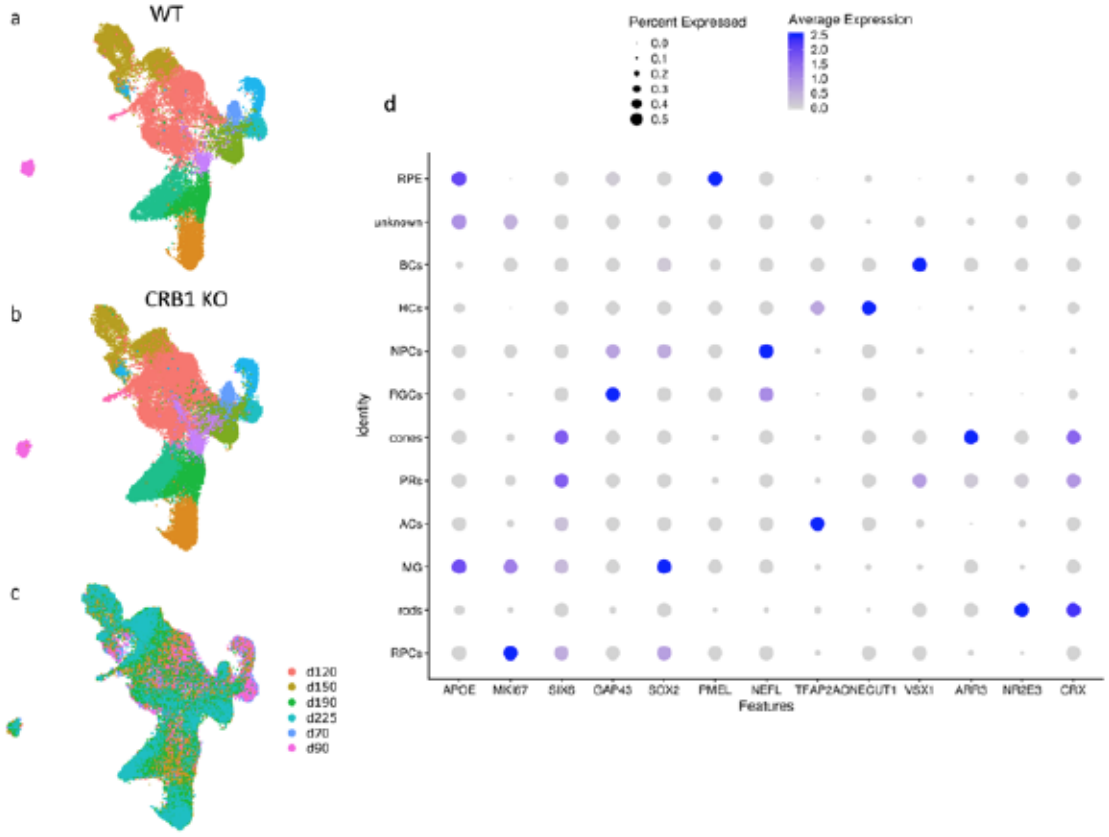

Supplementary Figure 4: Cell populations of merged WT and RPGRIP1 KO organoids. A-B) UMAP showing only WT **(A)** and RPGRIP1 KO **(B)** cells. **C)** Cells

Figure 32

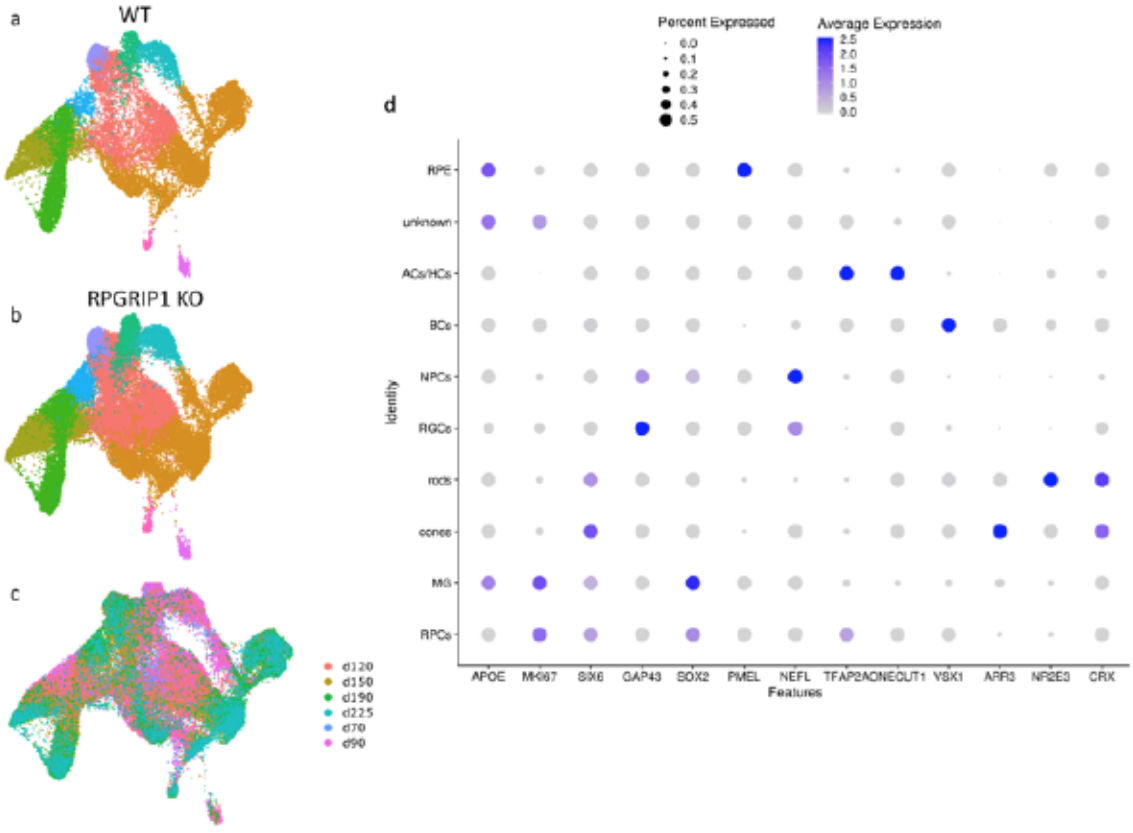

Supplementary Figure 5: Expression of some ciliary margin genes in unknown cell population of merged WT and CRB1 KO (A) or merged WT and RPGRIP1 KO (B) datasets.

Figure 33

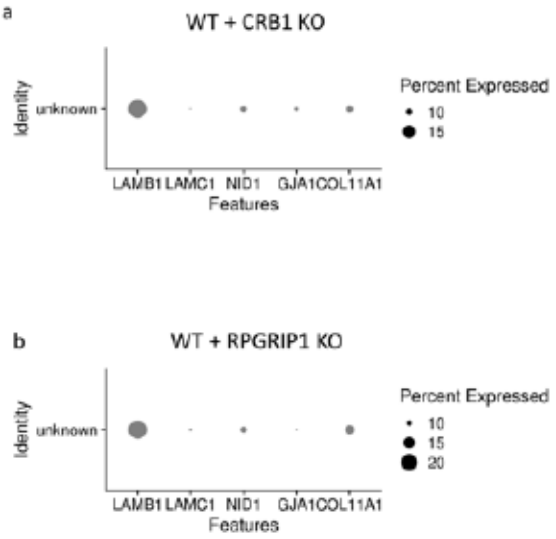

Supplementary Figure 6: Quality control metrics for clustering. A-C) UMAP labeling cells by percent mitochondrial gene content **(A)**, number of genes expressed **(B)**, and number of UMIs captured **(C)** in merged WT and CRB1 KO dataset. **D-F)** UMAP labeling cells by percent mitochondrial gene content **(D)**, number of genes expressed **(E)**, and number of UMIs captured **(F)** in merged WT and RPGRIP1 KO dataset.

Figure 34

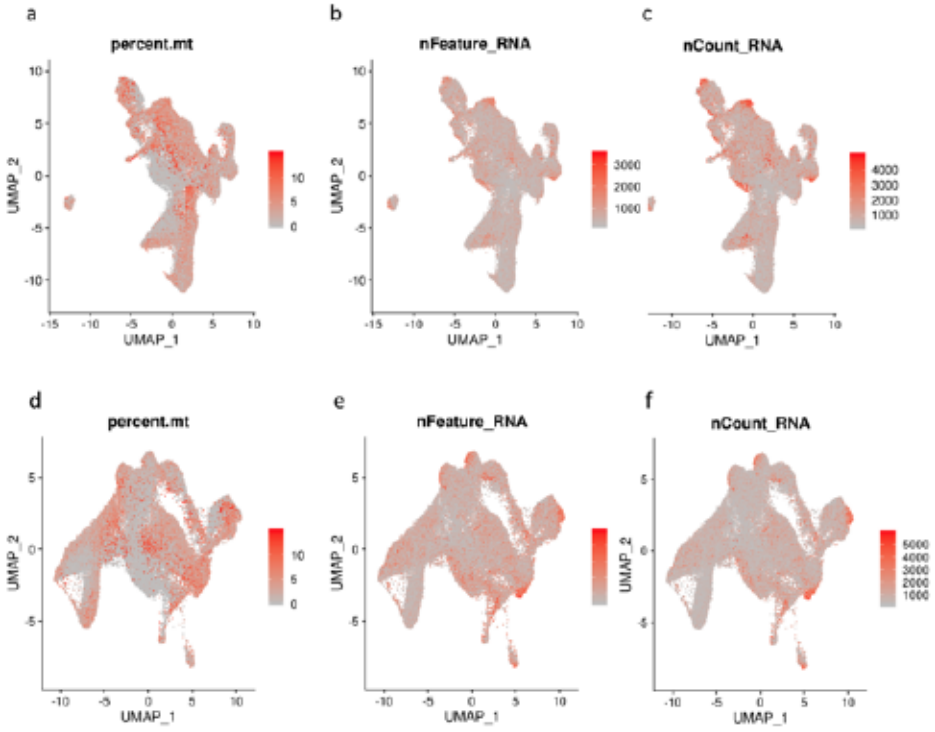

Supplementary Figure 7: Cell populations of merged WT, CRB1 KO, and RPGRIP1 KO photoreceptor dataset. A-C) Photoreceptors of CRB1 KO **(A)**, RPGRIP1 KO **(B)**, and WT **(C)** organoids. **D)** Expression of rod and cone marker genes in photoreceptor populations. **E-J)** Photoreceptors from day 70 **(E)**, 90 **(F)**, 120 **(G)**, 150 **(H)**, 190 **(I)** and 225 **(J)** organoids.

Figure 35

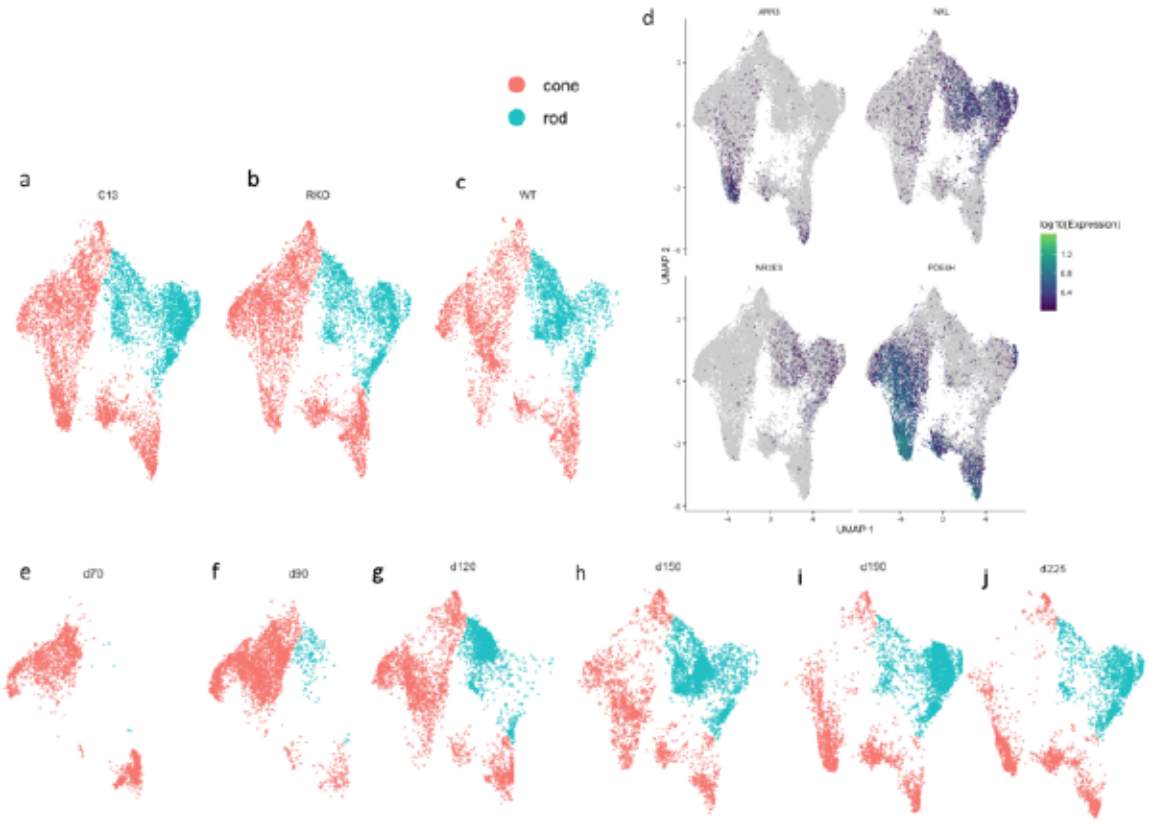

Supplementary Table 1: Genes differentially expressed between CRB1 KO and WT non-photoreceptor cells. Positive estimate indicates enrichment in WT.

Table 14

	amacrine cells		
gene_short_name	term	estimate	q_value
AC009245.3	genotypeWT	1.105443	0.000774976
ATP6AP2	genotypeWT	-0.5298982	0.02379234
BEX2	genotypeWT	-	1.32E-37

		0.9784325	
BEX3	genotypeWT	-0.4216971	2.72E-18
BTF3	genotypeWT	0.3719547	0.00261671
CHCHD2	genotypeWT	0.6691286	1.62E-15
DAAM1	genotypeWT	0.3718448	0.000634876
EIF1AX	genotypeWT	0.6921781	4.83E-06
HIST1H4C	genotypeWT	-0.3649891	9.58E-05
JUN	genotypeWT	-0.6379147	0.000187457
KRT10	genotypeWT	0.767613	8.79E-08
MALAT1	genotypeWT	0.224916	6.44E-14
MARCKSL1	genotypeWT	0.8131471	6.73E-33
MT-ND2	genotypeWT	-0.3886591	0.001632586
PPIAP22	genotypeWT	-1.101762	0.000195889
PTMAP5	genotypeWT	0.9630803	0.00474328
RP11-40C6.2	genotypeWT	1.75885	0.009890508
RPL10P9	genotypeWT	-0.6596682	1.86E-21
RPL21	genotypeWT	-0.1904466	0.005148095
RPL23	genotypeWT	-0.2280533	0.000285373
RPL26	genotypeWT	-0.2696256	1.48E-05
RPRM	genotypeWT	0.7013586	0.02564696
RPS10	genotypeWT	-0.3328271	0.0168075
RPS2	genotypeWT	0.3357718	3.04E-06
RPS24	genotypeWT	-0.1852551	0.015677804
TCEAL4	genotypeWT	-0.4693805	2.42E-06
TCEAL5	genotypeWT	-1.113582	5.31E-14
TCEAL7	genotypeWT	-0.8213461	2.20E-07
TCEAL9	genotypeWT	-0.5923942	0.014075418
TERF2IP	genotypeWT	0.2670183	0.003477486
TFAP2A	genotypeWT	0.5095079	7.52E-07
TMSB4X	genotypeWT	-0.5140416	1.81E-28

bipolar cells

gene_short_name	term	estimate	q_value

BEX2	genotypeWT	-1.089899	0.001816209
CHCHD2	genotypeWT	0.9674662	0.000242695
H3F3B	genotypeWT	0.3568437	0.001181288
MARCKSL1	genotypeWT	0.9111289	0.002200496
MT-RNR2	genotypeWT	-0.2800163	0.001121711
RPL10P9	genotypeWT	-0.7429476	0.01444468
RPL23	genotypeWT	-0.548478	0.000308981
RPL26	genotypeWT	-0.5452848	0.010893966
RPS15A	genotypeWT	-0.504775	0.002319625
RPS24	genotypeWT	-0.5106357	0.000416364
TMSB4X	genotypeWT	-0.4954409	0.008562084

horizontal cells

gene_short_name	term	estimate	q_value
BEX2	genotypeWT	-0.9322464	1.14E-18
BEX3	genotypeWT	-0.4446553	4.19E-08
CHCHD2	genotypeWT	0.6648687	6.86E-07
CNTNAP2	genotypeWT	0.5557652	0.00364442
MALAT1	genotypeWT	0.3303176	1.61E-05
MARCKSL1	genotypeWT	0.8844574	1.75E-13
MT-RNR1	genotypeWT	-0.5220851	0.04246545
PPIAP22	genotypeWT	-2.048635	0.006601536
RPL10P9	genotypeWT	-0.6280994	1.57E-07
RPS2	genotypeWT	0.4520894	1.72E-05
TCEAL5	genotypeWT	-0.9598012	0.002018592
TMSB4X	genotypeWT	-0.5595422	1.24E-09

RGCs

gene_short_name	term	estimate	q_value
AC009245.3	genotypeWT	1.750776	5.22E-12
ACSL4	genotypeWT	-0.6920428	0.012119796
ACTB	genotypeWT	-0.2364627	0.000252786
ACTG1	genotypeWT	-0.4016011	2.02E-23
ARF1	genotypeWT	0.3910266	6.88E-05

ARF4	genotypeWT	0.5025445	0.02490385
BEX2	genotypeWT	-0.7311269	2.58E-21
BEX3	genotypeWT	-0.6490533	2.35E-39
BTF3	genotypeWT	0.6270324	1.59E-21
C12orf57	genotypeWT	0.411425	0.006737939
CALM2	genotypeWT	-0.3424358	3.50E-18
CDKN1A	genotypeWT	1.616082	0.03565764
CHCHD2	genotypeWT	0.5615809	5.32E-12
CNTN2	genotypeWT	-0.7255532	0.001177934
CRABP1	genotypeWT	-0.2518086	0.002992368
DDX24	genotypeWT	0.4424281	0.03629786
EIF1	genotypeWT	0.1911652	0.005516469
EPB41L4A-AS1	genotypeWT	0.5716459	0.004953872
FABP7	genotypeWT	0.8281729	0.008875608
FNDC5	genotypeWT	-0.6703733	0.000474921
FTL	genotypeWT	0.3429372	2.03E-14
GAP43	genotypeWT	-0.3232445	2.58E-09
HNRNPA1	genotypeWT	-0.2320753	0.01069054
HSP90AA1	genotypeWT	-0.1566408	0.02458404
KRT10	genotypeWT	0.7663124	8.92E-06
LSM5	genotypeWT	1.175215	7.73E-08
MAGEH1	genotypeWT	0.6923011	0.01719704
MALAT1	genotypeWT	0.3785797	3.68E-15
MAP1B	genotypeWT	-0.2022967	0.009920126
MARCKSL1	genotypeWT	0.387417	0.000502258
MIAT	genotypeWT	-0.3274015	0.006690112
MIF	genotypeWT	0.4195675	5.90E-15
MPC1	genotypeWT	0.8019212	0.04143222
MT-CO1	genotypeWT	-0.3960208	9.00E-05
MT-ND4	genotypeWT	-0.373042	0.001995036
MT-RNR1	genotypeWT	-0.4624293	0.0395076
MT-RNR2	genotypeWT	-0.3288836	0.000142342

NEFL	genotypeWT	0.4534706	0.001129729
NOP58	genotypeWT	0.5891262	0.0473711
NPM1	genotypeWT	0.2688243	0.010176741
NR2F1	genotypeWT	-0.446382	0.00305653
NSG1	genotypeWT	0.4908336	2.32E-11
PCBD1	genotypeWT	1.120295	0.001026861
PJA1	genotypeWT	0.954684	1.58E-06
PRPH	genotypeWT	0.6275399	7.43E-10
PTMA	genotypeWT	-0.185162	7.81E-06
PTMS	genotypeWT	0.4674974	0.014996109
RPL10P9	genotypeWT	0.3899316	9.76E-08
RPL13P12	genotypeWT	0.5622842	0.00181817
RPL41	genotypeWT	0.203768	0.02040763
RPL7A	genotypeWT	0.2318222	0.00100761
RPL8	genotypeWT	0.1753384	0.03501734
RPS2	genotypeWT	0.2444862	0.0197661
RPS3	genotypeWT	-0.159321	0.03421632
SARAF	genotypeWT	0.3086741	0.01912449
SELENOM	genotypeWT	0.9557251	0.03213
SLC18A2	genotypeWT	0.7405699	0.001230962
SPINT2	genotypeWT	0.683353	0.000761388
STMN1	genotypeWT	0.1844336	0.00492201
STMN2	genotypeWT	0.1876817	6.17E-09
TCEAL4	genotypeWT	0.7448178	1.18E-10
TERF2IP	genotypeWT	0.2924867	0.0108024
TM9SF4	genotypeWT	1.447006	6.98E-07
TMSB10	genotypeWT	-0.195441	3.21E-08
TMSB4X	genotypeWT	0.8873862	1.23E-92
TRMT112	genotypeWT	0.4198918	0.004536252
TSC22D1	genotypeWT	0.5495897	0.001116924
TUBA1A	genotypeWT	0.2667807	2.45E-14
TUBB2B	genotypeWT	-0.214173	4.17E-06
UBBP4	genotypeWT	0.8539424	0.00799176
VAMP2	genotypeWT	0.4193473	0.02747286

ZNF667-AS1	genotypeWT NPCs	0.9329856	0.00035259
gene_short_name	term	estimate	q_value
AC009245.3	genotypeWT	1.227547	0.00018705
ACTB	genotypeWT	-0.3074082	1.44E-05
ACTG1	genotypeWT	-0.2902255	3.24E-07
BEX2	genotypeWT	-0.8320222	9.85E-27
BEX3	genotypeWT	-0.6815027	5.98E-50
BTF3	genotypeWT	0.8930798	4.46E-25
CHCHD2	genotypeWT	0.7206678	2.42E-13
COX7A2L	genotypeWT	0.4643326	0.01223296
EDF1	genotypeWT	0.2967636	0.013823887
EEF2	genotypeWT	0.3149527	0.000768686
EIF1	genotypeWT	0.2993	8.90E-06
ENO1	genotypeWT	0.3023484	0.000717162
FTL	genotypeWT	0.3952517	4.57E-11
GPM6B	genotypeWT	-0.9590727	0.000422318
HSP90AA1	genotypeWT	-0.233227	6.23E-05
IDI1	genotypeWT	0.8310832	0.002512692
INPP5F	genotypeWT	0.7350708	0.003607744
ISCU	genotypeWT	0.6864506	0.01786101
KDELR2	genotypeWT	0.7642626	0.00421951
KRT10	genotypeWT	0.7400691	0.000307911
LSM5	genotypeWT	0.9702124	0.03442404
MAP1B	genotypeWT	-0.2696213	0.000522191
MARCKSL1	genotypeWT	0.3585566	0.04310512
MIF	genotypeWT	0.3682849	1.17E-07
MT-ATP6	genotypeWT	-0.6624477	1.90E-07
MT-CO1	genotypeWT	-0.5256168	3.86E-11
MT-CO2	genotypeWT	-0.7229961	1.10E-09
MT-CO3	genotypeWT	-0.5374196	0.001311354
MT-CYB	genotypeWT	-0.7699502	0.000133523
MT-ND2	genotypeWT	-0.5258197	0.000206374

MT-ND4	genotypeWT	-0.5260744	3.58E-08
MT-RNR1	genotypeWT	-0.4969071	0.0016108
MT-RNR2	genotypeWT	-0.5313469	3.75E-17
NNAT	genotypeWT	-0.424482	7.47E-05
NR2F1	genotypeWT	-0.4034946	0.001609289
PNISR	genotypeWT	-0.3534987	0.02718872
PTMS	genotypeWT	-0.4957444	0.01229658
RPL10P9	genotypeWT	-0.3713759	7.79E-05
RPL13	genotypeWT	0.1998629	0.000204775
RPL13A	genotypeWT	0.2434585	4.92E-09
RPL13P12	genotypeWT	0.648207	0.013663806
RPL15	genotypeWT	0.1911715	0.009868074
RPL18A	genotypeWT	0.3284427	8.93E-08
RPL27A	genotypeWT	0.2788815	3.73E-06
RPL28	genotypeWT	0.257206	0.007132743
RPL32	genotypeWT	0.1889732	0.014611536
RPL35	genotypeWT	0.2327936	0.04005165
RPL4	genotypeWT	0.2216444	0.02686863
RPL41	genotypeWT	0.2543152	0.001292102
RPL8	genotypeWT	0.2116419	0.0265485
RPLP0	genotypeWT	0.2390986	0.000921721
RPLP2	genotypeWT	0.2070443	0.004718472
RPS11	genotypeWT	0.2191249	3.92E-05
RPS13	genotypeWT	0.2536352	8.26E-07
RPS16	genotypeWT	0.3144462	3.49E-11
RPS18	genotypeWT	0.2235607	0.001063392
RPS19	genotypeWT	0.3463354	1.14E-13
RPS2	genotypeWT	0.2734159	0.02879573
RPS25	genotypeWT	0.2366281	0.000312728
RPS27	genotypeWT	0.3097645	5.86E-06
RPS29	genotypeWT	0.2409408	0.00603825
RPS5	genotypeWT	0.2519428	0.000295033
SEC13	genotypeWT	0.6275591	0.005764874
SEC61G	genotypeWT	0.3963994	0.011799101
TCEAL1	genotypeWT	-0.8812663	0.008372

TCEAL3	genotypeWT	-0.7831803	0.000510941
TCEAL4	genotypeWT	-0.9923648	5.73E-22
TCEAL5	genotypeWT	-0.8773039	1.05E-07
TCEAL7	genotypeWT	-0.5667216	0.000921721
TMSB4X	genotypeWT	-0.8352675	6.72E-60
ZNF667-AS1	genotypeWT	1.178757	0.009788192

RPCs

gene_short_name	term	estimate	q_value
ABCA1	genotypeWT	0.925058	0.0449049
AC004453.8	genotypeWT	0.4721414	4.98E-05
AC007969.5	genotypeWT	0.2000276	1.72E-10
AC009245.3	genotypeWT	1.42256	3.54E-91
AC018738.2	genotypeWT	-1.387846	0.016880826
ACTA2	genotypeWT	-0.7196718	0.002051397
ACTB	genotypeWT	-0.2883742	1.91E-32
ACTG1	genotypeWT	-0.2133569	1.29E-28
ADIPOR1	genotypeWT	0.3751774	0.03531255
AIF1	genotypeWT	1.038466	2.06E-06
AKAP12	genotypeWT	0.4786876	1.26E-10
ALDOA	genotypeWT	0.1941154	3.34E-13
ANXA1	genotypeWT	1.259455	7.43E-12
ANXA2	genotypeWT	0.3363599	0.001314506
APOE	genotypeWT	0.9296276	3.68E-05
ARF1	genotypeWT	0.2679391	5.63E-10
ARF4	genotypeWT	0.3724506	7.42E-13
ARFGAP3	genotypeWT	0.2922631	0.007891364
ATP1A2	genotypeWT	-0.5850548	0.03989799
ATP5B	genotypeWT	0.2242118	3.05E-05
ATP6AP2	genotypeWT	-0.5087957	3.87E-14
ATP6V0B	genotypeWT	0.252107	0.000337875
ATP6V1G1	genotypeWT	0.184796	1.00E-06
AURKAIP1	genotypeWT	0.3372221	0.018947178
BEX2	genotypeWT	-0.8232045	4.83E-75
BEX3	genotypeWT	-	4.54E-136

		0.6150479	
BNIP3	genotypeWT	0.1637045	0.000178684
BNIP3L	genotypeWT	0.2405231	8.06E-06
BTF3	genotypeWT	0.6663938	1.26E-131
BTG2	genotypeWT	-0.4150391	0.000154553
C12orf57	genotypeWT	0.2653447	2.93E-08
C19orf43	genotypeWT	0.3118388	0.03927508
C19orf70	genotypeWT	0.3884225	9.18E-05
C6orf48	genotypeWT	0.1236606	0.003372628
CALM2	genotypeWT	-0.1812724	9.29E-08
CAMLG	genotypeWT	0.2322464	3.20E-05
CCDC152	genotypeWT	0.9658307	0.03426944
CCNI	genotypeWT	0.1628155	5.43E-06
CD63	genotypeWT	0.3876583	5.15E-31
CFI	genotypeWT	-0.4463055	0.000796936
CHCHD10	genotypeWT	0.5971959	1.25E-09
CHCHD2	genotypeWT	0.7277251	2.71E-108
CHD4	genotypeWT	-0.2188908	0.000717311
CHMP2A	genotypeWT	0.2377958	0.0455293
CIB1	genotypeWT	0.2998621	0.03572874
CLDN1	genotypeWT	-0.5758376	0.003184248
CLU	genotypeWT	0.3111244	8.94E-16
CNN2	genotypeWT	-0.3876738	0.0114669
COL9A1	genotypeWT	-0.4446958	0.001063078
COX7A2L	genotypeWT	0.172383	0.02801136
CRABP1	genotypeWT	-0.2373563	1.75E-16
CREB3	genotypeWT	0.4705531	5.97E-05
CRYAB	genotypeWT	0.4455643	0.000161475
CSDE1	genotypeWT	0.1780962	0.04761324
CTA-29F11.1	genotypeWT	0.4686425	9.85E-05
CYCS	genotypeWT	0.2723013	0.000968768
CYP1B1	genotypeWT	-0.432095	5.67E-09
DAD1	genotypeWT	0.3944239	3.30E-22
DAPL1	genotypeWT	-0.2728693	1.79E-14

DGUOK	genotypeWT	0.2229523	0.004963254
DLK1	genotypeWT	0.4402576	3.28E-05
EDF1	genotypeWT	0.1404997	0.00010102
EEF1D	genotypeWT	0.2853318	4.23E-19
EEF2	genotypeWT	0.1304353	0.000125166
EFNB1	genotypeWT	0.9379959	7.58E-07
EGR1	genotypeWT	-0.4656902	1.14E-14
EGR2	genotypeWT	-0.959305	0.000224647
EGR3	genotypeWT	-1.177005	0.001262153
EIF1	genotypeWT	0.1972439	7.15E-23
EIF1AX	genotypeWT	0.5871781	1.84E-17
EIF2S3	genotypeWT	0.203516	0.00061046
EIF3K	genotypeWT	0.1863399	0.04990798
EIF3L	genotypeWT	0.3113043	0.02550532
EIF3M	genotypeWT	0.2431647	9.30E-05
EIF4A2	genotypeWT	0.190188	1.27E-10
EIF4EBP1	genotypeWT	0.4398816	5.58E-07
EPB41L4A-AS1	genotypeWT	0.2168394	0.003937848
ERO1A	genotypeWT	0.5089634	0.039691
FAM162A	genotypeWT	0.2822458	6.26E-09
FAM96B	genotypeWT	0.2397762	7.69E-05
FAR2P1	genotypeWT	-1.147785	0.03635382
FAU	genotypeWT	0.1299446	1.09E-10
FOS	genotypeWT	-0.5262431	2.24E-23
FTL	genotypeWT	0.3558101	1.32E-49
FTLP3	genotypeWT	0.337862	3.64E-06
FUNDC1	genotypeWT	-0.5414968	0.000316919
FUS	genotypeWT	-0.2123964	3.87E-05
GAS5	genotypeWT	0.1922139	4.61E-18
GLTSCR2	genotypeWT	0.4362862	5.22E-17
GOLT1B	genotypeWT	0.5983234	1.88E-06
GPC3	genotypeWT	0.6896157	0.016379577
GPM6B	genotypeWT	-0.2492654	2.38E-05
GPT2	genotypeWT	0.5788354	0.04344496
GRIPAP1	genotypeWT	-0.5697512	7.16E-05
GUK1	genotypeWT	0.2439712	1.72E-05
HERPUD1	genotypeWT	0.3161268	2.67E-05

HES1	genotypeWT	-0.2156433	3.57E-05
HES6	genotypeWT	0.3887345	0.029887
HM13	genotypeWT	0.4660966	7.94E-13
HMGB1P5	genotypeWT	1.030007	1.09E-07
HMGN2	genotypeWT	-0.245759	1.43E-07
HMGN2P5	genotypeWT	-1.092545	4.25E-05
HNRNPA1	genotypeWT	-0.1763152	2.15E-12
HNRNPA1P48	genotypeWT	-0.3421737	0.02738555
HSP90AA1	genotypeWT	-0.1495406	1.34E-16
HSPA6	genotypeWT	0.3637559	0.02967942
IER2	genotypeWT	-0.2493196	0.000245618
IFITM1	genotypeWT	-0.3245357	0.001404521
IFITM2	genotypeWT	-0.5274989	4.55E-07
IFITM3	genotypeWT	-0.2760495	7.49E-11
IMPDH2	genotypeWT	0.2496168	0.000469997
JTB	genotypeWT	0.2577096	0.000612528
KDELR2	genotypeWT	0.4973601	1.81E-18
KRT10	genotypeWT	0.7543473	2.35E-57
LAMTOR5	genotypeWT	0.1759264	0.00170824
LAPTM4A	genotypeWT	0.2164366	7.14E-05
LGALS1	genotypeWT	0.6973592	0.003665725
LITAF	genotypeWT	0.4690294	2.78E-05
LRRC75A-AS1	genotypeWT	0.20242	4.71E-15
LSM5	genotypeWT	0.7593162	3.64E-26
MAGEH1	genotypeWT	0.4051497	5.59E-05
MAP1B	genotypeWT	-0.1726355	0.00013986
MAP2K1	genotypeWT	0.6859372	0.0250884
MARCKSL1	genotypeWT	0.4898608	4.40E-26
MATR3	genotypeWT	-0.1606373	0.000394499
MDK	genotypeWT	-0.3183493	1.16E-19
MED10	genotypeWT	0.272001	0.03009456
MID1IP1	genotypeWT	-0.9754605	1.59E-08
MIF	genotypeWT	0.268106	8.47E-26

MPC1	genotypeWT	0.3562089	1.72E-05
MRPL18	genotypeWT	0.2578506	0.001795929
MRPL55	genotypeWT	0.3252391	0.005423719
MT-ATP6	genotypeWT	-0.1881743	0.013453489
MT-CO1	genotypeWT	-0.4371335	5.53E-48
MT-CO2	genotypeWT	-0.2994978	5.15E-11
MT-CO3	genotypeWT	-0.3311539	2.34E-12
MT-CYB	genotypeWT	-0.3919821	1.49E-11
MT-ND1	genotypeWT	-0.232605	0.019259952
MT-ND2	genotypeWT	-0.3159077	6.39E-08
MT-ND3	genotypeWT	-0.3401897	0.001756364
MT-ND4	genotypeWT	-0.205204	4.06E-06
MT-ND5	genotypeWT	-0.2627145	4.17E-07
MT-ND6	genotypeWT	-0.4881938	3.12E-06
MT-RNR1	genotypeWT	-0.4393727	4.61E-21
MT-RNR2	genotypeWT	-0.2555685	5.61E-22
MT1G	genotypeWT	1.452649	8.31E-06
MT1X	genotypeWT	0.9485744	2.34E-07
MT2A	genotypeWT	0.9944136	2.15E-10
MTHFD2	genotypeWT	0.5194933	2.72E-10
MYL6	genotypeWT	-0.1303393	0.002089014
MZT2B	genotypeWT	0.3449151	0.00584226
NACA	genotypeWT	0.1086126	9.42E-06
NANS	genotypeWT	0.571878	0.000723569
NDUFA4	genotypeWT	0.1281028	0.008978541
NDUFS7	genotypeWT	0.2524824	0.002995993
NPRL2	genotypeWT	0.4219484	0.000344154
NR2F1	genotypeWT	-0.2657238	8.28E-14
NR4A1	genotypeWT	-0.6142015	0.000962523
NRIP1	genotypeWT	-0.3420212	0.01948812
NRN1	genotypeWT	0.7105191	3.33E-06

NUBP2	genotypeWT	0.4439861	0.000253991
OAZ1	genotypeWT	0.205916	1.82E-10
OFD1	genotypeWT	-0.4005772	3.37E-07
P4HA1	genotypeWT	0.2348018	0.006406722
P4HB	genotypeWT	0.3092024	1.31E-06
PABPC1	genotypeWT	0.1408151	2.87E-12
PAX6	genotypeWT	-0.2408935	1.38E-05
PBX1	genotypeWT	-0.2973632	0.0104635
PCBP1	genotypeWT	0.3153124	4.08E-13
PCNP	genotypeWT	0.257767	0.000480465
PDIA3	genotypeWT	-0.1668775	0.04657132
PFDN5	genotypeWT	0.1599976	2.53E-08
PGK1	genotypeWT	0.1712124	8.34E-05
PHPT1	genotypeWT	0.2722158	2.18E-15
PJA1	genotypeWT	0.7109385	8.51E-08
PLPP5	genotypeWT	0.3973515	7.60E-06
PPIA	genotypeWT	-0.2775752	4.47E-25
PPIAP22	genotypeWT	-0.775318	1.96E-11
PRDX5	genotypeWT	0.2281079	1.70E-07
PRSS23	genotypeWT	-0.3105741	0.000264474
PTGDS	genotypeWT	-0.7871846	3.71E-09
PTMA	genotypeWT	-0.1247688	1.73E-07
PTMAP5	genotypeWT	0.7343819	0.000251904
PTMS	genotypeWT	-0.2641425	0.006427352
PUS7L	genotypeWT	0.6745011	0.02446236
QKI	genotypeWT	0.377386	0.018300625
RAC1	genotypeWT	0.1810268	0.018864428
RBP1	genotypeWT	-0.1461012	0.004733118
RHOA	genotypeWT	0.2314364	6.21E-06
RNF187	genotypeWT	0.5564394	3.82E-11
RP11-20O24.4	genotypeWT	-1.032543	5.05E-06
RP11-247C2.2	genotypeWT	-0.5725961	0.03844128
RP11-371A22.1	genotypeWT	-0.3839906	1.58E-07

RP11-40C6.2	genotypeWT	1.468624	3.26E-17
RP11-475C16.1	genotypeWT	0.4660641	2.83E-10
RP11-84E17.1	genotypeWT	-0.2827772	1.34E-26
RP11-864N7.2	genotypeWT	0.4484591	2.30E-13
RPAP2	genotypeWT	-0.4906637	0.04219376
RPL10P6	genotypeWT	-0.7215294	1.70E-12
RPL10P9	genotypeWT	-0.4176672	4.83E-72
RPL13A	genotypeWT	0.1450946	2.54E-34
RPL13AP25	genotypeWT	-0.4549607	0.002681856
RPL13P12	genotypeWT	0.2537065	1.92E-07
RPL14P1	genotypeWT	0.3682743	0.012303312
RPL15	genotypeWT	0.1155184	6.59E-12
RPL18A	genotypeWT	0.1720617	1.42E-23
RPL23	genotypeWT	-0.1741234	1.76E-30
RPL26	genotypeWT	-0.1116153	3.54E-08
RPL26P19	genotypeWT	-0.6346686	0.004586955
RPL27A	genotypeWT	0.1269085	2.60E-14
RPL3	genotypeWT	0.1333189	1.07E-19
RPL39	genotypeWT	-0.1229073	0.000690078
RPL39P3	genotypeWT	0.7969832	3.73E-10
RPL3P7	genotypeWT	0.6126683	0.005946676
RPL4	genotypeWT	0.0765092	0.02821905
RPL41	genotypeWT	0.0865286	0.000200302
RPL5	genotypeWT	-0.1101072	8.39E-09
RPL5P1	genotypeWT	1.263313	4.78E-21
RPL6P27	genotypeWT	-0.5737761	3.85E-06
RPL7A	genotypeWT	-0.1675996	1.50E-17
RPL7AP50	genotypeWT	-0.6877784	5.55E-05
RPL7P1	genotypeWT	0.4923507	1.02E-11
RPL8	genotypeWT	0.1531018	3.96E-19
RPL9P9	genotypeWT	-0.2610567	2.73E-24
RPLP0	genotypeWT	0.153618	2.37E-25

RPLP0P6	genotypeWT	0.3296383	2.97E-09
RPLP1	genotypeWT	0.0628296	0.00795378
RPLP2	genotypeWT	0.1011748	2.66E-09
RPS10	genotypeWT	-0.2910324	7.03E-37
RPS11	genotypeWT	0.1509204	2.29E-28
RPS12	genotypeWT	0.0626016	0.017277442
RPS13	genotypeWT	0.1647721	8.11E-28
RPS16	genotypeWT	0.1170766	5.68E-13
RPS18	genotypeWT	0.1027005	4.51E-10
RPS19	genotypeWT	0.2616305	1.09E-95
RPS19BP1	genotypeWT	0.3347274	0.006323276
RPS19P1	genotypeWT	0.6621483	0.001588844
RPS2	genotypeWT	0.3501933	2.40E-76
RPS20	genotypeWT	0.071521	0.007556813
RPS24	genotypeWT	-0.089966	3.89E-06
RPS25	genotypeWT	0.1538643	3.03E-23
RPS27	genotypeWT	0.0984566	8.06E-06
RPS27A	genotypeWT	0.1173703	5.20E-15
RPS27L	genotypeWT	0.2528488	5.00E-08
RPS2P46	genotypeWT	-0.8277444	1.08E-09
RPS2P5	genotypeWT	0.4028816	1.29E-16
RPS3AP26	genotypeWT	0.3411847	0.000400775
RPS3AP5	genotypeWT	0.6401966	3.86E-11
RPS5	genotypeWT	0.1903752	2.88E-31
RPS7P1	genotypeWT	0.3692154	2.15E-06
S100A10	genotypeWT	0.6932389	0.000281253
SAP18	genotypeWT	0.2145392	0.001431705
SEC13	genotypeWT	0.2501433	0.01767402
SEC61B	genotypeWT	0.2013192	0.004670512
SEC61G	genotypeWT	0.3615836	2.73E-23
SELENOK	genotypeWT	0.2816972	9.55E-06
SELENOM	genotypeWT	0.58503	2.92E-19
SERF2	genotypeWT	0.1252133	0.000688013
SERP1	genotypeWT	0.3463818	2.62E-11
SF3B2	genotypeWT	0.1891206	0.00736912
SFRP2	genotypeWT	-0.4469986	4.82E-17
SLC25A6	genotypeWT	0.2254759	8.47E-05
SLC39A7	genotypeWT	0.3670114	0.00303775

SMS	genotypeWT	0.3741873	0.000602097
SNHG16	genotypeWT	0.3230691	0.000224647
SNHG5	genotypeWT	0.360204	3.45E-29
SNHG7	genotypeWT	0.5786886	3.17E-11
SNHG8	genotypeWT	0.3582097	7.28E-11
SNU13	genotypeWT	0.2065214	0.019968095
SNX3	genotypeWT	0.3031582	0.001172055
SPCS1	genotypeWT	0.197599	0.002013776
SRPRB	genotypeWT	0.4149633	0.03385314
SRSF3	genotypeWT	-0.1657088	0.019468141
SRSF5	genotypeWT	-0.1500986	0.001389913
SSR4	genotypeWT	0.3008102	8.85E-13
STMN1	genotypeWT	-0.1822766	5.46E-08
SVIL-AS1	genotypeWT	3.888992	0.009124608
TAF1D	genotypeWT	0.2712503	7.29E-07
TAGLN	genotypeWT	-1.012943	0.000319002
TCEAL1	genotypeWT	-0.6388383	6.53E-08
TCEAL3	genotypeWT	-0.390673	1.15E-05
TCEAL4	genotypeWT	-0.580284	6.93E-46
TCEAL5	genotypeWT	-1.141199	4.32E-33
TCEAL7	genotypeWT	-0.6979852	2.20E-30
TCEAL8	genotypeWT	-0.436464	1.23E-07
TCEAL9	genotypeWT	-0.5819777	2.42E-35
TMEM208	genotypeWT	0.4634191	2.27E-05
TMSB15A	genotypeWT	-0.2335876	0.01612932
TMSB4X	genotypeWT	-0.5953951	9.92E-129
TMSB4XP6	genotypeWT	-1.308952	8.19E-11
TMSB4XP8	genotypeWT	-0.7249307	0.010630408
TPM4	genotypeWT	-0.301311	1.41E-07
TPT1	genotypeWT	0.1539798	6.45E-15
TRAM1	genotypeWT	0.3185114	0.000908044
TRH	genotypeWT	-0.2620373	0.03218292
TRMT112	genotypeWT	0.218177	1.79E-11
TSC22D1	genotypeWT	-0.3069485	5.95E-10

UBA52	genotypeWT	0.1790368	6.64E-19
UBB	genotypeWT	0.1565573	3.63E-09
UBBP4	genotypeWT	0.5318618	6.98E-15
UFM1	genotypeWT	0.2936094	8.84E-05
UQCRHL	genotypeWT	-0.6217958	0.00055597
UQCRQ	genotypeWT	0.1907028	1.74E-05
USMG5	genotypeWT	0.1801104	0.00839293
VDAC2	genotypeWT	0.1941477	0.007473438
VIM	genotypeWT	0.1310365	5.80E-05
VTRNA1-3	genotypeWT	1.171527	4.93E-19
WIF1	genotypeWT	0.5378418	7.27E-09
WSB1	genotypeWT	0.1356304	0.001766759
YBX1	genotypeWT	0.1228561	8.11E-05
YIF1A	genotypeWT	0.4888068	2.04E-11
YWHAE	genotypeWT	-0.2024297	4.00E-07
ZCCHC18	genotypeWT	-1.040975	0.014602858
ZFP36L1	genotypeWT	-0.2975203	2.17E-11
ZNF248	genotypeWT	0.7853154	0.02905378
ZNF568	genotypeWT	1.537617	1.44E-06
ZNF667-AS1	genotypeWT	0.6915955	7.60E-11
ZNF880	genotypeWT	1.072155	6.43E-05
MIR4458HG	genotypeWT	-4.036707	0.014164194
OPTC	genotypeWT	1.06889	0.001770867

RPE

gene_short_name	term	estimate	q_value
BEX2	genotypeWT	-1.429969	0.001321083
BTF3	genotypeWT	0.8934872	0.010040851
CLU	genotypeWT	-0.8420198	0.000107693
DDIT3	genotypeWT	-1.157134	0.02465957
RPLP1	genotypeWT	0.3194085	0.00462924
RPS19	genotypeWT	0.4591927	0.000150827
RPS27A	genotypeWT	0.3223112	0.02068776

unknown cluster

gene_short_name	term	estimate	q_value
AC009245.3	genotypeWT	1.584101	2.19E-06
APOE	genotypeWT	1.059468	0.01477852
B2M	genotypeWT	0.3630064	0.00059867
BEX3	genotypeWT	-0.001144064	

		0.3451346	
BTF3	genotypeWT	0.7795798	1.24E-13
CHCHD2	genotypeWT	0.7689046	3.41E-06
COL3A1	genotypeWT	-0.3808459	2.03E-07
FOS	genotypeWT	-0.6004871	0.001506708
FTH1	genotypeWT	0.2426059	0.0214676
GPC3	genotypeWT	0.9786012	2.51E-05
IFITM2	genotypeWT	0.5726134	0.0018972
IGFBP7	genotypeWT	0.7056868	1.94E-06
JUN	genotypeWT	-0.5448475	0.004435464
LGALS1	genotypeWT	0.3053507	0.006317991
MGP	genotypeWT	-0.5478862	2.12E-05
NDUFS7	genotypeWT	0.9991122	0.011657184
POSTN	genotypeWT	-0.6764383	0.000213527
RP11-40C6.2	genotypeWT	2.46217	0.03790864
RPL10P9	genotypeWT	-0.3465499	0.012241954
RPL13A	genotypeWT	0.171147	0.00092515
RPL7	genotypeWT	0.1939053	0.03498438
RPLP0	genotypeWT	0.2759338	1.25E-05
RPS14	genotypeWT	0.2012091	0.002901392
RPS19	genotypeWT	0.2777626	8.76E-08
RPS2	genotypeWT	0.6565726	1.63E-18
RPS4X	genotypeWT	0.1587286	0.007837652
RPS5	genotypeWT	0.2567781	0.02119032
SSR4	genotypeWT	0.5024034	0.02815678
TCEAL4	genotypeWT	-0.6613403	4.77E-05
TCEAL7	genotypeWT	-0.9267293	0.00099764
TMSB4X	genotypeWT	-0.5986735	1.15E-30
TPM4	genotypeWT	-0.512094	6.91E-07
VTRNA1-3	genotypeWT	2.377013	0.009106085
DCN	genotypeWT	-0.652956	9.34E-07

muller glia

gene_short_name	term	estimate	q_value
AARS	genotypeWT	0.6167087	0.000250492
ABCA1	genotypeWT	1.260689	5.04E-09

ABCD4	genotypeWT	0.849024	3.65E-19
ABI3BP	genotypeWT	0.6524397	0.000140033
AC004453.8	genotypeWT	-0.6103413	0.001143112
AC009245.3	genotypeWT	1.314496	1.21E-22
AC016739.2	genotypeWT	-0.642193	0.00089245
ACER3	genotypeWT	0.8223497	0.000149338
ACLY	genotypeWT	0.6251939	6.04E-05
ACTA2	genotypeWT	-0.8935922	0.01286869
ACTB	genotypeWT	-0.4747006	1.18E-68
ACTG1	genotypeWT	-0.3105621	2.15E-51
ADAMTS1	genotypeWT	-1.057159	1.31E-20
ADD3	genotypeWT	-0.2723036	0.016252236
ADGRB1	genotypeWT	1.61041	0.000223388
ADM	genotypeWT	0.7683999	1.63E-29
AEBP1	genotypeWT	0.7532656	1.92E-20
AFAP1	genotypeWT	0.8622998	0.0296639
AFDN	genotypeWT	0.6439871	5.05E-11
AGPAT2	genotypeWT	1.714619	7.37E-23
AGPAT4	genotypeWT	0.9487637	2.91E-06
AK3	genotypeWT	0.5097048	0.03689388
AK4	genotypeWT	0.4736879	0.04032421
AKAP12	genotypeWT	0.7416548	4.71E-69
AKR1A1	genotypeWT	0.5225431	5.84E-05
ALDH1A3	genotypeWT	-0.7972661	0.0080787
ALPL	genotypeWT	1.372287	5.87E-13
ANGPTL4	genotypeWT	0.653411	9.22E-06
ANKRA2	genotypeWT	0.574812	0.00339416
ANKRD10	genotypeWT	0.7903959	8.53E-12
ANKRD11	genotypeWT	0.3625448	0.02546817
ANKRD12	genotypeWT	0.26563	0.00995596
ANKRD65	genotypeWT	0.9128439	0.01246729
ANXA1	genotypeWT	0.6133867	0.000146241
AP1S2	genotypeWT	-0.4356349	9.36E-15
AP2M1	genotypeWT	0.5646142	2.50E-19
AP3D1	genotypeWT	0.48664	0.04981707
APOE	genotypeWT	0.8093166	1.25E-36

AQP1	genotypeWT	0.7847034	3.15E-06
ARF1	genotypeWT	0.2383694	0.003163232
ARF4	genotypeWT	0.4202188	1.13E-06
ARHGAP6	genotypeWT	1.121697	0.000164065
ARHGEF10	genotypeWT	0.7433033	0.004681152
ARHGEF7	genotypeWT	0.715591	0.01955646
ARID4B	genotypeWT	0.3746843	0.000861565
ARL4A	genotypeWT	-0.6731473	1.55E-08
ARL4C	genotypeWT	0.7720463	5.10E-39
ARL6IP6	genotypeWT	0.5308009	0.00231672
ARMCX3	genotypeWT	0.4128034	9.17E-07
ARNT2	genotypeWT	0.9024616	0.007407015
ARPC2	genotypeWT	0.2566835	3.42E-08
ASNS	genotypeWT	0.733948	0.000134024
ATAD5	genotypeWT	1.139168	1.38E-08
ATF3	genotypeWT	-0.7629828	0.000306662
ATG12	genotypeWT	0.4085992	0.007062548
ATP13A3	genotypeWT	1.202544	0.00092904
ATP1B1	genotypeWT	0.4914854	2.24E-08
ATP1B2	genotypeWT	-0.4285505	9.78E-11
ATP5B	genotypeWT	0.271749	0.000295047
ATP5E	genotypeWT	-0.15301	0.04508072
ATP6AP1	genotypeWT	0.4346267	0.008500544
ATP6AP2	genotypeWT	-0.4368609	5.50E-11
ATP6V1G1	genotypeWT	0.2165002	5.59E-06
AUP1	genotypeWT	0.4090912	0.000844227
BASP1	genotypeWT	0.5539766	8.38E-07
BAZ1B	genotypeWT	0.3566788	0.000579522
BCAT1	genotypeWT	0.8402168	1.37E-08
BDP1	genotypeWT	0.4782112	0.000886688
BEST1	genotypeWT	-0.9991359	2.35E-07
BEX1	genotypeWT	-0.4449282	4.06E-28
BEX2	genotypeWT	-1.0877149	3.79E-93
BEX3	genotypeWT	-0.6754587	4.95E-177
BHLHE41	genotypeWT	0.6500864	3.90E-10

BIRC2	genotypeWT	0.6304006	0.002008448
BMP2	genotypeWT	1.489077	0.00076891
BMPR1B	genotypeWT	0.8640649	6.80E-06
BNIP2	genotypeWT	0.6160893	0.03975504
BNIP3	genotypeWT	0.2403598	3.15E-06
BSDC1	genotypeWT	0.6463499	0.001708153
BST2	genotypeWT	0.7690409	7.75E-09
BTF3	genotypeWT	0.584217	8.06E-55
BTG2	genotypeWT	0.5394857	0.000198217
C16orf45	genotypeWT	0.3707235	0.02623139
C19orf43	genotypeWT	0.4590431	0.000269882
C19orf66	genotypeWT	0.6534589	0.001349374
C1orf43	genotypeWT	0.2990838	0.003105851
C1orf61	genotypeWT	0.6354895	2.49E-43
C4orf48	genotypeWT	0.2660629	8.82E-05
C6orf48	genotypeWT	0.211899	1.77E-07
CA2	genotypeWT	0.3875736	1.21E-06
CA9	genotypeWT	0.7079218	0.000106062
CADM1	genotypeWT	0.3142941	8.91E-09
CALB1	genotypeWT	-1.530379	1.14E-15
CALM2	genotypeWT	0.3998726	6.51E-34
CALU	genotypeWT	0.5596798	1.85E-17
CAMK1D	genotypeWT	1.453859	2.65E-15
CARD19	genotypeWT	0.825631	1.08E-05
CAV1	genotypeWT	0.5492964	1.88E-05
CBR1	genotypeWT	0.4091779	0.000118676
CCDC47	genotypeWT	0.3966564	0.002951982
CCDC82	genotypeWT	0.5460277	0.000221456
CCDC85B	genotypeWT	0.7044717	0.018507735
CCND1	genotypeWT	1.445616	1.22E-166
CCNG1	genotypeWT	0.6497309	3.93E-08
CCNL2	genotypeWT	0.3446394	0.000198217
CD151	genotypeWT	0.4070946	9.95E-07
CD164	genotypeWT	0.3608606	0.0136896
CD63	genotypeWT	0.2910897	2.79E-14
CD81	genotypeWT	0.840102	6.70E-10

CD9	genotypeWT	-0.3495995	3.40E-09
CDC16	genotypeWT	0.5432985	1.08E-06
CDIP1	genotypeWT	1.569113	5.39E-64
CDK5RAP3	genotypeWT	0.3591766	1.97E-05
CDKN1A	genotypeWT	0.4511514	8.07E-07
CDKN1C	genotypeWT	0.9029673	6.21E-07
CELF1	genotypeWT	0.5884827	1.27E-08
CEP152	genotypeWT	1.104698	0.000811435
CEP85L	genotypeWT	0.6122766	0.016730192
CFI	genotypeWT	-0.4756023	2.52E-17
CHCHD2	genotypeWT	0.7776387	2.37E-86
CHD2	genotypeWT	0.3400795	0.02089203
CHPF	genotypeWT	0.7571822	6.12E-19
CHRDL1	genotypeWT	-0.4041386	0.01879346
CHST9	genotypeWT	-0.9713882	0.000275693
CISD1	genotypeWT	0.7029794	1.02E-22
CKB	genotypeWT	0.4089305	5.64E-38
CLCN6	genotypeWT	1.038476	0.002682561
CLDN1	genotypeWT	-0.8014167	0.00723424
CLIC1	genotypeWT	0.4378007	2.13E-05
CLN8	genotypeWT	0.935223	0.000641412
CLTC	genotypeWT	0.4896164	0.013384491
CLU	genotypeWT	-0.447746	4.54E-32
CMIP	genotypeWT	0.8555533	2.11E-13
CNDP2	genotypeWT	0.6670259	2.53E-07
CNN3	genotypeWT	-0.1761354	0.02070252
CNOT7	genotypeWT	0.3600265	0.02432558
CNPPD1	genotypeWT	0.7047383	0.04412793
COA1	genotypeWT	0.4441756	0.009783998
COL11A1	genotypeWT	0.2955144	0.000151655
COL15A1	genotypeWT	1.760081	1.44E-20
COL18A1	genotypeWT	0.9270256	5.93E-19
COL1A1	genotypeWT	1.209831	8.72E-24
COL1A2	genotypeWT	-0.8382452	7.81E-44
COLGALT1	genotypeWT	0.8811683	0.002913696
COMT	genotypeWT	-	0.006525411

		0.3651376	
COPS8	genotypeWT	0.3777192	0.02565832
COTL1	genotypeWT	0.3869154	0.02127204
COX4I1	genotypeWT	0.1657479	0.000233052
CP	genotypeWT	-0.6020007	2.02E-17
CPNE1	genotypeWT	0.5300727	1.26E-06
CRABP1	genotypeWT	-0.252272	8.98E-13
CRACR2B	genotypeWT	0.907482	2.67E-07
CRIP2	genotypeWT	0.4862881	4.54E-08
CRYZL1	genotypeWT	0.5897225	2.58E-05
CSGALNACT2	genotypeWT	0.8113725	0.00696669
CST3	genotypeWT	0.4541025	0.002682561
CTA-29F11.1	genotypeWT	0.5825961	0.02508781
CTC-444N24.11	genotypeWT	0.9108217	0.000116359
CTD-2287O16.1	genotypeWT	-1.346901	2.11E-05
CTTN	genotypeWT	0.6626268	8.37E-05
CWC25	genotypeWT	0.5088989	0.014148926
CXADR	genotypeWT	0.6840882	2.02E-06
CXXC5	genotypeWT	0.3083982	0.00882657
CYBA	genotypeWT	1.129495	1.39E-05
CYP1B1	genotypeWT	-0.8778631	1.09E-08
CYR61	genotypeWT	-0.4865459	0.000117326
CYSTM1	genotypeWT	-0.3888072	0.000635631
DAG1	genotypeWT	0.6605165	0.0386123
DAPL1	genotypeWT	-0.5386164	8.62E-32
DAZAP2	genotypeWT	0.4070082	0.002951982
DDB2	genotypeWT	1.110354	1.61E-13
DDIT4	genotypeWT	0.3345888	2.79E-05
DDX21	genotypeWT	0.4799059	0.001532631
DEK	genotypeWT	0.2708061	0.00404754
DGKD	genotypeWT	0.9805888	1.50E-05
DGUOK	genotypeWT	0.2807839	0.0359456
DLG5	genotypeWT	0.7197435	3.00E-07
DNAJA1	genotypeWT	-0.4015489	1.08E-14
DNAJB1	genotypeWT	-0.766503	4.78E-39
DNAJB4	genotypeWT	-0.9642394	3.84E-09

DNER	genotypeWT	0.9553764	2.24E-20
DNMT1	genotypeWT	0.4522177	0.003509506
DSG2	genotypeWT	0.8928832	0.011740365
DST	genotypeWT	-0.2705787	0.03556878
DTYMK	genotypeWT	0.7140234	2.36E-09
DYNC1LI2	genotypeWT	0.3321101	2.05E-05
EBLN3P	genotypeWT	0.5356128	0.000463397
ECHDC2	genotypeWT	-0.8687341	0.001877612
ECI1	genotypeWT	0.7776132	0.02203515
EEF1A1	genotypeWT	-0.2078316	1.87E-35
EEF1D	genotypeWT	0.1741002	0.03042465
EFNB1	genotypeWT	1.015403	2.54E-05
EFTUD2	genotypeWT	0.7753102	0.000575675
EGFL7	genotypeWT	1.055902	1.19E-13
EGR1	genotypeWT	-0.6134647	1.27E-26
EGR2	genotypeWT	-1.467299	1.10E-06
EGR3	genotypeWT	-1.610164	0.002547996
EIF1	genotypeWT	0.2554516	1.50E-23
EIF1AX	genotypeWT	0.8254555	1.31E-22
EIF2AK2	genotypeWT	0.5469231	1.15E-07
EIF4A2	genotypeWT	0.2578349	3.52E-13
EIF4EBP1	genotypeWT	0.4511245	0.006218073
ELOVL6	genotypeWT	0.6752484	0.018621838
ELP4	genotypeWT	-0.6075644	0.000403437
ENC1	genotypeWT	0.6331861	0.00903575
ENO1	genotypeWT	-0.2029973	6.66E-11
ENO2	genotypeWT	0.3496449	4.30E-08
EPAS1	genotypeWT	0.804019	4.14E-17
EPB41L4A-AS1	genotypeWT	0.3962476	8.17E-08
EPHB3	genotypeWT	1.380952	0.046222
EPSTI1	genotypeWT	1.683233	6.31E-06
ERF	genotypeWT	0.7715427	0.000741871
ERO1A	genotypeWT	0.7173657	1.93E-07
ESF1	genotypeWT	0.3517681	0.014263371
ETV5	genotypeWT	1.019329	9.36E-09
F12	genotypeWT	1.233316	0.000360896
FABP5	genotypeWT	-2.53E-36	

		0.9280835	
		-	
FABP7	genotypeWT	0.3167111	2.02E-20
FAM107A	genotypeWT	1.414186	2.47E-13
FAM127A	genotypeWT	0.2633876	0.008730874
FAM173A	genotypeWT	1.048393	9.24E-10
FAM174A	genotypeWT	0.862424	1.78E-05
FAM19A5	genotypeWT	1.192649	1.07E-06
FAM20C	genotypeWT	1.374394	0.000157667
FAM219B	genotypeWT	0.7822176	1.20E-06
FAM96B	genotypeWT	0.2917906	0.000158047
FAP	genotypeWT	-1.138088	0.000428541
FASN	genotypeWT	0.9893951	0.011758968
FASTKD1	genotypeWT	0.8306185	0.04641057
FBLN2	genotypeWT	1.842007	3.61E-109
FDPS	genotypeWT	0.4947222	1.02E-05
FER1L4	genotypeWT	1.05022	1.49E-14
		-	
FILIP1L	genotypeWT	0.9393762	0.000124305
FKBP10	genotypeWT	0.811597	1.81E-22
FLNB	genotypeWT	1.225619	4.85E-10
FN1	genotypeWT	0.4561501	3.54E-08
FNBP1	genotypeWT	0.5885109	0.02756448
FNIP1	genotypeWT	0.8170488	0.000295047
		-	
FOS	genotypeWT	0.7842405	3.99E-70
		-	
FOSB	genotypeWT	0.7282068	0.01974716
FRZB	genotypeWT	0.2371055	0.002027655
		-	
FTH1	genotypeWT	0.2332868	2.90E-26
FUCA2	genotypeWT	0.6195754	0.02127204
FUT11	genotypeWT	0.7295325	1.30E-09
FXYD6	genotypeWT	0.4807703	1.31E-13
FZD8	genotypeWT	0.8283447	0.005930232
		-	
GABARAP	genotypeWT	0.3753319	0.03099384
GABPB1-AS1	genotypeWT	0.4169271	0.000691652
GAD2	genotypeWT	0.5580708	0.000680063
GADD45B	genotypeWT	0.8788031	5.99E-19
GAS5	genotypeWT	0.3629507	9.65E-34
GAS6	genotypeWT	1.20051	5.40E-56
GAS7	genotypeWT	1.168777	0.03556878

GCK	genotypeWT	0.7377688	0.017915054
GLTSCR2	genotypeWT	0.4151279	2.37E-07
GLUL	genotypeWT	0.4837246	4.00E-10
GNAS	genotypeWT	0.2502587	4.75E-10
GNB1	genotypeWT	0.4476518	3.53E-05
GNB2	genotypeWT	0.5836451	1.91E-05
GNG4	genotypeWT	1.900468	5.10E-19
GNG7	genotypeWT	0.8723025	3.92E-05
GNL3	genotypeWT	0.3822965	0.012734904
GNPAT	genotypeWT	0.5456302	0.0467901
GOLGA2	genotypeWT	0.7673052	5.31E-16
GOLGA4	genotypeWT	0.3033217	0.000674285
GOPC	genotypeWT	0.5753805	0.001185603
GPAT4	genotypeWT	1.026979	0.001866119
GPM6B	genotypeWT	-0.3011304	2.19E-24
GPT2	genotypeWT	0.9546836	2.63E-08
GPX3	genotypeWT	0.4849873	0.001218231
GRAMD4	genotypeWT	1.138006	0.02699304
GRINA	genotypeWT	0.4021214	4.99E-06
GSE1	genotypeWT	0.7417631	1.97E-10
GSN	genotypeWT	-0.4871806	5.73E-05
GTF2E2	genotypeWT	0.9526024	0.0003822
GYPC	genotypeWT	1.035058	2.92E-12
H19	genotypeWT	0.6314935	0.003836322
H1F0	genotypeWT	-0.3467372	2.48E-06
H2AFV	genotypeWT	0.4705919	7.54E-07
H2AFZ	genotypeWT	0.2985762	1.04E-08
H3F3A	genotypeWT	-0.4987538	3.08E-13
H3F3B	genotypeWT	-0.1241568	0.001565406
HAGHL	genotypeWT	0.6977976	0.02337154
HAP1	genotypeWT	1.26222	1.54E-06
HELZ2	genotypeWT	1.485577	0.000281489
HERC2P2	genotypeWT	0.5021705	0.0405132
HES5	genotypeWT	-0.6102687	0.002586468
HIGD2A	genotypeWT	0.2920824	0.005796056
HILPDA	genotypeWT	0.3086998	0.000152425
HIST1H1D	genotypeWT	-0.691975	0.000805667

HIST1H1E	genotypeWT	-0.5972713	1.32E-07
HIST1H2BG	genotypeWT	-0.3379009	0.0241353
HIST1H4C	genotypeWT	-0.2607632	0.00314427
HK2	genotypeWT	0.6900473	0.01816346
HLA-E	genotypeWT	0.423779	0.000267955
HMGB1	genotypeWT	0.2252644	1.42E-07
HMGCS1	genotypeWT	0.5731128	3.80E-05
HMGN2	genotypeWT	-0.5201427	2.34E-20
HMGN2P5	genotypeWT	-1.734494	3.70E-06
HN1	genotypeWT	0.4110828	1.34E-05
HN1L	genotypeWT	0.7342782	0.00172923
HNRNPA1	genotypeWT	-0.1997811	7.76E-10
HOXB9	genotypeWT	-0.6871408	0.006582474
HSF4	genotypeWT	0.5722753	3.56E-06
HSP90AA1	genotypeWT	-0.281984	4.66E-38
HSP90AB1	genotypeWT	-0.154988	5.11E-11
HSPA1A	genotypeWT	-0.4962013	2.24E-19
HSPA1B	genotypeWT	-0.5554734	1.12E-33
HSPA6	genotypeWT	-0.9103453	1.20E-05
HSPA8	genotypeWT	-0.5666488	7.58E-51
HSPB1	genotypeWT	-0.7105754	3.39E-49
HSPB11	genotypeWT	0.5381904	6.49E-05
HSPD1	genotypeWT	-0.1683641	0.00091941
HSPE1	genotypeWT	-0.1992326	0.003028844
HSPH1	genotypeWT	-0.4719505	1.31E-08
IARS	genotypeWT	0.4793176	0.04774
ICAM1	genotypeWT	0.884725	0.04905873
ID2	genotypeWT	0.6651497	8.85E-32
IER2	genotypeWT	-0.3213884	0.000175498
IFI27L2	genotypeWT	-0.2975091	0.015240036
IFI44	genotypeWT	1.165351	2.32E-09

IFI44L	genotypeWT	1.333359	1.01E-46
IFI6	genotypeWT	1.0782134	3.99E-79
IFIT1	genotypeWT	0.840102	1.09E-05
IFITM1	genotypeWT	-0.5958949	7.07E-13
IFITM2	genotypeWT	-0.7466609	3.85E-25
IFITM3	genotypeWT	-0.2565875	7.50E-12
IGF1R	genotypeWT	0.9345273	5.88E-15
IGFBP2	genotypeWT	0.5297661	3.52E-08
IGFBP4	genotypeWT	0.9582125	0.00096358
IGFBP5	genotypeWT	0.6802646	2.09E-60
IKBIP	genotypeWT	0.8540901	5.09E-05
ING5	genotypeWT	0.5549837	0.00711917
INSIG1	genotypeWT	0.7325405	2.98E-05
INSIG2	genotypeWT	0.7068474	3.79E-12
IP6K2	genotypeWT	0.3912742	0.000150108
IREB2	genotypeWT	0.7623548	6.62E-05
IRF9	genotypeWT	1.138006	0.02222444
IRS2	genotypeWT	1.467842	7.30E-28
ISG15	genotypeWT	1.487801	2.17E-32
ITIH5	genotypeWT	1.470371	1.19E-20
JAM3	genotypeWT	1.018256	2.21E-11
JARID2	genotypeWT	0.6825301	0.01936675
JKAMP	genotypeWT	0.5482275	0.013498303
JUN	genotypeWT	-0.4978385	1.24E-28
JUNB	genotypeWT	-0.4594334	5.61E-06
KATNBL1	genotypeWT	0.3612165	0.04546038
KAZN	genotypeWT	0.9970275	2.91E-14
KBTBD11	genotypeWT	1.194033	1.65E-05
KCNQ3	genotypeWT	1.618372	0.03042465
KDELR2	genotypeWT	0.6588171	4.63E-15
KIAA0895L	genotypeWT	0.6917186	0.001457407
KIAA0907	genotypeWT	0.5885652	0.003413268
KISS1R	genotypeWT	1.015403	0.000767012
KLHL8	genotypeWT	-0.4816756	6.19E-07
KPNB1	genotypeWT	0.3610042	2.05E-05
KRT10	genotypeWT	0.9333079	9.36E-38
LAMB2	genotypeWT	0.715591	0.00637175

LAMP1	genotypeWT	0.7083533	1.35E-10
LARS	genotypeWT	0.3057415	0.01458896
LCA5	genotypeWT	-0.5271602	0.000567951
LDHA	genotypeWT	-0.3336451	8.55E-15
LDLR	genotypeWT	1.433987	0.004297433
LGALS1	genotypeWT	0.420067	6.17E-11
LGALS3	genotypeWT	-0.9173646	1.56E-54
LGALS3BP	genotypeWT	0.4773817	7.90E-05
LGI4	genotypeWT	0.3373827	3.06E-07
LINC01021	genotypeWT	0.7186142	0.001434286
LINC01551	genotypeWT	-1.36525	0.00189287
LITAF	genotypeWT	0.4872588	1.60E-11
LMAN1	genotypeWT	0.3273373	3.12E-08
LMNA	genotypeWT	0.5003227	0.012524268
LMO3	genotypeWT	0.6748081	0.03023488
LMO4	genotypeWT	0.4178298	0.00102722
LOXL3	genotypeWT	0.9399081	5.73E-13
LPCAT4	genotypeWT	1.015403	5.67E-06
LPP	genotypeWT	0.7986023	0.000283415
LRRC75A	genotypeWT	-0.3272542	0.03137484
LSM5	genotypeWT	0.7753605	1.47E-15
LST1	genotypeWT	-1.17453	1.92E-14
LTBP3	genotypeWT	0.7745372	8.01E-08
LUC7L3	genotypeWT	0.3730095	1.31E-34
LYN	genotypeWT	0.8436346	5.37E-09
LYPD1	genotypeWT	-0.6129141	5.38E-06
MAB21L1	genotypeWT	-0.3244196	0.008002176
MAF	genotypeWT	1.052085	1.49E-60
MAFB	genotypeWT	0.5580332	0.009573054
MALAT1	genotypeWT	0.1887688	3.13E-16
MAP7	genotypeWT	-0.6809136	0.015410373
MAP7D2	genotypeWT	1.260223	0.017303968
MARCH6	genotypeWT	0.3556574	0.018811656
MARCKSL1	genotypeWT	0.8414346	2.09E-44
MATR3	genotypeWT	-0.1955755	0.000940556

MCRIP1	genotypeWT	0.334136	0.007637089
MCRIP2	genotypeWT	0.6556952	0.04070217
MCUB	genotypeWT	0.7992028	2.29E-33
MDFI	genotypeWT	1.2237	0.000903972
MDH2	genotypeWT	0.3974647	0.000388
ME1	genotypeWT	0.5406792	1.95E-06
MED10	genotypeWT	0.6815206	5.14E-14
METRN	genotypeWT	1.148546	3.43E-52
MGRN1	genotypeWT	1.319572	3.17E-37
MGST3	genotypeWT	0.3167255	8.35E-08
MID1IP1	genotypeWT	-0.8203099	0.00024275
MIEN1	genotypeWT	0.362809	0.0296639
MIF	genotypeWT	-0.5495323	5.87E-72
MINDY2	genotypeWT	0.7297589	2.39E-11
MIR100HG	genotypeWT	0.4099575	7.54E-08
MLC1	genotypeWT	1.295836	7.07E-08
MLEC	genotypeWT	0.5251936	0.000811435
MLF2	genotypeWT	0.338853	0.0210815
MLLT11	genotypeWT	0.4404288	1.43E-07
MOGS	genotypeWT	1.160955	8.87E-06
MORF4L2	genotypeWT	-0.2065193	0.014914515
MPHOSPH8	genotypeWT	0.3299056	0.000395719
MRC2	genotypeWT	0.6430786	0.008959782
MRPL14	genotypeWT	0.3743074	0.0359456
MRPS5	genotypeWT	0.3756683	9.46E-06
MSMO1	genotypeWT	0.5674183	0.04792845
MT-CO1	genotypeWT	-0.3060832	1.69E-32
MT-CO3	genotypeWT	-0.2039707	0.000691652
MT-ND1	genotypeWT	0.2453328	0.000374459
MT-ND2	genotypeWT	0.3569089	1.84E-13
MT-ND5	genotypeWT	-0.1498632	0.0290928
MT-ND6	genotypeWT	-0.6979863	4.97E-26
MT-RNR2	genotypeWT	-0.5036977	4.17E-94
MT1X	genotypeWT	0.8123085	3.90E-10
MTCH1	genotypeWT	0.5970573	8.08E-21

MTDH	genotypeWT	0.477889	2.55E-12
MTG1	genotypeWT	0.8271565	4.67E-06
MTHFD2	genotypeWT	0.7625847	1.21E-07
MTSS1	genotypeWT	0.5504462	0.00103297
MVD	genotypeWT	0.791183	0.000952069
MYDGF	genotypeWT	0.3895496	2.54E-05
MYLK	genotypeWT	-1.238687	5.93E-08
MZT2A	genotypeWT	0.4523773	0.000653005
MZT2B	genotypeWT	0.4259763	8.23E-05
N4BP2L2	genotypeWT	0.324028	3.49E-07
NCAN	genotypeWT	1.220244	0.015240036
NDFIP2	genotypeWT	0.8801765	0.013308372
NDRG1	genotypeWT	0.801322	5.13E-26
NDUFA4	genotypeWT	-0.1515795	0.000944378
NDUFS2	genotypeWT	0.4873633	5.08E-07
NDUFS5	genotypeWT	-0.2061328	0.002143299
NEAT1	genotypeWT	0.6311149	8.78E-24
NEK6	genotypeWT	0.8319744	1.04E-07
NETO2	genotypeWT	0.9636522	0.04811436
NFIB	genotypeWT	0.4172622	0.0359456
NFIC	genotypeWT	0.4706902	0.003317192
NINJ1	genotypeWT	0.7595315	3.17E-06
NKTR	genotypeWT	0.2928503	0.000424707
NME4	genotypeWT	0.4387609	0.004931072
NNAT	genotypeWT	-0.4417565	3.12E-08
NOL3	genotypeWT	0.4655507	2.91E-09
NORAD	genotypeWT	0.4207114	0.00884534
NPAS2	genotypeWT	1.094988	0.002740174
NPM1P27	genotypeWT	-0.7315644	0.016385698
NR2E1	genotypeWT	0.5337686	3.10E-05
NR2F1	genotypeWT	-0.2249598	1.21E-07
NR4A1	genotypeWT	-1.335205	7.27E-13
NRN1	genotypeWT	0.8063815	9.37E-30
NRP1	genotypeWT	1.131736	1.76E-19
NSD3	genotypeWT	0.3284725	0.03080413
NSUN6	genotypeWT	0.6217304	0.00208548
NUBP2	genotypeWT	0.6651593	0.000397639

NUCKS1	genotypeWT	0.1755644	0.000246621
NUDT16L1	genotypeWT	1.012724	2.47E-33
NUDT21	genotypeWT	0.5209408	0.001272309
NUDT4	genotypeWT	-0.3754366	8.66E-05
NUFIP2	genotypeWT	0.6310635	5.83E-06
OAZ1	genotypeWT	0.2223805	2.39E-07
OCIAD2	genotypeWT	-0.4179436	0.016137949
OIP5-AS1	genotypeWT	0.625225	6.08E-06
OLFM1	genotypeWT	0.5133449	0.000936734
OPRK1	genotypeWT	1.467963	8.12E-05
ORC6	genotypeWT	0.9832993	2.89E-05
P4HB	genotypeWT	0.3653576	1.75E-05
PABPC1	genotypeWT	0.1741664	6.09E-10
PAX2	genotypeWT	0.9496169	1.59E-14
PAX5	genotypeWT	2.653917	7.11E-18
PAX6	genotypeWT	-0.4917005	1.08E-12
PAX8	genotypeWT	0.8125833	4.21E-07
PBX1	genotypeWT	-0.3585778	0.013002462
PCBP1	genotypeWT	0.2338064	0.02642148
PCDH10	genotypeWT	0.8712095	9.27E-11
PCDH9	genotypeWT	0.6515445	3.04E-05
PCOLCE2	genotypeWT	1.296699	1.00E-26
PDDC1	genotypeWT	0.6341487	0.012046551
PFDN5	genotypeWT	0.1535199	3.57E-05
PFKP	genotypeWT	0.422342	0.000312453
PFN1	genotypeWT	0.2417002	0.02642148
PHC3	genotypeWT	0.9581426	0.0026441
PHF1	genotypeWT	0.6581248	0.000422811
PHPT1	genotypeWT	0.1686265	0.00437429
PISD	genotypeWT	0.9272846	0.000998305
PLA2G16	genotypeWT	-0.4357142	1.99E-09
PLCXD1	genotypeWT	1.871975	4.36E-18
PLK2	genotypeWT	-0.6833205	0.013460602
PLOD2	genotypeWT	0.3361253	1.02E-05
PLP1	genotypeWT	0.3249346	0.000306662
PLPP5	genotypeWT	0.5158417	0.002605635
PNISR	genotypeWT	0.3488701	1.22E-23

PNN	genotypeWT	0.3476274	1.31E-15
PPIAP22	genotypeWT	-1.248061	1.37E-22
PPIF	genotypeWT	1.005616	3.53E-05
PPIG	genotypeWT	0.3373609	1.10E-06
PPP1CC	genotypeWT	0.6228974	1.02E-05
PPP1R14B	genotypeWT	0.9545567	0.001303112
PPP1R17	genotypeWT	-1.039828	0.01718976
PPP1R1B	genotypeWT	0.7460848	0.004757961
PPP2CB	genotypeWT	0.6352554	0.000184817
PRDX1	genotypeWT	-0.3218786	5.66E-11
PRDX3	genotypeWT	0.3508856	0.003989925
PRELP	genotypeWT	-0.6759154	0.0290928
PRKAB2	genotypeWT	0.8503236	0.04375045
PROS1	genotypeWT	0.5918129	4.97E-05
PRPF4B	genotypeWT	0.4040365	0.00062213
PRPH	genotypeWT	0.9649865	1.44E-07
PRPS1	genotypeWT	-0.9261684	0.00589203
PRSS23	genotypeWT	-0.4902835	5.40E-08
PSPH	genotypeWT	0.7871844	2.50E-10
PTAR1	genotypeWT	0.754625	0.006851576
PTGDS	genotypeWT	-0.5195731	1.03E-18
PTMAP5	genotypeWT	1.109606	0.000331843
PTN	genotypeWT	0.2650494	2.42E-17
PTPRF	genotypeWT	0.6727182	9.80E-16
PUS7L	genotypeWT	0.821336	0.007425868
QKI	genotypeWT	0.3910289	0.000961695
QSOX2	genotypeWT	1.138006	0.017821007
RAB9A	genotypeWT	-0.5868684	4.64E-05
RABGGTB	genotypeWT	0.4495396	0.002143299
RABL6	genotypeWT	0.7922598	0.04716959
RAC1	genotypeWT	0.2721648	7.74E-06
RBM17	genotypeWT	0.297835	0.006025876
RBM23	genotypeWT	-0.5037452	8.44E-07
RBM25	genotypeWT	0.2250827	0.000140033
RBM33	genotypeWT	0.5332048	0.001210559
RBM5	genotypeWT	0.2806812	0.017896806

RBMS3	genotypeWT	1.142079	0.001765848
RBP1	genotypeWT	-0.4048079	1.07E-19
RBPJ	genotypeWT	0.3244033	0.000205958
RC3H2	genotypeWT	0.7846864	0.04356168
RCC1	genotypeWT	1.109338	0.000523395
RCN1	genotypeWT	-0.2950279	1.20E-06
REEP3	genotypeWT	0.7409869	0.001297379
RGS16	genotypeWT	-0.237786	0.02146144
RGS2	genotypeWT	-0.5722883	0.000442092
RHBDF1	genotypeWT	1.855004	1.53E-07
RHOA	genotypeWT	0.2799202	1.68E-09
RHOBTB3	genotypeWT	0.468919	6.72E-05
RHOT2	genotypeWT	0.5688619	0.00466213
RN7SK	genotypeWT	1.225379	1.24E-06
RNF114	genotypeWT	0.456158	0.04792845
RNF187	genotypeWT	0.8846912	5.91E-21
RNF213	genotypeWT	0.5327279	0.02279802
RNH1	genotypeWT	0.4777562	0.001403431
RNMT	genotypeWT	0.4059964	0.007062548
ROMO1	genotypeWT	-0.2478154	5.38E-05
RP11-1000B6.3	genotypeWT	0.6662614	0.01974716
RP11-169K16.8	genotypeWT	-0.6693856	0.004604813
RP11-20O24.4	genotypeWT	-0.913265	0.000172017
RP11-278C7.1	genotypeWT	0.66028	0.04868205
RP11-36C20.1	genotypeWT	-0.7720735	0.000202082
RP11-371A22.1	genotypeWT	-1.330059	2.33E-63
RP11-40C6.2	genotypeWT	1.07403	1.06E-06
RP11-425L10.1	genotypeWT	-0.82882	2.19E-11
RP11-466H18.1	genotypeWT	-1.064924	3.99E-13
RP11-660L16.2	genotypeWT	0.8095016	0.003547704
RP11-778D9.4	genotypeWT	-0.7874448	0.002432304
RP11-84E17.1	genotypeWT	0.7808171	7.31E-167
RP11-889L3.1	genotypeWT	-0.9261684	1.96E-08
RP4-604A21.1	genotypeWT	-0.4864985	3.25E-20

RP4-706A16.3	genotypeWT	-1.016159	0.000849992
RP5-940J5.9	genotypeWT	-1.305658	2.15E-06
RPH3AL	genotypeWT	1.733697	7.63E-05
RPL10A	genotypeWT	-0.1271661	1.65E-07
RPL10P6	genotypeWT	-0.6864622	1.03E-10
RPL10P9	genotypeWT	-0.6439684	8.84E-129
RPL12	genotypeWT	-0.1111029	0.009937257
RPL13	genotypeWT	-0.0971219	2.16E-08
RPL13AP25	genotypeWT	-0.7989789	1.87E-11
RPL13AP5	genotypeWT	-0.8166631	6.62E-31
RPL13P12	genotypeWT	-0.7018035	1.55E-33
RPL14	genotypeWT	-0.2682433	1.36E-27
RPL15P3	genotypeWT	-0.8050994	2.20E-08
RPL17P36	genotypeWT	-1.071489	2.94E-12
RPL21	genotypeWT	-0.1555793	1.29E-17
RPL22	genotypeWT	-0.2913218	6.11E-22
RPL23	genotypeWT	-0.3113418	5.47E-78
RPL24	genotypeWT	-0.1217681	1.15E-05
RPL24P8	genotypeWT	-1.610866	0.002413125
RPL26	genotypeWT	-0.2651983	1.69E-39
RPL26P19	genotypeWT	-1.155651	1.01E-09
RPL27	genotypeWT	-0.1577128	9.25E-17
RPL28	genotypeWT	-0.2659426	1.28E-31
RPL29	genotypeWT	-0.2774979	1.95E-19
RPL30	genotypeWT	-0.1796794	4.00E-19
RPL31	genotypeWT	-0.0833658	0.01037826
RPL34	genotypeWT	-0.1704931	2.04E-18
RPL35A	genotypeWT	-	6.45E-12

		0.1336209	
RPL35P2	genotypeWT	-1.984726	3.44E-06
RPL36	genotypeWT	-0.2780786	3.36E-35
RPL36A	genotypeWT	-0.256583	1.40E-14
RPL37	genotypeWT	-0.2381298	1.46E-26
RPL37A	genotypeWT	-0.2386803	2.03E-40
RPL38	genotypeWT	-0.2358662	3.70E-26
RPL39	genotypeWT	-0.3347962	3.48E-31
RPL3P4	genotypeWT	0.2619485	0.000136928
RPL41	genotypeWT	-0.0878499	0.009073728
RPL5	genotypeWT	-0.1964275	4.96E-22
RPL5P1	genotypeWT	1.231978	1.28E-08
RPL6	genotypeWT	-0.1328197	1.04E-11
RPL6P27	genotypeWT	-1.336749	3.02E-22
RPL7A	genotypeWT	-0.1538337	1.80E-09
RPL7AP50	genotypeWT	-0.7999363	9.59E-06
RPL7AP6	genotypeWT	-1.189897	0.000465312
RPL7P9	genotypeWT	-0.4226421	0.005181209
RPL9	genotypeWT	-0.1322443	1.80E-09
RPL9P9	genotypeWT	-0.561064	4.13E-73
RPLP0	genotypeWT	0.1658024	8.44E-17
RPLP0P6	genotypeWT	-0.4538047	5.00E-07
RPLP1	genotypeWT	-0.2359234	1.86E-46
RPLP2	genotypeWT	-0.155711	5.58E-15
RPS10	genotypeWT	-0.4436384	7.54E-66
RPS12	genotypeWT	-0.1258049	4.87E-11
RPS15	genotypeWT	-0.0819542	0.000703204
RPS15A	genotypeWT	-0.2268628	2.51E-38
RPS17	genotypeWT	-0.1020445	0.000231122

RPS19	genotypeWT	0.2654462	2.13E-56
RPS2	genotypeWT	0.2865331	1.38E-29
RPS21	genotypeWT	-0.1730999	1.93E-09
RPS23P8	genotypeWT	-0.8544245	8.12E-14
RPS24	genotypeWT	-0.2363188	1.24E-40
RPS26	genotypeWT	-0.4191829	6.14E-40
RPS27	genotypeWT	-0.2388164	1.68E-35
RPS27A	genotypeWT	0.0754749	0.03347225
RPS27AP16	genotypeWT	-0.5791995	2.43E-14
RPS27L	genotypeWT	0.2295534	0.000388
RPS28	genotypeWT	-0.0929795	0.001970028
RPS29	genotypeWT	-0.2069649	5.10E-23
RPS2P46	genotypeWT	-1.530514	2.38E-24
RPS3A	genotypeWT	-0.1408872	2.00E-15
RPS3AP49	genotypeWT	0.8481707	1.02E-05
RPS3AP5	genotypeWT	0.8110295	5.51E-05
RPS4X	genotypeWT	-0.0994808	1.71E-07
RPS4XP3	genotypeWT	-0.7729076	0.0359456
RPS6	genotypeWT	-0.2329417	5.28E-53
RPS7	genotypeWT	-0.1467509	7.60E-10
RPS8	genotypeWT	-0.1719516	2.19E-27
RPSAP58	genotypeWT	-0.812603	1.31E-10
RSF1	genotypeWT	0.2739007	0.009016994
RSRP1	genotypeWT	0.3604711	5.36E-05
RTN3	genotypeWT	-0.2590838	6.35E-07
RTN4R	genotypeWT	1.264088	0.015315216
RXRA	genotypeWT	1.261422	1.50E-13
S100A10	genotypeWT	0.5357969	1.21E-13
S100A16	genotypeWT	-0.8039649	6.89E-05
S100A6	genotypeWT	-0.7302743	6.76E-31

SAMD14	genotypeWT	1.008548	8.70E-07
SARAF	genotypeWT	0.2376698	8.22E-05
SBNO1	genotypeWT	0.7519708	5.82E-09
SC22CB-1E7.1	genotypeWT	-0.7192684	0.000223388
SCD	genotypeWT	0.7039854	9.10E-12
SCG2	genotypeWT	0.5268008	9.88E-06
SCML1	genotypeWT	0.7316473	0.0001115
SCRG1	genotypeWT	0.6732192	4.29E-15
SDCBP	genotypeWT	0.3482316	0.00314427
SEC31A	genotypeWT	0.338895	0.03404428
SEC61A1	genotypeWT	0.7053448	0.012333462
SELENBP1	genotypeWT	0.8797708	0.000519545
SELENOP	genotypeWT	-0.6183595	8.51E-20
SEMA4B	genotypeWT	1.254237	3.80E-10
SEMA5A	genotypeWT	1.12866	0.0057771
SEMA5B	genotypeWT	1.152507	9.95E-19
SEPT11	genotypeWT	0.3245882	9.48E-06
SERPINB1	genotypeWT	-1.247467	0.023945
SERPINE1	genotypeWT	1.026196	1.89E-20
SETD5	genotypeWT	0.3808393	0.000422811
SF3B2	genotypeWT	0.3826292	1.15E-13
SFMBT2	genotypeWT	1.225448	4.89E-06
SFRP2	genotypeWT	-0.5894679	4.39E-26
SFSWAP	genotypeWT	0.3614769	0.04222647
SFT2D1	genotypeWT	0.6049569	8.60E-07
SFXN1	genotypeWT	0.6057251	0.001632878
SFXN3	genotypeWT	1.184372	6.80E-05
SH3GL1	genotypeWT	1.267485	3.13E-18
SHISA5	genotypeWT	0.4106937	0.002258919
SIKE1	genotypeWT	0.6063459	0.001345577
SIX3	genotypeWT	0.3139729	0.003643731
SKI	genotypeWT	1.409939	0.00089245
SLC11A2	genotypeWT	0.6365698	0.008481753
SLC1A3	genotypeWT	-0.3810482	4.67E-06
SLC25A3	genotypeWT	0.2133065	0.0496288
SLC25A37	genotypeWT	0.4474609	0.02813727
SLC25A6	genotypeWT	0.4080637	1.14E-17
SLC2A3	genotypeWT	0.8677153	1.00E-18

SLC39A1	genotypeWT	0.668002	0.000168722
SLC39A7	genotypeWT	0.6485449	1.08E-08
SLC6A8	genotypeWT	0.7072227	0.000718664
SLC7A5	genotypeWT	1.049595	6.37E-05
SLIT1	genotypeWT	0.9706534	0.008883336
SMAD5	genotypeWT	0.4491969	0.011375872
SMC4	genotypeWT	0.4351023	0.0130594
SMCO4	genotypeWT	0.8355813	2.13E-06
SMNDC1	genotypeWT	0.5741172	1.83E-07
SMOC2	genotypeWT	1.193236	4.94E-21
SNHG1	genotypeWT	0.6321183	3.15E-16
SNHG25	genotypeWT	0.8567545	1.32E-21
SNHG3	genotypeWT	0.7969228	1.23E-14
SNHG5	genotypeWT	0.2438677	2.17E-06
SNHG7	genotypeWT	1.023291	1.55E-17
SNHG8	genotypeWT	0.4943639	2.72E-10
SNRPA1	genotypeWT	0.467848	7.67E-05
SNRPG	genotypeWT	-0.339137	7.60E-10
SNX3	genotypeWT	0.359827	9.90E-08
SOD1	genotypeWT	-0.1565042	0.02089203
SON	genotypeWT	0.249319	5.61E-05
SORCS2	genotypeWT	0.6305527	0.0386123
SOX4	genotypeWT	0.3813725	9.61E-19
SPAG4	genotypeWT	0.7825305	0.000988683
SPATS2	genotypeWT	0.5163482	0.02070252
SPG7	genotypeWT	1.059702	3.34E-14
SPINT2	genotypeWT	-0.7352819	2.33E-11
SPP1	genotypeWT	-0.3772392	7.20E-31
SPTSSA	genotypeWT	0.5139851	0.000351212
SQLE	genotypeWT	0.7172933	4.27E-07
SREBF1	genotypeWT	1.175301	0.001206754
SREBF2	genotypeWT	0.9121111	0.000117709
SRI	genotypeWT	0.2386167	0.02470608
SRPRA	genotypeWT	0.4076674	0.03480568
SRSF1	genotypeWT	0.6926946	5.75E-18
SRSF10	genotypeWT	0.3321211	0.000426624
SRSF11	genotypeWT	0.327679	1.09E-10
SRSF9	genotypeWT	0.3814709	0.00027762

SSPN	genotypeWT	1.009184	6.08E-09
ST13	genotypeWT	-0.2359712	2.43E-07
ST8SIA1	genotypeWT	1.082242	0.000227249
ST8SIA4	genotypeWT	1.098458	0.00424006
STAC2	genotypeWT	0.6897787	3.00E-12
STARD4	genotypeWT	0.978041	0.000830716
STAT1	genotypeWT	0.6040576	0.004451139
STC1	genotypeWT	0.646108	0.01602365
STK25	genotypeWT	0.763939	3.16E-07
STK32C	genotypeWT	0.9024616	0.00148439
STMN4	genotypeWT	-0.4643651	0.012122772
SUDS3	genotypeWT	0.5817177	0.001005992
SUGP2	genotypeWT	0.4509534	0.000209833
SULF2	genotypeWT	0.6859931	1.59E-15
SUMO3	genotypeWT	0.4612188	0.00521946
TAF1D	genotypeWT	0.6654299	7.38E-29
TAGLN2	genotypeWT	-0.5222046	1.57E-07
TARDBP	genotypeWT	0.5939414	5.98E-06
TCEAL1	genotypeWT	-0.3941704	0.02699304
TCEAL2	genotypeWT	-0.6897796	3.56E-06
TCEAL3	genotypeWT	-0.6150204	6.20E-25
TCEAL4	genotypeWT	-0.6193643	2.45E-70
TCEAL5	genotypeWT	-1.344319	4.30E-42
TCEAL7	genotypeWT	-1.031871	5.38E-43
TCEAL8	genotypeWT	-0.7717075	1.23E-22
TCEAL9	genotypeWT	-0.6667145	2.77E-46
TCERG1	genotypeWT	0.4079739	2.22E-05
TDG	genotypeWT	0.5640961	0.00293284
TECR	genotypeWT	0.8079281	3.62E-08
TERF2IP	genotypeWT	0.3018917	1.12E-05
TGFA	genotypeWT	2.1524	2.67E-12
TGM2	genotypeWT	0.6520964	0.001611705
THOC2	genotypeWT	0.5074801	4.54E-13
THUMPD3-AS1	genotypeWT	0.5960491	0.000215651
TIMM13	genotypeWT	0.2933803	0.003201642

TIMP2	genotypeWT	0.5079915	0.001725455
TM2D3	genotypeWT	0.683949	7.88E-07
TM7SF3	genotypeWT	1.016116	5.59E-05
TM9SF4	genotypeWT	0.5636666	0.0038554
TMED4	genotypeWT	0.3178824	0.000341528
TMEM132A	genotypeWT	0.8842251	0.001881378
TMEM219	genotypeWT	0.3902949	0.006525411
TMEM248	genotypeWT	0.6992833	0.007100298
TMEM259	genotypeWT	0.7764763	0.001989239
TMEM68	genotypeWT	0.7179344	0.03194543
TMSB10	genotypeWT	-0.2159953	2.85E-17
TMSB4X	genotypeWT	-0.6884761	1.24E-221
TMSB4XP4	genotypeWT	-1.404859	0.001201014
TMSB4XP6	genotypeWT	-1.288877	6.94E-11
TMSB4XP8	genotypeWT	-1.188844	1.30E-12
TMTC4	genotypeWT	0.8100159	3.62E-08
TMX1	genotypeWT	0.4434877	0.03423375
TNFRSF10B	genotypeWT	0.8042059	1.48E-05
TNFRSF25	genotypeWT	0.8551898	0.01936675
TNS1	genotypeWT	1.192275	0.001077405
TPBG	genotypeWT	-0.6825743	0.000148373
TPM4	genotypeWT	-0.3952463	8.25E-10
TPT1	genotypeWT	-0.1879292	8.85E-16
TRH	genotypeWT	-1.0855231	2.85E-53
TRIM2	genotypeWT	0.3294842	0.00558482
TRIM56	genotypeWT	0.7300745	1.70E-06
TRIM9	genotypeWT	0.7034816	1.28E-10
TRIOBP	genotypeWT	0.5630018	0.03232632
TRNT1	genotypeWT	0.5912871	0.04375045
TROVE2	genotypeWT	0.4032138	0.001827577
TSC22D1	genotypeWT	-0.5356105	1.13E-20
TSC22D4	genotypeWT	0.6846926	2.04E-19
TSPAN2	genotypeWT	1.169221	0.010915256
TSPAN4	genotypeWT	0.6578067	7.26E-05
TSPAN9	genotypeWT	1.455732	2.97E-08
TSPO	genotypeWT	0.3896001	0.000136546

TSTD1	genotypeWT	-1.634583	1.24E-08
TTYH3	genotypeWT	1.345411	7.56E-29
TUBA1B	genotypeWT	0.2514086	5.83E-06
TXNIP	genotypeWT	-0.6133802	1.74E-42
U2SURP	genotypeWT	0.2388023	0.02508781
UBA5	genotypeWT	0.5700216	0.004470176
UBA6	genotypeWT	0.8610444	8.38E-08
UBAC1	genotypeWT	0.8183905	2.82E-07
UBALD1	genotypeWT	1.763275	8.44E-26
UBB	genotypeWT	-0.1766559	1.11E-06
UBE2I	genotypeWT	0.3942278	2.00E-07
UBXN4	genotypeWT	0.3896496	3.81E-21
UCHL1	genotypeWT	-0.3203491	9.33E-10
UFM1	genotypeWT	0.4134493	3.92E-05
UNC5B	genotypeWT	0.8767431	9.89E-05
UQCRH	genotypeWT	0.2349694	0.000172786
UQCRHL	genotypeWT	-0.9881809	9.68E-08
VAMP2	genotypeWT	0.4622379	1.06E-07
VAT1	genotypeWT	0.5903095	0.000219525
VBP1	genotypeWT	0.3477408	0.04849368
VCAN	genotypeWT	0.3625778	0.00596843
VDAC3	genotypeWT	0.3550546	0.02203515
VEGFA	genotypeWT	0.6030921	7.37E-37
VIM	genotypeWT	-0.1446647	1.55E-13
VOPP1	genotypeWT	0.6451338	0.01047381
VSNL1	genotypeWT	0.9009868	3.27E-07
VTRNA1-3	genotypeWT	1.465509	2.04E-06
WASF2	genotypeWT	0.5751953	9.20E-13
WDR25	genotypeWT	0.6944532	8.00E-05
WDR45B	genotypeWT	0.4509468	0.000120615
WIF1	genotypeWT	0.3676128	1.17E-23
WNK1	genotypeWT	0.8234045	1.43E-27
XBP1	genotypeWT	0.5917496	0.02432558
XPNPEP1	genotypeWT	0.5581872	0.004604813
XXYLT1	genotypeWT	1.023949	2.85E-05
YIPF6	genotypeWT	0.8420248	3.12E-05
YKT6	genotypeWT	0.746405	6.27E-05

YWHAE	genotypeWT	0.3540342	1.19E-26
YY1	genotypeWT	0.3416555	0.04184652
ZCCHC17	genotypeWT	0.5535551	8.79E-16
ZEB1	genotypeWT	0.5549156	1.09E-13
ZFAS1	genotypeWT	0.1644746	3.30E-05
ZFP36L2	genotypeWT	0.5915256	2.07E-13
ZIC2	genotypeWT	0.8788599	2.34E-08
ZMAT3	genotypeWT	1.252886	1.05E-16
ZNF207	genotypeWT	0.4769997	2.98E-05
ZNF24	genotypeWT	0.5487654	2.04E-07
ZNF395	genotypeWT	0.9340226	2.32E-16
ZNF471	genotypeWT	0.9871828	0.0205119
ZNF558	genotypeWT	1.661254	2.31E-07
ZNF638	genotypeWT	0.3746429	0.000107614
ZNF667-AS1	genotypeWT	0.7423349	0.000490491
ZNF880	genotypeWT	1.286426	0.003893752
ZRANB2	genotypeWT	0.2427304	0.013919275
ZSCAN18	genotypeWT	0.6914879	9.03E-09
ZSWIM8	genotypeWT	0.9098993	4.87E-05
DMBX1	genotypeWT	0.7911963	3.83E-11
FTH1P2	genotypeWT	-4.508618	1.35E-11
SH3RF3	genotypeWT	1.50643	0.03556878
CLEC2B	genotypeWT	0.7967393	0.0488704
FERMT3	genotypeWT	1.954978	0.008424492
FGFBP2	genotypeWT	-1.973037	0.003528606
LINC01139	genotypeWT	1.805835	1.17E-08
NKX6-1	genotypeWT	1.269034	0.03137484
NR0B1	genotypeWT	1.064981	0.000625974
OAS3	genotypeWT	2.191156	0.005508074
PHEX	genotypeWT	2.133838	6.98E-15
CCL28	genotypeWT	1.139671	5.10E-15
ADGRL4	genotypeWT	1.406094	3.19E-10
PLCXD3	genotypeWT	2.17356	1.23E-08
EPO	genotypeWT	1.010905	0.004259112
MIR4458HG	genotypeWT	-1.498781	0.03994408
AGXT	genotypeWT	1.113835	0.0035668
CHP2	genotypeWT	3.056398	9.60E-07

Supplementary Table 2: Genes differentially expressed between RPGRIP1 KO and WT non-photoreceptor cells. Positive estimate indicates enrichment in WT.

Table 15

amacrine/horizontal cells			
gene_short_name	term	estimate	q_value
BEX2	genotypeWT	-0.637973	0.00021604
BEX3	genotypeWT	0.5113237	4.02E-10
MARCKSL1	genotypeWT	0.4353592	0.0372325
MORF4L2	genotypeWT	0.6968735	2.00E-05
MT-RNR2	genotypeWT	0.3168686	0.02372108
RPS2	genotypeWT	0.4508504	0.002332528
TMEFF2	genotypeWT	1.697402	0.03630774
TMSB4X	genotypeWT	0.4699128	2.31E-05
bipolar cells			
gene_short_name	term	estimate	q_value
BEX2	genotypeWT	-1.0656	4.49E-05
BEX3	genotypeWT	0.5998571	6.51E-07
CHGB	genotypeWT	1.555392	5.39E-07
FAM162A	genotypeWT	1.454296	4.48E-06
PEG10	genotypeWT	1.314295	0.0167772
RPL10P9	genotypeWT	0.8443683	7.54E-08
RPL22	genotypeWT	-0.685351	0.000326259
RPL23	genotypeWT	0.3725722	0.004624977
RPL26	genotypeWT	-0.649772	1.05E-09
RPL34	genotypeWT	0.3599286	0.002156068
RPL35A	genotypeWT	0.3511144	0.002006109
RPL37A	genotypeWT	0.3652403	0.004011336
RPL38	genotypeWT	0.5615115	4.36E-06
RPL39	genotypeWT	0.6686562	0.00082161
RPL5	genotypeWT	0.4616362	1.56E-05
RPL6	genotypeWT	-	0.01623279

		-0.3197229	
RPL9	genotypeWT	-0.3700051	0.01459694
RPLP1	genotypeWT	-0.3883664	0.000692004
RPS15A	genotypeWT	-0.4270738	4.81E-05
RPS24	genotypeWT	-0.6165376	1.20E-13
RPS29	genotypeWT	-0.425169	0.000522795
RPS8	genotypeWT	-0.3276818	0.002851805
TMSB4X	genotypeWT	-0.7764946	2.08E-17

RGCs

gene_short_name	term	estimate	q_value
AC007969.5	genotypeWT	0.4964581	2.35E-06
ACSL4	genotypeWT	-1.127494	2.39E-07
AKAP12	genotypeWT	-0.6789144	1.06E-05
APC	genotypeWT	-0.8450719	0.000126056
ARF4	genotypeWT	0.4828389	0.04429096
ATP5C1	genotypeWT	0.3907217	0.04031049
ATP5H	genotypeWT	0.5444342	0.00682874
ATP5J	genotypeWT	0.384238	0.000144275
ATP6V0B	genotypeWT	0.4959978	0.000167927
ATP6V1F	genotypeWT	0.508686	0.04969848
BEX2	genotypeWT	-0.5611884	7.14E-09
BEX3	genotypeWT	-0.6201801	7.08E-29
C12orf57	genotypeWT	0.5307664	0.000104313
CALM2	genotypeWT	-0.2614343	1.72E-08
CEP170	genotypeWT	-0.4959852	0.001613879
CEP290	genotypeWT	-0.7179019	8.29E-05
COMMD6	genotypeWT	0.3038937	0.0487458
COX4I1	genotypeWT	0.312802	6.75E-05
COX5A	genotypeWT	0.4343891	7.04E-05
COX5B	genotypeWT	0.3452817	0.012505584
COX7A2	genotypeWT	0.4522869	5.80E-10
DAAM1	genotypeWT	-0.4746263	0.001741493

DAD1	genotypeWT	0.5544718	3.12E-05
DST	genotypeWT	-0.5935247	0.000193491
EDF1	genotypeWT	0.3685296	3.76E-06
EEF1A1	genotypeWT	0.251458	9.85E-07
EIF1	genotypeWT	0.3795543	1.42E-16
EIF4A2	genotypeWT	0.3031573	0.002220108
ELOB	genotypeWT	0.3366255	0.00201285
EMD	genotypeWT	0.7551425	0.03697152
EPB41L4A-AS1	genotypeWT	0.6133224	0.001661712
FAU	genotypeWT	0.3525336	2.12E-11
FNBP1L	genotypeWT	-0.4051687	0.000155942
FNDC5	genotypeWT	-0.7811902	0.00247535
FTH1	genotypeWT	0.2273001	4.21E-06
FTL	genotypeWT	0.5288666	2.75E-29
FTLP3	genotypeWT	0.857695	0.01993125
FUNDC2	genotypeWT	0.8521613	0.000169515
GAPDH	genotypeWT	0.3478468	1.53E-12
GAS5	genotypeWT	0.2788743	0.02327824
GNAS	genotypeWT	0.434142	1.59E-07
GSTP1	genotypeWT	0.4911216	0.002108568
H2AFZ	genotypeWT	0.3648287	0.000767136
HIST1H1E	genotypeWT	-1.210186	9.60E-07
HIST1H2AC	genotypeWT	0.8692558	0.02774082
HIST3H2A	genotypeWT	0.8057424	0.001256028
HSP90AB1	genotypeWT	0.2445396	5.01E-10
ISL1	genotypeWT	-0.6099053	0.003400545
KRT10	genotypeWT	0.6626415	0.000684072
LDHB	genotypeWT	0.3111449	0.03760424
MALAT1	genotypeWT	-0.441736	4.25E-27
MAP1B	genotypeWT	-0.3878542	4.56E-14
MAP2	genotypeWT	-0.3464604	0.002921778
MDH1	genotypeWT	0.6950644	6.89E-08
MIAT	genotypeWT	-0.3998563	6.71E-05
MIF	genotypeWT	0.4480648	1.01E-16
MORF4L2	genotypeWT	-0.4166042	2.63E-06

MT-ATP6	genotypeWT	-0.5549578	0.014813834
MT-ND2	genotypeWT	-0.5947576	2.82E-05
MT-ND4	genotypeWT	-0.3988648	0.00781697
MT-RNR2	genotypeWT	-0.8789011	1.31E-32
NACA	genotypeWT	0.2984165	1.49E-05
NDUFA4	genotypeWT	0.2935732	0.000343699
NDUFB11	genotypeWT	0.5725781	2.00E-05
NDUFS5	genotypeWT	0.3176544	0.002858093
NR2F1	genotypeWT	-0.677278	2.44E-09
NSG1	genotypeWT	-0.4559306	8.60E-07
OAZ1	genotypeWT	0.381382	2.51E-06
OCIAD2	genotypeWT	0.3954187	0.01255265
OFD1	genotypeWT	-0.9885779	0.00033253
PCBD1	genotypeWT	1.128117	0.005202634
PFDN5	genotypeWT	0.2923423	0.0309236
PHPT1	genotypeWT	0.4630103	1.62E-05
PJA1	genotypeWT	0.8537516	0.000364458
PNN	genotypeWT	-0.4155316	0.02805792
PRDX4	genotypeWT	0.8366189	1.13E-08
PRDX5	genotypeWT	0.4090986	9.79E-05
PSMB1	genotypeWT	0.4982312	0.001981024
RACK1	genotypeWT	0.340137	2.07E-09
RPL10	genotypeWT	0.26041	3.09E-08
RPL10A	genotypeWT	0.3719335	5.74E-13
RPL12	genotypeWT	0.2807335	0.0309236
RPL13	genotypeWT	0.3037254	2.06E-14
RPL13A	genotypeWT	0.4114645	2.77E-31
RPL13P12	genotypeWT	0.7996221	8.31E-10
RPL15	genotypeWT	0.2117089	0.000848591
RPL18	genotypeWT	0.3596249	3.16E-09
RPL18A	genotypeWT	0.3709183	2.41E-11
RPL19	genotypeWT	0.3337375	2.73E-11
RPL21	genotypeWT	0.2946091	1.15E-09
RPL23A	genotypeWT	0.3225404	1.20E-07
RPL24	genotypeWT	0.3722009	8.05E-15
RPL26	genotypeWT	0.2168003	0.04444749

RPL27	genotypeWT	0.2797772	1.55E-07
RPL27A	genotypeWT	0.3853092	1.51E-13
RPL28	genotypeWT	0.2909299	0.000193491
RPL3	genotypeWT	0.3648679	4.97E-17
RPL30	genotypeWT	0.3279819	4.62E-10
RPL31	genotypeWT	0.2198408	0.003559749
RPL32	genotypeWT	0.3108912	2.75E-11
RPL35	genotypeWT	0.3710224	3.66E-10
RPL35A	genotypeWT	0.2980827	2.66E-09
RPL37A	genotypeWT	0.2455787	4.80E-05
RPL38	genotypeWT	0.3530799	1.78E-09
RPL39	genotypeWT	0.3435131	0.002778432
RPL3P4	genotypeWT	0.5594978	0.014050188
RPL4	genotypeWT	0.2982004	1.32E-07
RPL41	genotypeWT	0.3675555	3.21E-12
RPL6	genotypeWT	0.1914367	0.014240671
RPL7	genotypeWT	0.2257055	0.000132447
RPL8	genotypeWT	0.4254107	2.78E-18
RPL9	genotypeWT	0.2809941	2.92E-08
RPL9P9	genotypeWT	0.3225964	0.03697152
RPLP0	genotypeWT	0.2039331	0.0051072
RPLP1	genotypeWT	0.326425	1.01E-13
RPLP2	genotypeWT	0.3854084	2.59E-18
RPS11	genotypeWT	0.4677736	7.27E-30
RPS12	genotypeWT	0.4098815	2.33E-19
RPS13	genotypeWT	0.3536774	4.68E-16
RPS14	genotypeWT	0.3754633	1.82E-18
RPS15	genotypeWT	0.3290798	1.31E-14
RPS15A	genotypeWT	0.2797546	1.05E-07
RPS16	genotypeWT	0.3862019	1.75E-17
RPS17	genotypeWT	0.2955115	1.69E-09
RPS18	genotypeWT	0.3593657	4.23E-14
RPS19	genotypeWT	0.3521416	4.18E-19
RPS2	genotypeWT	0.6118748	1.23E-24
RPS20	genotypeWT	0.2859719	0.000366034
RPS21	genotypeWT	0.2480497	0.007163346
RPS23	genotypeWT	0.3113675	9.74E-09
RPS25	genotypeWT	0.3143863	5.55E-10
RPS27	genotypeWT	0.3325943	1.62E-08
RPS27A	genotypeWT	0.2869712	1.41E-08

RPS28	genotypeWT	0.3319474	4.78E-10
RPS29	genotypeWT	0.3274032	7.40E-09
RPS2P5	genotypeWT	0.6911805	0.003767032
RPS3	genotypeWT	0.191312	0.01355665
RPS3A	genotypeWT	0.2865264	3.28E-11
RPS4X	genotypeWT	0.2853867	5.56E-13
RPS5	genotypeWT	0.3801022	1.41E-13
RPS6	genotypeWT	0.2667534	3.27E-05
RPS9	genotypeWT	0.3430543	2.63E-07
SCG2	genotypeWT	0.7365312	0.006526004
SEC61G	genotypeWT	0.4957737	2.83E-06
SF3B6	genotypeWT	0.521802	0.005952334
SLC18A2	genotypeWT	-0.7700351	0.03522298
SNRPD2	genotypeWT	0.39727	0.000219049
SOX11	genotypeWT	-0.5806964	0.000223832
SOX4	genotypeWT	-0.2803931	0.006239187
SRP14	genotypeWT	0.2686032	0.00343226
SSR4	genotypeWT	0.4396931	0.005075598
SYNE2	genotypeWT	-0.8330323	0.03044731
TCEAL4	genotypeWT	-0.6675429	1.35E-06
TIMM17B	genotypeWT	0.7858742	2.03E-05
TMSB10	genotypeWT	0.1804225	0.002108568
TMSB4X	genotypeWT	-0.5970095	6.62E-36
TOMM7	genotypeWT	0.4175453	0.002347737
TPT1	genotypeWT	0.4325094	3.18E-15
TRMT112	genotypeWT	0.5784825	2.61E-07
TTC3	genotypeWT	-0.2356261	0.03522298
UBA52	genotypeWT	0.3661786	1.01E-08
UBB	genotypeWT	0.4335563	2.94E-10
UBBP4	genotypeWT	0.9000274	0.000115506
UBC	genotypeWT	0.4338325	1.13E-07
UQCRB	genotypeWT	0.3485246	0.008837408
UQCRH	genotypeWT	0.6005496	1.72E-11
WSB1	genotypeWT	-0.2669257	0.002539071
YBX1	genotypeWT	0.3152554	1.05E-07

	RPCs		
gene_short_name	term	estimate	q_value
AC004453.8	genotypeWT	0.5188801	2.31E-05
AC007969.5	genotypeWT	0.4221974	1.66E-48
AC009245.3	genotypeWT	0.6595475	2.55E-26
ACSL4	genotypeWT	-0.6195421	0.00102583
AFG3L2	genotypeWT	-0.5768791	0.001585199
ASPM	genotypeWT	-1.188619	0.02630528
ATP5A1	genotypeWT	0.2932023	1.00E-07
ATXN7L3B	genotypeWT	-0.3179922	0.03102748
BAZ2B	genotypeWT	-0.2350526	0.001173972
BEX2	genotypeWT	-0.7284225	4.38E-49
BEX3	genotypeWT	-0.5397637	2.08E-94
C12orf57	genotypeWT	0.3454363	5.47E-13
C1orf61	genotypeWT	0.4720821	0.0447663
C6orf48	genotypeWT	0.2454355	3.81E-13
CASK	genotypeWT	-0.7820544	9.98E-05
CD63	genotypeWT	0.3321505	6.02E-13
CEBPZOS	genotypeWT	-0.45102	0.04968502
CENPF	genotypeWT	-0.740378	0.001194452
CEP350	genotypeWT	-0.3535558	0.002943083
CHCHD10	genotypeWT	0.5527817	0.000544051
CHD4	genotypeWT	-0.2501629	2.23E-05
COX4I1	genotypeWT	0.2352316	3.81E-12
CRABP1	genotypeWT	0.1171017	0.014865603
CRYAB	genotypeWT	0.6039426	0.000517286
CTD-3014M21.1	genotypeWT	-0.4750212	0.04660991
CUTA	genotypeWT	0.2058608	0.002840316
CYC1	genotypeWT	0.3028766	0.03738644
DAD1	genotypeWT	0.2462813	0.00100528
DAPL1	genotypeWT	0.201015	0.00267592
DNAJB1	genotypeWT	0.3224582	1.00E-11
EDF1	genotypeWT	0.2095736	3.25E-10
EEF1A1	genotypeWT	0.1901957	9.72E-32

EEF1A1P5	genotypeWT	0.5386828	0.008659549
EEF1D	genotypeWT	0.2338436	9.34E-07
EIF1	genotypeWT	0.1108011	0.000513189
EIF1AX	genotypeWT	0.5449322	1.05E-14
EIF3E	genotypeWT	0.1863969	0.000158583
EIF3L	genotypeWT	0.3304634	0.03451392
EIF4A2	genotypeWT	0.1620461	1.01E-05
EIF4G3	genotypeWT	-0.3690554	0.03389925
ELOB	genotypeWT	0.1825782	5.94E-05
EPB41L4A-AS1	genotypeWT	0.325705	3.45E-09
FABP7	genotypeWT	0.8417467	4.77E-22
FAU	genotypeWT	0.2243839	6.12E-29
FIS1	genotypeWT	0.3318416	0.008187258
FKBP4	genotypeWT	0.3325354	0.0402584
FNBP1L	genotypeWT	-0.2220599	0.04251159
FOS	genotypeWT	-0.3821967	3.92E-06
FTH1	genotypeWT	0.1345748	7.34E-08
FTL	genotypeWT	0.3470225	7.15E-65
FTLP3	genotypeWT	0.564024	2.05E-11
FUS	genotypeWT	-0.1877647	0.02610104
GABARAP	genotypeWT	0.3656844	0.001056626
GAD2	genotypeWT	0.6576063	0.00300468
GAPDH	genotypeWT	0.1517226	9.35E-11
GAS5	genotypeWT	0.1429809	9.58E-06
GLTSCR2	genotypeWT	0.3172869	1.66E-05
GNAS	genotypeWT	0.2503349	2.83E-10
GPC3	genotypeWT	0.9125108	0.03574482
GPM6B	genotypeWT	-0.3734512	1.29E-11
GSTP1	genotypeWT	0.2228017	2.23E-07
H3F3B	genotypeWT	0.1082001	5.14E-05
HIST1H1D	genotypeWT	-0.8289718	2.07E-17
HIST1H1E	genotypeWT	-0.764859	1.46E-29
HIST1H2AC	genotypeWT	0.3040499	0.01513216
HIST1H4C	genotypeWT	0.2353614	2.35E-05
HLTF	genotypeWT	-0.3343525	5.65E-05
HMGB1P5	genotypeWT	0.8443025	0.000375175

HSP90AB1	genotypeWT	0.1025362	3.45E-07
HSPA6	genotypeWT	0.6572386	1.79E-08
HSPB1	genotypeWT	0.3857488	2.63E-18
HSPD1	genotypeWT	0.1470407	0.000766469
ID2	genotypeWT	0.3725274	1.15E-05
IER2	genotypeWT	-0.3698661	6.86E-07
IFITM2	genotypeWT	-0.5414922	0.003992132
IFITM3	genotypeWT	-0.2594739	0.001036079
IGFBP2	genotypeWT	-0.4273996	0.001223224
KCNQ1OT1	genotypeWT	-0.4171251	0.000731478
KRT10	genotypeWT	0.2666145	0.000778793
LAMTOR5	genotypeWT	0.1814084	0.02548572
LDHB	genotypeWT	0.1544265	0.009501492
LRRC75A-AS1	genotypeWT	0.1659052	3.28E-06
MAGI3	genotypeWT	-0.4744233	0.001589239
MALAT1	genotypeWT	-0.3553586	1.15E-117
MARCKSL1	genotypeWT	0.4415677	7.26E-27
MIAT	genotypeWT	-0.2567086	8.85E-08
MICU2	genotypeWT	-0.330496	0.04230828
MIF	genotypeWT	0.2194318	4.91E-15
MIS18BP1	genotypeWT	-0.6293291	0.0269205
MORF4L2	genotypeWT	-0.6030064	6.48E-63
MRPL18	genotypeWT	0.3852063	4.30E-06
MT-CO1	genotypeWT	-0.2751945	7.36E-18
MT-ND2	genotypeWT	-0.2446478	0.000232983
MT-ND4	genotypeWT	-0.2276851	5.34E-09
MT-ND5	genotypeWT	-0.2302447	3.22E-05
MT-RNR1	genotypeWT	-0.2323038	0.005432064
MT-RNR2	genotypeWT	-0.5172036	4.51E-94
MYO6	genotypeWT	-0.4186706	0.04374168

NACA	genotypeWT	0.1960573	7.98E-19
NDUFB7	genotypeWT	0.2736287	0.00859826
NME2	genotypeWT	0.5622306	1.48E-06
NPM1P39	genotypeWT	1.251248	1.74E-09
NR2F1	genotypeWT	-0.3053995	4.33E-14
NSMCE1	genotypeWT	0.8919799	4.28E-07
NUDC	genotypeWT	0.207079	0.02240495
OAZ1	genotypeWT	0.2370004	8.42E-11
OFD1	genotypeWT	-0.6323281	3.36E-22
PALLD	genotypeWT	-0.3244159	0.009029352
PCBP1	genotypeWT	0.2320994	0.000939406
PCM1	genotypeWT	-0.2503616	0.004074246
PFDN5	genotypeWT	0.2402153	4.97E-16
PJA1	genotypeWT	0.5944337	1.95E-06
PLEKHA1	genotypeWT	-0.2435922	0.002819871
PNISR	genotypeWT	-0.1831294	9.21E-06
PNN	genotypeWT	-0.2144624	1.45E-05
PNRC1	genotypeWT	-0.3765639	0.00055845
PQBP1	genotypeWT	0.3501093	0.04066722
PRDX4	genotypeWT	0.3289684	1.63E-07
PRDX5	genotypeWT	0.2180145	0.000282453
PRRC2C	genotypeWT	-0.1999381	0.00041226
PTMAP5	genotypeWT	0.8461445	4.70E-10
RAB9B	genotypeWT	-0.7197782	0.011556968
RACK1	genotypeWT	0.1928163	1.15E-21
RAN	genotypeWT	0.1687842	0.008002508
RCVRN	genotypeWT	0.6227418	0.005658125
ROCK2	genotypeWT	-0.4710401	0.016899498
RP11-15A1.3	genotypeWT	3.057031	1.22E-18
RP11-40C6.2	genotypeWT	1.458803	7.44E-19
RP11-475C16.1	genotypeWT	0.6003732	3.65E-15
RP11-84E17.1	genotypeWT	0.1845955	5.06E-07
RP11-864N7.2	genotypeWT	0.7823272	5.81E-33
RP4-604A21.1	genotypeWT	0.2501494	3.69E-05

RP4-765C7.2	genotypeWT	1.868807	0.020556
RPL10	genotypeWT	0.2032624	7.60E-38
RPL10A	genotypeWT	0.1497893	1.28E-13
RPL11	genotypeWT	0.1933371	1.85E-30
RPL12	genotypeWT	0.1976218	8.64E-15
RPL13	genotypeWT	0.176501	7.41E-33
RPL13A	genotypeWT	0.2347294	4.45E-67
RPL13AP5	genotypeWT	0.3274395	1.83E-06
RPL13P12	genotypeWT	0.3033014	2.56E-09
RPL14	genotypeWT	0.1513947	6.99E-09
RPL15	genotypeWT	0.1157059	4.92E-08
RPL18	genotypeWT	0.1715959	4.04E-14
RPL18A	genotypeWT	0.2331299	5.00E-35
RPL19	genotypeWT	0.219233	2.95E-36
RPL21	genotypeWT	0.1619134	9.72E-21
RPL23	genotypeWT	0.1218305	1.89E-09
RPL23A	genotypeWT	0.1937583	2.99E-22
RPL24	genotypeWT	0.1308092	1.77E-09
RPL27	genotypeWT	0.1554839	7.77E-18
RPL27A	genotypeWT	0.240834	6.98E-42
RPL28	genotypeWT	0.1263393	8.12E-06
RPL3	genotypeWT	0.1865984	3.05E-31
RPL30	genotypeWT	0.1948388	1.50E-27
RPL31	genotypeWT	0.11576	1.38E-07
RPL32	genotypeWT	0.1954553	1.67E-30
RPL34	genotypeWT	0.0969134	0.000811719
RPL35	genotypeWT	0.1564836	1.45E-11
RPL35A	genotypeWT	0.1735964	7.18E-24
RPL36	genotypeWT	0.1349691	3.88E-06
RPL37	genotypeWT	0.1236134	6.20E-06
RPL37A	genotypeWT	0.1886012	4.56E-25
RPL38	genotypeWT	0.093279	0.03800085
RPL39P3	genotypeWT	0.6223157	0.000362842
RPL3P4	genotypeWT	0.2492961	2.08E-05
RPL4	genotypeWT	0.1913858	1.13E-21
RPL41	genotypeWT	0.281296	3.43E-54
RPL5P1	genotypeWT	1.632091	6.87E-28
RPL7	genotypeWT	0.1512795	8.79E-19
RPL7P1	genotypeWT	0.5566205	5.30E-13
RPL8	genotypeWT	0.2611428	8.02E-44

RPL9	genotypeWT	0.101416	9.79E-06
RPLP0	genotypeWT	0.0900058	0.000179179
RPLP1	genotypeWT	0.1995477	5.61E-35
RPLP2	genotypeWT	0.2612536	8.83E-57
RPS11	genotypeWT	0.2719817	3.95E-71
RPS12	genotypeWT	0.2436319	5.26E-52
RPS13	genotypeWT	0.2402445	7.98E-45
RPS13P2	genotypeWT	0.3304153	0.000162692
RPS14	genotypeWT	0.1924596	6.66E-32
RPS15	genotypeWT	0.1636183	4.50E-25
RPS15A	genotypeWT	0.1541035	8.64E-17
RPS16	genotypeWT	0.2048267	2.49E-34
RPS17	genotypeWT	0.1761018	1.76E-22
RPS18	genotypeWT	0.2400178	9.10E-47
RPS19	genotypeWT	0.2320731	5.47E-56
RPS2	genotypeWT	0.5065518	1.32E-122
RPS20	genotypeWT	0.2022577	2.49E-27
RPS21	genotypeWT	0.1521141	4.88E-10
RPS23	genotypeWT	0.2142737	3.01E-32
RPS25	genotypeWT	0.232123	3.78E-42
RPS27	genotypeWT	0.1718187	2.51E-17
RPS27A	genotypeWT	0.1868169	2.10E-30
RPS27AP16	genotypeWT	0.2833992	0.014557896
RPS28	genotypeWT	0.1734729	8.65E-21
RPS29	genotypeWT	0.1497252	1.46E-11
RPS2P5	genotypeWT	0.6288519	2.41E-30
RPS3	genotypeWT	0.1107208	1.48E-08
RPS3A	genotypeWT	0.1297308	7.21E-15
RPS3AP26	genotypeWT	0.4061053	4.04E-05
RPS3AP5	genotypeWT	0.5047954	4.27E-05
RPS3AP6	genotypeWT	0.6784447	7.33E-16
RPS4X	genotypeWT	0.2009002	1.70E-38
RPS5	genotypeWT	0.257666	1.83E-44
RPS6	genotypeWT	0.1385249	2.03E-15
RPS7	genotypeWT	0.1424008	5.46E-11
RPS8	genotypeWT	0.0784212	0.000706786
RPS9	genotypeWT	0.207342	6.82E-23
RPSA	genotypeWT	0.1426479	1.26E-08
SAT1	genotypeWT	0.3046853	0.000161462
SEC31A	genotypeWT	-	0.000424607

		0.3109838	
SEC61G	genotypeWT	0.1766445	0.03143691
SELENOM	genotypeWT	0.4076972	0.000369009
SELENOW	genotypeWT	0.2183802	0.010796625
SLC18A2	genotypeWT	-1.151056	0.03225722
SLC25A6	genotypeWT	0.2505681	2.13E-05
SMARCA5	genotypeWT	-0.2621866	2.89E-05
SMC4	genotypeWT	-0.4474771	2.79E-05
SNHG5	genotypeWT	0.343763	2.49E-19
SNHG7	genotypeWT	0.4316962	0.002449615
SNRPD2	genotypeWT	0.1958341	3.25E-08
SRSF5	genotypeWT	-0.2551191	1.47E-12
SSR4	genotypeWT	0.2129203	0.001387699
SYNE2	genotypeWT	-0.3974106	3.49E-05
TCEAL1	genotypeWT	-0.4412742	0.001237579
TCEAL3	genotypeWT	-0.4280476	1.98E-06
TCEAL4	genotypeWT	-0.4626531	2.20E-24
TCEAL7	genotypeWT	-0.6180415	2.45E-18
TCEAL8	genotypeWT	-0.5028997	2.09E-07
TCEAL9	genotypeWT	-0.5393675	6.94E-18
TFAP2A	genotypeWT	0.4543416	0.000457564
TIMP1	genotypeWT	0.3990185	0.001262228
TMSB4X	genotypeWT	-0.428671	4.91E-61
TMSB4XP6	genotypeWT	-0.9883668	0.0287686
TOP2A	genotypeWT	-0.6891168	1.49E-05
TPI1	genotypeWT	0.1936075	5.36E-12
TPT1	genotypeWT	0.2953759	4.49E-45
TRIM24	genotypeWT	-0.4289093	0.001367176
TSPAN6	genotypeWT	-0.5646465	0.005904738
TTC3	genotypeWT	-0.1239049	0.0482502
TXNIP	genotypeWT	-0.1512744	0.0447663

UBA52	genotypeWT	0.2649428	5.13E-33
UBB	genotypeWT	0.2718833	1.35E-26
UBBP4	genotypeWT	0.6058915	8.43E-16
UBC	genotypeWT	0.2392735	1.82E-09
UPF3B	genotypeWT	-0.2880807	0.017289278
UQCRB	genotypeWT	0.1633798	0.006048462
UQCRH	genotypeWT	0.2329652	4.11E-06
USP9X	genotypeWT	-0.4357833	0.009193449
VIM	genotypeWT	0.1497659	0.001418513
WIF1	genotypeWT	0.5545073	3.26E-05
WSB1	genotypeWT	-0.1220278	0.018747984
YBX1	genotypeWT	0.2506845	5.48E-24
ZCCHC11	genotypeWT	-0.2880927	1.71E-08
ZFAS1	genotypeWT	0.1694959	1.80E-07
ZFP36L1	genotypeWT	-0.3309884	9.85E-07
ZNF33A	genotypeWT	-0.4202095	0.003107429
ZNF404	genotypeWT	3.366692	0.001188332
ZNF608	genotypeWT	-0.310228	0.011618095
ZNF711	genotypeWT	-0.4116123	0.02281494
ZRANB2	genotypeWT	-0.2731343	1.59E-05

NPCs

gene_short_name	term	estimate	q_value
AC007969.5	genotypeWT	0.6146665	4.76E-10
ACTB	genotypeWT	-0.4659176	2.01E-18
ACTG1	genotypeWT	-0.2831789	4.94E-07
ATRX	genotypeWT	-0.5301227	1.56E-05
BEX2	genotypeWT	-0.7313599	4.46E-20
BEX3	genotypeWT	0.6503891	1.27E-51
C12orf57	genotypeWT	0.4547379	6.82E-05
C6orf48	genotypeWT	0.508496	2.65E-05
CALM1	genotypeWT	-0.3930445	7.46E-10
CAMLG	genotypeWT	0.3877109	0.0347165

CEBPZOS	genotypeWT	-1.445625	0.001354834
CHMP2A	genotypeWT	0.5301381	0.0232578
EDF1	genotypeWT	0.3377662	1.08E-05
EEF1A1	genotypeWT	0.2574472	5.87E-06
EEF1D	genotypeWT	0.6463134	0.004275404
EEF2	genotypeWT	0.261489	0.008195216
ENO1	genotypeWT	0.2755596	0.001315022
EPB41L4A-AS1	genotypeWT	0.5089144	0.03280756
FAU	genotypeWT	0.3568704	1.83E-10
FDFT1	genotypeWT	0.7334751	0.009150134
FTL	genotypeWT	0.4460312	1.37E-20
FTLP3	genotypeWT	1.040483	0.000865195
GPM6B	genotypeWT	-0.9701376	8.69E-05
H1FX	genotypeWT	0.8994502	0.014598292
HIST1H1E	genotypeWT	-1.139698	5.34E-05
HIST1H2BD	genotypeWT	0.823274	0.01896265
HIST3H2A	genotypeWT	0.8295889	0.004402476
HLTF	genotypeWT	-0.5855586	0.008624622
HOXA4	genotypeWT	1.271054	0.000482173
HOXB5	genotypeWT	-0.6630991	3.02E-08
KRT10	genotypeWT	0.7264242	0.000228342
MALAT1	genotypeWT	-0.235248	0.000221969
MAP1B	genotypeWT	-0.3574379	4.17E-11
MARCKSL1	genotypeWT	0.3685378	0.008210645
MIF	genotypeWT	0.2981784	1.08E-05
MORF4L2	genotypeWT	-0.4883983	4.68E-12
MT-ATP6	genotypeWT	-0.6039051	1.07E-05
MT-CO1	genotypeWT	-0.4239233	5.79E-06
MT-CYB	genotypeWT	-0.6342665	0.001193883
MT-ND2	genotypeWT	-0.4792803	0.00810006
MT-ND4	genotypeWT	-0.3793212	0.001206576
MT-RNR2	genotypeWT	-0.6424577	1.03E-25
NACA	genotypeWT	0.2455787	0.005709026
NPM1	genotypeWT	0.2788942	0.01370668

NR2F1	genotypeWT	-0.4222251	7.09E-05
OFD1	genotypeWT	-0.7527816	0.03598824
PCBP1	genotypeWT	0.4742576	0.02930568
PHPT1	genotypeWT	0.3317692	0.01007408
PJA1	genotypeWT	0.6682682	0.015489792
PNISR	genotypeWT	-0.3382002	0.04538055
PRDX4	genotypeWT	0.5185505	0.02309995
RACK1	genotypeWT	0.311014	5.36E-07
RP11-834C11.4	genotypeWT	0.5319222	5.41E-06
RP11-84E17.1	genotypeWT	0.4601682	0.000491722
RP4-604A21.1	genotypeWT	0.8533995	2.08E-09
RPL10	genotypeWT	0.2401066	4.27E-06
RPL10A	genotypeWT	0.2843369	7.02E-06
RPL11	genotypeWT	0.2918314	2.10E-08
RPL13	genotypeWT	0.3806682	3.58E-25
RPL13A	genotypeWT	0.4086741	1.46E-32
RPL13AP5	genotypeWT	0.7706303	0.002010582
RPL13P12	genotypeWT	0.9076151	4.75E-08
RPL14	genotypeWT	0.3968201	7.22E-10
RPL15	genotypeWT	0.2028836	0.001138091
RPL18	genotypeWT	0.4237186	4.84E-15
RPL18A	genotypeWT	0.4301173	1.30E-16
RPL19	genotypeWT	0.3480351	1.16E-12
RPL21	genotypeWT	0.3480548	2.65E-14
RPL22	genotypeWT	0.4065026	8.47E-05
RPL23	genotypeWT	0.3186688	4.92E-10
RPL23A	genotypeWT	0.362372	7.45E-12
RPL24	genotypeWT	0.3982933	7.76E-18
RPL26	genotypeWT	0.3450007	7.75E-09
RPL27	genotypeWT	0.3767955	7.43E-17
RPL27A	genotypeWT	0.4411979	7.75E-20
RPL28	genotypeWT	0.4111764	6.30E-12
RPL29	genotypeWT	0.4089827	1.97E-05
RPL3	genotypeWT	0.3038153	2.19E-10
RPL30	genotypeWT	0.4270954	3.40E-17
RPL31	genotypeWT	0.3168595	1.84E-10
RPL32	genotypeWT	0.3984189	5.41E-20
RPL34	genotypeWT	0.2605797	1.76E-05

RPL35	genotypeWT	0.3247846	9.06E-08
RPL35A	genotypeWT	0.4456163	9.14E-24
RPL36	genotypeWT	0.2482432	0.0207142
RPL36A	genotypeWT	0.5616876	3.24E-10
RPL37	genotypeWT	0.2753418	0.004992037
RPL37A	genotypeWT	0.422567	2.49E-19
RPL38	genotypeWT	0.3504068	3.27E-09
RPL39	genotypeWT	0.4888064	1.07E-08
RPL4	genotypeWT	0.4400662	5.71E-18
RPL41	genotypeWT	0.4760141	8.06E-20
RPL4P4	genotypeWT	0.8485918	0.02787575
RPL5	genotypeWT	0.2584007	4.36E-05
RPL7	genotypeWT	0.2514381	9.32E-06
RPL7A	genotypeWT	0.3227986	7.40E-06
RPL8	genotypeWT	0.4145408	1.88E-16
RPL9	genotypeWT	0.2871707	1.56E-08
RPLP0P6	genotypeWT	0.7795989	0.00032892
RPLP1	genotypeWT	0.2381071	3.49E-06
RPLP2	genotypeWT	0.4654313	1.62E-25
RPS10	genotypeWT	0.359311	0.00261662
RPS11	genotypeWT	0.4477991	2.73E-27
RPS12	genotypeWT	0.4335	7.87E-22
RPS13	genotypeWT	0.5341044	9.58E-38
RPS13P2	genotypeWT	0.8651211	0.005947858
RPS14	genotypeWT	0.3429923	3.43E-15
RPS15	genotypeWT	0.307658	2.21E-12
RPS15A	genotypeWT	0.467356	6.23E-24
RPS16	genotypeWT	0.5189539	4.92E-34
RPS17	genotypeWT	0.4185222	2.84E-18
RPS18	genotypeWT	0.4077462	1.62E-18
RPS19	genotypeWT	0.4503422	3.18E-28
RPS2	genotypeWT	0.734132	1.96E-31
RPS20	genotypeWT	0.3792	2.83E-08
RPS21	genotypeWT	0.4773004	2.90E-14
RPS23	genotypeWT	0.2931925	1.81E-06
RPS24	genotypeWT	0.3311597	1.96E-12
RPS25	genotypeWT	0.4475368	8.75E-22
RPS26	genotypeWT	0.3590642	0.00441815
RPS27	genotypeWT	0.512093	3.26E-22
RPS27A	genotypeWT	0.2737364	2.55E-08

RPS28	genotypeWT	0.3030733	1.76E-07
RPS29	genotypeWT	0.3240074	2.56E-08
RPS2P5	genotypeWT	1.00869	1.14E-06
RPS3	genotypeWT	0.1899815	0.02851112
RPS3A	genotypeWT	0.2238387	1.31E-06
RPS4X	genotypeWT	0.2827487	2.97E-12
RPS5	genotypeWT	0.4298655	2.31E-18
RPS7	genotypeWT	0.342961	9.65E-08
RPS8	genotypeWT	0.2408224	4.80E-09
RPSA	genotypeWT	0.2615657	0.004163994
SEC61G	genotypeWT	0.3941465	0.002377444
SNRPD2	genotypeWT	0.3776488	0.000139258
SSR4	genotypeWT	0.5325792	6.40E-06
STMN2	genotypeWT	-0.1978553	0.02214687
SUCO	genotypeWT	0.6268677	0.005199048
TCEAL4	genotypeWT	-0.8134084	5.84E-14
TCEAL7	genotypeWT	-0.641806	8.14E-07
TCF7L2	genotypeWT	-2.313817	5.77E-06
TMSB4X	genotypeWT	-0.8804051	7.22E-64
TOMM20	genotypeWT	0.4798487	0.02246412
TPT1	genotypeWT	0.5825604	8.66E-24
TRMT112	genotypeWT	0.4415988	0.00059865
UBA52	genotypeWT	0.4756275	1.02E-14
YBX1	genotypeWT	0.3924091	6.30E-12
ZFAS1	genotypeWT	0.3874896	0.004354896
ZIC2	genotypeWT	-1.90028	5.35E-05
ZIC4	genotypeWT	-0.7791953	0.010328472

RPE

gene_short_name	term	estimate	q_value
DCT	genotypeWT	0.8849135	0.004286656
RGR	genotypeWT	-0.9405609	0.03993072
RPL13A	genotypeWT	0.2462205	0.03007225
RPLP0	genotypeWT	0.3871244	0.003824206
RPS19	genotypeWT	0.3593436	0.007817634
RPS4X	genotypeWT	0.2913059	0.01619408
TMEM98	genotypeWT	0.4777809	0.04187512

unknown population

gene_short_name	term	estimate	q_value
B2M	genotypeWT	0.4653088	0.003360636
BEX3	genotypeWT	-0.5959846	4.44E-12
GPC3	genotypeWT	1.396363	0.000493266
GPM6B	genotypeWT	-1.592554	2.91E-06
HSPA1A	genotypeWT	0.5693053	0.02818749
MORF4L2	genotypeWT	-0.8803587	6.71E-08
NUPR1	genotypeWT	0.630554	0.04349722
RPL13A	genotypeWT	0.1855269	0.012795762
RPL26	genotypeWT	-0.3290661	0.001243918
RPL9P9	genotypeWT	-0.4536162	0.0382239
RPS2	genotypeWT	0.5249035	3.97E-06
TGFBI	genotypeWT	-0.5054303	0.006836094
TMSB4X	genotypeWT	-0.5893548	8.44E-23
TPM4	genotypeWT	-0.4075812	0.02175368
UBB	genotypeWT	0.3741789	0.005368875
RSPO3	genotypeWT	1.507384	0.000754651

muller glia

gene_short_name	term	estimate	q_value
ABCA1	genotypeWT	0.935263	1.11E-09
ABCD4	genotypeWT	0.4977214	3.22E-11
ABI3BP	genotypeWT	0.7467911	7.64E-11
AC004556.1	genotypeWT	-0.945292	6.08E-12
AC009245.3	genotypeWT	0.7273996	1.32E-21
AC018738.2	genotypeWT	-2.222102	0.007251585
ACER3	genotypeWT	0.7288369	7.53E-06
ACLY	genotypeWT	0.5263501	2.85E-05
ACSL4	genotypeWT	-0.7770128	0.011264112
ACTB	genotypeWT	-0.4274039	2.87E-88
ACTG1	genotypeWT	-0.1817712	1.11E-25
ADAMTS1	genotypeWT	-0.6654927	1.84E-09
ADGRB1	genotypeWT	1.463647	1.02E-05
ADI1	genotypeWT	0.396129	0.04288364
ADM	genotypeWT	0.7834316	1.06E-43

AEBP1	genotypeWT	0.3594289	4.38E-07
AFDN	genotypeWT	0.5260295	5.47E-11
AGPAT2	genotypeWT	1.044632	7.03E-19
AGPAT4	genotypeWT	0.6793893	9.07E-05
AKAP12	genotypeWT	0.288332	5.36E-14
AKAP17A	genotypeWT	0.5153662	0.04937031
AKR1A1	genotypeWT	0.291079	0.0305205
ALPL	genotypeWT	1.177123	2.96E-15
AMER2	genotypeWT	0.8681066	6.69E-05
ANGPTL4	genotypeWT	0.4496935	0.011954986
ANK3	genotypeWT	-0.4997926	0.0232218
ANKRD10	genotypeWT	0.4906397	3.56E-08
AP1S2	genotypeWT	-0.2757957	2.12E-06
AP2M1	genotypeWT	0.4516247	3.86E-20
AP3D1	genotypeWT	0.5130731	3.25E-06
APOE	genotypeWT	0.4844114	2.14E-17
AQP1	genotypeWT	0.5780432	0.000255217
ARF1	genotypeWT	0.2536683	2.61E-10
ARF4	genotypeWT	0.2055061	0.0224103
ARHGAP6	genotypeWT	0.7608755	0.015230583
ARHGEF10	genotypeWT	0.5853524	0.000632817
ARHGEF7	genotypeWT	0.5818507	0.005458815
ARL4A	genotypeWT	-0.3764053	5.94E-05
ARL4C	genotypeWT	0.5155186	7.36E-28
ARMCX3	genotypeWT	0.3422377	1.34E-07
ARPC2	genotypeWT	0.1472867	0.001473192
ATAD5	genotypeWT	0.5165319	0.02098728
ATP13A3	genotypeWT	0.9271109	0.000435914
ATP1A2	genotypeWT	0.2676845	0.04632732
ATP1B1	genotypeWT	0.356351	1.07E-06
ATP1B2	genotypeWT	-0.353014	2.95E-08
ATP2A2	genotypeWT	0.5923565	0.00303104
ATP5B	genotypeWT	0.2770928	1.99E-10
ATP5E	genotypeWT	-0.2265607	2.24E-15
ATP6AP1	genotypeWT	0.3772635	0.000138678
ATP6V0B	genotypeWT	0.2119904	0.0453136
ATP6V1G1	genotypeWT	0.1697624	1.05E-06
B2M	genotypeWT	0.1947097	1.50E-11

BCAT1	genotypeWT	0.5285153	4.35E-06
BEST1	genotypeWT	-0.7021977	2.79E-05
BEX1	genotypeWT	-0.2676058	4.31E-12
BEX2	genotypeWT	-0.7135573	5.23E-65
BEX3	genotypeWT	-0.6141262	2.85E-212
BHLHE41	genotypeWT	0.66722	1.91E-15
BNIP3L	genotypeWT	0.1739847	0.011792934
BST2	genotypeWT	0.7285575	1.22E-13
BTG2	genotypeWT	-0.540325	1.95E-10
C16orf74	genotypeWT	1.460687	5.57E-05
C19orf43	genotypeWT	0.3406196	0.000238809
C1QL1	genotypeWT	1.074251	0.04429978
C1QTNF3	genotypeWT	0.9030068	0.000318882
C1orf43	genotypeWT	0.2080383	0.0123624
C1orf61	genotypeWT	-0.3070586	1.66E-08
C4orf48	genotypeWT	0.2290201	2.01E-06
C6orf48	genotypeWT	0.2385583	3.99E-20
CA2	genotypeWT	-0.3679064	5.05E-07
CACYBP	genotypeWT	-0.2242082	0.000190682
CADM1	genotypeWT	0.3104011	3.20E-12
CALB1	genotypeWT	-1.26631	3.75E-14
CALM2	genotypeWT	-0.1596269	2.59E-06
CALU	genotypeWT	0.3359742	3.07E-11
CAMK1D	genotypeWT	1.174291	4.21E-17
CAMLG	genotypeWT	0.209592	0.000563125
CAPN10-AS1	genotypeWT	1.088813	0.0264654
CAPN6	genotypeWT	-1.004767	0.00417384
CAPZB	genotypeWT	-0.2228484	0.03336088
CARD19	genotypeWT	0.6619696	1.01E-07
CASK	genotypeWT	-0.609101	0.003255366
CCND1	genotypeWT	0.9030514	3.50E-125
CCNG1	genotypeWT	0.367049	0.000140114
CCNL2	genotypeWT	0.3407561	2.54E-08
CD151	genotypeWT	0.2923724	7.94E-05
CD63	genotypeWT	0.2282382	2.66E-15

CD81	genotypeWT	0.6392614	2.19E-09
CDC16	genotypeWT	0.3353167	0.0014035
CDCA7L	genotypeWT	0.3512567	0.014315886
CDIP1	genotypeWT	1.33384	9.03E-80
CDKN1A	genotypeWT	0.2210929	0.04957104
CDKN1C	genotypeWT	0.4203996	0.0272757
CEBPZOS	genotypeWT	-0.5612553	5.17E-10
CELF1	genotypeWT	0.4031495	4.93E-06
CFI	genotypeWT	-0.3667944	9.20E-13
CHCHD10	genotypeWT	0.482727	1.02E-05
CHD2	genotypeWT	0.2719207	0.004275722
CHPF	genotypeWT	0.6368823	3.04E-21
CISD1	genotypeWT	0.3879308	6.36E-10
CKB	genotypeWT	0.4540374	2.21E-56
CLCN6	genotypeWT	0.7789834	0.00399009
CLN8	genotypeWT	0.6289404	0.01102032
CLTB	genotypeWT	0.5432627	0.005499436
CLU	genotypeWT	-0.2167709	2.10E-09
CMIP	genotypeWT	0.4618816	1.04E-05
CNDP2	genotypeWT	0.4821255	5.42E-06
CNOT7	genotypeWT	0.261251	0.02281552
CNP	genotypeWT	0.3736599	0.008595136
COL11A1	genotypeWT	0.3112825	4.91E-08
COL15A1	genotypeWT	1.403238	6.12E-26
COL18A1	genotypeWT	0.333883	0.02261292
COL1A1	genotypeWT	1.008788	5.22E-26
COL1A2	genotypeWT	-0.4617147	1.24E-20
COL2A1	genotypeWT	0.4380039	0.001323669
COL9A1	genotypeWT	-0.5146432	1.62E-14
COMT	genotypeWT	0.3270185	0.01923872
COPS8	genotypeWT	0.3667835	3.30E-05
COTL1	genotypeWT	0.4104235	1.23E-06
CP	genotypeWT	-1.0786865	2.83E-69
CPNE1	genotypeWT	0.420053	2.12E-07
CRACR2B	genotypeWT	0.6445745	1.15E-06
CRIP2	genotypeWT	0.5245522	5.55E-15
CST3	genotypeWT	0.5736252	4.76E-15

CTD-2287O16.1	genotypeWT	-0.991812	0.000757963
CTD-2371O3.3	genotypeWT	1.214062	0.000101009
CTNNA2	genotypeWT	1.161715	4.49E-07
CTTN	genotypeWT	0.4170265	0.0325504
CUTA	genotypeWT	0.1639148	0.004071739
CXADR	genotypeWT	0.4733712	8.13E-05
CXCR4	genotypeWT	0.2882466	0.002745392
CXXC5	genotypeWT	0.3284389	1.86E-06
CYR61	genotypeWT	-0.3383058	0.004479645
DAG1	genotypeWT	0.5815818	0.004438952
DAZAP2	genotypeWT	0.2959073	0.007638576
DCLK1	genotypeWT	0.3109316	0.005071104
DDB2	genotypeWT	0.5258187	1.94E-05
DDIT4	genotypeWT	0.2918784	8.77E-08
DDR2	genotypeWT	-0.7513853	2.93E-05
DGKD	genotypeWT	0.5587854	0.014437536
DGUOK	genotypeWT	0.2329195	0.000325022
DHX9	genotypeWT	-0.2646588	0.03072246
DIRAS3	genotypeWT	-1.089119	0.02484408
DKK3	genotypeWT	0.1730069	0.000265495
DLG5	genotypeWT	0.5623761	3.56E-06
DNAH11	genotypeWT	0.9150603	1.28E-05
DNAJA1	genotypeWT	-0.343538	2.01E-22
DNAJB1	genotypeWT	-0.3361264	1.61E-14
DNAJB4	genotypeWT	-0.4928553	0.000306553
DNER	genotypeWT	0.8354176	2.23E-23
DPP7	genotypeWT	0.5255402	4.94E-10
DPYSL3	genotypeWT	0.6145412	5.85E-07
DRAM2	genotypeWT	0.4489406	0.02970954
DSC2	genotypeWT	0.4708166	0.002581992
DTYMK	genotypeWT	0.4504683	6.06E-07
DYNC1LI2	genotypeWT	0.2027183	0.013278447
EBLN3P	genotypeWT	0.5119988	8.05E-08
ECE1	genotypeWT	0.4936351	3.99E-07
ECHDC2	genotypeWT	-0.6438442	0.002438905
EEF1A1	genotypeWT	-0.0986262	3.02E-10

EEF1D	genotypeWT	0.2145759	1.12E-10
EFEMP1	genotypeWT	-0.6221979	0.000329104
EFHC1	genotypeWT	0.5632398	0.004805985
EFNB1	genotypeWT	0.7417716	7.22E-06
EFTUD2	genotypeWT	0.5128233	0.02484408
EGFL7	genotypeWT	0.681075	5.52E-09
EGR1	genotypeWT	-0.5122154	2.86E-29
EGR2	genotypeWT	-1.188522	3.04E-10
EGR3	genotypeWT	-0.990368	0.01641073
EI24	genotypeWT	0.4865672	0.00020035
EIF1	genotypeWT	0.1516316	9.27E-14
EIF1AX	genotypeWT	0.6094494	1.46E-23
EIF2AK2	genotypeWT	0.338762	0.00266383
EIF2S3	genotypeWT	0.1774474	0.019258155
EIF4A2	genotypeWT	0.2608232	6.24E-25
ELAVL1	genotypeWT	0.4068253	0.03782124
ELN	genotypeWT	1.098983	0.00490776
ELOVL2	genotypeWT	0.5787461	0.03558975
EMX1	genotypeWT	-2.922455	2.31E-07
ENC1	genotypeWT	0.6060102	0.000162938
ENO1	genotypeWT	-0.1523221	1.94E-10
ENO2	genotypeWT	0.262456	2.22E-07
EPAS1	genotypeWT	0.45397	3.03E-07
EPB41L4A	genotypeWT	-0.8064555	0.000458443
EPB41L4A-AS1	genotypeWT	0.2565386	4.11E-05
EPSTI1	genotypeWT	1.043319	0.000236762
ERF	genotypeWT	0.7381263	1.50E-06
ERICH5	genotypeWT	-0.6839474	1.20E-05
ERO1A	genotypeWT	0.5689673	4.00E-09
ETV5	genotypeWT	0.5546377	0.003133287
FABP5	genotypeWT	-0.6682692	4.50E-23
FAM107A	genotypeWT	1.493024	4.20E-20
FAM173A	genotypeWT	0.7979698	1.14E-10
FAM174A	genotypeWT	0.6449631	4.01E-05
FAM19A5	genotypeWT	1.189194	7.37E-11
FAM20C	genotypeWT	1.069611	3.71E-06
FAM219B	genotypeWT	0.6195815	3.66E-07

FAM8A1	genotypeWT	0.6593266	0.02220766
FAP	genotypeWT	-0.9038819	0.02687124
FBLN2	genotypeWT	1.196372	2.26E-93
FDPS	genotypeWT	0.3306579	0.000417429
FER1L4	genotypeWT	0.6449202	1.56E-08
FEZ1	genotypeWT	0.2422259	0.008595136
FILIP1L	genotypeWT	-0.6277523	0.002745392
FKBP10	genotypeWT	0.5698005	1.06E-18
FLNB	genotypeWT	0.8474286	5.66E-08
FLNC	genotypeWT	0.6108171	0.001532545
FN1	genotypeWT	0.3254191	9.98E-05
FOS	genotypeWT	-0.6247332	1.67E-63
FOSB	genotypeWT	-0.7780607	3.10E-09
FTH1	genotypeWT	-0.2100645	3.51E-29
FUNDC1	genotypeWT	-0.4573832	2.49E-06
FUT11	genotypeWT	0.6121995	1.65E-10
FXYD6	genotypeWT	0.6043767	2.55E-31
FZD3	genotypeWT	0.4300849	1.43E-05
FZD8	genotypeWT	0.7176553	0.001798289
GABARAPL2	genotypeWT	0.1676063	0.018099216
GAD2	genotypeWT	1.251389	6.37E-26
GADD45B	genotypeWT	0.697873	2.25E-23
GAS5	genotypeWT	0.2556892	6.82E-32
GAS6	genotypeWT	0.9455058	5.38E-60
GATM	genotypeWT	0.8470954	2.25E-10
GDI1	genotypeWT	0.2765778	0.00366413
GLO1	genotypeWT	-0.2021515	0.008453052
GLTSCR2	genotypeWT	0.2574488	0.000203008
GLUL	genotypeWT	0.471713	1.93E-17
GNAS	genotypeWT	0.223841	3.52E-13
GNB1	genotypeWT	0.3219905	0.000442062
GNG4	genotypeWT	1.260725	1.21E-21
GOLGA2	genotypeWT	0.3408018	9.18E-05
GOLM1	genotypeWT	0.3863623	0.00096911
GPC3	genotypeWT	0.4676095	0.00649833
GPM6A	genotypeWT	0.202265	0.0284914

GPRC5B	genotypeWT	0.5580159	2.97E-05
GPT2	genotypeWT	0.7827286	3.74E-11
GRAMD4	genotypeWT	1.199817	1.86E-05
GRINA	genotypeWT	0.3702118	7.97E-09
GSE1	genotypeWT	0.5807837	1.08E-09
GUCD1	genotypeWT	0.8390873	0.00366413
H2AFV	genotypeWT	0.4512415	1.61E-12
H2AFZ	genotypeWT	0.1907482	2.26E-06
H3F3A	genotypeWT	-0.2973923	1.13E-05
HAGHL	genotypeWT	0.8431726	8.47E-09
HAP1	genotypeWT	0.8675209	1.73E-05
HAS2	genotypeWT	-1.011122	2.34E-06
HELZ2	genotypeWT	1.181494	4.46E-05
HGF	genotypeWT	-0.7753799	0.003623367
HILPDA	genotypeWT	0.2547253	8.61E-06
HIST1H1D	genotypeWT	-0.8393085	7.67E-15
HIST1H1E	genotypeWT	-0.8959385	5.14E-33
HIST1H4E	genotypeWT	0.6817364	0.001710284
HLA-E	genotypeWT	0.373301	1.48E-05
HMGB1P5	genotypeWT	0.9250298	1.98E-06
HMGCS1	genotypeWT	0.5066694	3.34E-07
HMGN2	genotypeWT	-0.2573363	5.28E-06
HMGN2P5	genotypeWT	-1.084229	0.003969822
HNRNPA1	genotypeWT	-0.1480419	3.25E-08
HNRNPA1P48	genotypeWT	-0.4182295	0.000140313
HNRNPK	genotypeWT	-0.1265422	0.03761975
HS3ST1	genotypeWT	0.9023751	0.04409874
HSF4	genotypeWT	0.3911646	0.001372788
HSP90AA1	genotypeWT	-0.2328258	2.13E-45
HSP90AB1	genotypeWT	-0.1575534	3.99E-21
HSPA1A	genotypeWT	-0.3389805	2.43E-16
HSPA1B	genotypeWT	-0.3244876	1.14E-19
HSPA5	genotypeWT	-	5.43E-05

		0.2237181	
HSPA8	genotypeWT	-0.3904864	7.48E-46
HSPB1	genotypeWT	-0.4003652	2.04E-30
HSPB11	genotypeWT	0.3496657	0.00488755
HSPD1	genotypeWT	-0.1758721	2.63E-10
HSPE1	genotypeWT	-0.1619986	0.000279888
HSPH1	genotypeWT	-0.2546019	0.000288106
HTRA1	genotypeWT	0.5370926	9.13E-07
ID1	genotypeWT	0.7652493	1.52E-09
ID2	genotypeWT	0.6930278	4.22E-54
ID3	genotypeWT	0.2491822	0.04795048
IER2	genotypeWT	-0.3570416	5.46E-13
IFI44	genotypeWT	0.9278829	1.25E-10
IFI44L	genotypeWT	0.8911649	2.57E-37
IFI6	genotypeWT	0.979115	1.23E-94
IFITM1	genotypeWT	-0.530713	4.23E-14
IFITM2	genotypeWT	-0.9394269	8.60E-59
IFITM3	genotypeWT	-0.3977762	3.77E-45
IGF1R	genotypeWT	0.4834192	5.04E-05
IGF2	genotypeWT	-0.3503285	0.000909656
IGFBP5	genotypeWT	0.6622306	3.80E-88
ING5	genotypeWT	0.4953045	0.00020137
INSIG1	genotypeWT	0.5687357	4.35E-06
INSIG2	genotypeWT	0.5039088	1.36E-10
IREB2	genotypeWT	0.528536	0.000405111
IRS2	genotypeWT	1.148242	1.61E-33
ISG15	genotypeWT	0.723328	8.94E-14
ITIH5	genotypeWT	1.058904	1.44E-21
JAM3	genotypeWT	0.6934109	3.06E-09
JTB	genotypeWT	0.2374074	0.001108458
JUN	genotypeWT	-0.3736503	7.32E-26
JUNB	genotypeWT	-0.5782439	8.58E-20
KATNBL1	genotypeWT	0.3177219	0.003745644
KAZN	genotypeWT	0.9624438	3.40E-18

KBTBD11	genotypeWT	0.8525465	6.36E-05
KDELR2	genotypeWT	0.331728	2.98E-08
KIRREL	genotypeWT	0.8574825	0.016024968
KLHDC2	genotypeWT	0.3263806	0.00348024
KLHL29	genotypeWT	1.148173	0.001137085
KPNB1	genotypeWT	0.2140525	0.02464165
KRT10	genotypeWT	0.603407	1.44E-40
LAMB2	genotypeWT	0.6273131	0.001337969
LAMP1	genotypeWT	0.4268893	7.43E-06
LAMP5	genotypeWT	0.4386941	1.68E-10
LCA5	genotypeWT	-0.4824359	4.53E-08
LDHA	genotypeWT	-0.2503016	6.70E-15
LGALS1	genotypeWT	0.3326135	2.02E-09
LGALS3	genotypeWT	-0.5743006	1.22E-29
LGALS3BP	genotypeWT	0.3892261	9.71E-05
LGI4	genotypeWT	0.3846457	8.90E-12
LHX9	genotypeWT	1.089828	1.54E-05
LIFR	genotypeWT	0.9977732	6.83E-05
LINC01833	genotypeWT	0.3503739	6.25E-05
LITAF	genotypeWT	0.3357356	5.39E-09
LIX1	genotypeWT	-0.4874266	0.00270468
LMO4	genotypeWT	0.3023698	0.002070399
LOXL3	genotypeWT	0.7608288	7.94E-12
LPCAT4	genotypeWT	0.6024605	0.003745644
LPIN2	genotypeWT	0.5895571	0.00596848
LRRC17	genotypeWT	-0.5509349	0.0313313
LRRC75A-AS1	genotypeWT	0.1040115	0.0232218
LST1	genotypeWT	-0.8600081	3.27E-06
LTBP3	genotypeWT	0.6573106	3.64E-08
LUC7L3	genotypeWT	0.2725678	2.73E-27
LYN	genotypeWT	0.6621501	6.77E-09
MAF	genotypeWT	0.5919466	1.10E-30
MALAT1	genotypeWT	-0.2121712	6.02E-34
MAP4	genotypeWT	0.2079353	0.0081688
MARCKSL1	genotypeWT	0.5604288	3.16E-39
MATR3	genotypeWT	-	5.65E-06

		0.1765639	
MCRIP2	genotypeWT	0.5750615	0.000398961
MCUB	genotypeWT	0.6510775	9.26E-33
MDH2	genotypeWT	0.2597503	0.005866854
MED10	genotypeWT	0.4506748	6.77E-12
MEIS2	genotypeWT	0.5960812	5.98E-07
METRN	genotypeWT	0.9459685	2.23E-53
MGMT	genotypeWT	0.8779547	3.28E-07
MGRN1	genotypeWT	1.074053	1.75E-39
MGST3	genotypeWT	0.2861479	1.74E-11
MIEN1	genotypeWT	0.3112504	0.001602143
MIF	genotypeWT	-0.3044674	4.84E-36
MINDY2	genotypeWT	0.4216216	6.42E-06
MIR100HG	genotypeWT	0.3088195	4.39E-06
MLC1	genotypeWT	1.987639	4.48E-15
MLF2	genotypeWT	0.2936607	0.000583648
MLLT11	genotypeWT	0.2684935	0.002908444
MOGS	genotypeWT	0.9111407	5.59E-07
MORF4L1	genotypeWT	-0.134839	0.000548819
MORF4L1P1	genotypeWT	-0.7282107	5.70E-05
MORF4L2	genotypeWT	-0.6621231	6.98E-111
MPC1	genotypeWT	0.2772735	0.001669433
MRC2	genotypeWT	0.5441439	0.00835178
MRPL23	genotypeWT	-0.5383037	2.38E-06
MRPL33	genotypeWT	-0.2217269	0.000614355
MRPS21	genotypeWT	0.2040236	0.006803523
MRPS5	genotypeWT	0.2850021	6.89E-05
MSMO1	genotypeWT	0.4729985	0.006579426
MT-ATP6	genotypeWT	0.1694853	0.002438905
MT-CO1	genotypeWT	-0.2223262	5.39E-19
MT-ND2	genotypeWT	0.2805651	9.50E-11
MT-ND6	genotypeWT	-0.598203	2.23E-22
MT-RNR2	genotypeWT	-0.3881037	1.53E-66
MT1X	genotypeWT	0.4440495	0.001626602
MTATP6P1	genotypeWT	0.2451808	6.99E-05
MTCH1	genotypeWT	0.4230857	1.23E-18

MTDH	genotypeWT	0.2849963	2.80E-06
MTG1	genotypeWT	0.6321167	8.31E-05
MTHFD2	genotypeWT	0.3380428	0.001573501
MTPN	genotypeWT	0.3420713	6.71E-05
MTSS1	genotypeWT	0.4391624	0.005357114
MVD	genotypeWT	0.6748576	9.36E-05
MYL12A	genotypeWT	-0.2366201	0.03883603
MYL9	genotypeWT	-0.8944032	0.010837179
MZT2A	genotypeWT	0.437264	4.88E-07
MZT2B	genotypeWT	0.4711919	7.20E-13
NAT14	genotypeWT	0.9129572	0.00449988
NCAN	genotypeWT	2.70722	2.87E-08
NDRG1	genotypeWT	0.4259229	1.05E-10
NDUFA4	genotypeWT	-0.1699553	1.25E-10
NDUFA4L2	genotypeWT	-0.7237711	2.42E-21
NDUFS2	genotypeWT	0.4401797	6.81E-11
NDUFS7	genotypeWT	0.2520926	0.000112531
NDUFV1	genotypeWT	0.2640433	0.0232218
NEAT1	genotypeWT	0.355789	8.02E-15
NEK6	genotypeWT	0.7594561	6.48E-10
NFE2L2	genotypeWT	-0.3022731	0.040656
NFIC	genotypeWT	0.3711868	0.008270505
NFKBIZ	genotypeWT	-0.6756141	0.016126117
NINJ1	genotypeWT	0.5417492	2.51E-06
NKTR	genotypeWT	0.2177574	0.003867885
NME4	genotypeWT	0.3201838	0.028897
NPAS2	genotypeWT	0.7460945	0.0260608
NPM1	genotypeWT	-0.1030502	0.000585675
NPM1P27	genotypeWT	-0.6568834	0.000115405
NR2F1	genotypeWT	-0.1951726	4.58E-09
NR4A1	genotypeWT	-0.7200353	1.32E-06
NRIP1	genotypeWT	-0.4233979	0.006254028
NRN1	genotypeWT	0.459747	2.49E-13
NRP1	genotypeWT	0.7849096	1.36E-14

NSMCE1	genotypeWT	0.9499441	7.89E-14
NUDT16L1	genotypeWT	0.8093804	1.58E-32
NUDT4	genotypeWT	-0.2699441	0.011609876
OAZ1	genotypeWT	0.1753772	2.68E-08
OBSL1	genotypeWT	0.2858715	0.0244392
OFD1	genotypeWT	-0.401012	2.06E-11
OIP5-AS1	genotypeWT	0.365236	0.013521885
OLFM1	genotypeWT	0.5333343	1.22E-06
OPRK1	genotypeWT	1.299511	2.20E-06
ORC6	genotypeWT	0.7456777	7.35E-06
OST4	genotypeWT	-0.1261506	0.03538812
P4HB	genotypeWT	0.2485786	7.94E-05
PABPC1	genotypeWT	0.0997651	0.000103683
PALM	genotypeWT	0.9427442	0.000170329
PALMD	genotypeWT	-0.5345218	4.66E-06
PAX2	genotypeWT	0.6325516	8.88E-10
PAX5	genotypeWT	2.145165	2.50E-28
PAX8	genotypeWT	0.8401979	2.01E-11
PAX8-AS1	genotypeWT	0.9728343	0.0254525
PCBP1	genotypeWT	0.2215064	5.76E-06
PCDHA12	genotypeWT	2.776629	0.034578
PCOLCE2	genotypeWT	0.9372947	1.51E-21
PCP4	genotypeWT	-0.6736794	3.02E-08
PDDC1	genotypeWT	0.5942921	0.000249054
PDIA3	genotypeWT	-0.18024	2.74E-06
PDIA5	genotypeWT	0.6297371	0.000589756
PEA15	genotypeWT	0.1863307	0.006518446
PEBP1	genotypeWT	0.1101063	0.00270468
PFDN5	genotypeWT	0.1773413	1.07E-14
PHF1	genotypeWT	0.446222	0.002847276
PHKA2	genotypeWT	0.8500123	0.019644392
PIGX	genotypeWT	0.6081207	9.25E-06
PKM	genotypeWT	-0.1443151	0.00197005
PLCXD1	genotypeWT	1.17556	5.34E-15
PLK2	genotypeWT	-0.4205977	0.02565486
PLP1	genotypeWT	0.6297674	6.77E-24
PNISR	genotypeWT	0.1906266	1.71E-10

PNN	genotypeWT	0.2420487	2.08E-11
POLR2L	genotypeWT	-0.2663064	2.43E-06
PPIA	genotypeWT	0.1168085	0.000548819
PPIAP22	genotypeWT	-1.077033	2.44E-26
PPIF	genotypeWT	0.8558412	1.84E-07
PPP1CC	genotypeWT	0.4659431	3.54E-06
PPP1R14B	genotypeWT	0.6985473	0.000778466
PPP1R1B	genotypeWT	0.7369316	0.000318882
PPP2CB	genotypeWT	0.4725069	0.000647136
PPP4C	genotypeWT	0.3104957	0.04389768
PRDX1	genotypeWT	-0.2477591	6.46E-12
PRDX2	genotypeWT	-0.2073142	1.29E-05
PRDX4	genotypeWT	0.217115	0.000186367
PROS1	genotypeWT	0.385139	0.02362572
PRPH	genotypeWT	0.8075058	2.79E-08
PRR5L	genotypeWT	0.9136982	0.014194224
PRSS23	genotypeWT	-0.3654187	2.65E-06
PRSS35	genotypeWT	0.2974592	0.006111261
PRSS56	genotypeWT	1.688169	0.017162486
PSAP	genotypeWT	0.1910606	8.03E-07
PSPH	genotypeWT	0.493034	2.40E-06
PTGDS	genotypeWT	-0.7287306	3.92E-53
PTGES3P3	genotypeWT	-1.579497	0.00098544
PTMAP5	genotypeWT	0.8617109	7.66E-06
PTN	genotypeWT	0.253099	2.23E-20
PTPRF	genotypeWT	0.5888557	1.16E-16
PXN	genotypeWT	0.5895571	0.002969745
QKI	genotypeWT	0.4153683	2.62E-09
RAB18	genotypeWT	0.3659893	0.000936305
RAB9A	genotypeWT	-0.5196823	5.28E-06
RABGGTB	genotypeWT	0.3290906	0.001910786
RAC1	genotypeWT	0.226208	1.19E-07
RACK1	genotypeWT	0.0889471	3.04E-05
RBM23	genotypeWT	-0.4071798	1.17E-06
RBM25	genotypeWT	0.1854336	2.75E-05

RBM6	genotypeWT	0.23767	0.02058077
RBMS3	genotypeWT	0.8001112	0.007679048
RBP1	genotypeWT	0.2409264	3.28E-11
RBPJ	genotypeWT	0.2100072	0.02788498
RCVRN	genotypeWT	0.579331	0.01519055
RFX7	genotypeWT	0.8817294	0.002745392
RGS2	genotypeWT	0.4652726	5.05E-07
RHBDF1	genotypeWT	1.324253	4.46E-10
RHOBTB3	genotypeWT	0.3509431	0.002090796
RICTOR	genotypeWT	0.7053179	0.001736858
RN7SK	genotypeWT	1.145921	1.64E-10
RNF114	genotypeWT	0.360813	0.006660832
RNF187	genotypeWT	0.628853	3.15E-23
RNF213	genotypeWT	0.6656934	3.39E-08
ROMO1	genotypeWT	0.1983626	1.87E-05
RP11-1000B6.3	genotypeWT	0.5504866	0.019056235
RP11-108M9.6	genotypeWT	1.657398	0.00378621
RP11-115D19.1	genotypeWT	0.6399449	5.80E-06
RP11-15A1.3	genotypeWT	4.222347	1.06E-09
RP11-20O24.4	genotypeWT	0.9166089	1.34E-06
RP11-371A22.1	genotypeWT	-1.008494	1.22E-59
RP11-40C6.2	genotypeWT	1.401132	6.63E-18
RP11-425L10.1	genotypeWT	0.4841328	0.000114792
RP11-466H18.1	genotypeWT	0.8400427	5.71E-12
RP11-574K11.24	genotypeWT	0.4199022	0.004235013
RP11-660L16.2	genotypeWT	0.7718786	4.23E-06
RP11-84E17.1	genotypeWT	0.6933438	5.74E-179
RP11-864N7.2	genotypeWT	0.2624602	0.003214732
RP11-889L3.1	genotypeWT	0.5882793	0.000524204
RP4-604A21.1	genotypeWT	-0.314721	2.34E-12
RP4-665J23.1	genotypeWT	-1.330081	3.28E-11
RPH3AL	genotypeWT	1.077046	0.002357155
RPL10P6	genotypeWT	-0.73348	8.52E-18
RPL10P9	genotypeWT	0.5134575	3.38E-120

RPL13A	genotypeWT	0.0748244	1.27E-08
RPL13AP25	genotypeWT	-0.7276108	3.29E-13
RPL13AP5	genotypeWT	-0.2964176	0.000159047
RPL13P12	genotypeWT	-0.2691094	3.11E-06
RPL14	genotypeWT	-0.1794144	1.69E-19
RPL17P36	genotypeWT	-0.6834086	1.34E-05
RPL21	genotypeWT	-0.1214786	2.54E-16
RPL22	genotypeWT	-0.2752793	3.85E-32
RPL23	genotypeWT	-0.2228636	8.03E-57
RPL24	genotypeWT	-0.1328188	1.69E-14
RPL24P8	genotypeWT	-1.24768	0.001647033
RPL26	genotypeWT	-0.2013089	1.59E-34
RPL26P19	genotypeWT	-0.7897686	2.15E-05
RPL27	genotypeWT	-0.0837397	6.54E-06
RPL27A	genotypeWT	0.076526	0.00098544
RPL28	genotypeWT	-0.124477	3.23E-09
RPL29	genotypeWT	-0.1974885	2.85E-14
RPL3	genotypeWT	0.0644822	0.002541132
RPL34	genotypeWT	-0.1412003	5.41E-18
RPL35P2	genotypeWT	-1.211921	0.001237597
RPL36	genotypeWT	-0.2152196	1.28E-31
RPL36A	genotypeWT	-0.2844517	1.01E-30
RPL37	genotypeWT	-0.1335619	1.15E-11
RPL37A	genotypeWT	-0.1200186	2.53E-13
RPL38	genotypeWT	-0.1993547	3.91E-29
RPL39	genotypeWT	-0.2907858	1.12E-37
RPL41	genotypeWT	-0.0937789	3.22E-07
RPL5	genotypeWT	-0.176499	2.21E-29

RPL5P1	genotypeWT	1.506917	3.15E-22
RPL6	genotypeWT	-0.1519195	1.70E-27
RPL6P27	genotypeWT	-1.152592	6.14E-25
RPL7A	genotypeWT	-0.1127679	1.23E-07
RPL7AP50	genotypeWT	-0.7505479	1.76E-08
RPL9	genotypeWT	-0.1133647	8.43E-13
RPL9P9	genotypeWT	-0.4638627	3.18E-82
RPLP1	genotypeWT	-0.1066371	1.16E-14
RPS10	genotypeWT	-0.3443074	7.23E-61
RPS11	genotypeWT	0.0785996	6.81E-06
RPS15A	genotypeWT	-0.1136291	1.18E-12
RPS19	genotypeWT	0.1712661	1.49E-40
RPS2	genotypeWT	0.2204566	3.91E-30
RPS23P8	genotypeWT	-0.5252281	1.31E-06
RPS24	genotypeWT	-0.2306164	2.74E-61
RPS26	genotypeWT	-0.2625755	6.66E-24
RPS27	genotypeWT	-0.1343618	7.63E-15
RPS27AP16	genotypeWT	-0.312697	6.25E-05
RPS29	genotypeWT	-0.1498942	2.68E-17
RPS2P46	genotypeWT	-1.225894	8.45E-23
RPS3A	genotypeWT	-0.0756587	1.04E-05
RPS3AP5	genotypeWT	0.5839757	7.22E-07
RPS5	genotypeWT	0.1176204	4.27E-10
RPS6	genotypeWT	-0.1961756	8.29E-61
RPS8	genotypeWT	-0.1418427	6.90E-30
RPS9	genotypeWT	0.0760188	0.02119
RPSAP58	genotypeWT	-0.4464155	0.002357155
RTN4R	genotypeWT	1.082034	0.003214732
RXRA	genotypeWT	0.9437999	2.01E-14
S100A10	genotypeWT	0.4930628	6.19E-17

S100A6	genotypeWT	-0.4391552	1.75E-19
S100B	genotypeWT	0.6834413	1.44E-07
SALL1	genotypeWT	1.360413	0.00030451
SAMD14	genotypeWT	1.082856	5.81E-12
SAT1	genotypeWT	0.3808136	1.73E-36
SAT2	genotypeWT	0.1690306	0.04187362
SBNO1	genotypeWT	0.3961764	0.000442062
SCD	genotypeWT	0.6638424	3.52E-17
SCG5	genotypeWT	-0.7072958	0.004663284
SCML1	genotypeWT	0.5341286	0.000325022
SCRG1	genotypeWT	0.7030452	4.62E-23
SDCBP	genotypeWT	0.2612093	0.000526234
SEC11C	genotypeWT	0.2620871	6.02E-06
SELENBP1	genotypeWT	0.5823159	0.03275223
SELENOP	genotypeWT	-0.3033954	0.000164982
SEMA3B	genotypeWT	0.4416896	0.000242915
SEMA4B	genotypeWT	0.8100998	2.53E-07
SEMA5A	genotypeWT	1.114369	8.29E-05
SEMA5B	genotypeWT	1.078029	1.84E-24
SEPT11	genotypeWT	0.2787258	2.22E-06
SEPT8	genotypeWT	0.992581	1.17E-05
SERPINE1	genotypeWT	0.85889	3.13E-23
SETD5	genotypeWT	0.3870894	7.16E-09
SF3B2	genotypeWT	0.1955024	6.83E-05
SFMBT2	genotypeWT	0.7566111	0.003194568
SFXN1	genotypeWT	0.5292563	4.68E-06
SFXN3	genotypeWT	0.9471561	1.47E-05
SH3GL1	genotypeWT	0.7690558	6.30E-13
SIX3	genotypeWT	0.2858095	0.000337315
SKI	genotypeWT	1.055542	0.00162463
SKP1	genotypeWT	-0.1051088	0.03518647
SLC15A4	genotypeWT	0.6285187	0.000244962
SLC1A3	genotypeWT	-0.342853	6.71E-05
SLC22A5	genotypeWT	0.7524065	0.02626311
SLC25A1	genotypeWT	0.4460106	0.001966046
SLC25A6	genotypeWT	0.2550973	1.78E-11
SLC2A3	genotypeWT	0.6851009	4.09E-20
SLC39A1	genotypeWT	0.4674111	0.001802302

SLC39A7	genotypeWT	0.3554831	0.000145663
SLC4A4	genotypeWT	0.902178	0.000632817
SLC7A5	genotypeWT	1.093083	2.42E-10
SLIT1	genotypeWT	0.9953411	0.000107589
SMCO4	genotypeWT	0.4892876	0.02687124
SMOC2	genotypeWT	0.6758752	4.41E-12
SNHG1	genotypeWT	0.3404489	2.41E-08
SNHG18	genotypeWT	0.5649285	4.11E-05
SNHG25	genotypeWT	0.7303029	4.52E-27
SNHG3	genotypeWT	0.5261645	9.95E-12
SNHG5	genotypeWT	0.2027599	8.91E-09
SNHG7	genotypeWT	0.6588015	3.27E-17
SNHG8	genotypeWT	0.2304522	0.001702164
SNRPA1	genotypeWT	0.4010965	2.72E-07
SNRPE	genotypeWT	-0.1856993	0.02808714
SNX3	genotypeWT	0.2704878	1.32E-06
SNX32	genotypeWT	0.8380558	0.005357114
SNX5	genotypeWT	0.355983	0.005580939
SOD1	genotypeWT	-0.1938055	5.53E-11
SORCS2	genotypeWT	0.7398807	6.83E-06
SORCS3	genotypeWT	0.8166145	0.010532592
SOX4	genotypeWT	0.3228653	2.71E-20
SOX9	genotypeWT	0.4261208	6.11E-13
SPAG4	genotypeWT	0.5803845	0.011894366
SPARCL1	genotypeWT	0.3437688	0.000355809
SPATS2	genotypeWT	0.4311077	0.00112072
SPG7	genotypeWT	0.4053529	0.007088863
SPX	genotypeWT	-1.347813	0.016877952
SQLE	genotypeWT	0.5144017	5.83E-07
SREBF1	genotypeWT	0.8307191	0.003867885
SREBF2	genotypeWT	0.7070641	0.00010677
SRI	genotypeWT	0.1914434	0.02808714
SRRM2	genotypeWT	0.250447	9.75E-07
SRSF1	genotypeWT	0.4434981	7.04E-12
SRSF11	genotypeWT	0.2533814	2.67E-11
SRSF5	genotypeWT	-0.1250594	0.04207482
SRSF9	genotypeWT	0.3682862	8.61E-08
SSNA1	genotypeWT	0.4012577	0.001044875

SSPN	genotypeWT	0.8844141	5.13E-10
ST13	genotypeWT	-0.2373494	4.25E-15
ST8SIA1	genotypeWT	0.9246413	6.58E-05
ST8SIA4	genotypeWT	0.8705179	0.00592789
STAT2	genotypeWT	0.537732	0.00470396
STC1	genotypeWT	0.6087224	0.000294251
STK25	genotypeWT	0.3865395	0.010532592
STK32C	genotypeWT	0.6765684	0.003337099
STK36	genotypeWT	0.9070921	0.02991156
STXBP6	genotypeWT	-0.8513196	0.000815279
SULF2	genotypeWT	0.5759295	7.00E-15
SYNE2	genotypeWT	-0.3019339	5.45E-05
TAF1D	genotypeWT	0.406535	1.20E-19
TCEAL1	genotypeWT	-0.4955151	2.48E-09
TCEAL2	genotypeWT	-0.5028052	4.60E-05
TCEAL3	genotypeWT	-0.6107115	1.21E-36
TCEAL4	genotypeWT	-0.6009327	1.09E-91
TCEAL5	genotypeWT	-0.5770733	3.12E-08
TCEAL7	genotypeWT	-0.8916709	2.85E-53
TCEAL8	genotypeWT	-0.7049066	4.27E-31
TCEAL9	genotypeWT	-0.7121599	9.98E-87
TCF3	genotypeWT	0.6048112	0.001667463
TECR	genotypeWT	0.5375532	1.36E-07
TERF2IP	genotypeWT	0.1790891	0.01063361
TGFA	genotypeWT	1.443824	3.64E-12
TGM2	genotypeWT	0.7215568	6.18E-08
THOC2	genotypeWT	0.2985023	3.09E-06
THUMPD3	genotypeWT	0.562131	6.29E-07
THUMPD3-AS1	genotypeWT	0.4244815	0.000164578
TIAL1	genotypeWT	0.2618407	0.000983435
TIMP1	genotypeWT	-0.2157319	0.013075118
TIMP2	genotypeWT	0.4456262	0.000452298
TKT	genotypeWT	-	6.99E-05

		0.2455129	
TM2D3	genotypeWT	0.3957782	0.007170228
TM9SF3	genotypeWT	0.3768694	0.012810572
TM9SF4	genotypeWT	0.3984682	0.009002133
TMA7	genotypeWT	-0.1705351	3.41E-05
TMEM176A	genotypeWT	-0.8364776	5.81E-12
TMEM176B	genotypeWT	-0.8190127	1.36E-11
TMEM255B	genotypeWT	1.762758	0.000708734
TMSB10	genotypeWT	-0.1837174	9.27E-19
TMSB4X	genotypeWT	-0.5540114	4.77E-224
TMSB4XP4	genotypeWT	-1.065181	0.006315033
TMSB4XP6	genotypeWT	-1.160539	8.06E-15
TMSB4XP8	genotypeWT	-1.013791	6.01E-14
TMTC4	genotypeWT	0.5312026	0.000183698
TNFRSF25	genotypeWT	0.705556	0.0400501
TNS1	genotypeWT	1.13415	2.05E-05
TOPBP1	genotypeWT	0.5032156	0.001493638
TPBG	genotypeWT	-0.7785301	3.17E-10
TPD52	genotypeWT	0.4549705	0.00016274
TPM1	genotypeWT	-0.3275623	0.000355809
TPM4	genotypeWT	-0.3309475	9.29E-11
TRIM2	genotypeWT	0.4341935	2.10E-09
TRIM24	genotypeWT	-0.4332869	0.000288106
TRIM56	genotypeWT	0.4269532	0.003194568
TRIM9	genotypeWT	0.6244524	1.14E-11
TRIO	genotypeWT	0.5880818	0.03944214
TRNT1	genotypeWT	0.6044309	0.000175469
TSC22D1	genotypeWT	-0.3531633	3.63E-16
TSC22D4	genotypeWT	0.7307027	5.85E-28
TSEN34	genotypeWT	0.3670968	0.000247008
TSPAN2	genotypeWT	0.9843181	0.000548819
TSPAN6	genotypeWT	-0.3513766	0.008473055
TSPAN7	genotypeWT	0.4692009	1.14E-07
TSPAN9	genotypeWT	1.062831	1.68E-08

TSTD1	genotypeWT	-0.8443728	2.38E-05
TTR	genotypeWT	-3.3605864	0.000827561
TTYH2	genotypeWT	0.440916	0.016858395
TTYH3	genotypeWT	0.844604	1.68E-21
TUBA1B	genotypeWT	0.15626	0.013278447
TXNIP	genotypeWT	-0.4728614	5.48E-41
UBA2	genotypeWT	0.3560028	0.00706878
UBA5	genotypeWT	0.4128788	0.008737192
UBA6	genotypeWT	0.5429171	5.53E-06
UBAC1	genotypeWT	0.622368	1.49E-06
UBALD1	genotypeWT	1.320016	2.88E-31
UBE2D2	genotypeWT	0.2441907	2.89E-05
UBE2I	genotypeWT	0.3112446	7.60E-09
UBXN4	genotypeWT	0.2310725	1.78E-11
UCHL1	genotypeWT	-0.2455006	2.34E-11
UFM1	genotypeWT	0.2779857	0.000161924
UNC5B	genotypeWT	0.5667325	0.000801021
UQCRH	genotypeWT	0.1622377	0.001301158
UQCRHL	genotypeWT	-0.9710571	2.01E-13
VAMP2	genotypeWT	0.2818606	0.000747729
VAT1	genotypeWT	0.3780755	0.002847276
VCAN	genotypeWT	0.6701623	3.23E-21
VDAC2	genotypeWT	0.1843268	0.004418712
VDAC3	genotypeWT	0.3449799	1.36E-05
VEGFA	genotypeWT	0.41558	3.32E-25
VPS26B	genotypeWT	0.7491391	0.04207482
VSNL1	genotypeWT	0.6115836	0.000296294
VTRNA1-3	genotypeWT	0.7029552	4.03E-05
WASF2	genotypeWT	0.4367566	1.70E-12
WFDC1	genotypeWT	1.579436	0.002765475
WFDC2	genotypeWT	-0.5771528	1.47E-05
WIF1	genotypeWT	0.4410927	1.14E-42
WLS	genotypeWT	-1.09461	7.84E-12
WNK1	genotypeWT	0.6255239	3.05E-24
WRB	genotypeWT	0.3843379	1.64E-06
WSB1	genotypeWT	0.1636584	7.24E-08
XPNPEP1	genotypeWT	0.5519439	9.02E-06

XXYLT1	genotypeWT	0.6138698	0.011406395
YIPF6	genotypeWT	0.5357959	9.81E-05
YWHAE	genotypeWT	-0.260974	2.67E-20
ZCCHC17	genotypeWT	0.3107356	1.12E-06
ZEB1	genotypeWT	0.3504465	2.33E-07
ZFAS1	genotypeWT	0.1717743	3.79E-12
ZFP36	genotypeWT	-0.5312431	0.03680816
ZFP36L2	genotypeWT	0.3285684	1.11E-05
ZIC2	genotypeWT	0.5388701	4.85E-05
ZMAT3	genotypeWT	0.7729886	2.20E-15
ZNF207	genotypeWT	0.3767199	3.26E-05
ZNF24	genotypeWT	0.336045	0.000813265
ZNF395	genotypeWT	0.6507989	5.73E-12
ZNF404	genotypeWT	3.840636	0.011060594
ZNF558	genotypeWT	1.153871	2.41E-08
ZNF677	genotypeWT	0.7473766	9.73E-05
ZSCAN18	genotypeWT	0.5626242	9.94E-10
ZSWIM8	genotypeWT	0.8291127	5.69E-07
DMBX1	genotypeWT	0.4329286	0.001841169
FTH1P2	genotypeWT	-4.599503	2.20E-14
GFAP	genotypeWT	1.836149	1.83E-12
LINC01291	genotypeWT	1.910847	0.006416904
LUM	genotypeWT	1.492318	0.03417288
RSPO2	genotypeWT	-2.992472	3.46E-06
SYNPO	genotypeWT	0.7244969	0.01508934
FERMT3	genotypeWT	1.325752	0.008392209
IL7R	genotypeWT	1.592859	0.03903744
LINC01139	genotypeWT	0.7450362	0.04045471
NKX6-1	genotypeWT	1.384104	4.07E-05
OAS3	genotypeWT	1.84664	0.000610276
PHEX	genotypeWT	2.436423	4.16E-25
RP11-693N9.2	genotypeWT	-0.9792354	0.0075981
CCL28	genotypeWT	0.7634344	5.51E-11
ADGRL4	genotypeWT	1.071434	1.95E-10
PLCXD3	genotypeWT	1.040534	0.00011643
NPVF	genotypeWT	-2.221151	6.43E-09
AGXT	genotypeWT	1.185144	6.27E-05
C14orf180	genotypeWT	1.880541	0.000803036
CHP2	genotypeWT	4.627811	4.75E-05

LINC00473	genotypeWT	2.086393	0.007373786

Supplementary Table 3: GO enrichment of CRB1 KO vs WT non-photoreceptor or MG populations.

Table 16

CRB1 KO RGCs

GO biological process (parent)	fold enrichment	raw P value	FDR
electron coupled proton transport	>100	3.62E-05	2.30E-02
regulation of transepithelial transport	>100	3.62E-05	2.13E-02
positive regulation of microtubule polymerization or depolymerization	54.16	2.92E-05	2.32E-02
regulation of microtubule polymerization	47.69	1.92E-06	6.12E-03
negative regulation of microtubule polymerization or depolymerization	45.13	4.88E-05	2.50E-02
negative regulation of protein polymerization	35.1	6.12E-06	9.73E-03
negative regulation of supramolecular fiber organization	21.64	3.73E-06	8.47E-03
vesicle-mediated transport in synapse	18.72	6.62E-05	3.10E-02
axonogenesis	10	2.74E-05	2.30E-02
microtubule cytoskeleton organization	9.43	1.57E-06	8.35E-03

WT RGCs

GO biological process (parent)	fold enrichment	raw P value	FDR
no statistically significant results			

CRB1 KO RPCs

GO biological process (parent)	fold enrichment	raw P value	FDR
electron transport coupled proton transport	>100	3.86E-06	1.58E-03
cellular response to mycotoxin	>100	3.48E-04	4.42E-02
regulation of transepithelial transport	>100	3.48E-04	4.39E-02
positive regulation of tau-protein kinase activity	87.61	1.31E-05	4.17E-03
rostrocaudal neural tube patterning	51.11	4.88E-05	1.25E-02
glomerulus vasculature development	32.28	1.61E-	2.73E-

		04	02
negative regulation of viral entry into host cell	32.28	1.61E-04	2.70E-02
mitochondrial electron transport, cytochrome c to oxygen	30.66	1.85E-04	3.00E-02
response to salt stress	25.55	3.01E-04	4.16E-02
response to interferon-alpha	25.55	3.01E-04	4.13E-02

WT RPCs

GO biological process (parent)	fold enrichment	raw P value	FDR
suppression by symbiont of host innate immune response	35.14	1.60E-04	1.68E-02
SRP-dependent cotranslational protein targeting to membrane	32.95	8.14E-31	1.85E-27
peptidyl-proline hydroxylation to 4-hydroxy-L-proline	31.95	2.03E-04	2.05E-02
viral transcription	26.48	1.40E-27	1.86E-24
nuclear-transcribed mRNA catabolic process, nonsense-mediated decay	25.38	3.67E-27	4.49E-24
polyamine biosynthetic process	25.1	3.72E-04	3.50E-02
detoxification of copper ion	21.96	5.23E-04	4.60E-02
formation of cytoplasmic translation initiation complex	21.96	5.23E-04	4.57E-02
protein exit from endoplasmic reticulum	18.74	9.99E-05	1.14E-02
virion assembly	18.5	1.83E-06	2.88E-04

CRB1 KO NPCs

GO biological process (parent)	fold enrichment	raw P value	FDR
electron transport coupled proton transport	>100	5.98E-08	1.19E-04
regulation of transepithelial transport	>100	2.23E-05	2.09E-02
mitochondrial electron transport, cytochrome c to oxygen	>100	2.99E-06	3.66E-03

WT NPCs

GO biological process (parent)	fold enrichment	raw P value	FDR
SRP-dependent cotranslational protein targeting to membrane	>100	2.18E-41	6.94E-38
viral transcription	>100	5.03E-42	2.00E-38
nuclear-transcribed mRNA catabolic process, nonsense-mediated decay	92.94	2.19E-39	3.87E-36

translational initiation	81.38	5.82E-40	1.16E-36
ribosomal small subunit assembly	76.56	1.22E-05	2.10E-03
cytoplasmic translation	46.5	2.66E-10	5.80E-08
regulation of ATP metabolic process	15.77	1.34E-04	2.19E-02
rRNA processing	11.22	8.78E-05	1.47E-02

Supplementary Table 4: GO enrichment of RPGRIP1 KO vs WT non-photoreceptor or MG populations.

Table 17

RPGRIP1 KO RGCs

GO biological process complete (parent)	fold enrichment	raw P value	FDR
no statistically significant results			

WT RGCs

GO biological process complete (parent)	fold enrichment	raw P value	FDR
SRP-dependent cotranslational protein targeting to membrane	>100	1.99E-101	3.16E-97
viral transcription	87.09	1.33E-95	3.52E-92
nuclear-transcribed mRNA catabolic process, nonsense-mediated decay	83.46	1.05E-94	2.09E-91
translational initiation	72.33	6.64E-95	1.51E-91
suppression by symbiont of host innate immune response	65.67	1.22E-06	1.58E-04
ribosomal small subunit assembly	60.49	1.51E-10	2.40E-08
regulation of arachidonic acid secretion	54.73	4.58E-05	4.61E-03
cytoplasmic translation	53.98	1.43E-32	3.41E-30
ribosomal large subunit assembly	45.29	4.81E-11	7.81E-09
error-free translesion synthesis	32.84	1.24E-05	1.42E-03

RPGRIP1 KO RPCs

GO biological process complete (parent)	fold enrichmen	raw P value	FDR

	t		
chromosome condensation	25.97	2.36E-05	7.52E-02
positive regulation of nucleobase-containing compound metabolic process	2.84	2.42E-05	6.41E-02
regulation of transcription by RNA polymerase II	2.64	2.45E-05	5.56E-02

WT RPCs

GO biological process complete (parent)	fold enrichment	raw P value	FDR
SRP-dependent cotranslational protein targeting to membrane	93.28	4.69E-104	3.73E-100
positive regulation of intrinsic apoptotic signaling pahtway by p53 class mediator	80.2	2.19E-05	2.49E-03
viral transcription	77.87	4.85E-100	1.10E-96
nuclear-transcribed mRNA catabolic process, nonsense-mediated decay	75.74	5.31E-101	1.41E-97
translational initiation	67.3	1.75E-104	2.78E-100
ribosomal small subunit assembly	56.28	1.52E-11	2.40E-09
suppression by symbiont of host innate immune response	53.46	2.76E-06	3.64E-04
cytoplasmic translation	47.61	1.63E-33	3.93E-31
negative regulation of ubiquitin protein ligase activity	40.1	1.09E-04	1.05E-02
ribosomal large subunit assembly	36.87	2.48E-10	3.69E-08

RPGRIP1 KO NPCs

GO biological process complete (parent)	fold enrichment	raw P value	FDR
electron transport coupled proton transport	>100	8.40E-08	1.34E-03
regulation of transepithelial transport	>100	2.78E-05	4.03E-02
mitochondrial ATP synthesis coupled electron transport	32.68	7.70E-06	3.07E-02
organelle organization	3.12	1.47E-05	3.34E-02

WT NPCs

GO biological process complete (parent)	fold enrichment	raw P value	FDR
SRP-dependent cotranslational protein targeting to membrane	>100	1.06E-131	1.69E-127

viral transcription	>100	2.20E-127	6.99E-124
nuclear transcribed mRNA catabolic process, nonsense-mediated decay	>100	2.42E-126	6.42E-123
positive regulation of intrinsic apoptotic signaling pathway by p53 class mediator	>100	7.94E-06	1.07E-03
translational initiation	95.89	5.89E-122	1.04E-118
negative regulation of protein neddylation	93.92	4.11E-04	4.58E-02
ribosomal small subunit assembly	88.98	1.49E-14	2.43E-12
negative regulation of ubiquitin protein ligase activity	75.14	7.16E-07	1.01E-04
cytoplasmic translation	74.62	3.32E-43	7.78E-41
ribosomal large subunit assembly	51.82	1.63E-20	2.49E-09

Supplementary Table 5: Genes differentially expressed by age and genotype in rod and cone photoreceptors.

Table 18

cones	rods
BTF3	ADIPOR1
EEF1A1	AKAP9
EEF1B2	ANK2
EEF2	ARL6IP5
EIF3E	ATP6AP2
EIF3F	CADM2
EIF3H	CPLX4
EIF4A2	DPYSL3
EIF4B	ECHDC2
EPB41L4A-AS1	ENO2
FAU	FHOD3
FTL	FSTL5
GAS5	GABRR2
LRRC75A-AS1	GNGT2
NACA	GUCA1A
NACAP1	GUCA1B
NPM1	HOOK1
PABPC1	KCNV2

PFDN5	LBH
PHB2	LIMCH1
POLR1D	LINC00599
RACK1	MFGE8
RPL10	MPP4
RPL10A	MT1E
RPL11	MYL4
RPL13	MYL6
RPL13A	NDUFA4
RPL15	OTX2-AS1
RPL18	PCBP4
RPL18A	PCLO
RPL19	PDE6D
RPL3	PDE6H
RPL3P4	PEX5L
RPL4	PFKP
RPL5	PKIB
RPL6	PLEKHB1
RPL7	PPA1
RPL7A	PRCD
RPL8	PROM1
RPLP0	RABL3
RPS11	RD3
RPS14	RPGRIP1
RPS16	RS1
RPS18	RTBDN
RPS19	RTN4
RPS27A	SELENOK
RPS2P5	SRRM3
RPS3	SYT1
RPS3A	TPM1
RPS4X	TRAC
RPS5	TSPAN7
RPS9	TUBA1B
RPSA	TULP1
RSL1D1	VTN
SLC25A6	WRB
SNHG1	CABP4
SNRPD2	GUCA1C
TKT	IMPG1

TOMM20	BTF3
TPT1	EEF1A1
UBA52	EEF2
ANKRD33	EIF3E
ANP32E	EIF3F
APLP2	EIF4A2
BHLHE41	GAS5
CA2	PABPC1
CEP120	PFDN5
CHN2	RPL10
CREG1	RPL10A
DCAF1	RPL11
DEFB119	RPL13
DZIP3	RPL13A
GNGT2	RPL18A
GREM2	RPL19
GUCA1B	RPL27A
GUK1	RPL3
ITM2B	RPL30
ITM2C	RPL31
LRRC39	RPL32
MAP2	RPL3P4
MATN2	RPL4
MEF2C	RPL5
MFGE8	RPL6
MT1E	RPL7
MT1F	RPL7A
MT1X	RPL9
MT2A	RPLP0
MYL4	RPLP1
MYL6	RPS11
NME1	RPS12
PDE6D	RPS13
PLCD4	RPS14
PLS1	RPS16
PPA1	RPS17
PRCD	RPS19
RAB3IP	RPS20
RBP3	RPS23
RGS9BP	RPS27A

RS1	RPS3
RTBDN	RPS3A
RTN4	RPS3AP49
SEPT4	RPS4X
SH3GL2	RPS5
SLC4A7	RPS6
TMEM14B	RPS8
TMEM50B	RPS9
TRMT44	SNHG5
TSPAN3	TPT1
TTR	ZFAS1
TUBA1B	ARRDC3
VTN	C11orf57
AF131216.5	CACYBP
CABP4	CHORDC1
GUCA1C	DDIT3
FAM19A3	DNAJA1
C20orf141	DNAJB1
CTD-2521M24.11	DUSP1
IMPG1	EGR1
RP1L1	H1F0
RP11-240M16.1	HIST1H1D
AC017101.10	HIST1H1E
MIR4458HG	HIST1H2AC
AAK1	HIST1H2BD
ACSL6	HIST1H2BG
AHI1	HSP90AA1
AKAP9	HSP90AA2P
ALDOA	HSP90AB1
ANKRD36	HSP90AB3P
B3GAT2	HSPA1A
BICD1	HSPA1B
BNIP3	HSPA5
CADPS	HSPA6
CCDC82	HSPA8
CTBP2	HSPB1
DARS	HSPD1
DCT	HSPE1
DDIT4	HSPH1

DST	JUN
ENO2	MT-ATP6
FAM19A4	MT-ATP8
FZD3	MT-CO1
GNB3	MT-CYB
GOLGA8A	MT-ND1
GPM6A	MT-ND2
HK2	MT-ND3
HLTF	MT-ND4
INTU	MT-ND4L
KIDINS220	MT-ND5
KIF1B	MT-ND6
LDHA	MT-RNR1
LEMD1	MT-RNR2
LMO4	MT-TL1
LUC7L3	MTATP6P1
MYO3B	PCSK5
NCKAP5	PTGES3
NREP	RASSF9
ODF2L	TXNIP
PALMD	UBB
PCLO	UBBP4
PEG10	ZEB1
PFKP	AC009245.3
PRDX4	CCT6A
RCAN3	DCAF13
RNF157	FAR2P1
ROBO2	HNRNPCP2
RP11-15A1.3	KRT10
RRAD	MORF4L2
RUFY3	NPM1
RXRG	RP11-371A22.1
SCAPER	RP11-889L3.1
SLC12A2	RPL10P9
SLC1A2	RPL12
SLC8A1	RPL13AP5
SORBS2	RPL13P12
SPECC1	RPL14
SVIL-AS1	RPL14P1

TPI1	RPL18AP3
TTN	RPL23
TUBB4B	RPL23A
VAMP2	RPL23AP2
WRB	RPL23AP42
WWC1	RPL26
ACTB	RPL28
ACTG1	RPL29
AKAP12	RPL34
BEX1	RPL35A
BEX3	RPL36A
C4orf48	RPL37
CADM3	RPL37A
CCT2	RPL5P1
CD24	RPL6P27
CFL1	RPL7P1
CKB	RPL7P9
CNN3	RPL9P9
CRYBG3	RPLP2
DCX	RPS10
DUTP8	RPS13P2
ELAVL4	RPS15A
FABP7	RPS21
FNDC5	RPS24
FSCN1	RPS25
FXYD6	RPS26
GSG1	RPS28
HDAC2	RPS29
HN1	RPS7
HNRNPA0	RPS7P1
HNRNPA1	SNHG6
HNRNPA1P48	CTB-134H23.3
IFI6	AIPL1
LGI4	ARHGAP42
LHX4	ATP1B2
LINC00463	CABP5
LUC7L	CEP290
MIAT	CH17-472G23.4
NEUROD4	CNGB1

NNAT	COBLL1
OTX2	DDRGK1
POLR2B	DMD
PRDX2	EPB41L2
PTN	ERI1
RASD1	EZH1
RBP1	FAM161A
RGS16	FZD3
RP11-53O19.1	GPR137B
SELENOH	GPR160
SOX4	KRI1
SPP1	LENG8
SSTR2	MAK
STMN1	MATK
STMN2	MOK
STMN4	NRL
SUMO2	ODF2L
SVBP	OFD1
TAGLN3	OSBP2
TMSB10	PCMTD2
TMSB15A	PDC
TMSB4X	PDCD4
TPH1	PDE6B
TUBA1A	PLCD3
TUBB	PLOD2
TUBB2B	PPARA
VSX1	PRPH2
ANKRD12	PSIP1
APC	PTPN13
BPTF	REEP6
CCDC88A	ROM1
CCDC93	RP1
CEBPZOS	SAMD11
CHD9	SEC62
CLSTN3	SYCE1L
CRABP2	USP2
CYP26B1	WI2-1896O14.1
DYNC1LI2	RAX2
EID1	SAMD7

EIF1AX	GNAT1
FNBP1L	RP11-379K17.4
FSIP2	AC013470.6
FUBP1	ACTB
GIGYF2	ACTG1
GOLGA4	BEX3
GOLGB1	C8orf46
HIST1H1D	CADM3
HIST1H1E	CD24
HMP19	CENPBD1
KCNQ1OT1	CFL1
KHDRBS1	CTA-243E7.1
LINC00632	CTD-2291D10.4
MALAT1	FAM133A
MAP7	FASN
MARCKS	FHOD1
NEUROG1	GNA12
PARP1	GNG5
PJA1	HES6
PNN	HIST1H3J
PPP4R4	HMGA1
PUS7L	MAP1A
RABEP1	MIR7-3HG
RBM25	NAP1L1
RP11-834C11.4	NNAT
RTN3	OTX2
SERINC1	PHACTR1
SF3B2	PHLDA1
SLC38A5	PLCG1
SLF1	PLEKHA1
SMARCA5	PLPPR5
SRRM4	PPDPF
TAX1BP1	QPRT
TERF2IP	RASD1
THOC2	RBP1
THY1	RGS7BP
TM2D3	RP1-313I6.12

TTC3	RPS4XP6
USP11	SALL3
YTHDC1	SELENOW
ZC3H13	STMN2
ZNF248	TMSB10
ZNF638	TMSB4X
ACSL4	TUBA1A
ANK2	TUBB
ARL6IP1	VSX1
ARL6IP5	WSB1
ATP6AP2	RP11-288H12.3
C16orf74	AC020951.1
CADM2	RP11-290L1.3
CAMK1D	ABCA5
CD46	ACTN1
CDHR1	AIG1
CPE	ALDH2
CPLX4	ALDOC
CTD-2368P22.1	ANK3
EGR1	ATF4
ELOVL4	B2M
FAM107A	CADM1
FOS	CCKBR
FSTL5	CLUL1
GRIPAP1	CRNDE
IMPG2	CTD-3014M21.1
KCNB1	DGKD
KCNV2	ELOVL4
LAPTM4B	GNB1
LINC00599	GNGT1
MIR124-2HG	HPRT1
MPP4	IER2
PEA15	MXRA5
PLEKHB1	OCIAD2
PLXDC1	OPTN
PPM1N	OSBPL1A
PROM1	PDE6G
RD3	PPP2R2B

RGS11	PRUNE2
RGS9	RASSF2
RIMS2	RGS9
RPGR	RP11-96L14.7
RPGRIP1	SLC24A1
SGIP1	SNTB2
SLC2A11	SPTBN1
SRRM3	TACC1
STX3	TMEM237
STXBP1	YBX3
SV2B	PDE6A
SYP	RP11-536I6.2
SYT1	SAG
TPD52	AP000997.1
TPM1	PDZPH1P
TRAC	LINC02115
TRAK1	GABRR3
TSPAN7	RHO
TULP1	ABCD4
UNC119	ALDOA
ABCC5	AMER2
AFF1	BAZ2B
ARR3	BTG1
ASPH	CALD1
BMP7	COL16A1
C1D	ENAH
CC2D2A	ENO1
CLCN4	EYA2
CTBS	EZR
DHRS7	FABP7
EMB	INHBB
EPHX2	ITSN1
GABRG2	KMT2E
GNAI3	LAPTM4A
GNAT2	LGI4
GPR155	LHX4
GUCA1A	LINC00463
HOOK1	LINC01587
HRASLS	LOXL1

IQGAP2	LOXL1-AS1
KIF21A	MAP1LC3B
KIF2A	MGLL
LBH	MPPED2
LGALSL	NCOR2
LIMCH1	NEUROD4
MAP4	NIPAL1
MAPKBP1	NRIP1
MCF2	PGRMC2
NBEA	PIK3R1
NOS1AP	PKM
OPN1SW	PRDM1
PDE6C	PTPRF
PDE6H	SRRM2
PEX5L	SYTL4
PLA2G12A	TPI1
PPP1R15A	TPR
RABL3	ZNF146
RHOBTB1	MBD3L2
SLC24A2	ATP5A1
SLC44A1	CBX1
SPG20	CRABP2
TAPT1	DAAM1
TMEM30A	DCT
TP53BP2	DST
VOPP1	ELFN1
AC007349.7	FAM213A
CNGB3	FXYD7
COL4A3	GNG2
CTD-2050N2.1	GOLGA4
RAB41	GOLGB1
AC000124.1	HECTD4
AC007969.5	HMP19
AC009245.3	LEMD1
COX7C	LL22NC03-2H8.5
EIF3L	MALAT1
MIF	NEUROG1
RP11-371A22.1	NREP

RP11-40C6.2	PALMD
RP11-84E17.1	PCSK1N
RP11-864N7.2	PRDX1
RP4-604A21.1	PRMT1
RPL10AP6	RAX
RPL10P16	ROBO2
RPL10P9	RRAD
RPL13AP5	RXRG
RPL13P12	SIX6
RPL14P1	SLC12A9
RPL18AP3	SLC1A7
RPL22	SLC38A5
RPL23AP2	STAT6
RPL23AP42	SYNE2
RPL36	THUMPD3
RPL36A	TMEM145
RPL37	WWC1
RPL37A	NAT8L
RPL38	ADAR
RPL39	AGAP9
RPL41	BCL11A
RPL4P4	CCDC150P1
RPL5P1	CDK2AP1
RPL6P27	CLEC16A
RPL7AP50	CYR61
RPL7P1	EHD3
RPL7P9	GOLGA8B
RPL9P9	GREB1L
RPLP0P6	HOXB7
RPS10	KMT5C
RPS13P2	LINC01355
RPS21	LIPG
RPS26	MADCAM1
RPS27	MAPK7
RPS28	MFSD4B
RPS29	MTMR9LP
RPS3AP49	PCDH19
RPS3AP5	PIR

RPS3AP6	PSD3
RPS7P1	PYGO1
SNHG6	RNF213
CACYBP	RP11-732A19.1
CALR	RPAP2
CRYAB	SCFD1
DNAJB1	SLC26A2
DUSP1	SNRPGP10
DYNLL1	TNFRSF25
H2AFJ	TTPAL
H3F3B	ULK1
HERPUD1	VAT1
HIST1H1C	ZNF549
HIST1H2AC	BEX2
HIST1H2BD	CALM2
HIST1H2BG	COX17
HMGB2	GABARAP
HSP90AA1	H3F3A
HSP90AB1	HIST1H4C
HSP90AB3P	HMGB1P5
HSPA1A	HMGN2
HSPA1B	HMGN2P5
HSPA5	LSM5
HSPA6	NDUFB1
HSPB1	NDUFB4
HSPD1	PPIAP22
HSPE1	PTMS
HSPH1	RP11-641D5.1
JUN	RP11-84E17.1
KLF10	SNRPEP4
MRPL18	SON
MT-ATP6	TCEAL5
MT-CO1	TCEAL7
MT-CO2	TCEAL8
MT-CO3	TCEAL9
MT-ND1	TMA7
MT-ND2	UCHL1
MT-ND3	UQCR10

MT-ND4	UQCRHL
MT-ND4L	UQCRQ
MT-ND5	YWHAE
MT-ND6	AC004967.7
MT-RNR1	C19orf43
MT-RNR2	CCDC88A
MTATP6P1	CENPV
MTND2P28	CHCHD10
TXNIP	CHCHD2
UBB	CLTB
UBBP4	CRIP2
AIPL1	CTA-941F9.10
ANKRD33B	GADD45G
ATP1B2	GATSL3
BAZ2B	GLTSCR2
CBX1	GNB2
CLK4	GRAMD1C
DDX17	HNRNPU
DOCK8	ISOC1
ENAH	MAP1B
EPB41L2	MARCKS
EPS8	MARCKSL1
FAM161A	MZT2B
FEZ2	NENF
ITSN1	RP11-40C6.2
KDM5B	RPS2
KIAA0556	SLC40A1
KPNA3	TERF2IP
MAK	YPEL3
MAP1B	ABCA4
MAP1LC3B	ADD1
MARCH1	ARL3
MOK	ARL6IP1
MPPED2	CD47
NRIP1	CDHR1
NRL	CPE
NTM	FAM138E
PDC	HMGN1
PIK3R1	IFI27L2

PKM	MIR124-2HG
PPFIA2	PODXL
PPP2R5E	PRPF8
PTP4A3	RCVRN
PTPN13	RIMS2
PTPRF	RP11-356I2.4
RIC3	RP11-39E3.3
SEC62	SGIP1
SLC40A1	SLC2A11
SMC3	SNAP25
SRSF10	STX3
SYCE1L	TPD52
SYNE2	UNC119
TET1	
TMEM244	
UBXN4	
ZNF385B	
RAX2	
ATP5E	
ATP5H	
ATP5I	
ATP5J2	
CALM2	
CCDC181	
COX17	
COX6A1	
COX6C	
COX7A2	
COX8A	
ELOB	
HIST1H4C	
HMGB1P5	
HMGN2	
HNRNPM	
LINC00116	
MAN1A2	
MORF4L1	
NDUFA1	
NDUFA3	

NDUFA5
NDUFA6
NDUFB1
NDUFB4
NDUFC1
PTMA
PTMS
SELENOK
SLIRP
SNRPG
TCEAL4
TMA7
TOPORS-AS1
TTC1
UBL5
UQCR10
UQCR11
UQCRHL
UQCRQ
USMG5
YWHAE
ATP5A1
ATP5G2
ATP5G3
ATP5L
ATP6V1G1
BAG1
C19orf43
CENPV
CHCHD10
CLTB
COMT
COX4I1
GADD45G
GLTSCR2
GNAS
GSTP1
HINT1
IFT22
ISOC1

LDHB
MARCKSL1
MESP1
MZT2B
NDUFB11
NENF
PPIB
PRDX1
PRMT1
PTOV1
RNF187
RPS2
SNHG7
TMEM176B
UQCRB
UQCRH
YBX1
ZNF428
CTSF
AC004556.1
ARPC3
BLZF1
C12orf57
CD63
CEP95
CHCHD2
CYCS
DAD1
DNTTIP1
EDF1
EIF3I
EIF3K
FIS1
IMPDH2
KRT10
LSM5
MAGEF1
MGST3
MIA3
MORF4L2

MRPL23
NDUFB9
NDUFS8
OAZ1
PHPT1
PRDX5
PSMA7
PSMB6
RSU1
SAP18
SEC31A
SERF2
SSR4
TRMT112
UFM1
YIF1A
ZNF667-AS1
AC063980.3
ANAPC16
ATXN2L
BEX2
CCDC58
CDR1-AS
CNBP
CROT
CTD-3014M21.1
DDIT3
EIF1
FAM200B
FTH1
GLO1
ILF3-AS1
KIF5B
LINC00998
LINC01021
LINC02154
NDUFA4
PCAT4
PCP4
PKIB

PRL
RRM2B
SCG3
SQSTM1
TAF7
TCEAL7
TCEAL8
TCEAL9
TMEM38B
UCHL1
UFSP2
WASF3
XRCC4
ZNF793-AS1
BASP1
CABP7
CPNE3
CRABP1
CTC-378H22.2
DLL3
FAM57B
GNG5
GPC3
GPX1
HES6
HMGA1
HNRNPCP2
ID2
KDELR1
LMAN1
MDK
MIR7-3HG
NAP1L1
ONECUT1
PHLDA1
PLP1
PPP1R14A
PRDM1
PRRT2
PTH2

QPRT
RBP4
RCN1
RIMS1
S100A13
S100A6
SLC39A10
SYT4
TMEM176A
TRH
WSB1
COMMD6
PCBP2
RPL12
RPL14
RPL21
RPL23
RPL23A
RPL24
RPL26
RPL27
RPL27A
RPL28
RPL29
RPL30
RPL31
RPL32
RPL34
RPL35
RPL35A
RPL9
RPLP1
RPLP2
RPS12
RPS13
RPS15
RPS15A
RPS17
RPS20
RPS23

RPS24
RPS25
RPS6
RPS7
RPS8
SNHG5
ZFAS1
ABCA4
ALDOC
ARL3
CNGB1
COBLL1
DMD
GNGT1
GPR160
HMGN1
LENG8
PDE6G
PPP2R2B
PRPH2
RCVRN
ROM1
RP1
RP11-39E3.3
SETD3
SNAP25
SAMD7
SAG
AP000997.1

Supplementary Table 6: GO enrichment analysis of age-dependent modules of differentially expressed genes in rods and cones.

Table 19

cones - mature modules

GO term (parent)	fold enrichment	p value	FDR
positive regulation of guanylate cyclase activity	27.08	7.51 E-05	1.34 E-02

retinal cone cell development	16.92	4.49 E-05	9.12 E-03
detoxification of copper ion	16.92	2.75 E-04	3.58 E-02
rhodopsin mediated signaling pathway	14.1	8.83 E-05	1.52 E-02
regulation of rhodopsin mediated signaling pathway	10.83	3.17 E-06	1.38 E-03
cellular response to zinc ion	10.58	2.64 E-04	3.53 E-02
canonical glycolysis	10.3	1.75 E-05	4.39 E-03
regulation of cardiac muscle contraction by regulation of the release of sequestered calcium ion	9.67	9.54 E-05	1.55 E-02
photoreceptor cell maintenance	8.46	4.28 E-06	1.71 E-03
ATP biosynthetic process	7.81	2.59 E-04	3.55 E-02

cones - early modules

GO term (parent)	fold enrichment	p value	FDR
SRP dependent cotranslational protein targeting to membrane	34.74	5.82 E-83	4.31 E-79
positive regulation of instrinsic apoptotic signaling pathway by p53 class mediator	33.85	3.21 E-05	3.13 E-03
viral transcription	28.95	1.63 E-78	3.01 E-75
nuclear-transcribed mRNA catabolic process, nonsense-mediated decay	28.44	3.73 E-80	1.10 E-76
ribosomal small subunit assembly	23.8	2.46 E-09	3.47 E-07
negative regulation of ubiquitin protein ligase activity	18.8	1.69 E-04	1.46 E-02
ribosomal large subunit assembly	17.9	4.19 E-10	6.10 E-08
formation of cytoplasmic translation initiation complex	16.92	5.85 E-06	6.20 E-04
modulation by symbiont of host immune response	16.92	2.32 E-04	1.93 E-02
modulation by symbiont of host defense response	14.1	1.37 E-05	1.36 E-03

rods - mature modules

GO term (parent)	fold enrichment	p value	FDR
rhodopsin mediated signaling pathway	70.08	2.17 E-14	2.30 E-11

positive regulation of guanylate cyclase activity	67.27	2.21 E-06	7.62 E-04
regulation of rhodopsin mediated signaling pathway	37	1.95 E-13	1.81 E-10
detection of light stimulus involved in visual perception	21.02	7.69 E-05	1.68 E-02
eye photoreceptor development	21.02	1.71 E-08	9.04 E-06
photoreceptor cell maintenance	21.02	2.11 E-09	1.20 E-06
camera-type eye photoreceptor cell differentiaation	17.52	1.99 E-05	5.47 E-03
Wnt signaling pathway, calcium modulating pathway	12.74	7.73 E-05	1.57 E-02
synaptic vesicle exocytosis	9.52	6.46 E-05	1.50 E-02
actin-mediated cell contraction	7.42	2.30 E-04	4.31 E-02

rods - early modules

GO term (parent)	fold enrichment	p value	FDR
positive regulation of intrinsic apoptotic signaling pathway by p53 class mediator	40.57	1.60 E-05	1.99 E-03
telomerase holoenzyme complex assembly	38.03	2.36 E-04	2.18 E-02
electron transport coupled proton transport	38.03	2.36 E-04	2.16 E-02
SRP-dependent cotranslational protein targeting to membrane	31.49	4.52 E-62	6.70 E-58
viral transcription	26.69	7.29 E-60	1.80 E-56
nuclear-transcribed mRNA catabolic process, nonsense-mediated decay	25.99	2.40 E-60	8.89 E-57
translational initiation	22.98	9.58 E-60	2.03 E-56
negative regulation of ubiquitin protein ligase activity	22.54	8.52 E-05	9.43 E-03
cytoplasmic translation	16.43	2.18 E-19	7.34 E-17
chaperone-mediated protein complex assembly	15.85	4.11 E-05	4.80 E-03

Supplementary Table 7: GO enrichment analysis of genotype-dependent modules of differentially expressed genes in rods and cones.

Table 20

Cone modules 9 and 14 (KO enriched)

GO term (parent)	fold enrichment	p value	FDR
positive regulation of nucleotide-binding oligomerization domain containing 2 signaling pathway	>100	1.64 E-02	2.41 E-02
regulation of MHC class I biosynthetic process	>100	2.73 E-04	3.82 E-02
telomerase holoenzyme complex assembly	94.02	4.08 E-04	5.09 E-02
electron transport coupled proton transport	94.02	4.08 E-04	5.04 E-02
negative regulation of inclusion body assembly	62.68	3.02 E-05	6.13 E-03
ATF6-mediated unfolded protein response	62.68	3.02 E-05	6.04 E-03
PERK-mediated unfolded protein response	56.41	3.91 E-05	7.43 E-03
chaperone-mediated protein complex assembly	47.01	3.27 E-06	1.05 E-03
chaperone cofactor-dependent protein refolding	45.39	6.35 E-10	7.24 E-07
negative regulation of transcription from RNA polymerase II promoter in response to stress	43.39	7.57 E-05	1.35 E-02
protein refolding	41.79	1.75 E-08	1.18 E-05
mitochondrial electron transport, cytochrome c to oxygen	41.79	4.90 E-06	1.40 E-03
mitochondrial electron transport, NADH to ubiquinone	31.34	4.77 E-10	5.89 E-07
cellular response to heat	25.81	2.09 E-08	1.34 E-05
positive regulation of erythrocyte differentiation	24.53	3.38 E-04	4.44 E-02
aggrephagy	23.51	3.79 E-04	3.84 E-02

Rod modules 2, 8, 9, 12 (WT enriched)

GO term (parent)	fold enrichment	p value	FDR
SRP-dependent cotranslational protein targeting to membrane	38.68	1.37 E-45	1.01 E-41
viral transcription	33.08	1.26	3.73

		E-44	E-41
nuclear-transcribed mRNA catabolic process, nonsense mediated decay	32.51	1.52 E-45	7.49 E-42
translational initiation	29.22	2.96 E-46	4.38 E-42
ribosomal large subunit assembly	22.32	7.51 E-07	1.31 E-04
cytoplasmic translation	20.43	7.75 E-15	2.80 E-12
canonical glycolysis	16.82	1.54 E-04	2.35 E-02
ribosomal small subunit biogenesis	9.96	1.12 E-05	1.87 E-03
rRNA processing	6.54	5.91 E-08	1.14 E-05
positive regulation of translation	5.64	3.26 E-04	4.78 E-02

Rod modules 1, 3, 5, 11, 13 (KO enriched)

GO term (parent)	fold enrichment	p value	FDR
rhodopsin mediated signaling pathway	48.84	7.88 E-13	6.49 E-10
positive regulation of guanylate cyclase activity	48.89	9.10 E-06	1.93 E-03
telomerase holoenzyme complex assembly	43.96	1.55 E-04	2.11 E-02
electron transport coupled proton transport	43.96	1.55 E-04	2.09 E-02
regulation of rhodopsin mediated signaling pathway	25.79	9.70 E-12	7.57 E-09
response to light intensity	23.44	6.77 E-05	1.07 E-02
chaperone-mediated protein complex assembly	18.32	2.08 E-05	4.05 E-03
chaperone cofactor-dependent protein refolding	18.19	9.61 E-09	4.45 E-06
protein refolding	17.37	8.85 E-08	3.05 E-05
mitochondrial electron transport, ubuiquinol to cytochrome c	15.63	2.45 E-04	3.11 E-02

Chapter 4: Single cell transcriptomic analysis of human stem cell derived OPCs

Single-cell transcriptomic analysis reveals molecular diversity of PDGFRα+ human oligodendrocyte progenitor cells

Reworded content and figures/legends from:

Chamling, X., Kallman, A., Fang, W., Berlinicke, C., Mertz, J.L., Devkota, P., Morales Pantoja, I.E., Smith, M.D., Ji, Z., Chang, C., Kaushik, A., Chen, L., Whartenby, K., Calabresi, P.A., Mao, H-Q., Ji, H., Wang, T-H., Zack, D.J. Single-cell transcriptomic analysis reveals molecular diversity of PDGFRα+ human oligodendrocyte progenitor cells. Under review.

Abstract

Demyelinating diseases such as multiple sclerosis can result from oligodendrocyte injury or loss, and remyelination-based treatment strategies would benefit from an improved understanding of oligodendrocyte development. To address this, we performed single-cell transcriptomics over a time course of human stem cell-derived oligodendrocyte precursor cell development. We utilized a genome engineered stem cell line expressing a tag under the PDGFRα endogenous locus to purify and analyze OPCs. We characterized the transcriptional heterogeneity of stem cell derived PDGFRα+ OPCs and identified candidate regulatory factors controlling differentiation and myelination capacity. Specifically, we identified branch points separating oligodendrocyte and astrocyte cell fates and identified novel genes possibly involved in regulating this cell fate decision.

Introduction

Myelin is essential to neuronal health and function in vertebrates, and it functions to both protect axons and enable rapid saltatory conduction (115). Multiple sclerosis and other myelin disorders can be either inherited or acquired, resulting from genetic mutation, toxic injury, or autoimmune insult, and these disorders often lead to severe disability (116). While treatment options exist to modulate demyelination, these drugs are unable to effectively promote remyelination. Remyelination strategies could provide more impactful treatment avenues would benefit from better understanding of the molecular mechanisms underlying development of oligodendrocytes (OLs), the glial cells responsible for myelinating the central nervous system (CNS). Transcriptomic and pathways studies have led to identification of compounds that could target oligodendrocytes capable of myelination, however these studies utilized primarily rodent oligodendrocyte precursor cells (OPCs) and OLs (33, 117-119). Importantly, many differences exist between human and rodent OPCs and OLs, including over 200 human OPC genes not expressed in mouse OPCs and the expression of Ascl1, which is critical for OL development from mouse neural precursors but dispensable in humans (35, 120). As a result, more detailed transcriptomic analysis of human oligodendrocyte lineage cells (OLLCs) could greatly benefit disease modeling and ability to identify drugs to promote myelination.

Studies of human OLLCs are severely limited by difficulty in obtaining sufficient numbers of purified cells, as primary OPCs are rare, difficult to isolate, and cannot be expanded following isolation (52). Alternatively, OPCs differentiated from human pluripotent stem cells (hPSCs) provide another system for studying human OPCs, however challenges still exist in identifying and purifying OPCs from mixed cell populations (121-124). In this study, we utilized a genome engineered human

embryonic stem cell (hESC) reporter system in which an identification-and-purification (IAP) tag expressed under the endogenous PDGFRα locus enables scalable differentiation and purification of PDGFRα+ OPCs. Single cell capture via Dropseq and transcriptomic analysis was performed using this stem cell line at three time points over OPC differentiation (57). This single cell RNA sequencing (scRNAseq) and analysis enabled identification of transcriptionally distinct cell populations within the purified OPCs, thus revealing transcriptional heterogeneity of OPC populations and facilitating analysis of the various OPC differentiation pathways (57, 125). Comparing genes differentially expressed between OPCs and mature OLs identified pathways involved in OL maturation. Additionally, consistent with previous studies, we report the ability of PDGFRα+ OPCs to generate astrocyte cells, as well as identification of PDGFRα+ cells expressing mature astrocyte or oligodendrocyte markers (52, 53). We utilized the potential nature of the reporter OPCs and pseudotime analysis to characterize the trajectory of OPC development and the OL versus astrocyte lineages (77). This analysis identified OL or astrocyte enriched genes that could be involved in regulating OL versus astrocyte cell face specification.

Methods

Dropseq-based single cell capture and RNA-sequencing

Drop-seq-based single cell RNAseq was performed as previously described by Macosko et al. (16). Barcoded microparticles were purchased from Chemgenes Corporations. During differentiation, large number of differentiating cultures are PDGFRα+ on day 75, providing sufficient cell numbers for downstream analysis (121, 126). We observe a similar phenomenon with tdTomato expressing cells in our differentiation culture. Therefore, day 75 and two other time-points, two weeks apart were considered for time-course single cell capture. Since MACS purification and Drop-

seq could not be timed on the exact intended day, we ended up using cells from day 77, day 89 and day 104. The differentiating cells were MACS purified for Thy1.2 expression. Each time-point is from single batch of differentiation. Small fraction of the purified cells was used for FACS-based analysis to confirm that >90% of them were tdTomato+. Cells were MACS purified 2-3 times until ~90% purity was achieved. Using the microfluidic device, the purified reporter cells were captured into a ~1 nL size droplets containing barcoded nanoparticles and lysis buffer. Generated droplets were broken with perfluorooctanol (Sigma, 370533) in 30 ml of 6× SSC. The beads were then washed, reverse transcribed, PCR amplified, and the amplified cDNA quantified using a BioAnalyzer High Sensitivity Chip (Agilent). The cDNA was then fragmented and amplified for 3' prime end sequencing with the Nextera XT DNA sample prep kit (Illumina). cDNA and libraries for each sample were prepared independently, and an equimolar amount of each library was then pooled together for sequencing. The libraries were purified, quantified, and then sequenced on the rapid flow chip in Illumina HiSeq 2500. From the three independent timepoints, a combined total of ~4,800 purified cells were captured.

Quality control and clustering

The principal component analysis (PCA) and t-distributed stochastic neighbor embedding (tSNE) analyses were performed using a previously published R package, Seurat (76). As a quality control, only cells that had a minimum of 250 mRNA molecules and a maximum of 20% mitochondrial RNA were used for analysis. In order to eliminate probable doublets from the dataset, we bioinformatically filtered out cells with >30,000 unique molecular identifier (UMIs) (Figure S3a). Additionally, we removed cells that exhibited 1) expression of less than 250 genes or 2) greater than 20% mitochondrial gene content. The remaining 3271 cells were used for further bioinformatic analysis.

Genes that were expressed in a minimum of 3 cells were included for the analysis. 1874 highly variable genes were input for PCA analysis, and the 16 statistically significant PC's were used for clustering and t-SNE analysis. 1266 enriched genes were used to generate the expression heatmap. A gene that showed positive fold change with significant p value in a population when compared to all other populations is considered "enriched".

Pseudotemporal trajectory analysis

Time-series analysis to generate a pseudotemporal trajectory was performed using an unsupervised differential gene expression test based on sample age in Monocle, following previously published detailed instructions (77). The top 752 genes differentially expressed based on age were used for ordering and trajectory reconstruction. Differential gene expression was performed on each node of the resulting trajectory to identify genes with branch-dependent expression. Differential gene expression was performed using either Seurat or Monocle.

Calculation of Spearman correlations and human mouse overlap assessment

Total expression of all the genes expressed in both our dataset and the previously published snRNAseq dataset (13658 total genes) was used to normalize gene expression in each cell (127). The normalized expression was averaged across each population. 1195 variable genes expressed in both datasets were then used to calculate spearman correlation between each population. To combine all the oligodendrocyte subpopulation as one population, expression was weighted by number of cells in each sub-population. Similar weighted average was also used to combine the two astrocyte sub-populations. For the comparison with bulk RNAseq dataset, 767 highly variable genes from each human tissue-type published by Zhang et al. was compared to

each of our population's averaged normalized expression (128). For comparison with mouse cells, all the genes expressed in each of our clusters were compared to the genes from each of the mouse CNS cell-type previously published (119).

To assess the overlap of enriched genes in our hESC-derived OLLCs, ALCs, OPCs, and endothelial/pericyte cells to that of the enriched genes in the corresponding population from mouse dataset, we assigned clusters 0,1, and 3 as OPCs; 4,7, and 8 as OLLCs; 2,5,6, and 9 as ALCs; and 10 as endo/peri. All 1266 differentially expressed genes used for the expression heatmap (Figure 4b) were used for the comparison. From the mouse dataset3, genes expressed at levels > 20 FPKM and >5-fold relative to the average expression in all other populations, were considered enriched (119).

Results

Single cell transcriptome analysis of PDGFRα+ reporter OPCs

Development of scRNAseq technologies has allowed for the ability to profile thousands of single cells and identify transcriptional heterogeneity within cell populations (57, 125, 129). We utilized Dropseq, a microfluidic based single cell capture platform, to transcriptomically analyze differentiating OPCs and elucidate the gene expression changes associated with OL development and maturation (57). Reporter cells over three time points during *in vitro* differentiation, days 77, 89, and 104, were independently purified via MACs to obtain a 90% pure population of PDGFRα-tdTomato+ cells for single cell capture and RNA sequencing. These three stages yielded a total of 3271 cells after quality control filtering (Supplementary Fig. 1A-B). Cells were clustered using unsupervised t-distributed stochastic neighbor embedding (t-SNE) into 12 transcriptionally distinct cell populations (Fig 1A-B).

We also utilized spearman correlations with previously published single nucleus and bulk RNA sequencing to compare our dataset to primary human and murine CNS

cells (Fig. 1C and Supplementary Fig. 1C) (119, 127, 128). The correlations, gene expression patterns, and cell-type specific marker genes in Table 1 suggested that clusters 0, 1, and 3 are OPCs and clusters 5, 6, 9, and 2 are astrocyte lineage cells (ALCs), while more mature OLLCs correspond to clusters 4, 7, and 8 (Fig. 1, Supplementary Fig. 1C). Additionally, cluster 8 exhibited enrichment of the mature OL markers *MAG*, *MOG*, and *ZNF488*, indicating this population may be more mature that the OLs in clusters 4 and 7, which are likely newly formed OLs (nfOLs). Importantly, our in vitro differentiated OL populations were highly correlated with 6 previously described sub-populations of human brain OLs (Fig. 1C) (127). We also identified clusters 2, 5, 6, and 9 to have relatively higher correlation with fetal astrocytes (Supplementary Fig. 1C). Cluster 2 also exhibited high correlation with mature astrocytes, as well as enrichment for mature astrocyte markers including *SPARCL1*, *AQP4*, *IGFBP7*, *AGT*, and *EDNRB* (Fig. 1C, Supplementary Fig. 1C, Table 1) (128, 130). Proliferative genes associated with fetal astrocytes, including *TOP2A, HIST1H4C, PCLAF, HMGB2, NUSAP1, MKI67* and *TMSB15A,* were enriched in clusters 5, 6, and 9, but depleted in cluster 2 (Table 1). Additionally, cell cycle analysis revealed that the majority of the cells in clusters 5, 6 and 9 were in G2M or S phase, whereas the majority of the cells in clusters 2, 4, 7 and 8 were in G1 phase (Supplementary Fig. 1E). This data further confirms that cluster 5, 6 and 9 represent proliferative fetal astrocytes and cluster 2 is more akin to mature astrocytes.

Cluster 10, which was distant in the t-SNE space, exhibited higher correlation with endothelial cells and pericytes, in addition to enrichment for pericyte marker genes (*COL1A1, COL1A2, COL3A1, ATAC2, PDGFRβ*) and the endothelial marker gene *ANXA2* (Fig. 1C, Supplementary Fig. 1C, Table 1) (131, 132). This gene expression pattern suggests that this cluster could represent the VLMC-pericyte cells that are reported to arise from PDGFRα+ precursors (133). This cluster exhibited expression of

a few mature astrocyte markers (*SLC40A1, IGFBP7, SPARC*), and except for one or two cells, no OPC markers were detected (Fig. 1D, Table 1). It is also possible that this cluster could represent contaminating PDGFRα negative cells in the purified population.

Of all the single cells analyzed, 901 (27.5%) expressed *GFAP* and 733 (22.4%) expressed *MBP*, corresponding to ALCs and OLLCs, respectively (Supplementary Fig. 1D). As cells matured, the proportion of OPCs decreased while the *MBP+/PLP1+* and *GFAP+/AQP4+* populations increased in prevalence, supporting the finding that PDGFRα+ OPCs are able to differentiate into astrocytes and oligodendrocytes *in vitro* (Supplementary Fig. 1D and G) (52). Analysis of cells separately at each time point revealed that OPCs, OLs, and astrocytes are present at each time point (Supplementary Fig. 1H-J). While cells purified at the later time points are more enriched in the mature clusters, each cluster included cells over all three stages, thus confirming that purified hPSC-derived OPCs are heterogeneous with respect to their degree of differentiation even within the same *in vitro* stage (Supplementary Fig. 1F).

Validation of astrogenic potential in OPCs

To confirm that the ability of OPCs to form astrocytes was not a feature resulting from the reporter cell line or purification method, we also characterized OPCs differentiated from a second, non-reporter iPSC line, after 60 days in culture and purified using a PDGFRα antibody (Supplementary Fig. 2A-B). Very few cells expressed mature OL (*MBP, PLP1*) or astrocyte (*AQP4*) markers, which was unsurprising considering the time point (Supplementary Fig. 2C). Despite the lack of mature markers, the OL related genes *CNP* and *TCF7L2*, as well as transcription factors known to promote astrocyte development (*SOX9, NFIA*, and *NR2F1*), were enriched in day 60 cells. Additionally, many of these PDGFRα+ cells expressed *GFAP* (Supplementary Fig. 2C-D). As a second control, we also performed scRNAseq with day 89 reporter cells purified using

O4-antibody conjugated microbeads. Similarly to the other datasets, a subpopulation of these O4+ cells also expressed astrocyte markers (Supplementary Fig. 2E).

Identification of cell-type enriched genes

We next examined the clusters for highly enriched and differentially expressed genes, and found that the majority of differentially expressed genes in the OLLC and ALC populations were consistent with previous publications (119, 128). For example, *MBP, PLP1, CNP, CLDN11, UGT8, BCAS1, SIRT2, MOG, MAG, TNR, ENPP6*, and *CHN2* were enriched in the OLLCs; and *GFAP, CLU, AQP4, ID3, EDNRB, MGST1, AHCYL1, EZR, HSPB8, SPARC, DTNA*, and *FABP5* were enriched in the ALCs (Table 1, http://zacklab.org/OPCs/). We also report expected expression patterns for genes shown to be enriched specifically in human, but not mouse, OLs and astrocytes such as *APCDD1, HMGCS1, PMP2,* and *WIF1* (128, 134). We then sought to compare genes enriched in our hESC-derived OLLCs, ALCs, and OPCs to those enriched in the murine cell populations (119). While many known marker genes were enriched in both murine and human cells, we report some differences in gene expression enrichment (Supplementary Fig. 3A-D). In contrast to previous studies, we found OL enrichment of genes including *KCTD12, SLC7A14, HMGCS1, SPOCK1, FAM13C, FAM131C, TMEM206,* and *KIF21A* (Fig. 1D, Supplementary Fig. 3A, Table 1). *HMGCS1* has not been shown to be expressed in murine CNS cells, however it is also important for cholesterol biosynthesis and myeline production in the zebrafish CNS (119, 135). Contrary to the OL enrichment in our dataset, other human CNS data has shown its enrichment in fetal astrocytes (128). *KCTD12, TMEM206, FAM131C, FRMD4B* and *APCDD1* were OL-enriched in our dataset, but bulk RNAseq of purified murine CNS cells has shown *KCTD12* and *TMEM206* enrichment in microglia; *FAM131C* enrichment in neurons; and *FRMD4B* and *APCDD1* expression specifically in endothelial cells (119).

Additionally, while previous studies have shown specific expression of *CD9* in myelinogenic OLLCs, we report relatively ubiquitous *CD9* expression across all clusters, suggesting that *PDGFRα+/CD9+* expression is not specific to only myelinogenic precursors within the stem cell-derived OPC system (Fig. 1D) (52). In addition to protein coding genes, we identified numerous differentially expressed primary microRNAs (pri-miRNAs) (Supplementary Fig. 2H). Specifically, miR219-A2 was enriched in OL clusters whereas miR100HG and miR99AHG were astrocyte-enriched. These differentially expressed pri-miRNAs could be involved in regulating the developmental decision for an OPC to form either an OL or an astrocyte.

Trajectory analysis of the bi-potential nature of PDGFRα+ cells

We next utilized the Monocle R package to create a pseudotemporal trajectory of cell fate specification in PDGFRα+ cells over development (77). This trajectory presented two main cell fates for the precursor cells, suggesting that OPCs have the potential to form two distinct cell populations (Fig. 2A). Identification of differentially expressed genes and transcription factors (TFs) and the main node using the Branch Expression Analysis Modeling regression model enabled us to designate path II as OLLCs and path III as ALCs (Fig. 2B-C). In analyzing TFs specifically, *HES1, EGR1, ZFP36L1, NFIA*, and *JUNB* were enriched in ALCs, whereas *SOX10, SOX4, SOX6, TSC22D1*, and *RBPJ* were OLLC enriched (Fig. 2C). This data suggests that these TFs could be involved in OPC cell fate specification.

In assessing the specific cell populations of the trajectory, we identified 7 states across development (Fig. 3A). State 1 was comprised of precursor cells, state 2 astrocytes, and state 6 OLs. The expression of *MBP* and *PLP1* over pseudotime showed an enrichment in state 6 OLs, while *GFAP* and *AQP4* expression over pseudotime showed an enrichment in state 2 astrocytes (Fig. 3C). In analyzing smaller

sub-branches along path II towards mature OLs, states 5 and 7 diverged from the OL trajectory and exhibited enrichment of astrocyte markers (*GFAP, AQP4, NFIA, SOX9*), instead of OL markers (*PLP, MBP, SOX10, TCF7L2, OLIG2, NKX2.2*) (Fig. 3B, Supplementary Fig. 4B). We performed correlation between each branch, and unsurprisingly the state 5 and 7 cells were more highly correlated with state 2 astrocytes than state 6 OLs (Supplementary Fig. 4B). Additionally, cells from the astrocyte cluster in the t-SNE (cluster 2) were present in states 2, 5, and 7 (Supplementary Fig. 4C). To validate this bipotential cell fate in a second system, we performed parallel pseudotime analysis in the day 89 O4+ purified reporter cells. Similarly, this trajectory indicated two main branches, one representing the OL fate and the other the astrocyte fate, as well as the same trends in marker gene expression over pseudotime (Supplementary Fig. 4D-F).

Finally, utilized the same differential expression analysis regression model, we examined differential gene expression at nodes 1 and 2 and between states 2 and 6 to identify genes of potential interest (Fig. 3D-E, Supplementary Fig. 5A-C). In addition to the previously described TFs that could be important for OPC/OL/astrocyte differentiation, including *SOX10* and *TCF7L2*, we identified a number of TFs whose roles in development are less well characterized. Specifically, *ZEB2, TSC22D4, ARID4B, PARP1, E2F3,* and *ARHGAP35* were enriched in OLs, while *HES1, FOSB, NFIA, NR2F1,* and *ZFP36L1* were enriched in astrocytes. We also identified TFs such as *SOX4, SOX11, MLLT11, RBM22, ZNF711, EZH2,* and *DACH2* as depleted in ALCs and slightly enriched in OLs (Fig. 3D). A subset of these genes were also enriched in the day 60 hPSC-derived OPCs (Supplementary Fig. 2C). Finally, the purified PDGFRα+ cells from each time point (days 77, 89, and 104) were present across all branches of the trajectory, supporting the claim that these cells are heterogeneous both

transcriptionally and developmentally, to the degree that even some day 77 cells were already relatively mature (Supplementary Fig. 5C).

Discussion

In this study, we have characterized the transcriptional diversity and heterogeneity of PDGFRα+ OPCs using scRNAseq over a time course of differentiation of reporter OPCs, as well as a second non-reporter cell line. We identified distinct cell clusters, most of which represented OPCs and cells committed to OL or astrocyte cell fate. This is consistent with previous reports that OPCs are capable of developing into either astrocytes or OLs *in vitro* (52). Because previous studies have shown that only OPCs and pre-OLs, not mature OLs, express PDGFRα, the identification of PDGFRα+/tdTomato+ cells expressing mature astrocyte and OL markers was unexpected (Fig. 1, Table 1) (33, 115, 122, 136). Mature astrocyte markers such us the synapse-inducing protein (*SPARCL1*) and transmembrane proteins (*CLU* and *SPON1*) were detected and highly enriched in the astrocyte cluster (128). On the other hand, the OL cluster was enriched for genes associated with myelin production including *MBP, MYCRF, MAG*, and *MOG* (Table 1). Of note, the *PDGFRα* transcript was not detected in the clusters representing these mature cell types (Fig. 1D). This could be explained by presence of the PDGFRα protein, but not transcript, at the time or purification, a longer half-life of tdTomato and Thy1.2 enabling purification beyond the window of PDGFRα expression, or low abundance of the *PDGFRα* transcript in mature cells leading to drop out in the single cell dataset (57, 125, 129, 137, 138).

The identification of transcriptionally distinct cell clusters within the PDGFRα+ population was made possible by scRNAseq and would be undetectable by bulk RNAseq strategies. This analysis enabled identification of several novel human-specific OL (*KCTD12, SLC7A14, HMGCS1, SPOCK1, FAM13C, FAM131C, TMEM206,* and

KIF21A) and astrocyte (*S100A10, CD99, ID2, CRYAB*, and *CA2*) marker genes. Interestingly, we identified some OL and astrocyte specific genes (*KCTD12, HMGCS1, FAM131C APCDD1, S100A10, CD99*, and *ID2*) that have been shown to be expressed in primary microglia, neurons, and endothelial cells (119, 128). This could be a feature of differences between *in vitro* differentiated cells and their *in vivo* counterparts, or lower sequencing depth in scRNAseq compared to bulk RNAseq. However, it is also possible that immunopanning for primary cells from a mixture of dissociated brain cells led to contamination of OL and astrocyte populations with microglia and endothelial cells. Identification of such contaminating cell populations is now possible using various scRNAseq methods.

Because of the large window of PDGFRα expression in OPCs, we were able to utilize pseudotemporal trajectory analysis to better understand OPC differentiation. This analysis revealed that OPCs have two major cell fate decisions corresponding to the OL and astrocyte lineages. While t-SNE clustering identified a small population of cells expressing endothelial/pericyte markers, this population was not identified in the trajectory (Fig. 1, Table 1). The development of oligodendrocytes and astrocytes from our PDGFRα+/tdTomato+ cells is consistent with findings from *in vitro* cultured primary human OPCs, but contrasts with murine studies showing that Pdgfrα+ mouse OPCs can form OLs, neurons, or VLMC-pericytes, but not astrocytes *in vivo* (52, 133). To our knowledge there are no existing studies of the ability of *in vitro* cultured Pdgfrα+ mouse OPCs to form astrocytes. While our results derive from an in vitro culture system and must be confirmed in vivo, our findings suggest that human OPCs can differentiate into astrocytes (Fig. 2, Supplementary Fig. 3)

We have also identified TFs that could be important for directing differentiation of OPCs to either OLs or astrocytes. Various TFs, such as *ZEB2, TSC22D4, ARID4B, PARP1, E2F3, SOX10, TCF7L2, TSC22D1, RBPJ, ARHGAP35, SOX4, SOX11,*

MLLT11, RBM22, ZNF711, EZH2, and *DACH2*, were continuously upregulated in OLs and downregulated in astrocytes. On the other hand, *HES1, EGR1, FOSB, NFIA, NR2F1, ID3, KLF6*, and *ZFP36L1* were enriched in astrocytes and depleted in OLs. It is possible that these sets of TFs could drive specification OL or astrocyte cell fates. The relationships between most of these TFs and OPC differentiation have not been studied, making future studies necessary to ascertain the roles of these TFs in OPC development. The functions of SOX10 and TCF7L2 in OL development and NFIA and NR2F1 in astrocyte development have been well characterized, in addition to the recent identification of the role of ZFP36L1 in OL/astrocyte cell fate specification (139-141). Our identification of these TFs lends support to the possible role of the newly identified TFs in OPC development, however further loss and gain of function studies are necessary to validate and determine their specific impacts on development of OPCs, OLs, or astrocytes.

While Dropseq only captures polyadenylated RNAs and is thus unable to capture mature miRNAs, pri-miRNAs contain polyA tails prior to cleavage by Drosha and are thus able to be captured in this system. MiRNAs, in addition to regulatory genes and TFs, have been shown to be important for OPC specification and differentiation (142-144). To this end, we identified *miR219-A2* as highly enriched in the OL cluster, and it has also been shown to be important for myelination and re-myelination in mice (35, 117, 143-145). The reporter system described here and single cell transcriptomics could enable future studies of ALC and OLLC specific miRNAs in OPC development.

While human and murine OPCs and OLs have similar gene expression patterns and conserved pathways, import species-specific differences exist with regard to their transcriptomes, development, and regeneration (146). For example, gliogenesis in humans begins during gestation and myelination can continue until age 22, whereas rodent gliogenesis occurs postnatally and myelination is complete by day 60 (147, 148).

Additionally, in vitro expression of Ascl1 and Fgf2 promote development of OLs from OPCs in rodents, but not humans (35). Furthermore, animal models of MS are capable of regenerating myelin from newly formed OLs, while human patients have diminished capacity to generate new OLs and rather the limited remyelination likely originates from pre-existing OLs (149). Because of these differences, better understanding of human OL maturation is critical for improved disease modeling and drug discovery efforts. We hope that the hOPC purification system described here along with our scRNAseq dataset (http://zacklab.org/OPCs/) will help provide the basis for ongoing and future studies that will more fully define the molecular mechanisms of human OL differentiation, maturation and myelination.

Table 1: Top 40 differentially expressed genes per cluster ranked by fold change.

Table 21

Cluster 1	Cluster 2	Cluster 3	Cluster 4	Cluster 5	Cluster 6	Cluster 7	Cluster 8	Cluster 9	Cluster 10	Cluster 11
TRIO	GFAP	IFI6	BCAS1	HIST1H4C	PCLAF	PLP1	MBP	ASPM	COL3A1	RTN1
HES1	CLU	H19	MIR219A2	PCLAF	CLSPN	BCAS1	PLP1	CENPF	COL1A2	CRABP1
FGF12	AQP4	ISG15	SIRT2	TOP2A	GINS2	IFI6	CNP	UBE2C	HP	STMN2
PHLDA1	SPARCL1	IGFBP5	KIF21A	HMGB2	TYMS	SIRT2	RP11-89N17	PTTG1	SULF1	ELAVL4
HEY1	ID3	B2M	PLP1	NUSAP1	ORC6	ARHGAP5	CLDN11	TOP2A	CTGF	NNAT
SOX6	AGT	HLA-B	WASF1	MKI67	CENPF	FAM13C	PTGDS	CCNB1	TFF3	SOX4
ARL4A	S100A10	HLA-A	GPC3	TUBA1B	HMGN2	SLC44A1	UGT8	CENPE	COL1A1	DCX
ZFP36L2	CD99	HS3ST1	PRDX1	CDK1	SMC2	RP11-89N1	BCAS1	NUF2	ANXA2	SOX11

						7				
EGR1	EDNRB	HLA-C	UGT8	SMC4	DUT	PRDX1	KCTD12	HMGB2	TAGLN	MIAT
RPS2P5	NMB	CD9	SLC44A1	PCNA	MCM7	WASF1	MIR219A2	NUSAP1	MGP	NREP
MAP2	MGST1	FOS	FAM13C	RRM2	TMSB15A	CENPJ	SEMA4D	TPX2	IGFBP7	ETV1
RPL39	AHCYL1	WWTR1	CNP	HIST1H1D	MCM4	FERMT1	RGS16	MKI67	DCN	HMP19
KHDRBS3	TGFB2	IFI16	EPB41L2	TPX2	MAD2L1	FYN	SIRT2	CKS2	LGALS1	PEG10
RP4-765C7	CRYAB	SERPINE2	RAB33A	HMGN2	H2AFZ	CNP	NFASC	PRC1	SPARC	NRXN1
NKX2-2	VIM	TRIB2	SGK1	CENPF	TUBA1B	MBP	APLP1	KPNA2	ACTA2	TAGLN3
PLPPR1	HSPB8	PMP2	CADM2	SMC2	RPA2	RNF13	HMGCS1	SGO2	IGFBP5	FTX
RPL13P12	EZR	RBP1	SMOC1	BIRC5	TUBB	KIF21A	CDK18	NEK2	VIM	CD24
LIMA1	SPARC	BAALC	ARHGAP5	ESCO2	PCNA	CADM2	SLC44A1	KIF14	ELN	TERF2IP
HES5	DTNA	CNTN1	FERMT1	TYMS	RANBP1	RND2	DLG1	BIRC5	SFRP4	PIK3R1
GABPB1-AS1	FABP5	NUPL2	DYNLL1	CENPU	NASP	TNR	CHN2	SMC4	CALD1	CEP170
MTATP6P1	CA2	SAT1	NFASC	MAD2L1	TOP2A	ATCAY	FRMD4A	AURKA	EFNB3	NFIB
HIST3H2A	ID1	PLLP	FYN	PRC1	SNRPB	UGT8	MOG	ARL6IP1	ACTG2	KDM5B
RPL18A	ID2	WSCD1	GALNT13	KNL1	ARL6IP1	MIR219A2	KIF21A	CDK1	CYR61	HES6
RPL36A	ANOS1	C1orf21	TMEM206	ATAD2	SUPT16H	MOG	ARHGAP5	DLGAP5	IFITM3	FNBP1L
EPN2	PEA15	CARS	CENPJ	ZWINT	HMGB1	GNB4	CENPJ	MAD2L1	COL21A1	CRMP1
TAOK3	F3	CCND1	GPR17	DUT	RRM1	MYO5A	RAB33A	FAM64A	MYLK	TCF12
COL11A1	DCLK1	FABP7	SEMA6D	H2AFZ	SRSF2	EPB41L2	TNR	CDC20	S100A10	DLL3
CCND1	CNN3	MTSS1	FRMD4B	HIST1H1E	NUCKS1	SMOC1	ENPP6	GTSE1	CFC1	PKIA

GAS5	PSRC1	DBI	HIPK2	UBE2C	SMC3	SLC25A5	TM7SF3	CCNB2	SLC40A1	TTC3
STMN2	ATP1B2	NDFIP1	SLC25A5	NDC80	CKS1B	MOB3B	RND2	CDKN3	TPPP3	STMN4
ETV1	CST3	GPR37L1	ATCAY	TUBB	GNG4	CRB1	CTD-2636A23	CKAP2	MEIS2	MAP1B
TMEFF2	ID4	ATP1B2	E2F3	MCM4	SMC4	HIPK2	FAM13C	KNL1	NNMT	FAM110B
GRIA2	TNC	MALSU1	SGCD	DHFR	AP2S1	ERBB3	SGCD	CCNA2	TPM1	STMN1
RP11-343H5	B2M	HMP19	TNR	KIF15	CACYBP	MPZL1	PRDX1	KIF4A	DHRS3	ZNF292
RPSAP58	CCDC80	RAB31	APOD	CLSPN	HMGB3	PKP4	GOLIM4	CKS1B	PLTP	SLC38A1
CA10	IGFBP7	CD59	SOX10	ANP32E	BZW2	NFASC	TRIM2	HMGB3	NPC2	TCF4
AC007969	RGMA	HIP1	TCF7L2	MIS18BP1	PA2G4	GPR17	ARHGAP5-AS1	ANP32E	EZR	MAP2
RPS29	HOPX	PHLDA1	ENPP6	NUF2	NOP56	RAB33A	MAG	TUBB4B	NLRP1	HDAC2
TRAF4	PON2	TRIM9	SOX2-OT	TMSB15A	EXOSC8	CHN2	FYN	KIF20B	MYL12A	MLLT11
DANCR	SPON1	RGS16	GRIA2	PTTG1	HNRNPD	TNS3	FBXO32	NDC80	ID3	KIFAP3

Figure 1: Single cell transcriptomic analysis of purified OPCs. A) t-SNE based unsupervised clustering of the single cell transcriptional profiles of 3,271 purified PDGFRα-tdTomato+ OPCs. Cells (each dot represents a cell) are divided into 12 clusters (0 through 11) based on difference in gene expression profiles. **B)** An expression heatmap of all the enriched genes from each cluster. **C)** Spearman correlation of the single cell transcriptome-based clusters with snRNAseq data from primary human brain cells. "All oligos" and "all astros" are weighted averages of all 6 oligos or both astro sub-populations. **D)** Distribution of various genetic markers among the different clusters presented as an enrichment heatmap. Clusters 0,1,3 – OPCs; 2-Astrocytes; 5,6,9 – Fetal astrocytes; 4,8 – oligodendrocytes; and 10-Endothelial/pericyte.

Figure 36

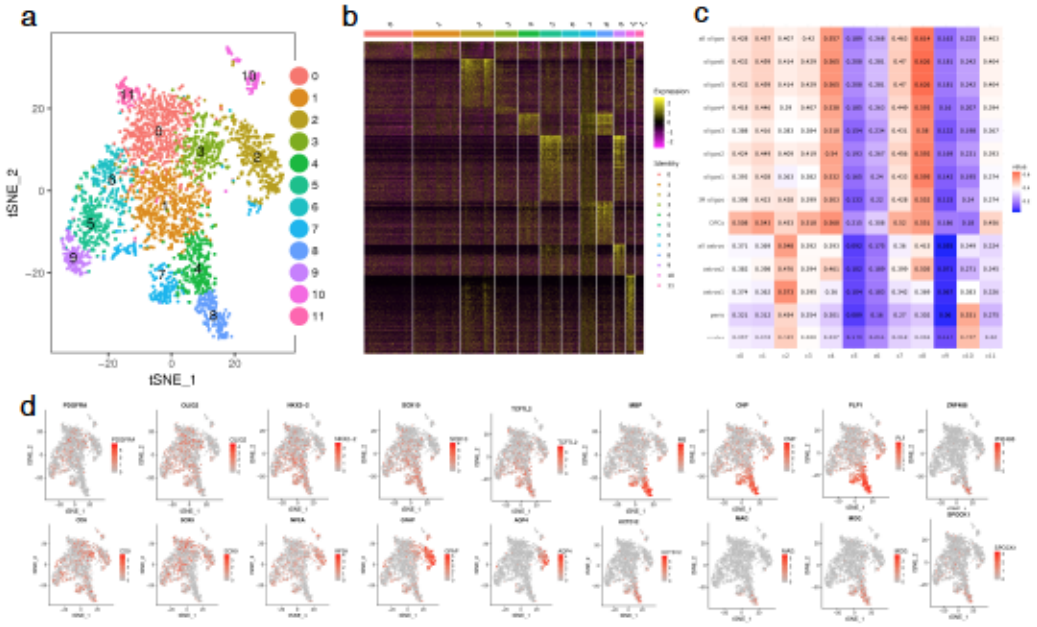

Figure 2: Pseudotemporal trajectory analysis of the single cell transcriptomes of the hOPCs. A) Developmental trajectories of the purified reporter OPCs generated, using Monocole-2, demonstrate two prominent paths for the OPCs. Darker colored dots (on Path I) represent developmentally younger cells and the lighter colored dots (on Paths II and III) represent more mature cells. **B-C)** Kinetic heatmap generated using BEAM regression model capturing the most differentially expressed genes **(B)** and transcription factors **(C)** between Paths II (oligodendrocytes) and III (astrocytes). The genes are hierarchically clustered based on their expression pattern.

Figure 37

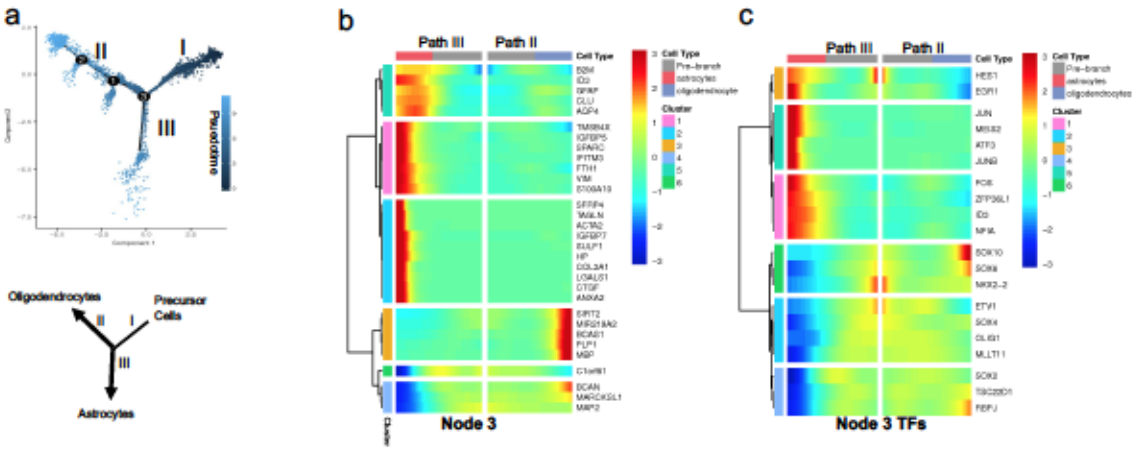

Figure 3: Pseudotemporal trajectory of differentiation based on single cell transcriptomes. A) Ordering cells along the trajectory divides the population into seven different states. State 1 cells are OPCs, state 2 cells are astrocytes, and state 6 cells are oligodendrocytes. **B)** Expression of OL and astrocyte markers within the trajectory further confirms Path III as the astrocyte and Path II as oligodendrocytes lineage cells. Astrocyte makers (*GFAP, AQP4, SOX9, NFIA*) are highly enriched in Path III and in the smaller branches that emerge from path II. OLLC markers (*SOX10, MBP, PLP, TCF7L2*) are enriched in Path II, but not in the smaller branches. **C)** Pseudotemporal expression pattern of OL and astrocyte genes show that the OL genes, *MBP* and *PLP1,* have similar kinetic trend and both are enriched in state 6 cells. The astrocyte marker *GFAP* is modelled to be expressed earlier than *AQP4,* although both are enriched in state 2 cells. **D-E)** Kinetic heatmap of the most differentially expressed non-transcription factor **(D)** and transcription factor genes **(E)** between state 6 (oligodendrocyte cells) and state 2 (astrocyte cells) identified by BEAM and clustered based on their expression pattern.

Figure 38

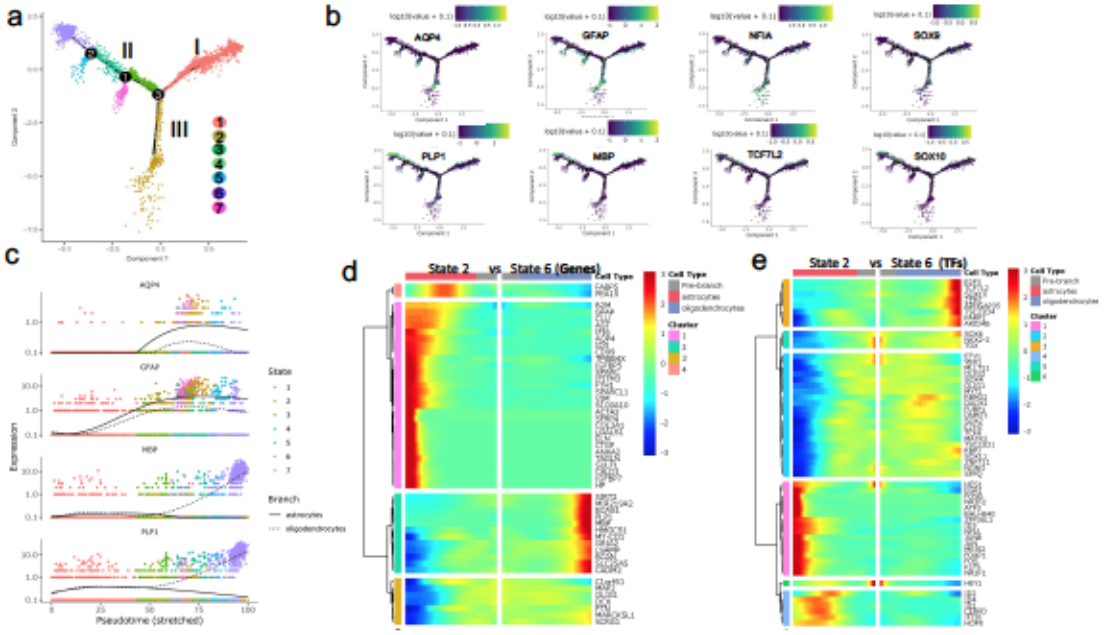

Supplementary Materials

Supplementary Figure 1: scRNAseq analysis of the purified PDTT reporter OPCs separated by different differentiation time-points. A-B) Quality control metrics applied to the scRNA seq data of MACs purified PD-TT derived OPCs. **A)** Violin plot showing number of UMIs by age. In order to remove probable doublets, cells with UMI above 30,000 were removed from the analysis. **B)** Percent mitochondrial gene content per cell. Cells with greater than 20% mitochondrial gene content were also removed from analysis. **C)** Spearman correlation of single cell transcriptome-based clusters with RNAseq data from primary mouse brain cells and primary human brain cells. **D)** table showing number and percentage of cells expressing OL and astrocyte markers at different time-points. **E)** Single cell transcriptome-based cell-cycle analysis. Majority of the cells in cluster 5,6 and 9 are at G2M of S phase, and majority of the cells in cluster 2, 4 and 8 are at G1 phase. **F)** Cells in the t-SNE plot labelled by day at which they were purified (day 77, 89, or 104). Although some enrichment of day 77 cells in OPC and day 104 cells in the mature clusters is noticeable, each cluster consists of cells from all three ages. **G)** A bar graph depicting the frequency of each cluster per time point. Overall reduction of progenitor (0,1,3) clusters and increase in mature clusters i.e OLC, ALC, and Endo-peri clusters is apparent. **H-J)** t-SNE based unsupervised clustering of single cells captured from PDGFRα+/tdTomato+ reporter OPCs at different stages of differentiation (day 77, day 89, and day 104). Cluster specific enrichment of various OL and astrocyte markers indicate OLLC and ALC subgroups of PDGFRα+ cells in each time-point.

Figure 39

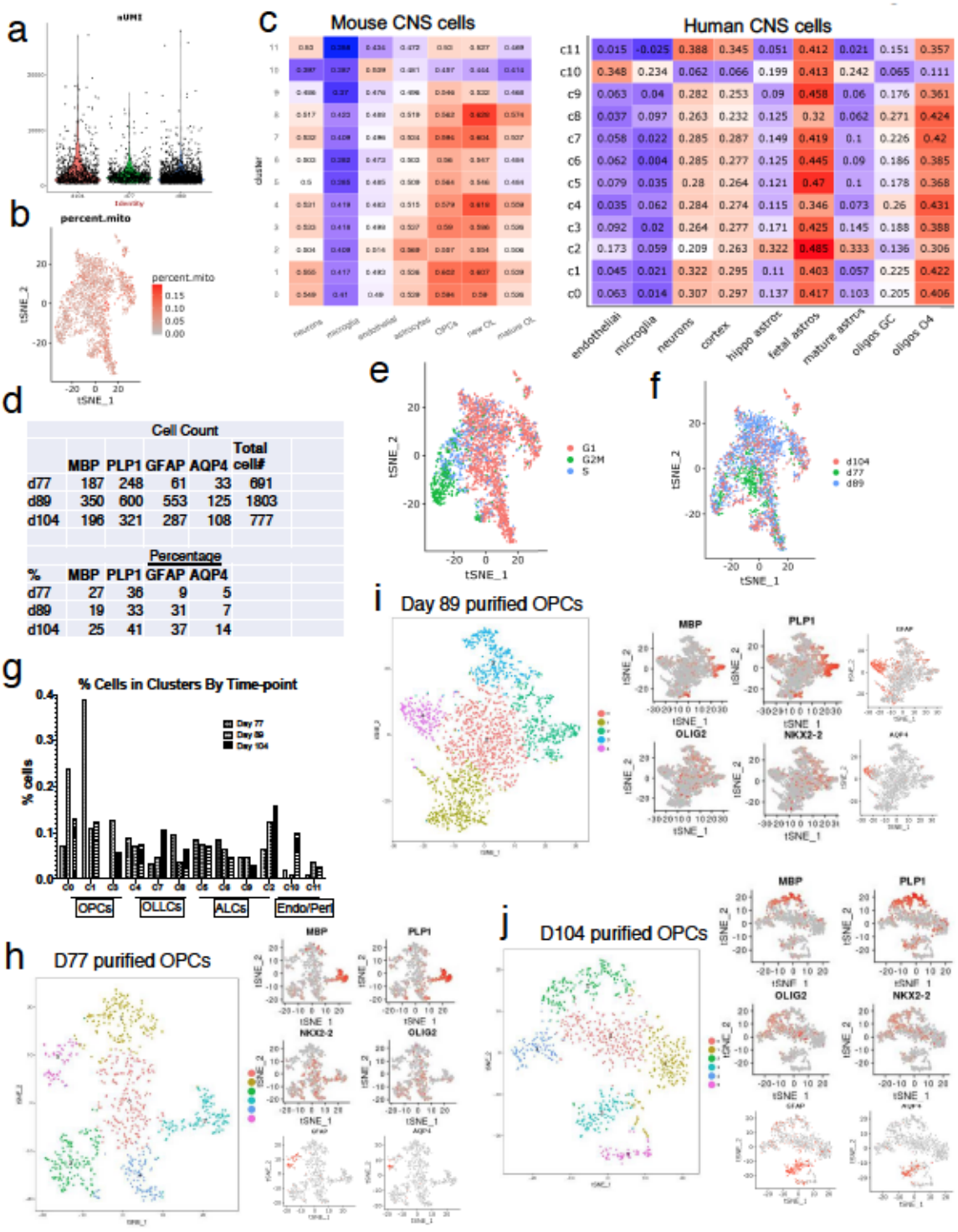

Cell Count					
	MBP	PLP1	GFAP	AQP4	Total cell#
d77	187	248	61	33	691
d89	350	600	553	125	1803
d104	196	321	287	108	777

Percentage				
%	MBP	PLP1	GFAP	AQP4
d77	27	36	9	5
d89	19	33	31	7
d104	25	41	37	14

Supplementary Figure 2: Bioinformatic analysis of the hiPSC-derived PDGFRα+ OPCs and O4+ cells A) hiPSC-derived, day 60 OPCs were stained with antibody against PDGFRα and FACS-purified. Single cells from the FACS-purified samples were captured using the 10X-genomics platform, and their transcriptome was sequenced and analyzed. **B)** t-SNE based unsupervised clustering divided cells into 5 clusters. **C)** Enrichment heatmap showing expression patterns for each cluster of previously reported OL and astrocyte markers. Enrichment of various OL and astrocyte genes is apparent. **D)** Scatterplot mapping cells that express PDGFRα and GFAP. Numerous cells express both the genes. **E)** PD-TT cells at day 89 of differentiation were MACS purified using O4 beads and processed for scRNAseq with Drop-seq. t-SNE based unsupervised clustering and heatmap showing expression patterns of OL and astrocyte markers of day 89 PDTT cells enriched using O4 microbeads.

Figure 40

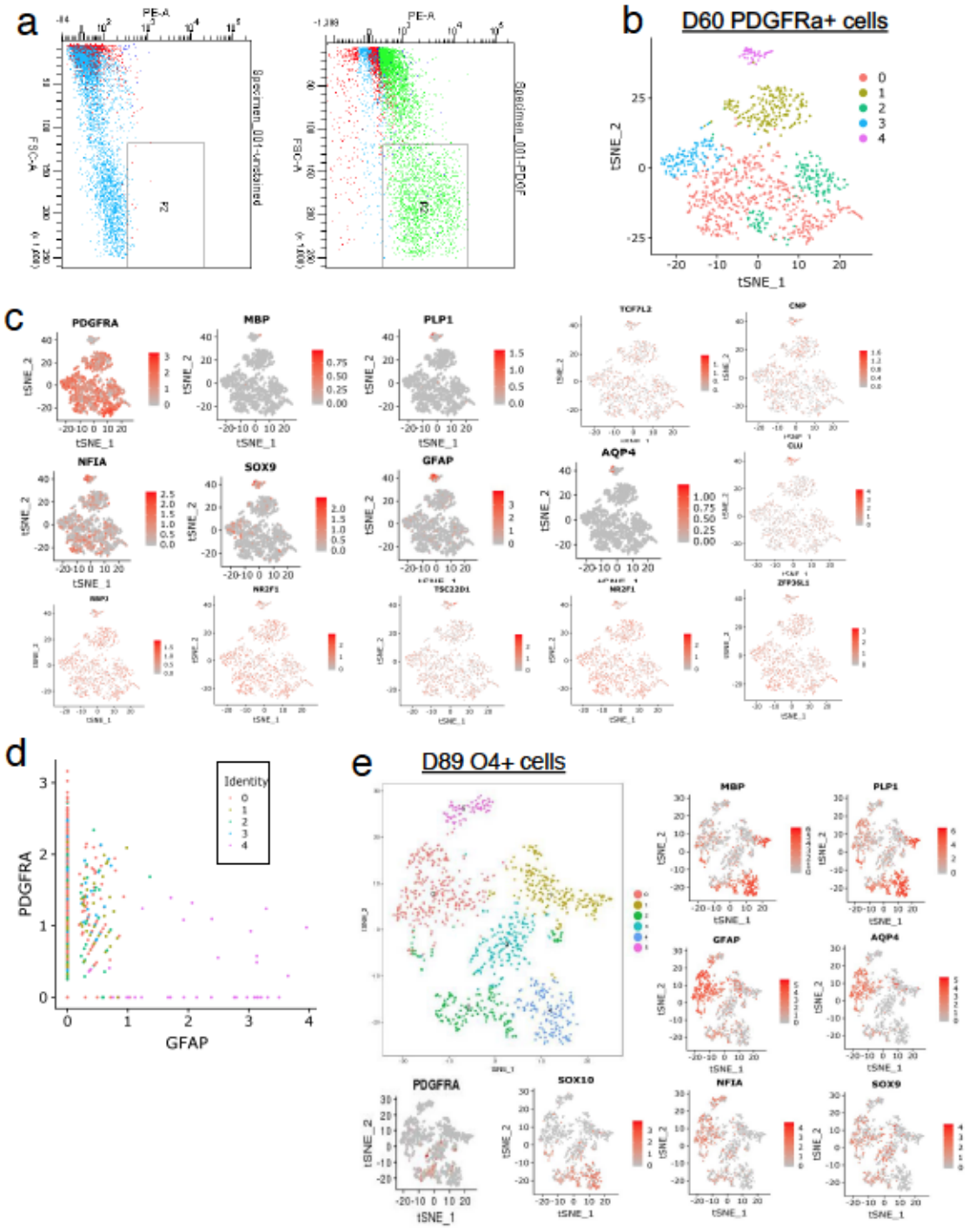
a
b
D60 PDGFRa+ cells
c
d
e
D89 O4+ cells
PDGFRA
MBP
PLP1
NFIA
SOX9
GFAP
AQP4
SOX10
tSNE_1
tSNE_2
GFAP
PDGFRA
Identity

Supplementary Figure 3: Species-specific similarity and differences between genes enriched in our hESC-derived populations vs primary mouse cells. A-D) Venn diagram depicting the overlap of genes enriched in human vs mouse **A)** OLLCs **B)** ALCs **C)** OPCs, and **D)** Endothelial/pericytes, with examples of overlapping and different genes. **E)** Heatmap of pri-microRNAs captured by scRNAseq analysis. miR219 is enriched in OL clusters, miR99AHG and miR100HG are enriched in astrocyte clusters.

Figure 41

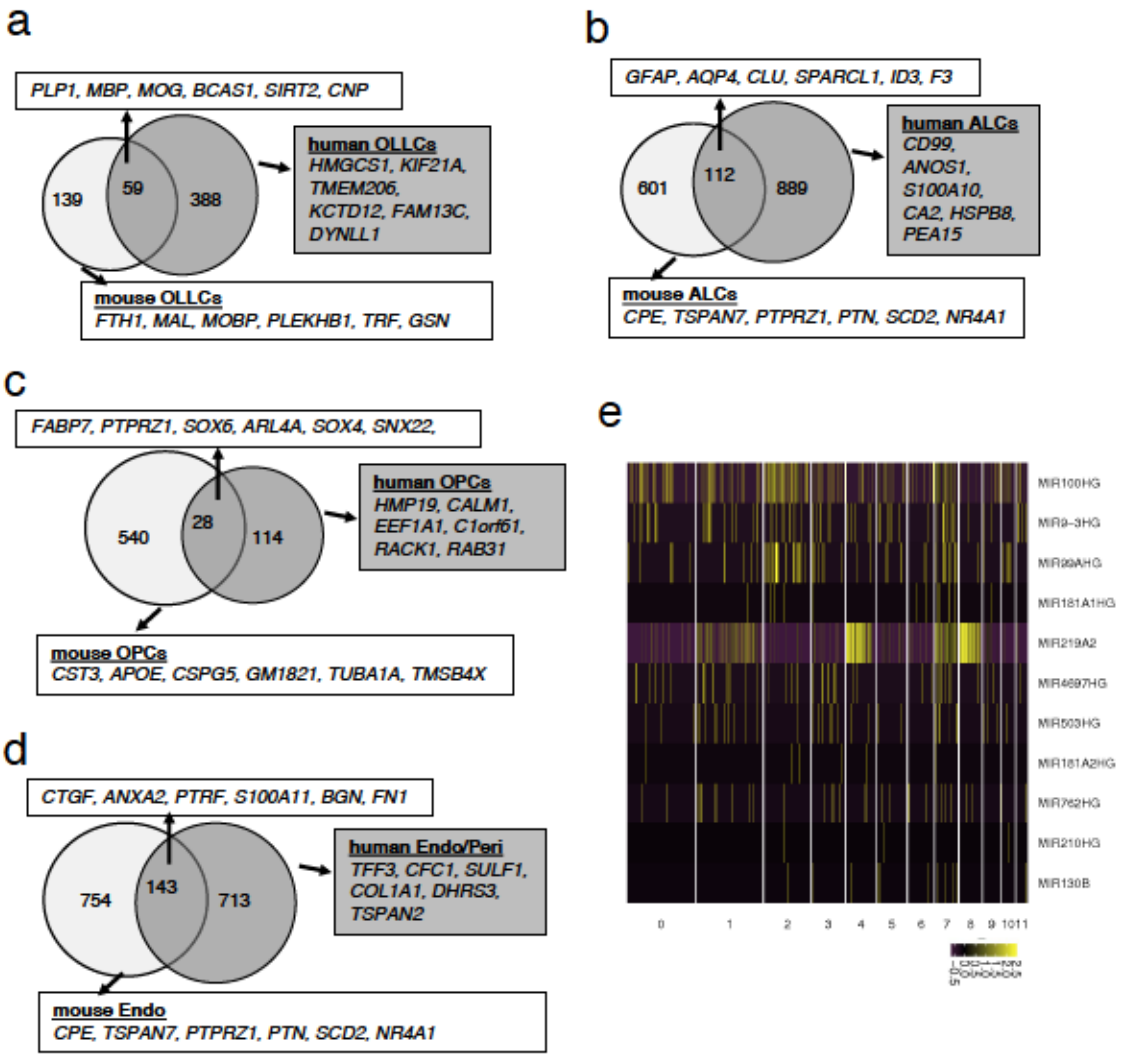

Supplementary Figure 4: Monocole-2 analysis of the PDTT reporter cells purified with Thy1.2 or O4+ microbeads. **A**) Within the trajectories derived from the PDTT OPCs purified with Thy1.2 microbeads, OLLC markers (OLIG2 and NKX2-2) show higher expression in Path I and II, but not in Path III or the smaller branches that emerge along Path II. **B)** Scatterplot showing the average gene expression of the cells in astrocyte vs oligodendrocyte states. Each dot represents a gene and axes are average number of transcripts per cell. Cells from the small branches (state 5 and 7) have higher correlation with astrocytes (state 2 cells) than oligodendrocytes (state 6 cells). Inset shows cells at different states. **C)** Overlay of cells from each cluster from figure 4a onto the pseudo-temporal trajectory showing where in the trajectory the cells from each cluster are located. Cells from cluster 0, 1, and 3 make up the majority of Path I population. Cells from astrocyte cluster (cluster 2) make up the majority of population on Path III (state 2 cells) and the sub-branches within Path II (state 5 and 7 cells). Cells from cluster 4 and 8 are located at the end of Path II (state 6 cells). Cells from cluster 10 are located at the end of Path III or state 2 cells. **D)** Developmental trajectories of the O4 microbead enriched day 89 reporter OPCs, generated using Monocole-2. Developmentally younger cells (A) represent OPCs and fall on shorter branch. OPCs have two prominent developmental paths B and C. **E)** Expression of OL and astrocyte markers within the trajectory show enrichment of astrocyte makers (GFAP, AQP4) on Path B and OLLC markers (MBP, PLP1) on Path C. **F)** Pseudotemporal expression pattern of OL and astrocyte genes showing kinetic trend of the OL, (MBP and PLP1) and astrocyte (GFAP and AQP4) marker genes.

Figure 42

Fig. S8

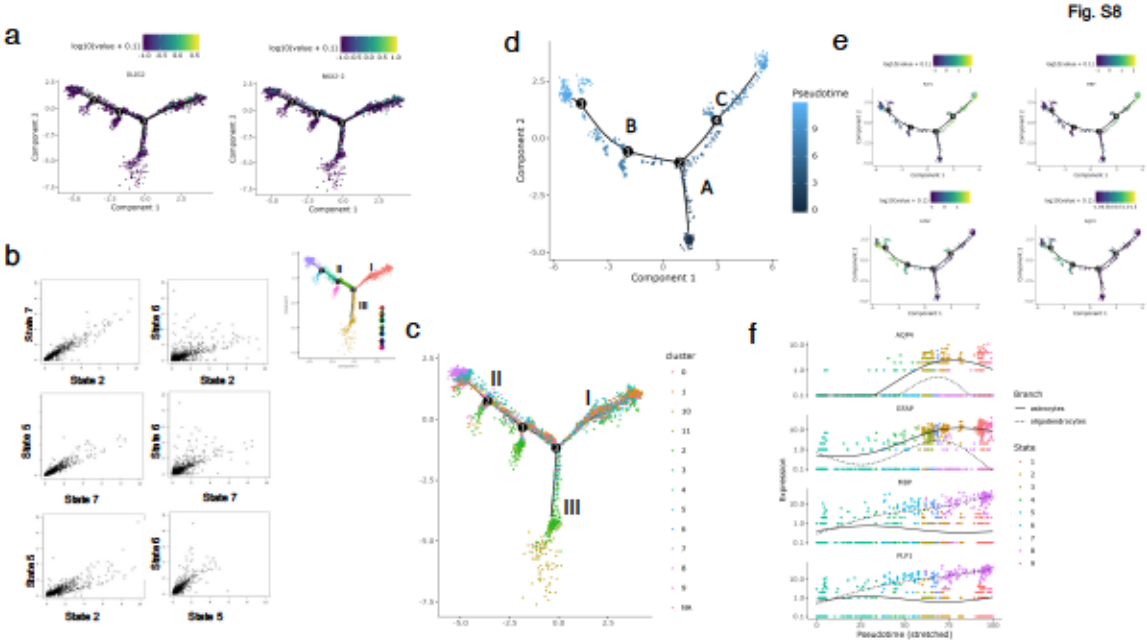
a
b
c
d
e
f
Pseudotime
Component 1
Component 2
State 2
State 5
State 6
State 7
I
II
III
A
B
C
Branch
State
Pseudotime (stretched)

Supplementary Figure 5: Heatmap of the most differentially expressed genes between different sub-branches of the monocole-2-based trajectories. A-B) Differential heatmap capturing the most differentially expressed genes **(A)** and transcription factors **(B)** between Paths II (oligodendrocytes) and III (astrocytes) identified by BEAM and clustered according to their expression pattern. Analysis of differential expression at node 2 represents genes from sub-branch A vs C **(B)**, and node 1 represents sub-branch B vs D **(A)**. See inset on the bottom right for labelling of nodes and sub-branches. **C)** Cells in each path of the trajectory are labelled by day at which they were purified (day 77, 89, or 104). Although some enrichment of day 104 cells is seen in the mature clusters, each path consists of cells from all three ages.

Figure 43

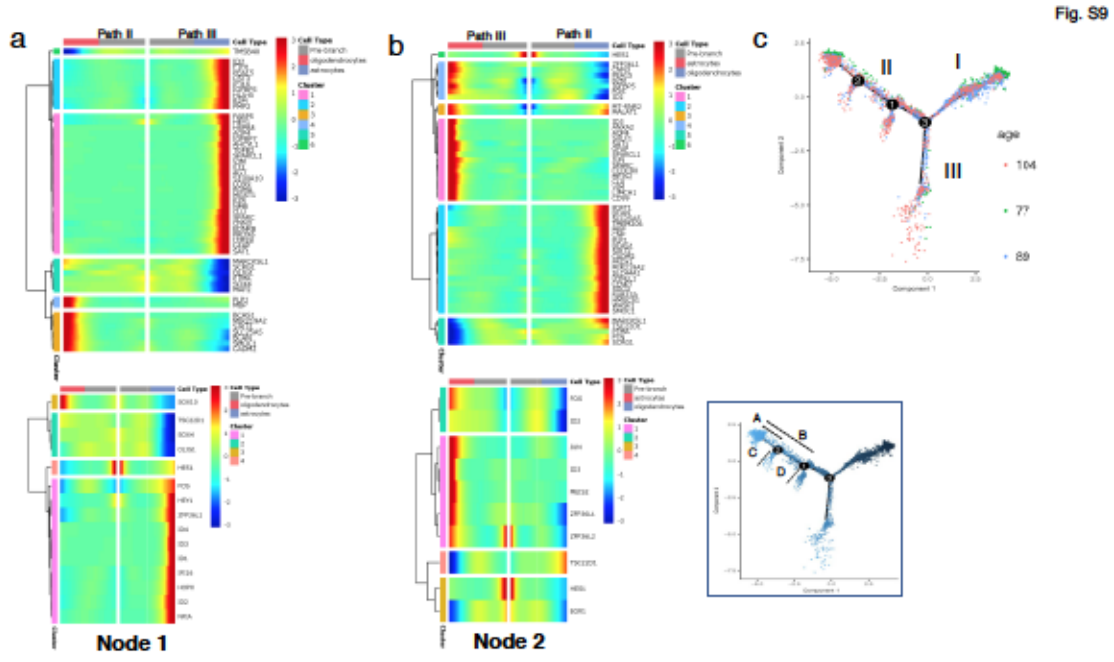

Chapter 5: Conclusions and Future Directions

Collectively, the work described in this thesis utilized human stem cell systems to gain insights into multiple facets of human retinal health and disease. While mouse models have provided many important insights, there are distinct difference between human and murine biology that necessitate human models. Utilizing human models of development and disease allows for identification of similarities with mouse models and features unique to human models. In the case of NRL loss, we identified many of the same transcriptional changes in murine and human photoreceptors, specifically decreased expression of *RHO, GNAT1, NR2E3, ROM1, RCVRN, GNB1* and *CNGA1* (17, 18). However, murine Nrl null photoreceptors still exhibit Sag expression, while SAG expression is absent in human NRL null photoreceptors. Additionally, human NRL null photoreceptors form 2 distinct S-opsin expressing populations which may explain the ESCS phenotype of enhanced cone function combined with some degree of retinal degeneration (12). These 2 *OPN1SW+* populations have not been identified in Nrl null mice, however this may stem from lack of single cell transcriptomic studies of Nrl null mice. Further studies of Nrl null photoreceptor at the single cell level would be helpful to identify if these populations also exist in mice. In addition to photoreceptor development, modeling photoreceptor degeneration can also provide important insights. In the case of LCA, mouse models of Crb1 and Rpgrip1 loss highlight both similarities and differences to the human models described here. In the case of Crb1 mice, retinas exhibited outer limiting membrane aberrations and rosette formation, but do not recapitulate the human phenotype of a thickened ONL (92, 101). The retinal organoid model of CRB1 loss, however, did recapitulate the *in vivo* ONL thickening. Additionally, CRB1 KO organoids exhibited aberrant RHO+ expression, a phenotype not described in Crb1 KO mice. In the case of Rpgrip1 KO mice, RPGRIP1 KO organoids recapitulate a similar phenotype of abnormal outer segment morphology, with human RPGRIP1 KO photoreceptors

completely lacking outer segment discs (102, 103). Of the human models described here, OPC development is possibly the most significantly different from murine OPCs, with human OPC lineage cells being bipotential in temrs of their ability to develop into astrocytes or oligodendrocytes. As such, human models of OPC development can identify gene expression changes important for skewing development toward oligodendrocytes and MBP expression. Identification and small molecule manipulation of oligodendrocyte development and myelin production could help promote re-myelination of neurons *in vivo*.

While identifying similarities and differences with mouse models highlights the importance of characterizing human models, arguably more significant insights from human models stem from the possibility of identifying avenues for therapeutic intervention in disease. For ESCS, targeting the cod photoreceptor population could help alleviate the phenotype. Because cods in human retinal organoids seem to result from a lack of the rod or cone gene expression programs and reintroduction of NRL led to expression of RHO, gene therapy to reintroduce NRL could potentially restore some rod function. On the other hand, LCA has extensive genetic heterogeneity that could benefit from a strategy targeting degenerative pathways as opposed to a specific gene. This study identified DDIT3 induction and ER stress as a common degenerative pathway in LCA photoreceptors. Studies of other human models of LCA or retinitis pigmentosa could reveal the extent of ER stress involvement across genetically different causes of photoreceptor cell death. Therapeutically targeting ER stress could help alleviate or slow photoreceptor degeneration, thus preserving some visual function for retinal degeneration patients.

Despite the insights into photoreceptor development and degeneration from this study, critical questions remain to be answered. In the case of photoreceptor development and the putative role of MEF2C, further studies are required to ascertain

the role of MEF2C in cone development and maturation. Specifically, knockdown studies of MEF2C are required to determine if its loss alters the distribution of rods and cones or if cones do not properly mature in its absence. Additionally, in the case of cods, it is important to determine if induction of MEF2C expression could lead cods to look more akin to the "normal" S cone population. For LCA and the utility of targeting ER stress to alleviate degeneration, it is critical to analyze other photoreceptor degenerations for ER stress involvement. While this study found a common pathway in two LCA models, over 20 genes are known to cause LCA and many more cause retinitis pigmentosa (RetNet). As such, more widespread generation and characterization of human models of photoreceptor degeneration are necessary. Finally, the link between CRB1 and RPGRIP1 loss and ER stress warrants further elucidation. While ER stress often results from accumulation of misfolded proteins, the mutant CRB1 and RPGRIP1 proteins in the described models would be expected to be degraded (98). ER stress can also result from perturbation of various other cell functions, and in this system, improper protein trafficking seems a likely cause of DDIT3 induction. Because photoreceptor function depends on trafficking opsins and various other phototransduction proteins to the outer segments, it is possible that loss of CRB1 or RPGRIP1 impair this function and lead to ER stress. Further studies of ER dynamics in these degeneration models and others can reveal important insights into how to combat ER stress and photoreceptor death in treating various forms of retinal degeneration.

References

1. Noback CRS, N.L. & Demarest, R.J. & Ruggiero, D.A. The human nervous system: Structure and function. 6 ed2005.
2. Rodieck RW. The first steps in seeing: Sinauer Associates; 1998.
3. Demb JB, Singer JH. Functional Circuitry of the Retina. Annu Rev Vis Sci. 2015;1:263-89.
4. Rivolta C, Sharon D, DeAngelis MM, Dryja TP. Retinitis pigmentosa and allied diseases: numerous diseases, genes, and inheritance patterns. Human Molecular Genetics. 2002;11(10):1219-27.
5. Koenekoop RK. An overview of Leber congenital amaurosis: a model to understand human retinal development. Surv Ophthalmol. 2004;49(4):379-98.
6. Zagozewski JL, Zhang Q, Pinto VI, Wigle JT, Eisenstat DD. The role of homeobox genes in retinal development and disease. Dev Biol. 2014;393(2):195-208.
7. Freund C, Horsford DJ, McInnes RR. Transcription factor genes and the developing eye: a genetic perspective. Human Molecular Genetics. 1996;5:1471-88.
8. Mansergh FC, Carrigan M, Hokamp K, Farrar GJ. Gene expression changes during retinal development and rod specification. Molecular Vision. 2015;21:61-87.
9. Chacon-Camacho OF, Zenteno JC. Review and update on the molecular basis of Leber congenital amaurosis. World J Clin Cases. 2015;3(2):112-24.
10. Cremers FP, van den Hurk JA, den Hollander AI. Molecular genetics of Leber congenital amaurosis. Hum Mol Genet. 2002;11(10):1169-76.
11. Littink KW, Stappers PTY, Riemslag FCC, Talsma HE, van Genderen MM, Cremers FPM, et al. Autosomal Recessive NRL Mutations in Patients with Enhanced S-Cone Syndrome. Genes (Basel). 2018;9(2).
12. Nishiguchi KM, Friedman JS, Sandberg MA, Swaroop A, Berson EL, Dryja TP. Recessive NRL mutations in patients with clumped pigmentary retinal degeneration and relative preservation of blue cone function. Proc Natl Acad Sci U S A. 2004;101(51):17819-24.
13. Cheng H, Khanna H, Oh EC, Hicks D, Mitton KP, Swaroop A. Photoreceptor-specific nuclear receptor NR2E3 functions as a transcriptional activator in rod photoreceptors. Hum Mol Genet. 2004;13(15):1563-75.
14. Akimoto M, Cheng H, Zhu D, Brzezinski JA, Khanna R, Filippova E, et al. Targeting of GFP to newborn rods by Nrl promoter and temporal expression profiling of flow-sorted photoreceptors. Proc Natl Acad Sci U S A. 2006;103(10):3890-5.
15. Daniele LL, Lillo C, Lyubarsky AL, Nikonov SS, Philp N, Mears AJ, et al. Cone-like morphological, molecular, and electrophysiological features of the photoreceptors of the Nrl knockout mouse. Invest Ophthalmol Vis Sci. 2005;46(6):2156-67.
16. Kim JW, Yang HJ, Brooks MJ, Zelinger L, Karakulah G, Gotoh N, et al. NRL-Regulated Transcriptome Dynamics of Developing Rod Photoreceptors. Cell Rep. 2016;17(9):2460-73.
17. Mears AJ, Kondo M, Swain PK, Takada Y, Bush RA, Saunders TL, et al. Nrl is required for rod photoreceptor development. Nat Genet. 2001;29(4):447-52.

18. Yoshida S, Mears AJ, Friedman JS, Carter T, He S, Oh E, et al. Expression profiling of the developing and mature Nrl-/- mouse retina: identification of retinal disease candidates and transcriptional regulatory targets of Nrl. Hum Mol Genet. 2004;13(14):1487-503.
19. Fan J, Rohrer B, Frederick JM, Baehr W, Crouch RK. Rpe65-/- and Lrat-/- mice: comparable models of leber congenital amaurosis. Invest Ophthalmol Vis Sci. 2008;49(6):2384-9.
20. Greenwald SH, Charette JR, Staniszewska M, Shi LY, Brown SDM, Stone L, et al. Mouse Models of NMNAT1-Leber Congenital Amaurosis (LCA9) Recapitulate Key Features of the Human Disease. Am J Pathol. 2016;186(7):1925-38.
21. Lakowski J, Baron M, Bainbridge J, Barber AC, Pearson RA, Ali RR, et al. Cone and rod photoreceptor transplantation in models of the childhood retinopathy Leber congenital amaurosis using flow-sorted Crx-positive donor cells. Hum Mol Genet. 2010;19(23):4545-59.
22. Lukovic D, Artero Castro A, Kaya KD, Munezero D, Gieser L, Davo-Martinez C, et al. Retinal Organoids derived from hiPSCs of an AIPL1-LCA Patient Maintain Cytoarchitecture despite Reduced levels of Mutant AIPL1. Sci Rep. 2020;10(1):5426.
23. Parfitt DA, Lane A, Ramsden CM, Carr AJ, Munro PM, Jovanovic K, et al. Identification and Correction of Mechanisms Underlying Inherited Blindness in Human iPSC-Derived Optic Cups. Cell Stem Cell. 2016;18(6):769-81.
24. Pawlyk BS, Bulgakov OV, Liu X, Xu X, Adamian M, Sun X, et al. Replacement gene therapy with a human RPGRIP1 sequence slows photoreceptor degeneration in a murine model of Leber congenital amaurosis. Hum Gene Ther. 2010;21(8):993-1004.
25. Ramamurthy V, Niemi GA, Reh TA, Hurley JB. Leber congenital amaurosis linked to AIPL1: a mouse model reveals destabilization of cGMP phosphodiesterase. Proc Natl Acad Sci U S A. 2004;101(38):13897-902.
26. Seeliger MW, Grimm C, Stahlberg F, Friedburg C, Jaissle G, Zrenner E, et al. New views on RPE65 deficiency: the rod system is the source of vision in a mouse model of Leber congenital amaurosis. Nat Genet. 2001;29(1):70-4.
27. Maguire AM, Russell S, Wellman JA, Chung DC, Yu Z-F, Tillman A, et al. Efficacy, Safety, and Durability of Voretigene Neparvovec-rzyl in RPE65 Mutation–Associated Inherited Retinal Dystrophy. Ophthalmology. 2019;126(9):1273-85.
28. Almasieh M, Wilson AM, Morquette B, Cueva Vargas JL, Di Polo A. The molecular basis of retinal ganglion cell death in glaucoma. Prog Retin Eye Res. 2012;31(2):152-81.
29. Carelli V, La Morgia C, Valentino ML, Barboni P, Ross-Cisneros FN, Sadun AA. Retinal ganglion cell neurodegeneration in mitochondrial inherited disorders. Biochim Biophys Acta. 2009;1787(5):518-28.
30. Shindler KS, Ventura E, Dutt M, Rostami A. Inflammatory demyelination induces axonal injury and retinal ganglion cell apoptosis in experimental optic neuritis. Exp Eye Res. 2008;87(3):208-13.
31. Bradl M, Lassmann H. Oligodendrocytes: biology and pathology. Acta Neuropathol. 2010;119(1):37-53.

32. Britze J, Pihl-Jensen G, Frederiksen JL. Retinal ganglion cell analysis in multiple sclerosis and optic neuritis: a systematic review and meta-analysis. J Neurol. 2017;264(9):1837-53.
33. Marques S, Zeisel A, Codeluppi S, van Bruggen D, Mendanha Falcao A, Xiao L, et al. Oligodendrocyte heterogeneity in the mouse juvenile and adult central nervous system. Science. 2016;352(6291):1326-9.
34. Sim FJ, Windrem MS, Goldman SA. Fate determination of adult human glial progenitor cells. Neuron Glia Biol. 2009;5(3-4):45-55.
35. Wang J, Pol SU, Haberman AK, Wang C, O'Bara MA, Sim FJ. Transcription factor induction of human oligodendrocyte progenitor fate and differentiation. Proc Natl Acad Sci U S A. 2014;111(28):E2885-94.
36. Capowski EE, Samimi K, Mayerl SJ, Phillips MJ, Pinilla I, Howden SE, et al. Reproducibility and staging of 3D human retinal organoids across multiple pluripotent stem cell lines. Development. 2019;146(1).
37. Collin J, Queen R, Zerti D, Dorgau B, Hussain R, Coxhead J, et al. Deconstructing Retinal Organoids: Single Cell RNA-Seq Reveals the Cellular Components of Human Pluripotent Stem Cell-Derived Retina. Stem Cells. 2019;37(5):593-8.
38. Deng WL, Gao ML, Lei XL, Lv JN, Zhao H, He KW, et al. Gene Correction Reverses Ciliopathy and Photoreceptor Loss in iPSC-Derived Retinal Organoids from Retinitis Pigmentosa Patients. Stem Cell Reports. 2018;10(4):1267-81.
39. Eiraku M, Sasai Y. Self-formation of layered neural structures in three-dimensional culture of ES cells. Curr Opin Neurobiol. 2012;22(5):768-77.
40. Eldred KC, Hadyniak SE, Hussey KA, Brenerman B, Zhang PW, Chamling X, et al. Thyroid hormone signaling specifies cone subtypes in human retinal organoids. Science. 2018;362(6411).
41. Fligor CM, Langer KB, Sridhar A, Ren Y, Shields PK, Edler MC, et al. Three-Dimensional Retinal Organoids Facilitate the Investigation of Retinal Ganglion Cell Development, Organization and Neurite Outgrowth from Human Pluripotent Stem Cells. Sci Rep. 2018;8(1):14520.
42. Gonzalez-Cordero A, Kruczek K, Naeem A, Fernando M, Kloc M, Ribeiro J, et al. Recapitulation of Human Retinal Development from Human Pluripotent Stem Cells Generates Transplantable Populations of Cone Photoreceptors. Stem Cell Reports. 2017;9(3):820-37.
43. Hallam D, Hilgen G, Dorgau B, Zhu L, Yu M, Bojic S, et al. Human-Induced Pluripotent Stem Cells Generate Light Responsive Retinal Organoids with Variable and Nutrient-Dependent Efficiency. Stem Cells. 2018;36(10):1535-51.
44. Kim S, Lowe A, Dharmat R, Lee S, Owen LA, Wang J, et al. Generation, transcriptome profiling, and functional validation of cone-rich human retinal organoids. Proc Natl Acad Sci U S A. 2019;116(22):10824-33.
45. Nakano T, Ando S, Takata N, Kawada M, Muguruma K, Sekiguchi K, et al. Self-formation of optic cups and storable stratified neural retina from human ESCs. Cell Stem Cell. 2012;10(6):771-85.

46. Phillips MJ, Jiang P, Howden S, Barney P, Min J, York NW, et al. A Novel Approach to Single Cell RNA-Sequence Analysis Facilitates In Silico Gene Reporting of Human Pluripotent Stem Cell-Derived Retinal Cell Types. Stem Cells. 2018;36(3):313-24.
47. Quinn PM, Buck TM, Mulder AA, Ohonin C, Alves CH, Vos RM, et al. Human iPSC-Derived Retinas Recapitulate the Fetal CRB1 CRB2 Complex Formation and Demonstrate that Photoreceptors and Muller Glia Are Targets of AAV5. Stem Cell Reports. 2019;12(5):906-19.
48. Volkner M, Zschatzsch M, Rostovskaya M, Overall RW, Busskamp V, Anastassiadis K, et al. Retinal Organoids from Pluripotent Stem Cells Efficiently Recapitulate Retinogenesis. Stem Cell Reports. 2016;6(4):525-38.
49. Wahlin KJ, Maruotti JA, Sripathi SR, Ball J, Angueyra JM, Kim C, et al. Photoreceptor Outer Segment-like Structures in Long-Term 3D Retinas from Human Pluripotent Stem Cells. Scientific Reports. 2017;7(1).
50. Welby E, Lakowski J, Di Foggia V, Budinger D, Gonzalez-Cordero A, Lun ATL, et al. Isolation and Comparative Transcriptome Analysis of Human Fetal and iPSC-Derived Cone Photoreceptor Cells. Stem Cell Reports. 2017;9(6):1898-915.
51. Zhong X, Gutierrez C, Xue T, Hampton C, Vergara MN, Cao LH, et al. Generation of three-dimensional retinal tissue with functional photoreceptors from human iPSCs. Nat Commun. 2014;5:4047.
52. Sim FJ, McClain CR, Schanz SJ, Protack TL, Windrem MS, Goldman SA. CD140a identifies a population of highly myelinogenic, migration-competent and efficiently engrafting human oligodendrocyte progenitor cells. Nat Biotechnol. 2011;29(10):934-41.
53. van Bruggen D, Agirre E, Castelo-Branco G. Single-cell transcriptomic analysis of oligodendrocyte lineage cells. Curr Opin Neurobiol. 2017;47:168-75.
54. Clark BS, Stein-O'Brien GL, Shiau F, Cannon GH, Davis-Marcisak E, Sherman T, et al. Single-Cell RNA-Seq Analysis of Retinal Development Identifies NFI Factors as Regulating Mitotic Exit and Late-Born Cell Specification. Neuron. 2019;102(6):1111-26 e5.
55. Hu Y, Wang X, Hu B, Mao Y, Chen Y, Yan L, et al. Dissecting the transcriptome landscape of the human fetal neural retina and retinal pigment epithelium by single-cell RNA-seq analysis. PLoS Biol. 2019;17(7):e3000365.
56. Lukowski SW, Lo CY, Sharov AA, Nguyen Q, Fang L, Hung SS, et al. A single-cell transcriptome atlas of the adult human retina. EMBO J. 2019;38(18):e100811.
57. Macosko EZ, Basu A, Satija R, Nemesh J, Shekhar K, Goldman M, et al. Highly Parallel Genome-wide Expression Profiling of Individual Cells Using Nanoliter Droplets. Cell. 2015;161(5):1202-14.
58. Peng YR, Shekhar K, Yan W, Herrmann D, Sappington A, Bryman GS, et al. Molecular Classification and Comparative Taxonomics of Foveal and Peripheral Cells in Primate Retina. Cell. 2019;176(5):1222-37 e22.
59. Shekhar K, Lapan SW, Whitney IE, Tran NM, Macosko EZ, Kowalczyk M, et al. Comprehensive Classification of Retinal Bipolar Neurons by Single-Cell Transcriptomics. Cell. 2016;166(5):1308-23 e30.

60. Voigt AP, Whitmore SS, Flamme-Wiese MJ, Riker MJ, Wiley LA, Tucker BA, et al. Molecular characterization of foveal versus peripheral human retina by single-cell RNA sequencing. Exp Eye Res. 2019;184:234-42.
61. Swaroop A, Kim D, Forrest D. Transcriptional regulation of photoreceptor development and homeostasis in the mammalian retina. Nat Rev Neurosci. 2010;11(8):563-76.
62. Bessant DAR, Holder GE, Fitzke FW, Payne AM, Bhattacharya SS, Bird AC. Phenotype of Retinitis Pigmentosa Associated With the Ser50Thr Mutation in the NRL Gene. Archives of Ophthalmology. 2003;121(6):793-802.
63. Meyer JS, Shearer RL, Capowski EE, Wright LS, Wallace KA, McMillan EL, et al. Modeling early retinal development with human embryonic and induced pluripotent stem cells. Proc Natl Acad Sci U S A. 2009;106(39):16698-703.
64. Meyer JS, Howden SE, Wallace KA, Verhoeven AD, Wright LS, Capowski EE, et al. Optic Vesicle-like Structures Derived from Human Pluripotent Stem Cells Facilitate a Customized Approach to Retinal Disease Treatment. Stem Cells. 2011;29(8):1206-18.
65. Phillips MJ, Wallace KA, Dickerson SJ, Miller MJ, Verhoeven AD, Martin JM, et al. Blood-derived human iPS cells generate optic vesicle-like structures with the capacity to form retinal laminae and develop synapses. Invest Ophthalmol Vis Sci. 2012;53(4):2007-19.
66. Phillips MJ, Capowski EE, Petersen A, Jansen AD, Barlow K, Edwards KL, et al. Generation of a rod-specific NRL reporter line in human pluripotent stem cells. Sci Rep. 2018;8(1):2370.
67. Reichman S, Terray A, Slembrouck A, Nanteau C, Orieux G, Habeler W, et al. From confluent human iPS cells to self-forming neural retina and retinal pigmented epithelium. Proc Natl Acad Sci U S A. 2014;111(23):8518-23.
68. Kuwahara A, Ozone C, Nakano T, Saito K, Eiraku M, Sasai Y. Generation of a ciliary margin-like stem cell niche from self-organizing human retinal tissue. Nat Commun. 2015;6:6286.
69. Mellough CB, Collin J, Khazim M, White K, Sernagor E, Steel DH, et al. IGF-1 Signaling Plays an Important Role in the Formation of Three-Dimensional Laminated Neural Retina and Other Ocular Structures From Human Embryonic Stem Cells. Stem Cells. 2015;33(8):2416-30.
70. Wiley LA, Burnight ER, DeLuca AP, Anfinson KR, Cranston CM, Kaalberg EE, et al. cGMP production of patient-specific iPSCs and photoreceptor precursor cells to treat retinal degenerative blindness. Sci Rep. 2016;6:30742.
71. Karunakaran DK, Al Seesi S, Banday AR, Baumgartner M, Olthof A, Lemoine C, et al. Network-based bioinformatics analysis of spatio-temporal RNA-Seq data reveals transcriptional programs underpinning normal and aberrant retinal development. BMC Genomics. 2016;17 Suppl 5:495.
72. Zelinger L, Karakulah G, Chaitankar V, Kim JW, Yang HJ, Brooks MJ, et al. Regulation of Noncoding Transcriptome in Developing Photoreceptors by Rod Differentiation Factor NRL. Invest Ophthalmol Vis Sci. 2017;58(11):4422-35.
73. Consugar MB, Navarro-Gomez D, Place EM, Bujakowska KM, Sousa ME, Fonseca-Kelly ZD, et al. Panel-based genetic diagnostic testing for inherited eye diseases is highly

accurate and reproducible, and more sensitive for variant detection, than exome sequencing. Genet Med. 2015;17(4):253-61.
74. Capowski EE, Schneider BL, Ebert AD, Seehus CR, Szulc J, Zufferey R, et al. Lentiviral vector-mediated genetic modification of human neural progenitor cells for *ex vivo* gene therapy. Journal of Neuroscience Methods. 2007;163(2):338-49.
75. Zufferey R, Nagy D, Mandel RJ, Naldini L, Trono D. Multiply attenuated lentiviral vector achieves efficient gene delivery in vivo. Nature Biotechnology. 1997;15:871-5.
76. Butler A, Hoffman P, Smibert P, Papalexi E, Satija R. Integrating single-cell transcriptomic data across different conditions, technologies, and species. Nat Biotechnol. 2018;36(5):411-20.
77. Qiu X, Mao Q, Tang Y, Wang L, Chawla R, Pliner HA, et al. Reversed graph embedding resolves complex single-cell trajectories. Nat Methods. 2017;14(10):979-82.
78. Wang J, Zibetti C, Shang P, Sripathi SR, Zhang P, Cano M, et al. ATAC-Seq analysis reveals a widespread decrease of chromatin accessibility in age-related macular degeneration. Nat Commun. 2018;9(1):1364.
79. Strettoi E, Mears AJ, Swaroop A. Recruitment of the rod pathway by cones in the absence of rods. J Neurosci. 2004;24(34):7576-82.
80. Stuck MW, Conley SM, Naash MI. Defects in the outer limiting membrane are associated with rosette development in the Nrl-/- retina. PLoS One. 2012;7(3):e32484.
81. Smiley S, Nickerson PE, Comanita L, Daftarian N, El-Sehemy A, Tsai EL, et al. Establishment of a cone photoreceptor transplantation platform based on a novel cone-GFP reporter mouse line. Sci Rep. 2016;6:22867.
82. Mi H, Muruganujan A, Huang X, Ebert D, Mills C, Guo X, et al. Protocol Update for large-scale genome and gene function analysis with the PANTHER classification system (v.14.0). Nat Protoc. 2019;14(3):703-21.
83. Hao H, Tummala P, Guzman E, Mali RS, Gregorski J, Swaroop A, et al. The transcription factor neural retina leucine zipper (NRL) controls photoreceptor-specific expression of myocyte enhancer factor Mef2c from an alternative promoter. J Biol Chem. 2011;286(40):34893-902.
84. Hoshino A, Ratnapriya R, Brooks MJ, Chaitankar V, Wilken MS, Zhang C, et al. Molecular Anatomy of the Developing Human Retina. Dev Cell. 2017;43(6):763-79 e4.
85. Veleri S, Lazar CH, Chang B, Sieving PA, Banin E, Swaroop A. Biology and therapy of inherited retinal degenerative disease: insights from mouse models. Dis Model Mech. 2015;8(2):109-29.
86. Kallman A, Capowski EE, Wang J, Kaushik AM, Jansen AD, Edwards KL, et al. Investigating cone photoreceptor development using patient-derived NRL null retinal organoids. Commun Biol. 2020;3(1):82.
87. Lotery AJ, Jacobson SG, Fishman GA, Weleber RG, Fulton AB, Namperumalsamy P, et al. Mutations in the CRB1 gene cause Leber congenital amaurosis. Arch Ophthalmol. 2001;119(3):415-20.
88. Dryja TP, Adams SM, Grimsby JL, McGee TL, Hong DH, Li T, et al. Null RPGRIP1 alleles in patients with Leber congenital amaurosis. Am J Hum Genet. 2001;68(5):1295-8.

89. Stuart T, Butler A, Hoffman P, Hafemeister C, Papalexi E, Mauck WM, 3rd, et al. Comprehensive Integration of Single-Cell Data. Cell. 2019;177(7):1888-902 e21.
90. Cao J, Spielmann M, Qiu X, Huang X, Ibrahim DM, Hill AJ, et al. The single-cell transcriptional landscape of mammalian organogenesis. Nature. 2019;566(7745):496-502.
91. den Hollander AI, Roepman R, Koenekoop RK, Cremers FP. Leber congenital amaurosis: genes, proteins and disease mechanisms. Prog Retin Eye Res. 2008;27(4):391-419.
92. Alves CH, Pellissier LP, Wijnholds J. The CRB1 and adherens junction complex proteins in retinal development and maintenance. Prog Retin Eye Res. 2014;40:35-52.
93. Li T. Leber congenital amaurosis caused by mutations in RPGRIP1. Cold Spring Harb Perspect Med. 2014;5(4).
94. Bringmann A, Pannicke T, Grosche J, Francke M, Wiedemann P, Skatchkov SN, et al. Muller cells in the healthy and diseased retina. Prog Retin Eye Res. 2006;25(4):397-424.
95. Mitter SK, Rao HV, Qi X, Cai J, Sugrue A, Dunn WA, et al., editors. Autophagy in the Retina: A Potential Role in Age-Related Macular Degeneration2012; Boston, MA: Springer US.
96. Athanasiou D, Aguila M, Bevilacqua D, Novoselov SS, Parfitt DA, Cheetham ME. The cell stress machinery and retinal degeneration. FEBS Lett. 2013;587(13):2008-17.
97. Metrailler S, Schorderet DF, Cottet S. Early apoptosis of rod photoreceptors in Rpe65(-/-) mice is associated with the upregulated expression of lysosomal-mediated autophagic genes. Exp Eye Res. 2012;96(1):70-81.
98. Schroder M. Endoplasmic reticulum stress responses. Cell Mol Life Sci. 2008;65(6):862-94.
99. Keestra-Gounder AM, Byndloss MX, Seyffert N, Young BM, Chavez-Arroyo A, Tsai AY, et al. NOD1 and NOD2 signalling links ER stress with inflammation. Nature. 2016;532(7599):394-7.
100. Sun KH, Chang KH, Clawson S, Ghosh S, Mirzaei H, Regnier F, et al. Glutathione-S-transferase P1 is a critical regulator of Cdk5 kinase activity. J Neurochem. 2011;118(5):902-14.
101. Mehalow AK, Kameya S, Smith RS, Hawes NL, Denegre JM, Young JA, et al. CRB1 is essential for external limiting membrane integrity and photoreceptor morphogenesis in the mammalian retina. Hum Mol Genet. 2003;12(17):2179-89.
102. Won J, Gifford E, Smith RS, Yi H, Ferreira PA, Hicks WL, et al. RPGRIP1 is essential for normal rod photoreceptor outer segment elaboration and morphogenesis. Hum Mol Genet. 2009;18(22):4329-39.
103. Zhao Y, Hong DH, Pawlyk B, Yue G, Adamian M, Grynberg M, et al. The retinitis pigmentosa GTPase regulator (RPGR)- interacting protein: subserving RPGR function and participating in disk morphogenesis. Proc Natl Acad Sci U S A. 2003;100(7):3965-70.
104. Koenekoop RK. RPGRIP1 is mutated in Leber congenital amaurosis: a mini-review. Ophthalmic Genet. 2005;26(4):175-9.

105. Sancho-Pelluz J, Arango-Gonzalez B, Kustermann S, Romero FJ, van Veen T, Zrenner E, et al. Photoreceptor cell death mechanisms in inherited retinal degeneration. Mol Neurobiol. 2008;38(3):253-69.
106. Chan P, Stolz J, Kohl S, Chiang WC, Lin JH. Endoplasmic reticulum stress in human photoreceptor diseases. Brain Res. 2016;1648(Pt B):538-41.
107. Griciuc A, Aron L, Ueffing M. ER stress in retinal degeneration: a target for rational therapy? Trends Mol Med. 2011;17(8):442-51.
108. Kroeger H, Messah C, Ahern K, Gee J, Joseph V, Matthes MT, et al. Induction of endoplasmic reticulum stress genes, BiP and chop, in genetic and environmental models of retinal degeneration. Invest Ophthalmol Vis Sci. 2012;53(12):7590-9.
109. Nakanishi T, Shimazawa M, Sugitani S, Kudo T, Imai S, Inokuchi Y, et al. Role of endoplasmic reticulum stress in light-induced photoreceptor degeneration in mice. J Neurochem. 2013;125(1):111-24.
110. Duricka DL, Brown RL, Varnum MD. Defective trafficking of cone photoreceptor CNG channels induces the unfolded protein response and ER-stress-associated cell death. Biochem J. 2012;441(2):685-96.
111. Thapa A, Morris L, Xu J, Ma H, Michalakis S, Biel M, et al. Endoplasmic reticulum stress-associated cone photoreceptor degeneration in cyclic nucleotide-gated channel deficiency. J Biol Chem. 2012;287(22):18018-29.
112. Zhang T, Zhang N, Baehr W, Fu Y. Cone opsin determines the time course of cone photoreceptor degeneration in Leber congenital amaurosis. Proc Natl Acad Sci U S A. 2011;108(21):8879-84.
113. Michalakis S, Geiger H, Haverkamp S, Hofmann F, Gerstner A, Biel M. Impaired opsin targeting and cone photoreceptor migration in the retina of mice lacking the cyclic nucleotide-gated channel CNGA3. Invest Ophthalmol Vis Sci. 2005;46(4):1516-24.
114. Ghosh R, Wang L, Wang ES, Perera BG, Igbaria A, Morita S, et al. Allosteric inhibition of the IRE1alpha RNase preserves cell viability and function during endoplasmic reticulum stress. Cell. 2014;158(3):534-48.
115. Baumann N, Pham-Dinh D. Biology of Oligodendrocyte and Myelin in the Mammalian Central Nervous System. Physiological Reviews. 2001;81(2).
116. Duncan ID, Radcliff AB. Inherited and acquired disorders of myelin: The underlying myelin pathology. Exp Neurol. 2016;283(Pt B):452-75.
117. de Faria O, Jr., Cui QL, Bin JM, Bull SJ, Kennedy TE, Bar-Or A, et al. Regulation of miRNA 219 and miRNA Clusters 338 and 17-92 in Oligodendrocytes. Front Genet. 2012;3:46.
118. Elbaz B, Popko B. Molecular Control of Oligodendrocyte Development. Trends Neurosci. 2019;42(4):263-77.
119. Zhang Y, Chen K, Sloan SA, Bennett ML, Scholze AR, O'Keeffe S, et al. An RNA-sequencing transcriptome and splicing database of glia, neurons, and vascular cells of the cerebral cortex. J Neurosci. 2014;34(36):11929-47.
120. Chanoumidou K, Mozafari S, Baron-Van Evercooren A, Kuhlmann T. Stem cell derived oligodendrocytes to study myelin diseases. Glia. 2020;68(4):705-20.

121. Douvaras P, Wang J, Zimmer M, Hanchuk S, O'Bara MA, Sadiq S, et al. Efficient generation of myelinating oligodendrocytes from primary progressive multiple sclerosis patients by induced pluripotent stem cells. Stem Cell Reports. 2014;3(2):250-9.
122. Goldman SA, Kuypers NJ. How to make an oligodendrocyte. Development. 2015;142(23):3983-95.
123. Marton RM, Miura Y, Sloan SA, Li Q, Revah O, Levy RJ, et al. Differentiation and maturation of oligodendrocytes in human three-dimensional neural cultures. Nat Neurosci. 2019;22(3):484-91.
124. Nistor GI, Totoiu MO, Haque N, Carpenter MK, Keirstead HS. Human embryonic stem cells differentiate into oligodendrocytes in high purity and myelinate after spinal cord transplantation. Glia. 2005;49(3):385-96.
125. Zheng GX, Terry JM, Belgrader P, Ryvkin P, Bent ZW, Wilson R, et al. Massively parallel digital transcriptional profiling of single cells. Nat Commun. 2017;8:14049.
126. Douvaras P, Fossati V. Generation and isolation of oligodendrocyte progenitor cells from human pluripotent stem cells. Nat Protoc. 2015;10(8):1143-54.
127. Jakel S, Agirre E, Mendanha Falcao A, van Bruggen D, Lee KW, Knuesel I, et al. Altered human oligodendrocyte heterogeneity in multiple sclerosis. Nature. 2019;566(7745):543-7.
128. Zhang Y, Sloan SA, Clarke LE, Caneda C, Plaza CA, Blumenthal PD, et al. Purification and Characterization of Progenitor and Mature Human Astrocytes Reveals Transcriptional and Functional Differences with Mouse. Neuron. 2016;89(1):37-53.
129. Klein AM, Mazutis L, Akartuna I, Tallapragada N, Veres A, Li V, et al. Droplet barcoding for single-cell transcriptomics applied to embryonic stem cells. Cell. 2015;161(5):1187-201.
130. Sloan SA, Darmanis S, Huber N, Khan TA, Birey F, Caneda C, et al. Human Astrocyte Maturation Captured in 3D Cerebral Cortical Spheroids Derived from Pluripotent Stem Cells. Neuron. 2017;95(4):779-90 e6.
131. Fujiwara K, Jindatip D, Kikuchi M, Yashiro T. In situ hybridization reveals that type I and III collagens are produced by pericytes in the anterior pituitary gland of rats. Cell Tissue Res. 2010;342(3):491-5.
132. Seet LF, Toh LZ, Chu SWL, Finger SN, Chua JLL, Wong TT. Upregulation of distinct collagen transcripts in post-surgery scar tissue: a study of conjunctival fibrosis. Dis Model Mech. 2017;10(6):751-60.
133. Marques S, van Bruggen D, Vanichkina DP, Floriddia EM, Munguba H, Varemo L, et al. Transcriptional Convergence of Oligodendrocyte Lineage Progenitors during Development. Dev Cell. 2018;46(4):504-17 e7.
134. Lee HK, Laug D, Zhu W, Patel JM, Ung K, Arenkiel BR, et al. Apcdd1 stimulates oligodendrocyte differentiation after white matter injury. Glia. 2015;63(10):1840-9.
135. Mathews ES, Mawdsley DJ, Walker M, Hines JH, Pozzoli M, Appel B. Mutation of 3-hydroxy-3-methylglutaryl CoA synthase I reveals requirements for isoprenoid and cholesterol synthesis in oligodendrocyte migration arrest, axon wrapping, and myelin gene expression. J Neurosci. 2014;34(9):3402-12.

136. Ellison JA, Vellis Jd. Platelet-Derived Growth Factor Receptor Is Expressed by Cells in the Early Oligodendrocyte Lineage. Journal of Neuroscience Research. 1994;37(1):116-28.
137. Ho AL, Vasudeva SD, Lae M, Saito T, Barbashina V, Antonescu CR, et al. PDGF receptor alpha is an alternative mediator of rapamycin-induced Akt activation: implications for combination targeted therapy of synovial sarcoma. Cancer Res. 2012;72(17):4515-25.
138. Muzumdar MD, Tasic B, Miyamichi K, Li L, Luo L. A global double-fluorescent Cre reporter mouse. Genesis. 2007;45(9):593-605.
139. Ehrlich M, Mozafari S, Glatza M, Starost L, Velychko S, Hallmann AL, et al. Rapid and efficient generation of oligodendrocytes from human induced pluripotent stem cells using transcription factors. Proc Natl Acad Sci U S A. 2017;114(11):E2243-E52.
140. Weng Q, Wang J, Wang J, He D, Cheng Z, Zhang F, et al. Single-Cell Transcriptomics Uncovers Glial Progenitor Diversity and Cell Fate Determinants during Development and Gliomagenesis. Cell Stem Cell. 2019;24(5):707-23 e8.
141. Zhao C, Deng Y, Liu L, Yu K, Zhang L, Wang H, et al. Dual regulatory switch through interactions of Tcf7l2/Tcf4 with stage-specific partners propels oligodendroglial maturation. Nat Commun. 2016;7:10883.
142. Galloway DA, Moore CS. miRNAs As Emerging Regulators of Oligodendrocyte Development and Differentiation. Front Cell Dev Biol. 2016;4:59.
143. Letzen BS, Liu C, Thakor NV, Gearhart JD, All AH, Kerr CL. MicroRNA expression profiling of oligodendrocyte differentiation from human embryonic stem cells. PLoS One. 2010;5(5):e10480.
144. Zhao X, He X, Han X, Yu Y, Ye F, Chen Y, et al. MicroRNA-mediated control of oligodendrocyte differentiation. Neuron. 2010;65(5):612-26.
145. Dugas JC, Cuellar TL, Scholze A, Ason B, Ibrahim A, Emery B, et al. Dicer1 and miR-219 Are required for normal oligodendrocyte differentiation and myelination. Neuron. 2010;65(5):597-611.
146. Dietz KC, Polanco JJ, Pol SU, Sim FJ. Targeting human oligodendrocyte progenitors for myelin repair. Exp Neurol. 2016;283(Pt B):489-500.
147. Craig A, Ling Luo N, Beardsley DJ, Wingate-Pearse N, Walker DW, Hohimer AR, et al. Quantitative analysis of perinatal rodent oligodendrocyte lineage progression and its correlation with human. Experimental Neurology. 2003;181(2):231-40.
148. Semple BD, Blomgren K, Gimlin K, Ferriero DM, Noble-Haeusslein LJ. Brain development in rodents and humans: Identifying benchmarks of maturation and vulnerability to injury across species. Prog Neurobiol. 2013;106-107:1-16.
149. Yeung MSY, Djelloul M, Steiner E, Bernard S, Salehpour M, Possnert G, et al. Dynamics of oligodendrocyte generation in multiple sclerosis. Nature. 2019;566(7745):538-42.

Curriculum Vitae

Alyssa Kallman

Education

University of California, Los Angeles
B.S, Microbiology, Immunology, and Molecular Genetics
Magna Cum Laude

Johns Hopkins University, School of Medicine
PhD Candidate, Human Genetics

Research Experience

- Utilized CRISPR/Cas9 and human stem cells to engineer organoids for analysis of genetic retinal disease and identification of novel therapeutic targets
- Mentored various scientists in stem cell derived organoid culture and computational analysis techniques
- Use of the R programming language to analyze large single cell RNA sequencing datasets for data visualization and presentation in lecture-style and poster presentations
- Immunohistochemical analysis and imaging of retinal organoids to observe retinal architecture and photoreceptor morphology
- Collaborated with scientists in bioinformatics, pathology, and engineering departments at JHU and retinal degeneration researchers at the Cleveland Clinic and University of Wisconsin
- TA for graduate pathobiology course

Consulting Experience

- Johns Hopkins Graduate Consulting Club 2019 Healthcare Case Competition
- Johns Hopkins Graduate Consulting Club 2018 Fall Case Competition

Awards

- Visual Science Training Program Graduate Fellowship

Publications

- Kallman, A., Capowski, E.E., Wang, J. et al. Investigating cone photoreceptor development using patient-derived NRL null retinal organoids. Commun Biol 3, 82 (2020). https://doi.org/10.1038/s42003-020-0808-5
- Masuda, T., Wan, J., Yerabelli, A., Berlinicke, C., Kallman, A., Qian, J., Zack, D. Off target, but sequence-specific, shRNA-associated trans-activation of promoter reporters in transient transfection assays. PLOS ONE 11, 12 (2016). https://doi.org/10.1371/journal.pone.0167867
- Chamling, X., Kallman, A., Berlinicke, C. et al. Single-cell transcriptomic analysis reveals molecular diversity of PDGFRα+ human oligodendrocyte progenitor cells. Under review.